DETERMINATION AND SIMULATION OF THE HEAT TRANSFER CHARACTERISTICS OF ELECTRONIC ASSEMBLIES

FARHAD SARVAR

A thesis submitted in partial fulfilment of the requirements of the Council for National Academic Awards for the degree of Doctor of Philosophy

APRIL 1992

Polytechnic of Wales

I dedicate this thesis to my parents

Dr Hassan Sarwar
and
Mrs Najieh Baghbani

Farhad Sarwar

ACKNOWLEDGMENTS

The author wishes to thank the staff of the Hybrid Electronic Unit of the Radio and Signals Research Establishment at Malvern for fabricating the test samples used in this project. Thanks are also due to AGEMA Limited for the loan of their thermal imaging equipment and the assistance of their representative for temperature measurements on hybrid resistors.

I am indebted to my supervisor Professor P A Witting, head of department of Electronics and Information Technology at the Polytechnic of Wales, for his helpful guidance, encouragement and enthusiasm during the course of this investigation.

I would also like to express my gratitude to Dr. N J Poole for his support and many hours of vigourous and stimulating discussion.

I am grateful to the staff of the Information Technology Centre at the Polytechnic for all their help with the software content of this project and to the staff of the Media and Resources for the preparation of the photographs presented in the thesis.

Finally, I wish to thank my wife for her patience and support during the many evenings I spent working on this thesis.

TABLE OF CONTENTS

ABSTRACT

This research project has developed a computer-assisted methodology whereby the temporal and spatial distribution of temperature in thick film circuits fabricated on ceramic substrates may be predicted. The analogy between thermal and electrical systems is used to define a thermal structure in electrical format which is then simulated using ASTEC3 electronic analysis package.

Procedures have been developed whereby the three heat transfer mechanisms namely conduction, convection and radiation may be modelled. Models have also been proposed which allow the more important sections of a thermal structure to be analysed in finer detail. These procedures have been used in the solution of some standard heat flow problems whose solutions have also been obtained by other more conventional techniques for comparison. Programs have been developed which facilitate the presentation of the results in the form of contour-maps or 3-D temperature distribution plots. Software has also been developed which can generate the electrical equivalent description of a device in ASTEC3 syntax. Estimates of the computing times required to carry out electro-thermal simulations of hybrid and VLSI devices have been made. The predicted computation times are feasible.

Confirmatory experiments have been carried out in large scale using partially heated samples prepared from printed circuit boards. These were heated electrically and temperature measurements were made using an infrared thermometer. These structures were modelled and simulated using ASTEC3 for comparison. It was found that for an accurate thermal analysis there was a need for reliable data for the thermal conductivity of the glass-fibre laminate and the heat transfer coefficients of convection. Experiments were designed to measure the thermal conductivity of the laminates tangential to the

plane of the boards. A standard Lees' disc apparatus was also used to measure this parameter in a direction normal to the boards. A Schlieren optics apparatus was used to study the convection plumes over the surface of the plates in a horizontal position with the heated side facing upwards which provided a significant insight into the flow regime over such surfaces. Values were subsequently determined for the convection coefficients from the boards. Using the measured thermal conductivities of FR4 boards and the estimated convection coefficients, excellent agreement was achieved between the measured and simulated results.

Temperature measurements were also conducted at reduced dimensional scale on especially designed thick film resistor samples. The samples were fabricated by R.S.R.E and temperature measurements were carried out using a thermal imaging equipment manufactured by AGEMA. Again the Schlieren apparatus was used to observe the convection plumes forming over the devices which led to a better understanding of the heat transfer mechanism from such devices. These observations were then used to estimate the natural convection coefficients from the surface of horizontally positioned resistor samples which were then included in the ASTEC3 model of the devices. The subsequent ASTEC3 thermal simulation showed an excellent agreement with the measured temperature profile.

1 INTRODUCTION

The main limitation to the increasing complexity of integrated circuits has been the chip size. As the necessary chip area increases the production costs also increase and a desired solution has been not to increase the chip size but to allow a greater density of active devices on the chip. The prime motivation for the increase in packing density is therefore the reduction in the cost of producing such circuits. The semiconductor industry is further stimulated by the information processing industry constantly requiring systems of higher performance and speed which can be accomplished by reduction in size and increased packing density and which in turn reduce the inter-chip interconnection delays [1]. Furthermore, the most unreliable aspect of any system design is the physical connection and the reliability of electronic systems is approximately inversely proportional to the number of joints [2]. Component integration has led to the replacement of printed circuit cards containing many individual circuits (built on chips with smaller numbers of components) with a single chip. The connection between the circuits is accomplished using thin film wires on the chip and these are less susceptible to problems with mechanical vibration, incomplete insertion and dirty contacts normally associated with circuit cards. The reduction in the number of mechanical connections therefore gives a more reliable product. The reduction in the physical size of a device however means an increase in electrical activity within a small area on a chip and consequently to excessive heat generation within that area. The resulting high temperatures can drastically affect the performance of a circuit and hence its reliability. There is, therefore, a need for a computer modelling tool allowing the prediction of the temperature profile on a circuit, preferably under accurately simulated working condition of electrical activity.

The transient aspects of the modelling is most crucial for devices operating under pulsed conditions since in these situations the phasing of the heat dissipation should be taken into account [3] to reduce the risks of under- or over-estimating the problem. This type of simulation cannot be carried out without coupling of the electrical and thermal models.

The original objective of this project was to develop a simulation tool capable of simultaneous analysis of both the electrical and thermal systems. In the event, the initial simulations indicated that a much closer understanding of the heat loss processes as applied to microelectronic circuits was needed. As a result the majority of the effort in this work was directed towards the elucidation of the heat loss mechanisms and further work still remains to be done to explore the combination of the electrical and thermal analysis.

The work carried out to date and reported in this thesis is as follows:

- A modelling process has been developed whereby the thermal characteristics of a structure can be simulated using an electronic simulation package. To allow the presentation of the temperature distribution in graphic form, programs have been developed to produce contour maps of a surface temperature. Also to minimise the effort involved in producing an error-free net-list of a structure, software has been developed to automatically generate such data-files.

- To reduce the computation times, techniques were devised and tested whereby the various sections of a circuit could be simulated at different resolutions.

- To demonstrate that ASTEC3 could be used for thermal modelling, standard heat flow problems were solved using the software and the results were successfully compared with the solution derived from more conventional techniques.

• To ascertain the validity of the modelling system in a practical situation, experiments were designed in macro-scale using partially heated PCB plates. The initial simulation results in this case showed large discrepancies with the measured temperatures. It was clear that for an accurate simulation, further analysis of the heat flow mechanisms from these boards was required. Instruments such as the Lees' disc apparatus are available commercially for the measurement of thermal conductivity in a normal direction for materials in the form of thin boards which was subsequently employed for this purpose. No such apparatus was however found capable of measuring conductivity in a direction tangential to the board. A novel experiment was therefore developed to measure the in-plane thermal conductivity of FR4 boards. Samples of the insulating board were heated from one end and temperatures measured along the specimen. This was carried out in a vacuum chamber so as to minimise the effect of convection which is a difficult process to quantify. These temperatures were then compared with a finite difference solution of the structure where the thermal conductivity along the board was varied in the solution until the calculated temperature profile best match the measured one. The resulting value was then taken to be the required tangential thermal conductivity. To develop a better understanding of the heat flow regime and hence the natural convection from partially heated structures, an optical method was used to observe the plumes forming over such surfaces. Using the results of these observations and an error optimisation technique, heat transfer coefficients were estimated for convection. This demonstrated that certain simplifying assumptions could be made concerning the convection coefficients. Good agreement between simulation and experiment was obtained.

• Having validated the macro-scale model, the modelling system was tested on small scale devices, namely a hybrid resistor sample. At this scale the measured temperatures again showed differences with the simulated data which required further

examination of the convection flow from the packaged hybrid samples. Again it was demonstrated that (different) simplifying assumptions could be made and good agreement between simulation and experiment was obtained.

At this point the program of research was terminated and further work will be needed to deal with the thermal modelling of devices fabricated on semiconducting substrates.

The ASTEC3 electronic simulation program was chosen as a vehicle for such analysis. It is particularly well suited for thermal simulation of devices as it incorporates two features of special significance in addition to its highly efficient electronic simulation capabilities. These are its powerful sub-modelling facility and its ability to handle large sets of first-order differential equations. The sub-modelling is highly useful in thermal modelling as a library of thermal models of standard components may be developed via this facility. These may then be called up within other circuits with the need of only the outer connections of the sub-model.

The software also makes it possible to model both thermal and electrical characteristics of the same device in one simulation. This is made possible by including in the circuit description file, an additional section describing the electrical equivalent network of the thermal aspects of the same circuit. The package allows exchange of parameters between the electrical and thermal sections. The instantaneous heat generation due to the passage of current is calculated as a parameter in ASTEC3 from the values of the electrical circuit parameters. This can then be assigned to the heat generator in the thermal model. In this way a *two-layer* combined electro-thermal model is produced.

Modelling procedures are described which can deal with one-, two- and three-dimensional heat flow situations. One- and two-dimensional models may be used where the heat flow

within the structure can be approximated to that scheme. It is however shown [4] that time-dependent problems and devices with very small heat sources cannot be accurately analysed using one- or two-dimensional models and therefore a three-dimensional approach has to be taken.

In order to demonstrate the importance of thermal modelling of devices, the following section is included examining the temperature effects on electronic components.

1.1 Effects of Temperature on Electronic Components

The elevated temperature of a device can cause a variety of strange effects in electronic circuits. An accelerated corrosion and interfacial diffusion process may be activated at high temperatures [5] leading to a premature failure of the circuit. Excessive temperatures may, for example, cause failure in the metallisation layer or bonded interfaces such as wire bonds and the chip to package bonding of a device. To test the reliability of a device and for quality control purposes, manufacturers normally rely on accelerated stress testing techniques. Many chemical and physical processes can be accelerated by temperature. The reaction rate R at which these processes proceed is related to temperature by the Arrhenius equation [6]:

$$R = R_0 e^{-E_a/kT} \qquad 1.1$$

where E_a is the activation energy (in Electron Volts), k is the Boltzmann constant and T is the absolute temperature in Kelvin. The results of such tests have shown that the failure rate of semiconductor devices with temperature follows the same relationship and that temperature rises as small as 10 °C can reduce the average time that a device functions before first failure (the mean time to failure) by a factor of two [5,7,8].

Operating temperature also influences the Performance of the circuit. The changed characteristics of the components in the hot regions may modify the behaviour of the whole circuit in such a way that the design specifications are no longer met. P-n junctions, which are the building blocks of electronic components fabricated on semiconducting substrates, are sensitive to high temperatures. Virtually all the characteristics of a semiconductor diode are affected by the changes in temperature. An example is shown in figure (1.1) [9]. The forward voltage is reduced with an increase in temperature but perhaps more importantly, the increasing temperatures lead to an increase in the reverse saturation current I_s of a p-n junction [9] in turn reducing the electrical isolation which is normally provided by the reverse-biased junction [5]. It has been found experimentally that the reverse saturation current of a diode increases approximately 7.2% per K [10]. The following equation represents the variation of I_s as a function of temperature [10]:

$$I_s(T_2) = I_s(T_1)e^{K_i(T_2 - T_1)} \qquad 1.2$$

where T_1 and T_2 are two different temperatures the latter being the higher one and K_i is equal to 0.072/K. Thus for a silicon diode with an I_s of 10 nanoAmperes at room temperature of 25 °C, a reverse saturation current of 81 microAmperes is expected at 150 °C. It is also obvious from figure (1.1) that the voltage level at which the Zener (Avalanche) breakdown occurs decreases with an increase in temperature.

A bipolar junction transistor is also a temperature sensitive circuit element. It is basically made up of two p-n junctions and hence all the temperature effects discussed above apply. Specifically, the reverse saturation current at the collector junction of a transistor I_{CBO} varies with temperature in the same way as defined by equation (1.2). The increase in the power developed at the junction increases the temperature of the junction which in turn causes a further increase in I_{CBO}. The collector current, I_C, of a common-emitter configuration for example is related to the reverse saturation current of the transistor by the following relationship [11,12]:

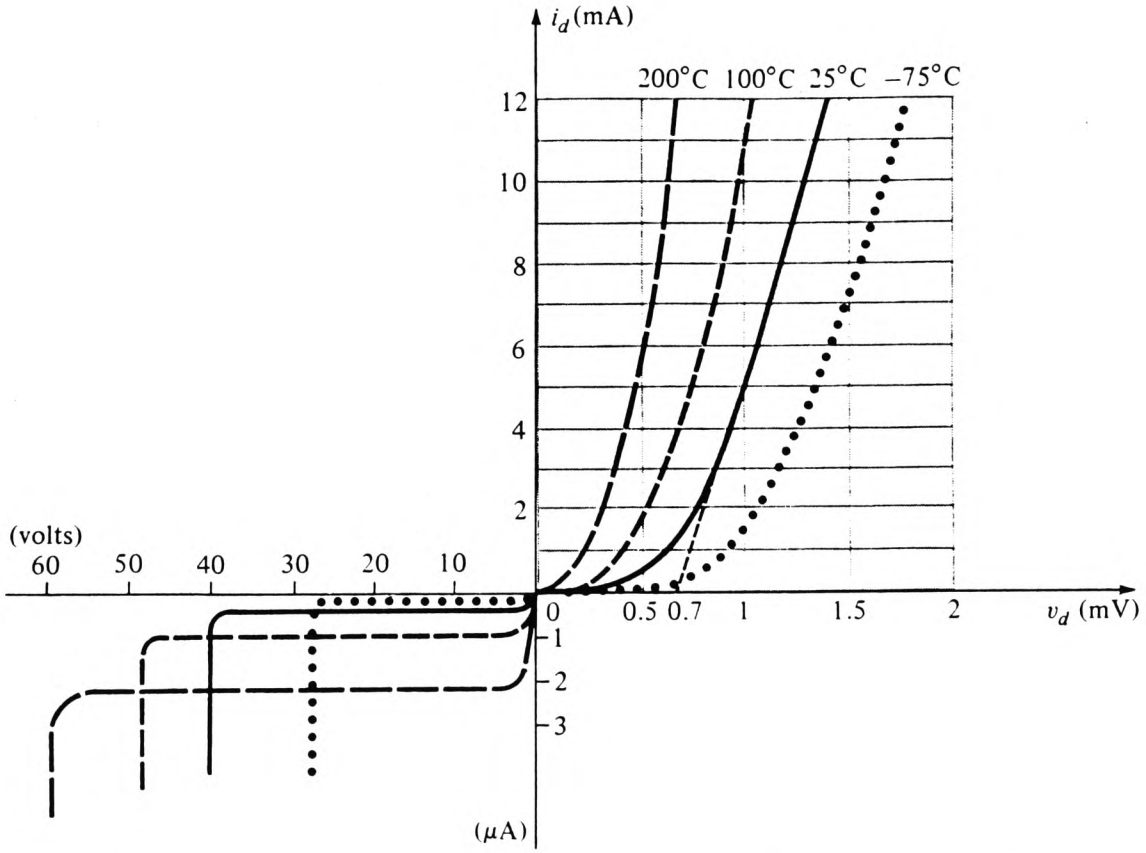

Figure (1.1) Variation in Diode Characteristics with Temperature Change

After Boylstad R and Nashelsky L [9]

$$I_C = \beta I_B + (1 + \beta) I_{CBO} \qquad 1.3$$

where β is the Common-Emitter Forward-Current Amplification Factor of the transistor [9]. It is therefore clear that an increase in I_{CBO} also increases the collector current. A regenerative heating cycle may occur at high temperatures (high ambient temperature, high developed power or perhaps a hot spot on a device) which can result in a phenomenon referred to as *thermal runaway* [11,12] and in extreme cases can lead to destruction of the transistor.

Even if a transistor does not burn out, high temperatures may cause the operating point to shift to such an extent that the circuit functions improperly [11]. Considering the typical output characteristics of a transistor in common emitter configuration, as shown in figure (1.2), if the line for I_B=0 moves upwards because of the increase in the reverse saturation current and hence the collector current I_C from equation (1.3), then the characteristics for other values of I_B also move upwards. The operating point which is normally chosen at half the value of V_{cc} (Supply Voltage) also moves up if I_B is forced to remain constant [12]. Thus a transistor originally biased to operate in the active region at room temperature may be pushed into saturation at temperatures above 100 °C [12].

The bipolar junction transistor can be represented as a two port network. Using standard notations [9], it is possible to set up the hybrid model which is often used for bipolar junction transistors operating under *small signal* conditions. The parameters of the hybrid model of a transistor vary with bias conditions and frequency as well as temperature. The variation in *h*-parameters is shown graphically as a function of temperature in figure (1.3) [9]. The parameters have all been normalised at room temperature of 25 °C. It can be seen that all the parameters increase in magnitude with increasing temperature.

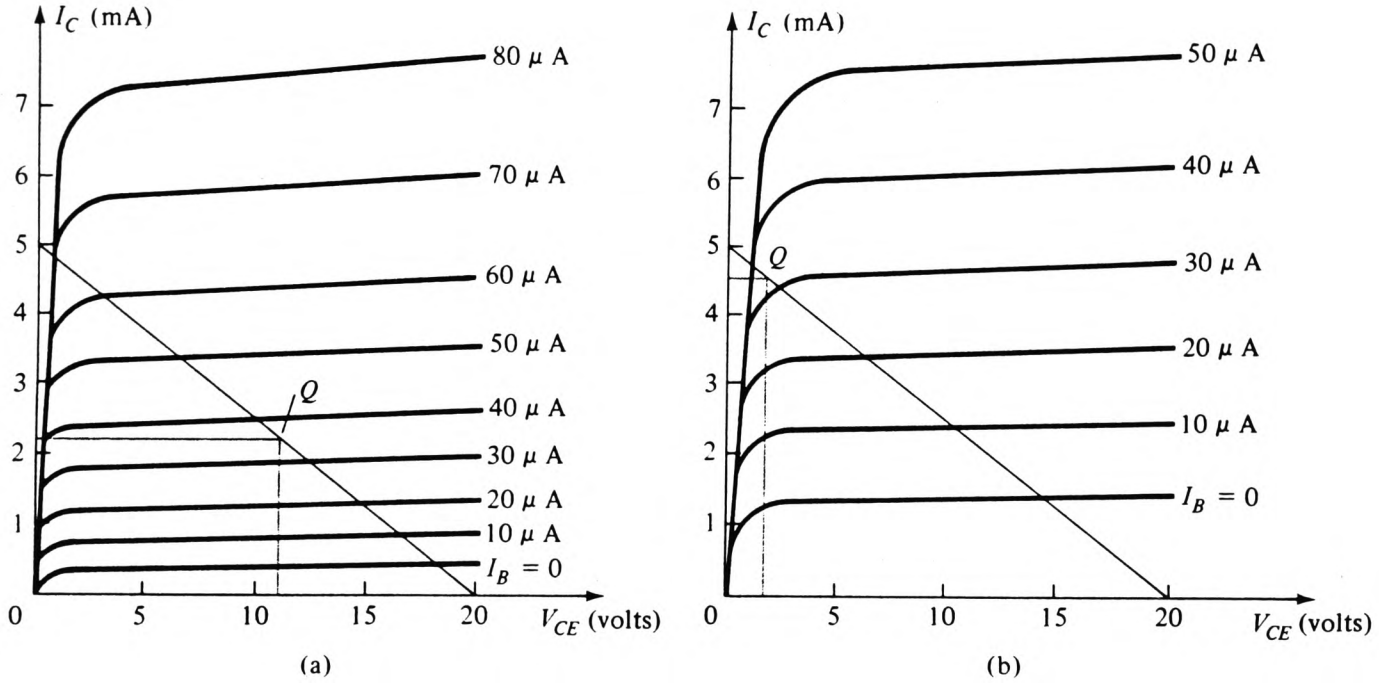

Figure (1.2) Shift in DC Bias Point (Q-Point) due to Change in Temperature: (a) 25 °C; (b) 100 °C

After Boylstad R and Nashelsky L [9]

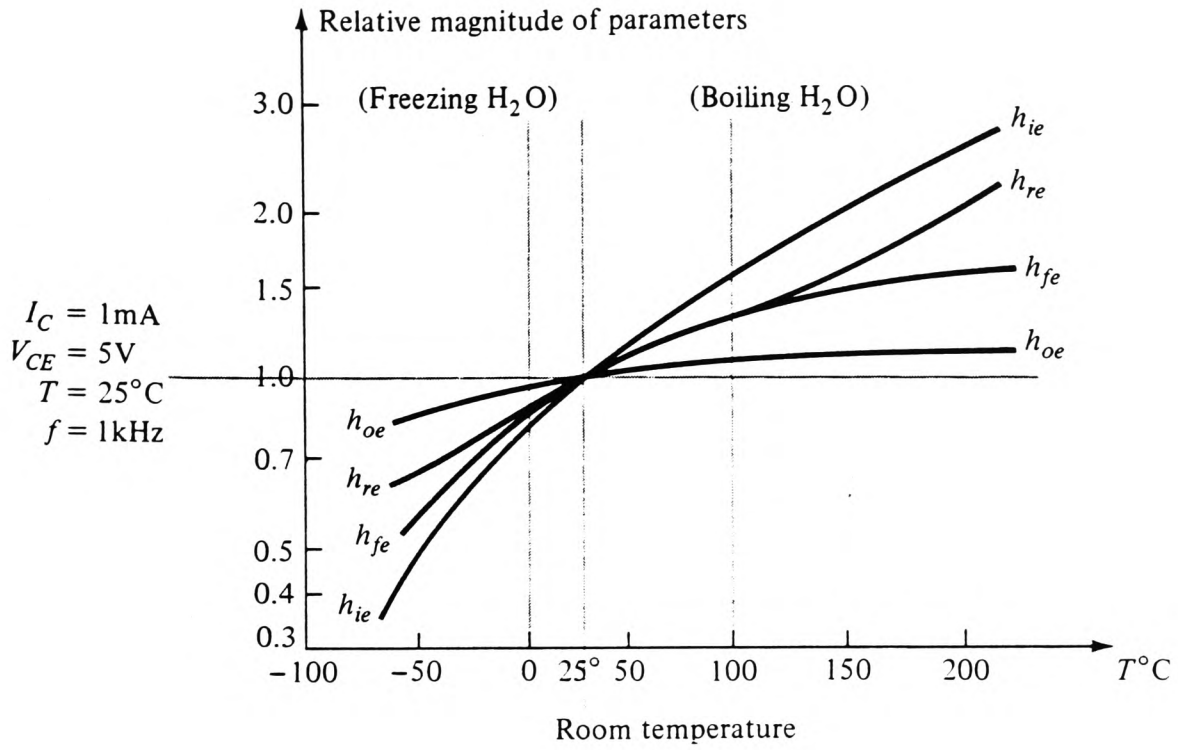

Figure (1.3) Hybrid Parameter Variation with Temperature

After Boylstad R and Nashelsky L [9]

h_{ie} (Input impedance parameter) increases at the greatest rate while h_{oe} (Output conductance) is least affected. h_{fe} (forward current gain) changes from 50% of its normalised value at -50 °C to 150% of its normalised value at +150 °C [9].

In MOS transistors the mobility of the carriers, μ, in the channel is an inverse function of the absolute temperature. The mobility at temperature T is related to mobility at room temperature of 300 K (27 °C) via the empirical relation given below [13]:

$$\mu(T) = \frac{\mu(300K)}{(T/300)^a} \qquad 1.4$$

where a is a constant which lies between 1.0 and 1.5 [13]. Thus a 100 °C temperature rise would result in approximately 30% fall in carrier mobility. Consequently, for a fixed applied voltage the drain current I_D decreases with an increase with temperature. The increased temperatures may therefore reduce the switching speeds of these devices [14].

1.2 Review of Thermal Analysis Techniques

The problems outlined above have to be foreseen and prevented at the design stage. The traditional approach, to construct and test an experimental layout, is obviously costly and time-consuming and also takes no account of tolerance variations. For many years designers have faced the problem of predicting temperature rise due to thermal dissipation in semiconductor integrated circuits [15,16] and also hybrid microcircuits [17-19]. Almost all the electrical energy consumed by electronic devices is converted directly into heat. An irreversible dominant heating process occurs when current passes through a material. This is called *Joule Heating* and it is proportional to the product of the square of the current and the electrical resistance of the material to the current flow (I^2R). A second independent heating or cooling process which occurs in a single material is called the *Thomson Effect* [20]. This appears when an electric current flows through a conductor along which there

is a temperature gradient [21,22]. This effect is proportional to the product of the current I and the temperature gradient dT/dx [21] and therefore reverses when current is reversed. A Thomson coefficient is defined for a material as the heat evolved when a charge of one coulomb flows from one point in a material to another at 1 °C lower. Thomson coefficient which is normally denoted by σ has units of Joules and is exceedingly small (in the order of 10^{-7} [23] for most metals). For this reason the *Thomson Effect* will be ignored in all the discussions and calculation throughout this thesis.

There is therefore a need for programs which facilitate the prediction of the local temperature rises in devices. These programs should preferably include both the thermal and electrical aspects of the design integrated.

A number of papers have been published attempting to deal with the thermal problem in electronic devices. One of the simplest approaches taken in the modelling of hybrid circuits is a one-dimensional model [8,24-26] where the heat is assumed to flow from the power dissipating element in the front to the back side of the substrate. The heat dissipation from the heat generator is confined to a fixed spreading angle measured from the normal to the substrate. The angle is taken to be approximately 45° but it is recommended that the angle should be verified experimentally. An average steady-state thermal resistance analog of the heat flow is determined by integrating over the thickness of the heat flow path. The back side is considered to be isothermal and heat losses by convection and radiation from the surfaces of the device are neglected. The model may be valid to some extent for substrates of small thermal conductivity such as glass but it is not suitable for ceramic substrates with relatively high thermal conductivities (around 24 *W/mK* compared to 1 *W/mK* for glass) where the lateral heat flux is not negligible. The technique is limited to steady-state thermal analysis and thermal coupling between different heat generating

elements is ignored by assuming that the distance between the adjacent elements is sufficiently large. This may of course be a significant effect in the conductive flow within a device [27].

In cases where there is considerable lateral heat flow due to high thermal conductivity of the substrate and the substrate thickness is much smaller than other dimensions, workers have taken a two-dimensional approach [19,28]. These models assume that the temperatures on the front and the rear sides of the substrate (top and bottom if placed horizontally) are identical and neglect temperature gradients perpendicular to the substrate faces [19]. The two-dimensional model does not however hold for thermal situations where very small heat sources result in temperature gradients in the direction normal to the large faces [15,29] or where fast thermal transients are present [4]. In such cases the three-dimensional heat equations have been solved in the appropriate form to obtain the temperature distribution in the device.

Various approaches have been proposed for the solution of the equations defining the heat flow in devices. A finite-difference method has been presented for two- [30,31] as well as three-dimensional cases [30]. This technique is based on the concept of *lumped parameters*. A device is divided into an array of discrete volumes called *nodes* and the mass of each volume is then *lumped* at a point within the volume it represents [32]. The paths for the heat flow from one volume to another are represented by conductors joining the appropriate nodes. Heat balances are subsequently made on each of the nodes giving rise to a system of linear algebraic equations defining the temperature of each node in terms of the temperatures of its surrounding nodes. The system of equations may be expressed in matrix notation as $A\mathbf{T}=\mathbf{b}$ [33] where A is the matrix including the coefficients of the temperature terms, $\mathbf{T}$ is the required solution vector and $\mathbf{b}$ is a column vector of constants. Solutions of these equations have either been by direct matrix inversion [33] or via iterative techniques

[28,30,34]. The latter is normally carried out using a *relaxation* technique which is a method whereby a temperature is ascribed to each node either by guessing or observation. Upon substitution of these temperatures a *residue* is obtained for each nodal equation. The temperature at the node with the greatest error is then *relaxed* (corrected) and subsequently a new error distribution is calculated across the network and the temperature of the node showing the greatest error is now relaxed. This process is repeated until the residues at every node reaches a required accuracy. The solution may be slow if a very fine grid is used in order to obtain more accurate results. This is particularly true in the three-dimensional cases for which the computing time becomes too large for the method to be useful [35].

The finite element technique has also been proposed [35,36] for the thermal analysis of electronic devices. For this method, the structure is divided into a number of small finite elements which are connected together at some nodes. For each node a heat flow balance is performed considering all the finite elements connected to it and the solution is expressed in terms of node temperatures. The advantage of this technique is that it is not geometrically restrictive [36] and it therefore gives a freedom of choice for the shape of elements [37].

The *Separation of variables* technique [37,38] has been used by some authors to derive analytical solutions for heat flow in hybrid [17,27] as well as integrated circuits [39-41]. This approach is used to reach a steady-state solution of the three-dimensional partial differential equation of heat conduction (Laplace's equation). The following assumptions are normally made to simplify the thermal problem:

- The lateral dimensions of all the different layers are assumed to be identical, that is the pattern of these layers is ignored.
- The heat losses due to convection and radiation are neglected from the top face as

well as the vertical sides of the substrate and the bottom surface of the hybrid is assumed to be isothermal as it is mounted on to a heat sink.

• The heat is only generated at the top surface and all resistors are taken to be of zero thickness.

• All layers are of uniform thickness with no voids and they are all rectangular in shape.

The solution of this technique proceeds by assuming that the temperature may be written as a multiplication of three separate functions such as $T(x,y,z)=X(x)Y(y)Z(z)$. This is substituted into the Laplace's equation from which three ordinary differential equations result in the form:

$$\frac{d^2X}{dx^2} \pm \lambda^2 x = 0 \qquad 1.5$$

for each of the variables X, Y and Z. The solution to each of these differential equations is then found in terms of simple hyperbolic or trigonometric functions depending on the sign of the linear coefficient (positive or negative). For the positive value for example the solution is in the form $X(x)=A\ sin\lambda x + B\ cos\lambda x$ and for a negative coefficient the solution is $Y(y)=Ce^{-\lambda y}+De^{\lambda y}$. Depending on the sign of the linear term solutions are found for $X(x)$, $Y(y)$ *and* $Z(z)$. Arbitrary constant A and B and others in the solutions for $Y(y)$ and $Z(z)$ are then evaluated by applying the particular boundary conditions. The parameter λ in $X(x)$ and the equivalent ones in Y and Z are also determined from the boundary conditions. These are normally found to be in the form of a summation over a range of values which when substituted in $T(x,y,z)$, a form of Fourier series is obtained. The accuracy of the calculations depends on how many terms are included between 0 and ∞. In practice the calculations of the series are truncated and Bessel's inequality formula [38] is used to measure the accuracy of the Fourier series approximation. The main disadvantage of the

technique is its limited use [36] and that even for simplest of geometries the solution is quite complex [37]. The series solution to the equations does not necessarily converge rapidly and an accurate solution could require evaluation of many terms [36].

Another analytical approach adopted by some workers involves the use of Laplace and Fourier transform techniques for the solution of the classical transient heat flow equation. This method has been used for two [35] as well as three-dimensional differential equations. The solution is found by applying multiple finite Fourier transforms with respect to x and y and then taking the Laplace transform over the discrete time interval. The resulting differential equation is then solved for the z variable in the composite structure with the appropriate boundary conditions. An inverse Laplace transform is subsequently performed to obtain a relationship for transient temperature in the structure. The accuracy of the solution depends on the number of terms in the series. It has been claimed that ±2 °C truncation error can be achieved using 400 terms [42].

For an accurate thermal analysis of electronic devices, accurate values are required for various parameters such as the thermal conductivity of the substrate, convection and radiation coefficients. Perhaps the only parameter for which reliable information may be available is the thermal conductivity which is normally specified in the manufacturers data sheets. The convection coefficient h_c is the most difficult parameter to quantify [35]. Its value depends strongly on the nature of the whole surface, the orientation of the substrate (vertical or horizontal) and the speed of the air flow (natural or forced convection). Perhaps because of the difficulties in ascertaining an accurate value, some authors [17,25,34] opt to ignore the effects of convection altogether assuming that these losses are too small compared to conduction losses. Some workers however include convection in their models by using values taken from other publications [35] or via a *rule of thumb* [15,31]. Some however use a very simplified experimental approach [43] to estimate a uniform convection

coefficient over the surface. These experiments basically involve the measurement of the surface and the ambient temperatures followed by a simple energy balance approach [43] to calculate an average heat transfer coefficient. Empirical relationships have also been used [18,28,44] to arrive at an average coefficient of convection. The empirical relationships assume that the rate of convection losses is the same over the whole of the chip assembly and are derived in various texts each yielding a different heat transfer coefficient. It is up to the designer to decide which to use in the model.

1.3 Thermal Analysis and Modelling Using ASTEC3

The modelling technique used in this thesis is based on the analogy between thermal and electrical systems. A thermal structure is divided into an appropriate number of conduction *cells* whose thermal resistances may be calculated in the three space directions. Thermal resistances are also determined for convection and radiation heat losses from the boundaries. An equivalent electrical network is constructed which is subsequently simulated using the ASTEC3 electronic simulation package.

Electronic analysis programs have been used in the past for thermal calculations in microelectronic circuits [45] and other applications [46]. In the case of electronic devices SPICE2 electronic analysis program has been used as the simulation tool. The method is limited in its applications as it is only applicable to monolithic integrated circuits [27] and it is therefore not suitable for thermal analysis of hybrid circuits [27]. The technique does not include thermal coupling between heat generating elements and it is limited to steady-state analysis [45]. In one publication [46] thermal analysis of heat exchangers and control loops of spacelab has been discussed where ASTEC3 is used as the simulation software.

The most difficult task in the thermal analysis of devices is the error-free preparation of the description file especially for very large thermal networks. Software has therefore been developed which can semi-automatically generate the electrical equivalent circuit of a thermal structure in ASTEC3 language. Programs have also been developed which make use of the ASTEC3 output results to plot two-dimensional temperature contour-maps or three-dimensional surface temperature profiles.

Procedures are also introduced which allow a user to define the more important parts of a circuit in finer detail. *Interface* cells are described which make the coupling of the *coarse* and *fine* mesh areas possible. These procedures are of special importance when simulating very large circuits as they reduce the computation time required for such simulations. Studies have been carried out to establish relationships between the size of the circuit and the CPU time needed for its thermal analysis. These relationships may be used to estimate the CPU time for a particular thermal simulation.

Verification of the modelling system is established in the first instance by application to standard heat flow problems. The solutions to these problems are readily available via a more standard method for comparison.

In practical levels, the accuracy of thermal simulations are limited by the accuracy of the thermal parameters used. In steady-state analysis these may include thermal conductivity, emissivity and heat transfer coefficients. In transient simulations the specific heat capacity of all the materials must also be included in the list of required parameters. The availability of such data is also an additional factor since they would have to be measured otherwise. This problem was encountered in this work during the analysis of a set of preliminary experiments designed to verify the modelling system.

2 ASTEC3 SIMULATION PACKAGE

The ASTEC3 software is primarily designed for the analysis of the electrical performance of circuits and is capable of displaying the results of a simulation in various graphical formats. For thermal modelling however some of the displaying techniques which are built into ASTEC3 had to be enhanced to allow the presentation of the results in the form of temperature contour maps or three dimensional distributions. For this reason a brief introduction is included in this chapter describing the capabilities of the simulation package. This is then followed by further sections discussing the software developed to achieve the displaying enhancement.

2.1 Introduction

ASTEC3 is a powerful analogue circuit analysis package which is capable of performing transient, AC small signal and DC steady-state simulations [1,2]. ASTEC3 is also suitable for providing solutions to first order differential equations and any system defined by such a format can be solved. Since electrical and thermal characteristics of any given network can be written in terms of analogous differential equations, this allows for the possibility of simulating both phenomena with ASTEC3.

ASTEC3 has many advantages over other analogue simulators and although other individual packages may be better than ASTEC3 in certain aspects, ASTEC3 is a package capable of simulation of both electrical and thermal characteristics of a given circuit and it is therefore suitable for this investigation. A brief comparison of ASTEC3 with a more popular circuit simulation package, SPICE, is given below.

Amongst ASTEC3's advantages over SPICE are its speed and efficiency [3] and also the ease and the speed with which models may be created. Accuracy is also another important advantage over SPICE, especially in time-dependent simulations [4]. It has been reported [4] that there is a certain amount of empiricism built into the mathematical formulae used in SPICE for time-integration which makes it less accurate than ASTEC3. There are also restrictions in the variables allowed in SPICE since only current and voltage can be made variable. With ASTEC3 however, any variable is permitted provided that it can be expressed in the form of a standard FORTRAN equation. This means that parameters such as temperature and thermal conductivity can be made variables and computed automatically. There are also other facilities in ASTEC3 which do not exist in SPICE. For example, the ability to store the final results of a simulation which can then be used as the starting point for further simulation on the same circuit. This takes away the need for repeating the whole sequence again. There is also a facility which allows the dynamic output of the simulation onto the screen. This means that the state of the simulation can be checked throughout the simulation and if not correct it may be stopped, preventing the wastage of computing resources and time.

Finally, the most attractive feature of ASTEC3 is its powerful sub-modelling facility. The simulator allows the description of sub-circuits (so-called *models*) which can be used within other models, and the main circuit, many times without the need to write out the sub-circuit description each time it is employed. These user-defined sub-models can also be stored in the form of a personalised library. The stored models may then be called up in any future circuits in the same way as if they had been defined as models in the description sequence of the particular ASTEC3 file.

The sub-modelling facility can be of great importance in thermal modelling since it makes it possible to develop a library of typical components which may then be used in the

development of more complicated circuits. This makes it possible to hide the details of the individual thermal/electrical models and greatly simplifies the work of the end-user of the package.

2.1.1 System Analysis with ASTEC3

In this section a brief description of all the possible forms of simulation will be given with particular reference to the transient and DC steady-state simulations. These are of particular importance in thermal simulations of semiconductor devices since they can provide the user with either the final steady-state temperatures of the device or its transient temperatures while it is heating up. The latter is especially important since critical temperatures leading to a device failure may occur well before a steady-state condition has been established.

It is also possible to carry out a statistical simulation on each of the above analyses. This may be adopted in thermal problems in order to include tolerances in the thermal properties of the materials. A brief description of these simulations is given below.

DC steady-state

This analysis is used to determine the steady-state values of a linear or non-linear circuit. For a circuit containing capacitive or inductive components, the steady-state values correspond to the state after the transients have disappeared and the currents and voltages reach their equilibrium values.

AC small signal

The AC analysis provides a small signal solution to a linear circuit at a particular frequency.

If the circuit contains non-linear elements the operating points of the system are first obtained by an automatic DC steady-state analysis and then small-signal AC analysis is carried out on a version of the circuit linearised at the calculated operating point using the stimulus sinusoidal signal supplied by the user.

Transient

The transient simulation routine determines the behaviour of a linear or non-linear network when subjected to an independent signal which may or may not vary with time. The initial conditions can either be supplied by the user or can be the DC steady-state values calculated in a previous simulation.

Statistical

This allows the production of statistical data for DC, AC and Transient simulations by carrying out a Monte-Carlo analysis [5]. This is a collection of the results of many simulations on the same circuit but with different, randomly generated, values for specified components or parameters, taken from a user-specified distribution. These may be based on component tolerances in the circuit or on parameter tolerances defined in the model or both. This may be used in thermal problems to specify the variation in the value of thermal parameters such as thermal conductivity and to study its effect on the results.

The results of such simulations can be presented in three different forms. A scatter diagram can show the correlation between the relevant parameters; a graph can be plotted showing the nominal, upper and lower cases; a histogram of the results may be plotted showing the number of times that a particular quantity has taken a value in a specified range.

2.1.2 ASTEC3 Data File

A file containing the particular circuit for simulation, normally has three well defined sections as follows:

Description

This is the stage where a circuit or system is described in a particular syntax based on a conventional circuit diagram with the position of each element defined by the nodes at its connections. This is illustrated in figure (2.1) by means of a simple circuit [6] capable of producing a square wave (V_{out}) at its output node if a sinewave (V_{in}) is applied to its input terminals. A listing of the circuit description file and the output produced by ASTEC3 is shown in figure (2.2).

The circuit components are specified using a keyword (R=resistor, C=capacitor, J=current source, etc.) followed by an alphanumeric sequence for naming the particular element in the circuit. This stage includes an "!OUTPUT" sequence in which the required final output results are declared (eg. VN3 and VN6 in figure (2.2)).

Simulation

In this part of the file, the type of simulation required is specified. The type of simulation may be one of transient, DC steady-state or AC small signal simulations. It is also possible to have a single type of simulation or a mixture of all three. There are two sequences "!CHANGE" and "!VARY" which allow the simulation of the circuit with parameter values other than those already given in the description stage.

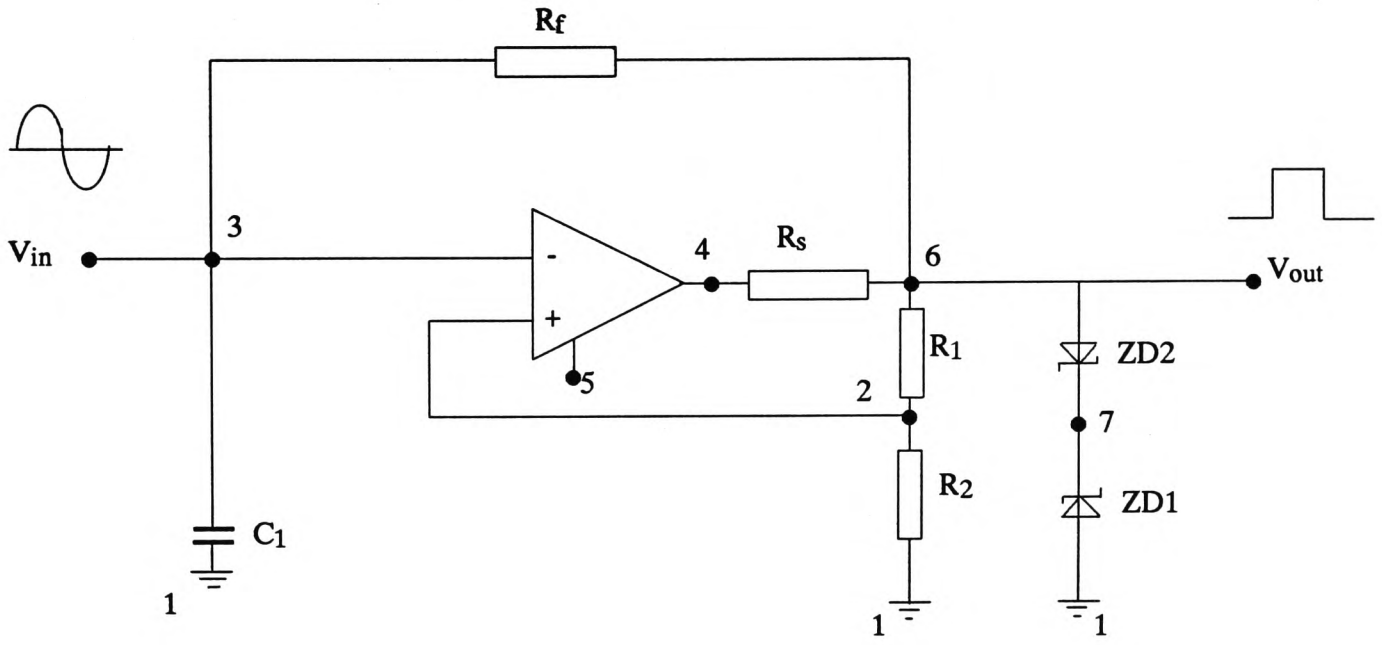

Figure (2.1) Circuit Diagram for the square Wave Generator

```
$DESC
!LIBS: ZENER1N.4740; AMPOP.LM741;

!CIRCUIT:

RF(6-3)22K;
RS(4-6)5K;
R1(6-2)1MG;
R2(2-1)1MG;
C1(3-1)0.1MC;
MZD2(6-7)ZENR1N.4740;
MZD1(1-7)ZENR1N.4740;
MAMP(1-2-3-4-5)AMPOP.LM741;
EIN(3-1)10*FSIN(2*3.14159*10*&T);

!OUTPUT: VN3;VN6;
!OPTION: TSCALE=1E-9;
!EXEC

$TRAN
!INIT:
!PARAM: TMAX=0.2;HOUT=0.0001;
!EXEC

$EDITTK
!PPLOT(TITLE=I/P & O/P OF SQ. WAVE GEN.),
VERSUS &T(RENAME=TIME SEC, LINSCALE= 0/0.2):
VN3(RENAME=INPUT,LINSCALE);
VN6(RENAME=OUTPUT,LINSCALE);
!EXEC

$END
```

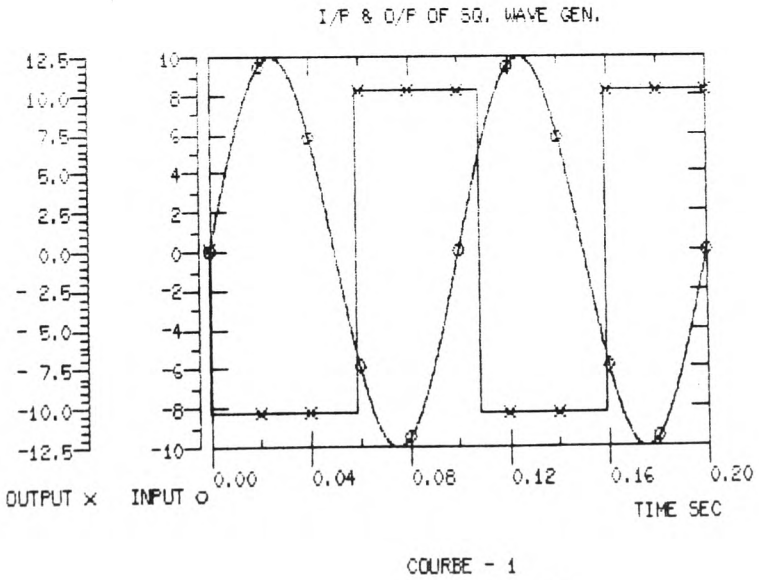

If the simulation is of a transient type then the starting point and the length of the simulation may be declared here as "TMIN" and "TMAX" values.

Presentation of results

This is the final stage where the format of the output results is specified which may be in the form of graphs or tables of results.

If a statistical analysis is carried out, then the results may be presented in the form of histograms or scatter diagrams derived from a number of runs. It is also possible to display an envelope graph showing the nominal, upper and lower performances achieved over many runs.

There also exists a facility within ASTEC3 which allows the user to store the whole of a simulation run in a specified file. This file may include tables of results which can then be used to obtain isothermal maps or temperature distribution plots as will be described in a later section.

2.2 Presentation of ASTEC3 output results for Thermal Systems

The ASTEC3 package has a very efficient and versatile graphics facility which allows the presentation of the results of a simulation in various forms. These may be graphs containing one or more curves from the same, or separate, simulations. In the case of statistical analysis, histograms, scatter diagrams or even envelope curves may be displayed representing the upper, lower and the mean values of the results. It is also possible to obtain tables containing the numerical values of the results, a sample of which is given in Table (2.1). The tabular form of the ASTEC3 output, normally contains a boxed section

Table (2.1) An Example of the Tabular Output of an ASTEC3 Simulation

```
PRINT  - 1

I-------------------------------------------------------------------I
I                                                                   I
I    SYMBOL      MINIMUM      MAXIMUM      ---- VARIABLE NAME ----  I
I                                                                   I
I       A        0.00E+00     6.00E+01     VN1                      I
I       B        0.00E+00     5.20E+01     VN3                      I
I       C        0.00E+00     4.40E+01     VN5                      I
I       D        0.00E+00     3.60E+01     VN7                      I
I       E        0.00E+00     2.80E+01     VN9                      I
I       F        0.00E+00     2.00E+01     VN11                     I
I                                                                   I
I-------------------------------------------------------------------I

&T          0.000E+00   4.500E+01   7.500E+01   1.200E+02   1.500E+02
VN1         0.000E+00   6.000E+01   6.000E+01   6.000E+01   6.000E+01
VN3         0.000E+00   3.790E+01   4.393E+01   4.837E+01   4.986E+01
VN5         0.000E+00   2.201E+01   3.103E+01   3.812E+01   4.054E+01
VN7         0.000E+00   1.481E+01   2.313E+01   3.012E+01   3.254E+01
VN9         0.000E+00   1.522E+01   2.010E+01   2.436E+01   2.586E+01
VN11        0.000E+00   2.000E+01   2.000E+01   2.000E+01   2.000E+01

&T          1.950E+02   2.250E+02   2.700E+02   3.000E+02   3.450E+02
VN1         6.000E+01   6.000E+01   6.000E+01   6.000E+01   6.000E+01
VN3         5.104E+01   5.143E+01   5.174E+01   5.185E+01   5.193E+01
VN5         4.244E+01   4.308E+01   4.359E+01   4.376E+01   4.389E+01
VN7         3.444E+01   3.508E+01   3.559E+01   3.576E+01   3.589E+01
VN9         2.704E+01   2.743E+01   2.774E+01   2.785E+01   2.793E+01
VN11        2.000E+01   2.000E+01   2.000E+01   2.000E+01   2.000E+01

&T          3.750E+02   4.200E+02   4.500E+02   4.950E+02   5.250E+02
VN1         6.000E+01   6.000E+01   6.000E+01   6.000E+01   6.000E+01
VN3         5.196E+01   5.198E+01   5.199E+01   5.200E+01   5.200E+01
VN5         4.394E+01   4.397E+01   4.398E+01   4.399E+01   4.400E+01
VN7         3.594E+01   3.597E+01   3.598E+01   3.599E+01   3.600E+01
VN9         2.796E+01   2.798E+01   2.799E+01   2.800E+01   2.800E+01
VN11        2.000E+01   2.000E+01   2.000E+01   2.000E+01   2.000E+01

&T          5.700E+02   6.000E+02   6.450E+02   6.750E+02   7.200E+02
VN1         6.000E+01   6.000E+01   6.000E+01   6.000E+01   6.000E+01
VN3         5.200E+01   5.200E+01   5.200E+01   5.200E+01   5.200E+01
VN5         4.400E+01   4.400E+01   4.400E+01   4.400E+01   4.400E+01
VN7         3.600E+01   3.600E+01   3.600E+01   3.600E+01   3.600E+01
VN9         2.800E+01   2.800E+01   2.800E+01   2.800E+01   2.800E+01
VN11        2.000E+01   2.000E+01   2.000E+01   2.000E+01   2.000E+01

&T          7.500E+02   7.950E+02   8.250E+02   8.700E+02   9.000E+02
VN1         6.000E+01   6.000E+01   6.000E+01   6.000E+01   6.000E+01
```

at the top of each table which shows the maximum and minimum values of all the logged variables (voltages at nodes N1, N2,...etc. in this case). It then gives the transient value of these variables at equal time intervals in the user-specified time-range. Time is denoted by the symbol &T and listed at the top row of each column followed by the values of the outputs at the particular time intervals.

The package is primarily designed for electrical simulations and it lacks the necessary routines to enable it to produce contour-maps or temperature distribution plots for a thermal system. It has therefore been necessary to develop additional programs which make use of the tabular form of ASTEC3 outputs to display the results in the mentioned formats as detailed below.

2.2.1 Production of Contour and Temperature Distribution Plots

There exists a facility within ASTEC3 which allows the user to store the whole of a simulation run in a specified file. This file is really a screen-dump of the run and therefore includes, apart from the tables of results, extra information which should be deleted before the file can be used in plotting graphs.

As mentioned above the actual tables are normally printed beginning with the symbol '&T' in the left hand side representing time and ending with the message 'Edit Ended'. A program has therefore been written in FORTRAN, which scans through the ASTEC3 output file and ignores the additional lines up to the symbol '&T' and after 'Edit Ended'. This program creates a second file containing only the tables. A listing of this program is given in appendix (1) as program (1).

The output file of program (1) is subsequently analysed using a second program (program

(2) in appendix (1)) for plotting of the required contour-maps. A brief list of the different stages of this program are given below:

i) The data file generated by program (1) is scanned and the time-intervals are read and stored in the array "store_time".

ii) The output values corresponding to each time interval are read and stored in a two-dimensional array "store_array" along with the corresponding time-interval.

iii) The information concerning the size and location of the point grid is read.

iv) The (x-y) coordinates are generated for the outputs in each time interval. This is carried out by allocating to the uppermost quantity in the table the coordinate (x_0,y_0) and the second output (x_1,y_0) until the row y_0 is complete and then the same at rows y_2, y_3 and so on.

v) The program asks the user the desired time-difference between the plots.

vi) The appropriate subroutines from the CAD graphics package GINO are initialised automatically to produce the desired contour-maps for the first time-interval using the grid generated in section (iv).

vii) The operator is given a few seconds to dump the graph onto a printer before the contour-map for the next time-interval is displayed.

At present the software uses the CAD package GINO which is only capable of handling square or rectangular planes with uniform grid pattern superimposed upon them an example of which is illustrated in figure (2.3).

For the program to operate correctly, the ASTEC3 outputs (normally temperatures at particular points on a plane although these could be any other parameter with a distribution over the area) should be arranged in the circuit description file, in order of nodes starting from the lowest x and y position (x_0,y_0 in figure (2.3)) and incremented in the x direction until the row is complete and then repeated for rows at the next y positions (y_1, y_2, y_3, ...etc.).

Figure (2.3) A Typical Grid Pattern for Plotting Contour Maps

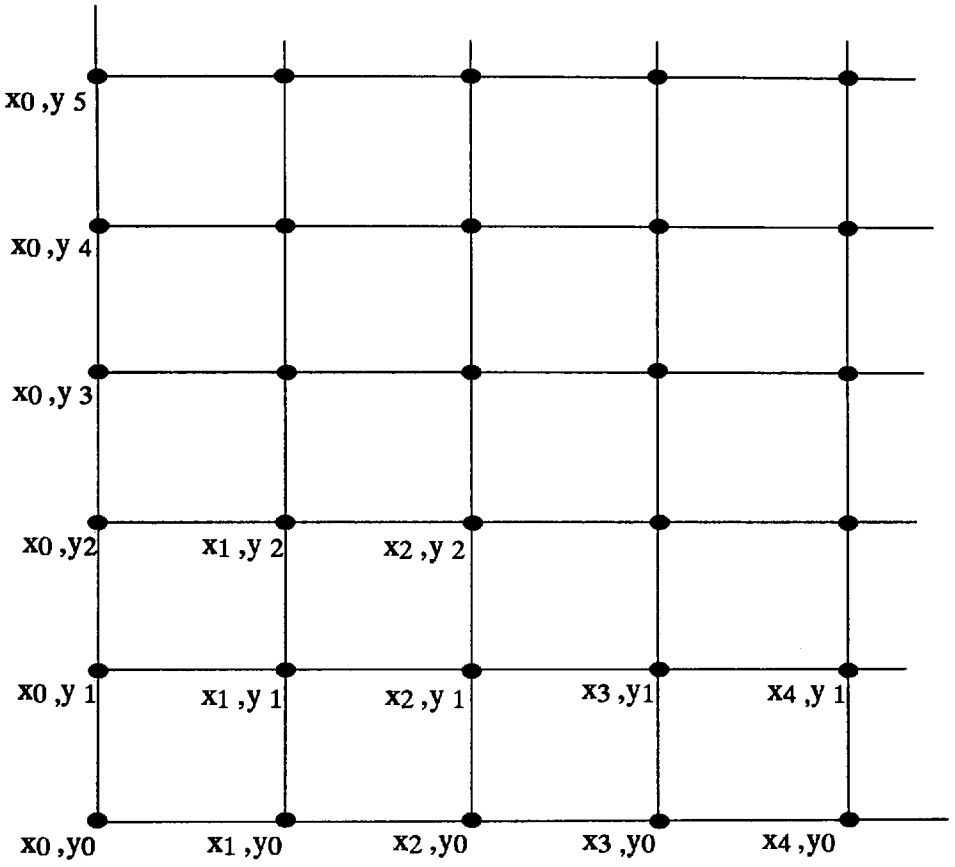

The program described above takes into account temperatures at the nodal points in one (x,y) grid to generate the contour map of the plane. This may not be satisfactory where greater accuracies are required for the temperature profile. This problem may be tackled in two ways. The first approach may be to use a finer grid for simulation of the structure which has the disadvantage of having to write a substantially greater data file which in turn needs greater computer time. This of course become more important when dealing with larger circuits. A second approach could be to develop the software to utilise the temperatures of other nodes which already exist within a 2-D model to plot the distribution. For 2-dimensional modelling, a particular structure is divided into a number of thermal cells (This will be described in detail in section 4) as shown in figure (2.4) for a structure with (5×3) cells. Three uniform grids can be observed within the model which are illustrated using symbols **x**, **o** and **+**. The program already given was extended to take into account the three grids in the plotting process. A listing of this program is given in appendix (1) program (3).

For this program the !OUTPUT nodes in the ASTEC3 data file should start with grid + first, grid o second and grid x last. The nodes of each grid should be arranged in the same way as described in program (2).

2.3 Conclusions

A brief description of ASTEC3 electronic simulation package has been given with particular reference to features such as its sub-modelling facility which make it suitable for thermal modelling.

Software which has been developed to allow the production of contour-maps and temperature distribution plots using the ASTEC3 simulation data has been described.

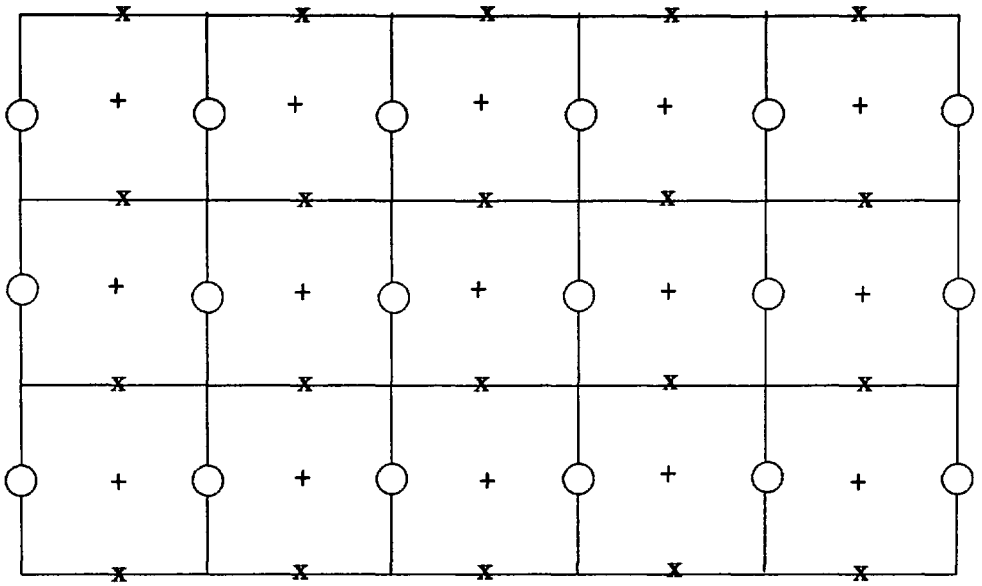

Figure (2.4) Diagram Showing the Three Grids in a Two-Dimensional Model

3 HEAT TRANSFER

There are three basic processes of heat transfer namely conduction, convection and radiation. A brief description will be given for each of these processes separately but bearing in mind that in most problems of practical importance two or sometimes all of these modes may occur simultaneously.

3.1 Conduction

This is a heat flow mechanism whereby thermal energy is transferred through a material from a region of high temperature to a region of lower temperature. In metallic conductors or any other electrically conducting solids, heat is carried through the lattice structure simultaneously by means of free electrons and vibrational energy (phonons) [1,2]. In non-metallic or dielectric materials heat is conveyed only by means of phonons [1].

The conduction of thermal energy by lattice waves may be described by considering the situation of an atom in a crystal vibrating about its equilibrium position. If this atom is vibrating with an amplitude say a at a temperature T, it exerts decaying periodic forces on its neighbouring atoms which in turn increase their amplitudes of vibration. This of course occurs if the other atoms were vibrating with lower amplitudes because of their lower temperature. If the ends of a solid are kept at different temperatures then heat will flow from the hot end to the colder end each atom oscillating with smaller and smaller amplitudes towards the cooler end.

The heat conduction by lattice vibrations is proportional to the mean free path of the phonons. The thermal conductivity of the material is therefore governed by the distance a

phonon can travel before it is scattered. If the energy transfer between the atoms of a solid were purely harmonic, there would be no mutual scattering of phonons [3]. In this case the scattering process would be dominated by collisions of lattice waves with the boundaries and lattice imperfections. In solids however, the heating causes a subsequent expansion of the structure which in turn changes the harmonic nature of the lattice waves. This anharmonicity then causes collisions between the different phonons and a subsequent scattering of the waves. Anharmonic interactions are dominant at high temperatures where the mean free path of the phonons is inversely proportional to the temperature [1]. There is another scattering process affecting thermal conduction at high temperatures called the Umklapp process. This is a random process by which the direction of flow of energy is changed after a phonon-phonon collision [1,3]. Collision of two phonons with wavevectors K_1 and K_2 travelling in the positive x direction in a crystal would at low temperatures be of the form $K_1+K_2=K_3$ where a third phonon is produced travelling in the same general direction. In the Umklapp process however collision of the energetic phonons gives rise to a third phonon whose wavevector falls outside the first Brillouin zone. According to the laws of conservation of momentum in a crystal all meaningful phonon K's should be contained in the first zone [3] and therefore the emitted phonon in the Umklapp process is brought back into the zone by a reversal of direction via $K_1+K_2=K_3+G$ where G is a reciprocal lattice vector.

Conduction in metals is dominated by movement in the solid of the electrons in partially filled bands although lattice conductivity may occasionally become important in situations where low temperature, high magnetic fields and large impurity contents exist [4]. The scattering processes which contribute to lattice resistance to heat conduction in metals may be due to electron-phonon interactions which is negligible at low temperatures and becomes important at higher temperatures. The other process is due to scattering of electrons by lattice defects which is not a temperature dependent process and depends solely on the

purity of the metal and lattice imperfections.

The basic equations of heat conduction have been well documented [5-7]. In one dimension the rate of heat transfer through a given area A is given by the Fourier rate equation :

$$q_x = -KA\frac{\partial T}{\partial x} \qquad 3.1$$

where K is the thermal conductivity of the material, T is the temperature and x is the displacement through the material of area A.

Equation (3.1) assumes that temperature varies only along the x direction and does not change with time t. This however is not sufficient where the temperature of the solid varies in the x, y and z directions and with time. The general equation of conduction in three dimensions for a uniform body with constant thermal conductivity and with heat sources present within the body [5,8] is given by :

$$K\left(\frac{\partial^2 T}{\partial x^2}+\frac{\partial^2 T}{\partial y^2}+\frac{\partial^2 T}{\partial z^2}\right)+q^* = \rho C_p \frac{\partial T}{\partial t} \qquad 3.2$$

where q^*, ρ and C_p are the heat generation per unit volume, density and the specific heat capacity of the material respectively.

The terms on the left hand side of equation represent the heat gains by conduction and generation respectively and the right hand side represents the rate of change of temperature with time in the solid.

By eliminating the appropriate terms in equation (3.2), suitable relationships can be obtained defining a particular situation. For example steady-state heat conduction in 2-dimensions with heat generation is of the form:

$$K\left(\frac{\partial^2 T}{\partial x^2}+\frac{\partial^2 T}{\partial y^2}\right)+q^{\cdot}=0 \qquad 3.3$$

The heat conduction equation may be solved to determine the temperature distribution in a medium as a function of space and time. For this, a set of boundary conditions and an initial condition are needed. The latter specifies the temperature distribution in the system at time t=0 and the former specifies the heat flow or temperature situation at the boundaries.

3.2 Convection

Convection is another mode of heat transfer where heat is exchanged between a solid body and an adjacent fluid. Heat transfer between the fluid and the solid surface takes place because of a combination of conduction within the fluid and energy transport which is due to the fluid motion.

There are two types of convection namely free convection and forced convection. Free convection takes place as a consequence of density differences caused by temperature gradients between the fluid and the body and within the fluid itself. Forced convection occurs when the fluid motion is induced by an external force. The rate of heat flow at the surface is conventionally described by equation (3.4) [5,6] which is applicable to forced as well as free convection regimes:

$$q = h_c A(T_s - T_f) \qquad 3.4$$

where A is the solid surface area exposed to the fluids, h_c is the convective heat transfer coefficient and T_f and T_s are the fluid and surface temperatures respectively.

3.2.1 Boundary Layer Fundamentals

When a fluid flows over a body, the velocity and temperature distribution in the vicinity of the surface influence the heat transfer by convection. In order to simplify the analysis of convective heat transfer, the boundary layer concept has been introduced [8]. There are essentially two types of boundary layers which form over a surface namely velocity boundary layer and thermal boundary layer. A brief description of these two kinds of boundary layers is given in the following sections.

3.2.1.1 Velocity Boundary Layer

The concept of velocity boundary layer may be illustrated by considering the flow past a plane, stationary plate as shown in figure (3.1). At the leading edge of the plate the fluid has a velocity U_f which is parallel to the surface. As the fluid moves over the plate, the fluid viscosity causes the particles near the surface to slow down. The fluid particles in the immediate vicinity of the surface adhere to it due to the interaction frictional forces and their velocity reduces to zero [9]. Other fluid molecules trying to slide over these stationary particles are retarded because of the interaction between the faster and slower moving particles. This retardation of molecules is reduced to zero at a position far from the plate where the fluid velocity reaches that of the main fluid velocity U_f. At each location along the plate there is a distance $\delta_v(x)$ from the surface where the axial velocity component U approaches 99 percent of U_f. The velocity boundary layer is defined as the locus of the points where $U = 0.99\ U_f$ [8].

Furthermore, as the fluid proceeds along the plate, the shearing forces cause more and more of the fluid to be slowed down and hence the thickness of the boundary increases [9].

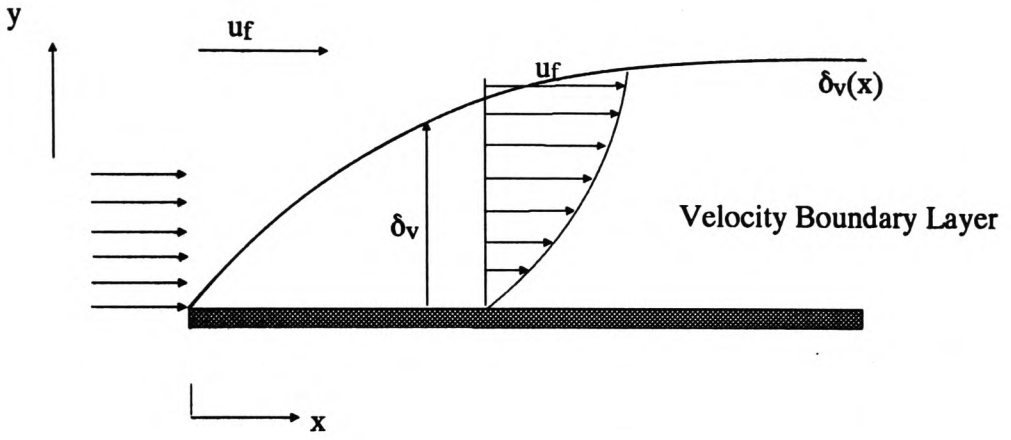

Figure (3.1) Velocity Boundary Layer on a Flat Plate

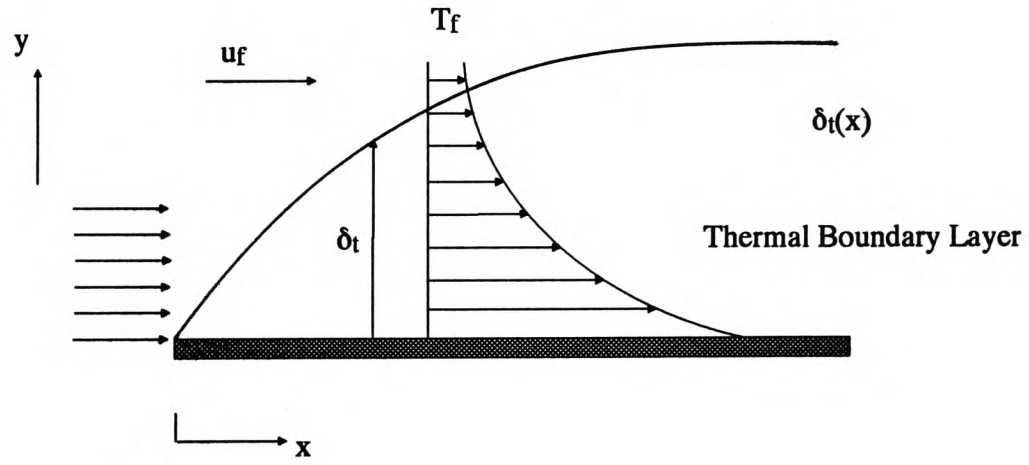

Figure (3.2) Thermal Boundary Layer on a Flat plate

3.2.1.2 Thermal Boundary Layer

Analogous to the fluid velocity behaviour, if a flat plate is maintained at a constant temperature T_s which is different from the main fluid temperature T_f, a thermal boundary layer develops [9]. The fluid temperature varies from the surface temperature to the free stream temperature within this boundary layer as shown in figure (3.2). The transition from the temperature in the boundary layer to the conditions in the main fluid flow takes place asymptotically [8] and hence the thickness of the thermal boundary layer $\delta_t(x)$ has been defined similar to the velocity boundary layer as the thickness where the temperature of the boundary reaches that of the main stream.

The thermal boundary layer contributes the main resistance to heat exchange between the surface and the fluid. In the immediate vicinity of the surface heat transfer takes place by way of conduction through the stationary particles in that layer relative to the boundary [9]. Further away from the surface, the energy transport is aided by the movement of the fluid. The temperature gradient is quite steep near the surface becoming less steep away from the wall and levelling out in the main flow.

3.2.1.3 Laminar and Turbulent Boundary Layers

The motion of the fluid in the boundary layer region is in two forms as illustrated in figure (3.3) for flow over a flat plate. The boundary layer starts at the edge of the plate as a laminar boundary layer in which the fluid moves in layers, each fluid particle following a smooth and continuous path. The molecules in these layers behave in an orderly manner and do not pass each other. In this type of motion the heat exchange is by molecular conduction within the fluid as well as at the interface between the surface and the fluid [10].

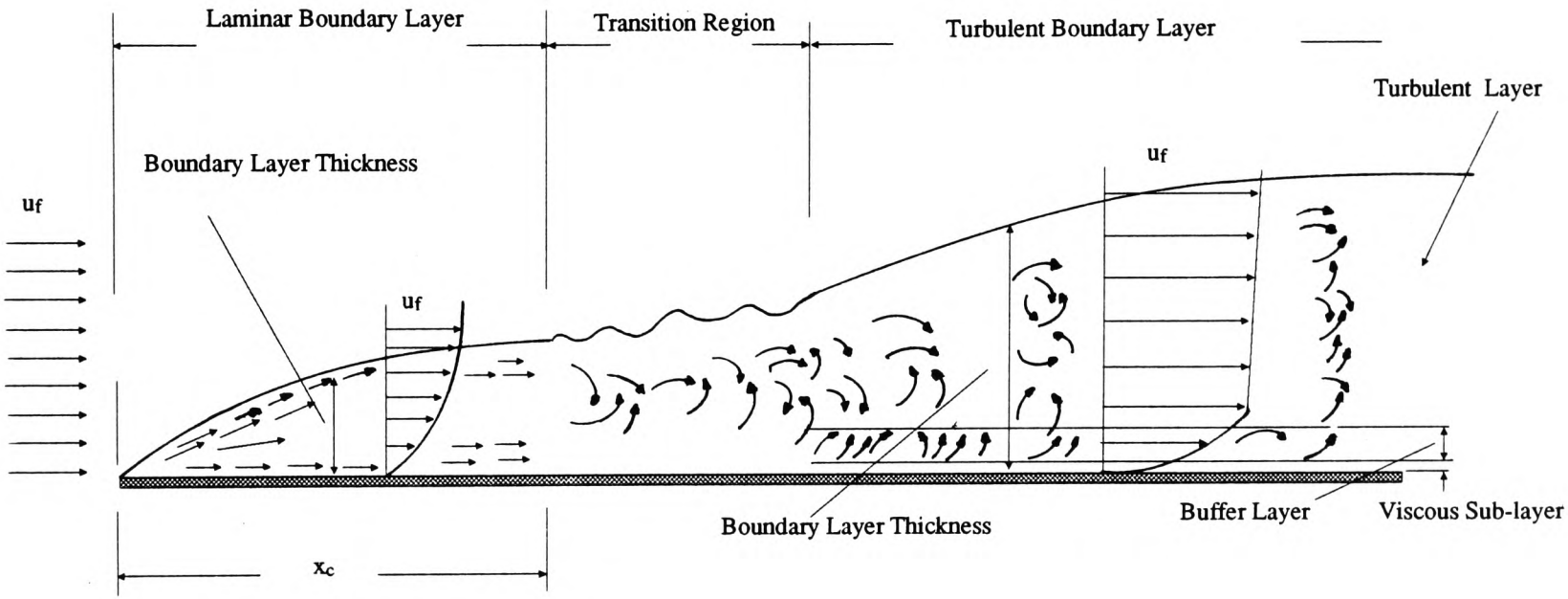

Figure (3.3) Boundary Layer Concept for Flow over a Flat Plate

After a transition distance, the flow becomes turbulent where irregular velocity fluctuations are superimposed on the fluid motion. The turbulent boundary layer consists of three sections. There exists a very thin layer in the immediate vicinity of the surface called the viscous sub-layer. Adjacent to this sub-layer there is a region called the buffer layer where there is a very small, fine-grained turbulence. Following the buffer layer the motion becomes completely turbulent.

The conduction mechanism in turbulent flows take place by eddies which convey lumps of fluid across the streamline. These lumps act as carriers of energy by mixing with other fluid particles.

3.2.2 Empirical Equations

The analysis of convective heat transfer is extremely complicated because of the interaction between the fluid motion and the temperature field. Therefore the determination of the temperature distribution in the fluid and hence the true local heat transfer coefficient involves the solution of the complete fluid mechanics problem in the region near the surface.

In general this would involve the simultaneous solution of equations for conservation of mass, momentum and energy and also the equations of state of the fluid [5].

Because of the complexity of the equations of motion and energy, it is extremely difficult to solve convective heat transfer problems by the above method except for very simple, idealised situations. Therefore, for most cases of practical interest convective heat transfer problems have been studied experimentally and the results are then presented in the form of empirical equations that involve some dimensionless groups [8].

Various methods may be employed to arrive at such dimensionless parameters. In one such method the dimensionless groups can be determined directly from the dimensionless form of the differential equations of motion and energy [5]. A simpler method however is the dimensional analysis approach which enables equations to be written relating the important physical quantities such as the fluid properties in dimensionless groups. Natural convection is only considered here since throughout this report convection will be assumed to be of this nature.

Many experiments have been carried out to establish the functional relationships between the dimensionless parameters for various geometric configurations and planforms [5,6,8]. It has been found for example that in natural convection relationships of the following form apply:

$$Nu = C(Gr.Pr)^n \qquad 3.5$$

where C and n are constants. Nu, Gr and Pr are Nusselt, Grashof and Prandtl numbers respectively given by:

$$Nu = h_c l/K \qquad 3.6$$

$$Gr = \Delta T \beta g l^3/\nu^2 \qquad 3.7$$

$$Pr = \mu C_p/K \qquad 3.8$$

where the parameters are as given in Table (3.1):

Table (3.1)	
β	The coefficient of cubical expansion
g	Acceleration due to gravity
l	Characteristic length for bodies with geometrically similar shapes
ν	The coefficient of kinematic viscosity
μ	Coefficient of dynamic viscosity
C_p	The specific heat capacity of the fluid
K	Fluid thermal conductivity
h_c	The heat transfer coefficient
ΔT	Temperature difference between the surface and the ambient fluid

The physical significance of Nusselt number may easily be arrived at by writing equation (3.6) in the following form [11]:

$$Nu = \frac{h_c l}{K} = \frac{h_c A \Delta T}{K A \Delta T / l} \qquad 3.9$$

which can be interpreted as the ratio of the heat transfer by convection to heat transfer by conduction across a fluid layer of thickness l.

Equation (3.8) describing Prandtl number can also be rearranged in the following form by introducing the fluid density ρ:

$$Pr = \frac{\mu C_p}{K} = \frac{\mu/\rho}{K/(\rho C_p)} \qquad 3.10$$

The Prandtl number is then seen to be the ratio of the kinematic viscosity to the thermal diffusivity. By incorporating these into equation (3.10) the following relationship can be obtained for the Prandtl number.

$$Pr = \frac{\nu}{\alpha} \qquad 3.11$$

Kinematic viscosity ν affects the velocity distribution and thermal diffusivity α influences the temperature profile in the fluid.

Finally, the Grashof number is another dimensionless group defined by equation (3.7). It has been shown experimentally that this parameter indicates the ratio of the buoyancy force to the viscous force in natural convection systems [9].

The values of C and n in equation (3.5) are normally quoted for a given range of Rayleigh number which is a product of Grashof and Prandtl numbers which determines whether the flow is laminar or turbulent [5,6,8,9]. Laminar flow corresponds to a flow where the fluid velocities are sufficiently small that the fluid moves in layers parallel to the surface without

mixing [9]. In contrast, fluid motion in turbulent flow is highly irregular and occurs at higher fluid velocities where, the mixing of the fluid layers is caused by an oscillatory motion of the particles normal to the main flow direction [12].

As an example the following relationships have been recommended [5] for uniformly heated horizontal plates with the heated side facing upwards:

$$Nu = 0.54(Gr.Pr)^{1/4} \qquad 2.6 \times 10^4 < Gr.Pr < 10^7$$

$$Nu = 0.15(Gr.Pr)^{1/3} \qquad 10^7 < Gr.Pr < 3 \times 10^{10}$$

The various properties are normally taken at a mean film temperature defined as $(T_s+T_f)/2$ where T_s and T_f are the surface and the ambient fluid temperatures.

Once the Nusselt number is determined for a certain situation, an average heat transfer coefficient can be calculated using a rearranged form of equation (3.6) which is $h_c=NuK/l$.

3.3 Radiation

The third mode of heat transfer is thermal radiation. This is a process in which bodies emit thermal energy by means of electromagnetic radiation extending from approximately 0.1 to 100 μm wavelength of the electromagnetic spectrum which includes part of the Ultra Violet and all of the visible and Infra-Red regions. This type of radiation is emitted in all possible directions and if it strikes another body, it may be partly absorbed, partly reflected and partly transmitted. The absorbed part of thermal radiation will appear as heat within the absorbing body.

In contrast to conduction and convection where the transfer of energy from one body to

another can occur only through a material medium, electromagnetic radiation may pass from one body to another without the need of a transport medium.

There is a maximum rate at which thermal radiant energy can be emitted and consequently absorbed by a body at a certain temperature. The surfaces which interchange radiant energy at such rates are called *black bodies* and it can be shown [6] that the radiation emitted by such surfaces at temperature T is given by the Stefan-Boltzmann law:

$$E_b = \sigma T^4 \qquad 3.12$$

where σ is the Stefan-Boltzmann constant ($5.67\times10^{-8}\ W/m^2K^4$), T is the absolute temperature in Kelvins and E_b is the *black-body* emissive power. In practice there are no surfaces that behave as a *black-body* and the radiation flux emitted by a *grey body* is always less than a *black-body* and is given by:

$$q = \varepsilon\sigma T^4 \qquad 3.13$$

where ε is called the emissivity which relates the radiation of the grey surfaces to that of a black surface.

The fourth power law derived by Stefan-Boltzmann can be used to determine the total amount of radiation leaving a surface. This concept is however inadequate when dealing with radiative transfer between bodies where only a portion of the radiation leaving one surface in a particular direction is intercepted by another. It is therefore necessary to introduce a quantity called the View or Shape factor which gives the fraction of the total radiation emitted by a surface which is received by another. Before an attempt is made to derive a general relationship for the View Factor, basic definitions will be given for Solid

Angle and Intensity of Radiation.

Solid Angle: The physical significance of solid angle may be illustrated by referring to figure (3.4) where x is the direction of propagation and dA is a small area normal to x at a distance r from a point source s. The solid angle ω in units of steradians is defined as [9]:

$$\omega = \frac{dA}{r^2} \qquad 3.14$$

using the above definition, for a complete hemispherical shell the solid angle may be calculated as $2\pi r^2/r^2$ which is equal to 2π steradians.

Intensity of Radiation: The radiation emitted by a surface propagates in all possible directions and if a small flat area is considered the entire radiation passes through a hemispherical surface surrounding the emitting area [13] as shown in figure (3.5). The Intensity of Radiation, I, describes the directional distribution of the radiant energy leaving a surface or incident upon it. It is defined as the rate of energy emission per unit time of the emitting surface per unit solid angle subtended at the surface. The variation in the intensity of radiation for a *black-body* is expressed by Lambert's Cosine Law which states that [13]:

$$I_\theta = I_N \cos\theta \qquad 3.15$$

By definition of radiation intensity, the energy dq_N emitted by dA through a solid angle $d\omega_N$ normal to dA is hence given by:

$$dq_N = I_N . d\omega_N \qquad 3.16$$

and radiation emitted in an angle θ through a solid angle $d\omega_\theta$:

$$dq_\theta = I_\theta . d\omega_\theta \qquad 3.17$$

which according to Lambert's Law may be written as :

$$dq_\theta = I_N . \cos\theta d\omega_\theta \qquad 3.18$$

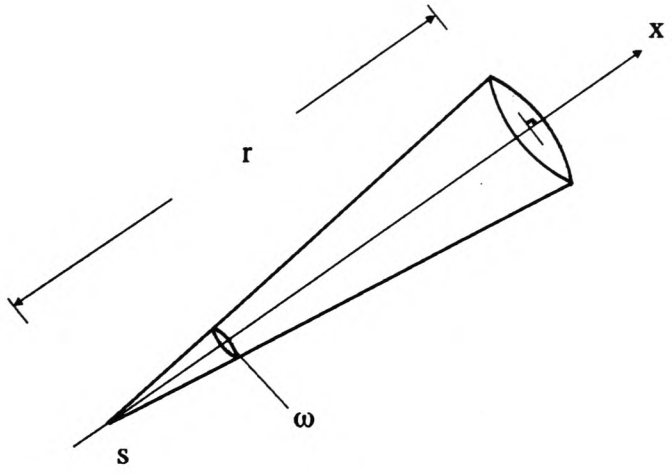

Figure (3.4) Solid Angle

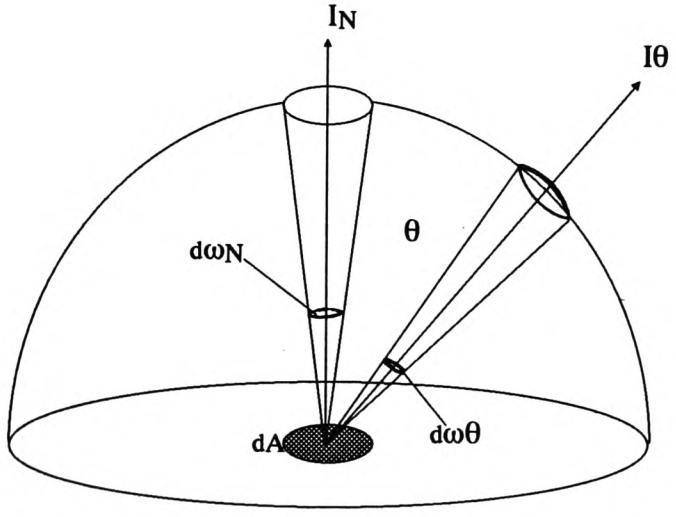

Figure (3.5) Emission from a Differential Element dA into a Hemispherical Shell.

It has been shown [13] that the radiation intensity in the normal direction, I_N may be expressed in terms of the absolute temperature of the emitting surface in the following form:

$$I_N = \frac{\varepsilon\sigma T^4}{\pi} \qquad 3.19$$

3.3.1 View Factor

This is a term which is used extensively in calculation of the radiant heat transfer between surfaces. It is defined as the fraction of the total diffuse radiation emitted from a surface which is intercepted directly by another.

In order to derive a general expression for the view factor, the arbitrary configuration illustrated in figure (3.6) is considered which shows two surfaces A_1 and A_2 at temperatures T_1 and T_2 respectively. The view factor $F_{1\rightarrow 2}$ can be derived by writing the appropriate equations defining the energy exchange between two differential area elements dA_1 and dA_2 and integrating over both surfaces. Subscripts ($1 \rightarrow 2$) represent a view factor for the radiation emitted by surface 1 which is received by surface 2. dA_1 and dA_2 are connected by a line of length x which makes angles of θ_1 and θ_2 with I_{N_1} and I_{N_2} respectively which are the normals to the elemental areas as shown in figure (3.6).

Radiation leaving dA_1 and arriving dA_2 is a product of (a) the radiation intensity, I_1, from each point on dA_1 in the direction of x, (b) the area dA_1 and (c) the solid angle $d\omega_{1\text{-}2}$ subtended by dA_2 when viewed from dA_1. Thus for the whole area dA_1:

$$dq_{1\rightarrow 2} = I_1 . d\omega_{1-2} . dA_1 \qquad 3.20$$

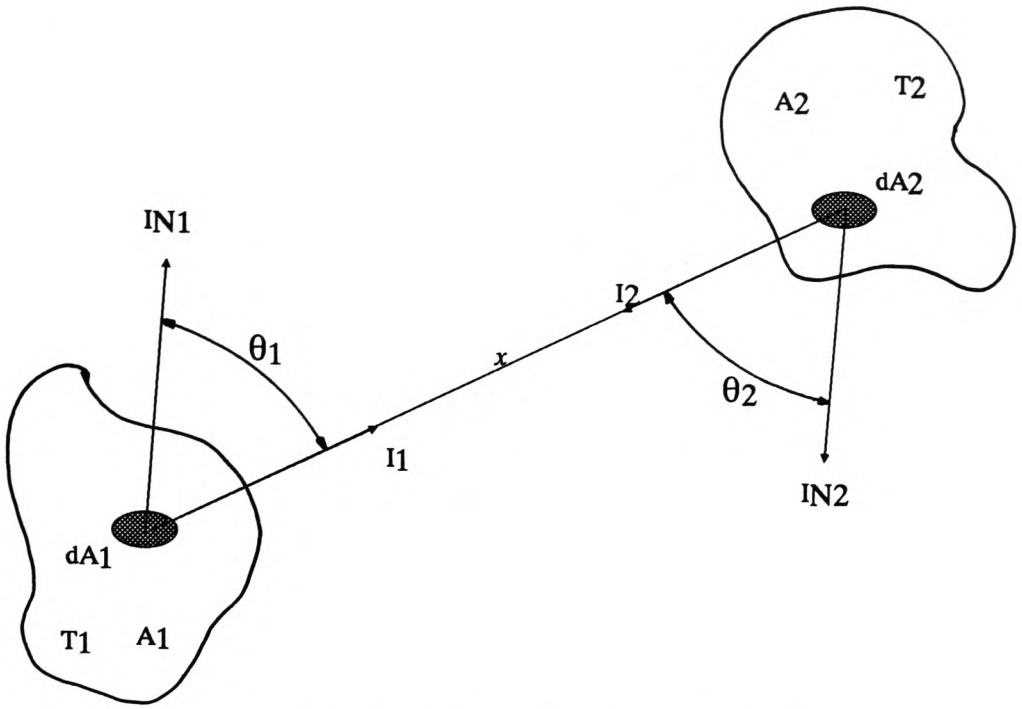

Figure (3.6) Notations for Geometrical View Factor

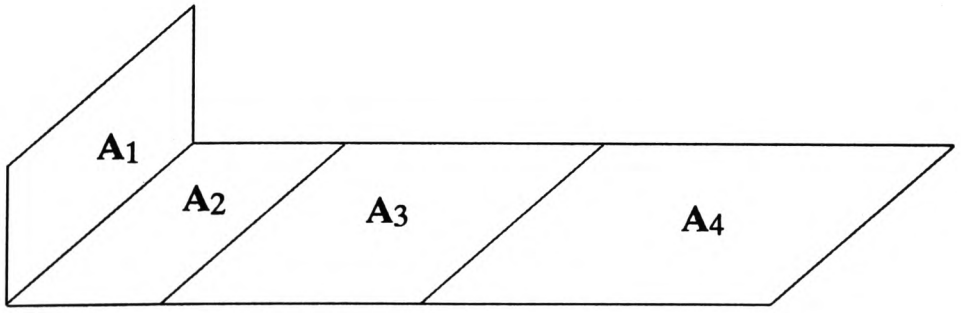

Figure (3.7) An Example of View Factor Evaluation for Non-Adjacent Surfaces

By definition of solid angle, $d\omega_{1\text{-}2}$ is equal to the projected area of the receiving element, dA_2, in a direction normal to the direction of incidence divided by the square of the distance x. I_1 is also equal to $I_{N1}cos\theta$ according to Lambert's Law. Therefore $dq_{1\to 2}$ becomes :

$$dq_{1\to 2} = I_{N_1}\cos\theta_1 . \frac{dA_2\cos\theta_2}{x^2} . dA_1 \qquad 3.21$$

which may be written as :

$$dq_{1\to 2} = I_{N_1} . \frac{\cos\theta_1\cos\theta_2}{x^2} . dA_1 dA_2 \qquad 3.22$$

in a similar manner :

$$dq_{2\to 1} = I_{N_2} . \frac{\cos\theta_1\cos\theta_2}{x^2} . dA_1 dA_2 \qquad 3.23$$

by substituting for I_N from equation (3.19) for a *black-body* with an emissivity (ε) of one and integrating over the two areas the total energy radiated from A_1 reaching A_2 is:

$$q_{1\to 2} = \int_{A_1}\int_{A_2} \frac{\cos\theta_1\cos\theta_2 dA_1 dA_2}{\pi x^2} . \sigma T_1^4 \qquad 3.24$$

The total energy emitted by A_1 is equal to $\sigma A_1 T_1^4$. The View Factor is by definition the fraction of the total energy emitted by A_1 which reaches A_2 and therefore:

$$F_{1\to 2} = \frac{q_{1\to 2}}{\sigma A_1 T_1^4} \qquad 3.25$$

which by substituting for $q_{1\to 2}$ becomes :

$$F_{1\to 2} = \frac{1}{A_1}\int_{A_1}\int_{A_2} \frac{\cos\theta_1\cos\theta_2 dA_1 dA_2}{\pi x^2} \qquad 3.26$$

similarly :

$$F_{2\to 1} = \frac{1}{A_2}\int_{A_1}\int_{A_2} \frac{\cos\theta_1\cos\theta_2 dA_1 dA_2}{\pi x^2} \qquad 3.27$$

Equations (3.26) and (3.27) may be used to evaluate the shape factor for various surfaces. It is a very tedious mathematical process involving the double integrals taken over the surfaces. Even for the simplest of geometries the calculations are quite laborious. Other workers have carried out such evaluations for most of the significant configurations which are readily available in various publications. These are normally either in the form of simple algebraic expressions [9] or in graphic form [9] where with a knowledge of a few dimensions the view factors can be obtained. More complex situations may generally be reduced to simpler cases and evaluated using view factor relations which will be given in the following section.

3.3.1.1 Properties of View Factors

There exist some very useful relationships between the view factors of radiating surfaces some of which will be given here.

Perhaps the most useful and important property of the shape factors is derived from equations (3.26) and (3.27) which suggest that :

$$A_1F_{1\to 2} = A_2F_{2\to 1} \qquad 3.28$$

which is called the reciprocity relationship.

If radiation from a surface i to a surface j is considered where surface j is divided into n sub-areas($A_{j_1}, A_{j_2}, \ldots, A_{j_n}$) then the radiation reaching the whole of j is the sum of the radiation received by its individual parts [9]. Thus:

$$F_{i\to j} = \sum_{1}^{n} F_{i\to j_n} \qquad 3.29$$

However if the radiating surface is divided into n smaller sections, each radiating to a surface j, then the shape factor for the whole of surface i to j is given by a summation of all the individual FA products [9] as :

$$A_i F_{i \to j} = \sum_{1}^{n} A_{i_n} F_{i_n \to j} \qquad 3.30$$

Consider the configuration shown in figure (3.7) which illustrates two perpendicular rectangles with a common edge one of which is divided into three sections. The shape factors $F_{1 \to 4}$ and $F_{4 \to 1}$ for radiation exchange between surfaces A_1 and A_4 is required.

The shape factors for perpendicular surfaces sharing a common edge are readily available in various references [9]. Figures may therefore be obtained for shape factors $F_{1 \to 2}$, $F_{1 \to (2+3)}$, $F_{1 \to (2+3+4)}$, etc.

According to relation (3.29), the total shape factor from surface A_1 to the combined surfaces of A_2, A_3 and A_4 is the sum of the individual shape factors. Thus:

$$F_{1 \to (2+3+4)} = F_{1 \to 2} + F_{1 \to 3} + F_{1 \to 4} \qquad 3.31$$

$$F_{1 \to (2+3)} = F_{1 \to 2} + F_{1 \to 3} \qquad 3.32$$

by combining equations (3.31) and (3.32) and rearranging for $F_{1 \to 4}$ we get the following relationship:

$$F_{1 \to 4} = F_{1 \to (2+3+4)} - F_{1 \to (2+3)} \qquad 3.33$$

where the two terms on the right hand side of the equation are known.

To derive a relationship for $F_{4 \to 1}$ use is made of the reciprocity relation given in equation (3.28) as follows:

$$A_4 F_{4 \to 1} = A_1 F_{1 \to 4} \qquad 3.34$$

by substituting for $F_{1\to 4}$ from equation (3.33) and rearranging, the shape factor $F_{4\to 1}$ is found to be:

$$F_{4\to 1} = \frac{A_1}{A_4}[F_{1\to(2+3+4)} - F_{1\to(2+3)}] \qquad 3.35$$

The net radiation exchange between two *black* surfaces may be determined as follows:

$$q_{1\to 2} = F_{1\to 2}\sigma A_1 T_1^4 \qquad 3.36$$

$$q_{2\to 1} = F_{2\to 1}\sigma A_2 T_2^4 \qquad 3.37$$

However according to reciprocity relation (3.28) :

$$A_1 F_{1\to 2} = A_2 F_{2\to 1} \qquad 3.38$$

and therefore $q_{2\to 1}$ becomes:

$$q_{2\to 1} = A_1 F_{1\to 2}\sigma T_2^4 \qquad 3.39$$

Thus the net exchange is given by:

$$q_{net} = F_{1\to 2}\sigma A_1(T_1^4 - T_2^4) \qquad 3.40$$

For a *black-body* at temperature T_1, totally enclosed in another much larger surface maintained at T_2, $F_{1\to 2} = F_{2\to 1} = 1$ [13] and therefore the net radiant energy exchanged [14] is given by:

$$q = \sigma A(T_1^4 - T_2^4) \qquad 3.41$$

where A is the surface area of the enclosed body.

For two grey bodies with emissivities of ε this becomes:

$$q = \varepsilon\sigma A(T_1^4 - T_2^4) \qquad 3.42$$

Similar to convection, a radiation heat-transfer coefficient h_r may be defined [5] as :

$$q = h_r A(T_1 - T_2) \qquad 3.43$$

where T_1 and T_2 are the temperatures of the two bodies exchanging heat by radiation. h_r may be determined for different surfaces with varying shapes and geometries [5]. By comparing equations (3.42) and (3.43) the following expression is obtained for the heat transfer coefficient as :

$$h_r = \varepsilon\sigma(T_1^2 + T_2^2)(T_1 + T_2) \qquad 3.44$$

3.4 Conclusions

In this chapter the general principles of heat transfer phenomena have been presented. It was chosen to deal with each of the three modes separately although in most practical problems at least two of the modes occur simultaneously.

In each section the appropriate equations describing the particular mode were outlined with particular reference to the equations which will later be used when dealing with various heat flow situations.

4 THERMAL SYSTEM MODELLING

4.1 Introduction

The thermal performance of a given system can be written as an electrical analogy by a suitable change of variables. The simple Ohm's law equation can be compared to equations (3.1, 3.4 and 3.44) for conductive, convective and radiative heat transfer respectively. This gives equivalent electrical resistances of:

$$R_{conduction} = \frac{\Delta x}{K \Delta y \Delta z} \qquad 4.1$$

$$R_{convection} = \frac{1}{h_c A} \qquad 4.2$$

$$R_{radiation} = \frac{1}{h_r A} \qquad 4.3$$

for conductive, convective and radiative processes respectively. The conductive thermal resistance $R_{conduction}$ is given for a cuboidal portion of a material of thermal conductivity K and dimensions Δx, Δy and Δz as shown in figure (4.1). h_c and h_r are the convective and radiative heat transfer coefficients respectively and A is the area.

It can also be seen by comparing the equation for the current in a charging capacitor ($i = C\, dV/dt$) with the equation for the rate of change of energy in a volume element ΔV ($q = \rho C_p \Delta V\, dT/dt$) that an equivalent electrical capacitance can be used to represent the thermal capacitance of a cell of volume ΔV of a body given by:

Figure (4.1) The Electrical Equivalent Model for a Cell in Three-dimensional Conduction

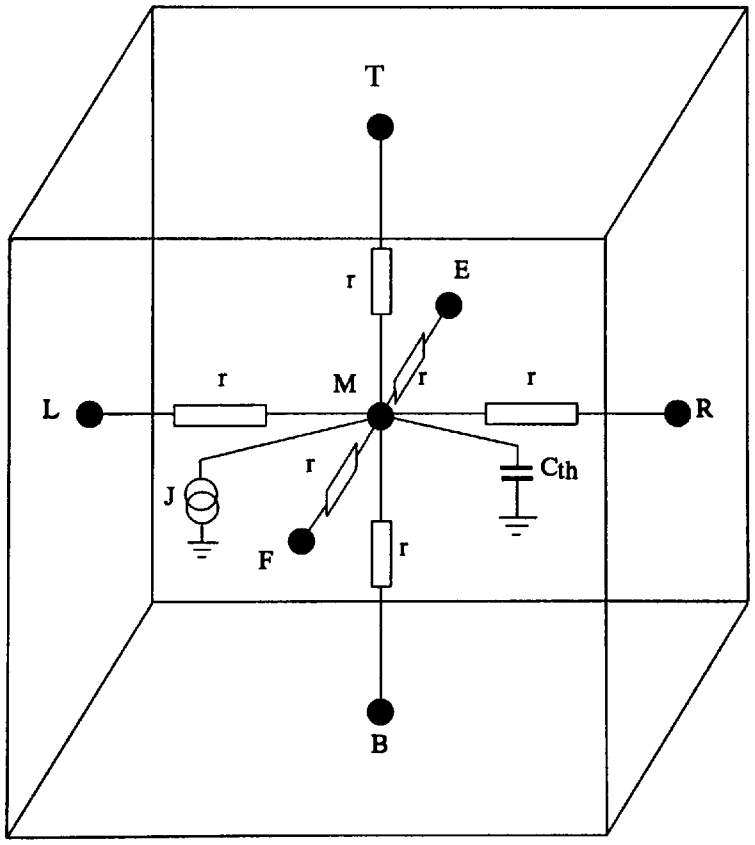

$r = 1/2\ R_{th}$

$$C_{thermal} = \rho C_p \Delta V = \rho C_p \Delta x \Delta y \Delta z \qquad 4.4$$

where ΔV is represented by $\Delta x \Delta y \Delta z$.

Since the flow of heat through a thermal resistance is analogous to flow of current through an electrical resistance, any form of heat flow into or out of a system can be modelled as current sources. Similarly there is an analogy between temperature in a thermal system and electrical potential. Fixed temperatures at a boundary can therefore be modelled as voltage sources of the same value.

4.2 Conduction

To model the heat flow by conduction in a physical system, such as an integrated circuit, the structure is divided into a number of cells each of volume ΔV and dimensions Δx, Δy and Δz. The thermal resistance in the x direction and capacitance for each of these cells as shown in figure (4.1) are defined by:

$$R_{th_x} = \frac{\Delta x}{K \Delta y \Delta z} \qquad 4.5$$

$$C_{th} = \rho C_p \Delta V = \rho C_p \Delta x \Delta y \Delta z \qquad 4.6$$

Similar expressions can also be written for R_{th} in the y and z directions. However, for simplicity, throughout this document the cells will be assumed to be of equal dimensions unless otherwise stated. This consequently means that the cells have equal resistances in all directions. For conduction in one-dimension, a value of unity is taken for Δy and Δz and for Δz in two dimensions [1].

Simple electrical equivalent models for thermal characteristics can be written using the analogous thermal resistance and capacitance quantities.

The ASTEC3 input language is based on a conventional circuit diagram with the positions of each element defined by the nodes at its connections. Figures (4.1-4.3) show the electrical configurations used for thermal cells in 3, 1 and 2 dimensional systems respectively. In each model the thermal resistance in each direction is divided by two and resistors of such values are connected from the node at the centre of the cell to nodes at the mid-point of each side. The thermal capacitance of value C_{th} and the optional current source representing the heat generation in the cell are connected between the centre-node and ground.

4.3 Convection

Convection at the boundaries, assuming that the value of convective heat transfer coefficient h_c is known, can be modelled using resistors of values $1/h_cA$ connected to voltage sources (ambient) where A is the convection surface-area ($A=\Delta y.\Delta z$). In 1-D this reduces to $1/h_c$ as Δy and Δz are taken as unity and in 2-D to $1/h_c\Delta y$.

4.4 Radiation

Radiation emitted from a plane surface may also be modelled in the same way as convection by using thermal resistances of values $1/h_rA$. The radiative heat transfer coefficient h_r defined in section (3.3) is used here instead of h_c. In situations where both convection and radiation are present, and when the temperature difference (T_1-T_2) driving the heat exchange is the same for both phenomena , a combined value of h may be used given by ($h_c + h_r$).

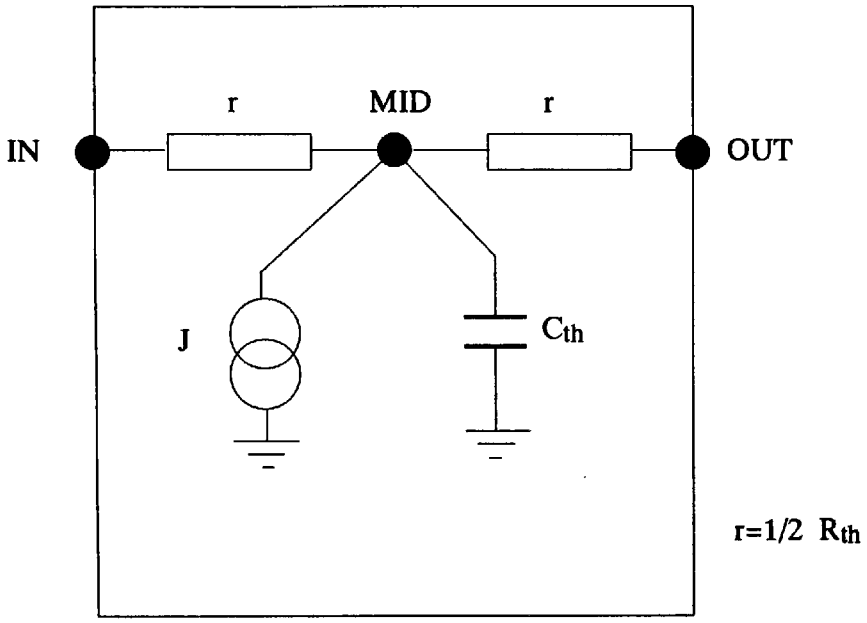

Figure (4.2) The Electrical Equivalent Model for a Cell in One-Dimensional Conduction

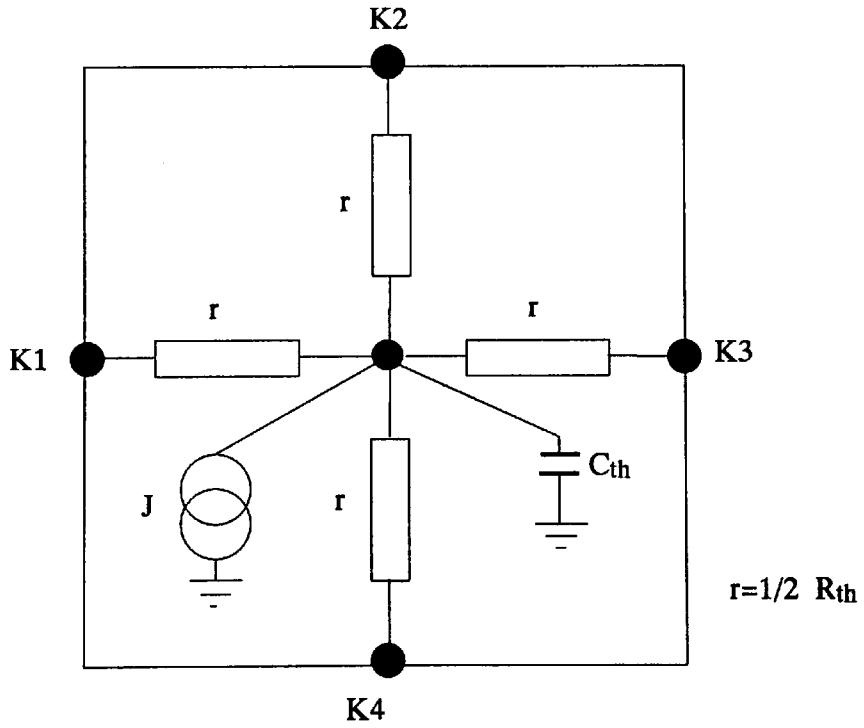

Figure (4.3) The Electrical Equivalent Model for a Cell in Two-Dimensional Conduction

4.5 ASTEC3 Code-Generation Programs

4.5.1 Introduction

For the thermal version of the ASTEC3 modelling package to be of any commercial or practical interest, it is important for it to be made user-friendly and automated as much as possible.

The most cumbersome task in thermal simulations is the actual writing of the circuit description in the ASTEC3 syntax, especially when dealing with a large number of thermal cells. It was therefore essential to develop the necessary software which would automatically generate the net-list required for a given thermal structure.

Programs have been developed which generate the electrical equivalent circuit description for uniform structures. Two programs will be described here the first of which is for 2-dimensional heat conduction and the second for 3-dimensional heat conducting structures.

It should be mentioned that the user must write a single thermal cell model described in section (4.2) as a *sub-model* and store it in his personalised library. This sub-model can then be called up within the circuit description file. The sub-models for the 2 and 3 dimensional conduction are as follows :

```
!MODEL 2D(L-R-T-B-C-G):PR1;PR2;PC;PJ;
RL(L-C)PR1;
RR(R-C)PR1;
RT(T-C)PR2;
RB(B-C)PR2;
CC(C-G)PC;
JC(G-C)PJ;
```

```
!MODEL 3D(L-R-T-B-F-E-C-GND):PR1;PR2;PR3;PC;PJ;
RL(L-C)PR1;
RR(R-C)PR1;
RT(T-C)PR2;
RB(B-C)PR2;
RF(F-C)PR3;
RE(E-C)PR3;
CC(C-GND)PC;
JC(GND-C)PJ;
```

where PR1, PR2 and PR3 are the thermal resistance values in the *x*, *y* and *z* directions respectively. PC and PJ are the thermal capacitance and generation per cell respectively.

The user should also decide on the size of the thermal cell required and store the so-called !TYPE of the !MODEL in his library. This incorporates the values of the thermal parameters for the particular material of that size. The following shows the format of such !TYPE for 2 and 3 dimensional sub-models:

```
!TYPE 2D.type : PR1=value;PR2=value;PC=value;PJ=value;
!TYPE 3D.type : PR1=value;PR2=value;PR3=value;PC=value;PJ=value;
```

The !TYPE can then be called up in the description section as many times as required in the following formats:

```
Mn(Ln-Rn-Tn-Bn-Cn-G)2D.type;
Mn(Ln-Rn-Tn-Bn-Fn-En-Cn-G)3D.type;
```

where n is the cell number and 2D.type and 3D.type are the !TYPE of the sub-model with the parameters for a cell of a particular size and material.

4.5.2 Program for 2-D Conduction

This program generates the ASTEC3 file for structures with conduction in 2-dimensions. The program is given in appendix (2) section (a). A run of the program for generating the ASTEC3 file for a 2-dimensional conducting structure of (5×3) cells, figure (4.4), is given in appendix (2) sections (b). The various sections of the program are as described below :

i) The program enquires the following information to generate the $DESC stage of the output file:

a) Name of the ASTEC3 2-D sub-model as stored in user's personal library.
b) The !TYPE of the sub-model which includes the thermal parameters for the particular material of that size.
c) The number of cells in the x and y direction.

Using the values given by the user following 'c' above the program generates the 2-Dimensional mesh. It displays the output on the screen and stores it in the output file.

ii) The program then automatically generates the !OUTPUT section of the file where all the required output results are declared for simulation. The results here are all the nodal temperatures needed for the contour plotting programs in the required order.

iii) The simulation type (Transient or Steady-state) is enquired and the necessary syntax for $TRAN or $DCAN is generated. If transient, the length of the simulation is also enquired.

Figure (4.4) The Arrangement Used for ASTEC3 Code-Generation of a Two-Dimensional Structure

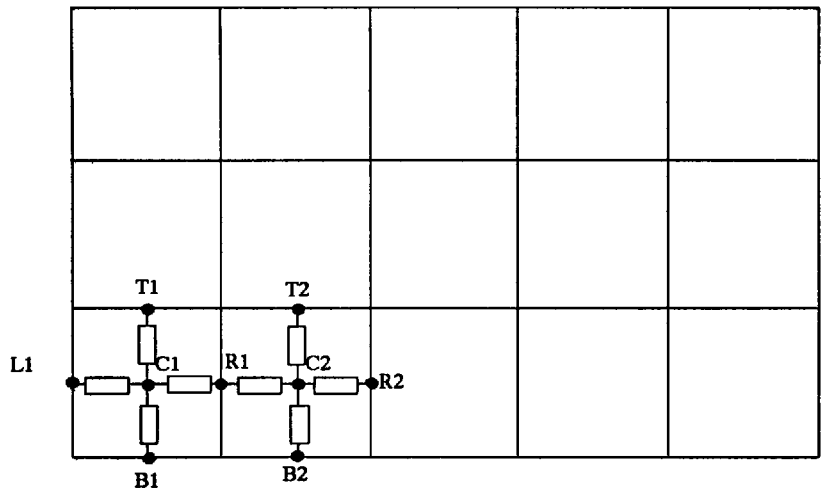

iv) The $EDIT section of the file is generated. The nodal temperatures are automatically written in the order needed for the plotting program given in section (2.3) which makes use of all the nodes in a model. The software also divides the output results into blocks of fifteen as required by ASTEC3.

4.5.3 Program for 3-Dimensional Conduction

This program generates the circuit description file for a 3-dimensional heat conducting structure. It should be noted that the program generates the thermal mesh assuming all the conduction cells are of the same size and thermal parameters are the same. In any real physical problem however, the structure is normally composed of various materials and hence different parameters. It is also appreciated that heat is probably only generated in certain cells. In these cases then the user should manually (at least at the present time) create a file containing the *odd* cell '!type's and the cell numbers. The format of this file is given in appendix (2) section (d).

A further file should also be created which includes the values of thermal resistances corresponding to the heat transfer coefficients of convection and radiation. The format of this file is also given in section (d) of appendix (2). The values, separated by commas are written in an order of nodes for a face, starting from the bottom left hand corner of the face to the right until the row is complete and the same for the next row until all the nodes on that face are included.

The program is given in appendix (2) section (c). A particular set of questions and answers for generating the ASTEC3 code for a 3-dimensional structure consisting of 7, 2 and 3 cells in the x, y and z directions and the subsequent output file are given in section (e).

Various stages of the program are as follows:

i) The program enquires the following information to generate the $DESC stage of the output file:

a) Name of the ASTEC3 3-D sub-model as stored in user's personal library.

b) The !TYPE of the sub-model which includes the thermal parameters for the particular material of that size.

c) The number of cells in the x and y and z direction.

d) The name of the file containing the number of those cells with different !TYPE extension.

e) The name of the file including the combined value for the heat transfer coefficients of convection and radiation.

ii) Using the information given by the user the program generates the necessary codes for the $DESC section of the file as shown in the output example in appendix (3) section (e). Note that in the mesh, the !type name has been changed to the corresponding one in the given file. A series of resistors is also created with the values supplied in the file for the heat transfer coefficients.

The remaining stages of the program are very similar to the program for 2-Dimensional conduction except in (iv) the nodes are in an order for the contour plotting program described in section (2.3). Here the nodes are chosen to be for the top face of the structure shown in figure (4.5) which can be easily extended to include any surface.

Figure (4.5) The Structure Used for Three-Dimensional ASTEC3 Code-Generation

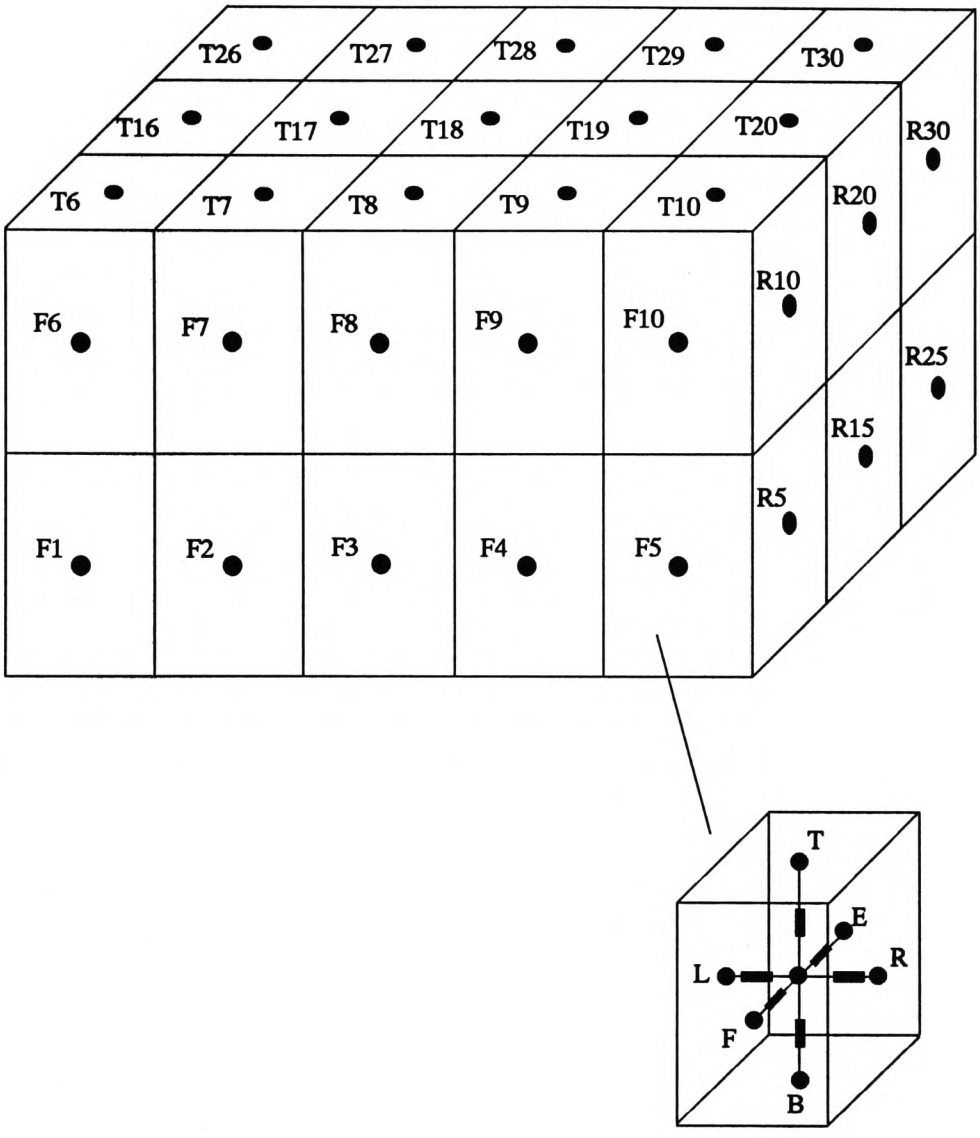

4.6 Conclusions

In this chapter, procedures have been described for modelling the three heat transfer mechanisms. An electrical analogy has been employed which allows the simulation of a thermal structure using the electronic analysis package ASTEC3.

Programs written to semi-automatically generate the electrical equivalent circuit description of a problem in ASTEC3 syntax have been described. Two programs have been presented the first of which is for code-generation of two-dimensional conduction models and second one for three-dimensional heat flow problems.

5 VALIDATION OF ASTEC3 MODELLING

5.1 Introduction

The principles described in chapter (4) must be verified in the context of ASTEC3 modelling. This is achieved here by applying them to a number of heat flow situations whose solutions may be determined directly from theory or by a separate, more conventional, technique. This approach is carried out here for one- and two-dimensional heat conducting arrangements.

In one-dimension the temperature distribution in a uniform slab is simulated and compared with the finite-difference and analytical solutions of the same structure. Two cases have been considered: conduction only and conduction with convection at the boundaries.

To verify the simulation performance in two-dimensional heat conduction, the flow in a rectangular plate is considered when subjected to a non-uniform external input. The simulated results are compared with the analytical solution of the problem.

A method will be described which makes it possible to model the more important sections of a thermal structure in finer detail. Subsequent measurements will demonstrate the reduction of computation-time when this method is employed.

A further investigation has also been carried out to establish a relationship between the number of conduction cells and the simulation time. This will allow the prediction of the computation time needed for a particular thermal structure.

5.2 One-dimension

5.2.1 Conduction only

As an example consider a slab of width 50 *mm* with uniform thermal conductivity of 17.3 W/mK and thermal diffusivity of 4.5 $\mu m^2/s$ where heat is generated at a constant rate of $2.06 MW/m^3$. The temperature distribution in the slab is required when constant temperature sources at 60 °C and 20 °C are applied to its boundary surfaces.

a ASTEC3 Solution

To achieve an ASTEC3 solution of this problem the slab may be divided into 5 segments of 10 *mm* length each. R_{th} and C_{th} are calculated for a one-dimensional cell using equations (4.5) and (4.6) and five such cells are connected in series as shown in figure (5.1).

The simulation is carried out starting from an initial linear distribution and the nodal-temperatures are recorded until a steady-state condition is reached. The ASTEC3 results are shown graphically in figure (5.2) which gives the variation of the temperature distribution in the slab with time.

b Finite difference solution

To validate the ASTEC3 simulation results a finite-difference technique was also used to determine the temperatures of the four interior nodes from an initial linear steady-state condition to a final steady state in steps of Δt. This is a method by which the partial differential equation of heat conduction is replaced by a system of linear algebraic

Figure (5.1) The Electrical Configuration used for the One-dimensional Conduction only Problem

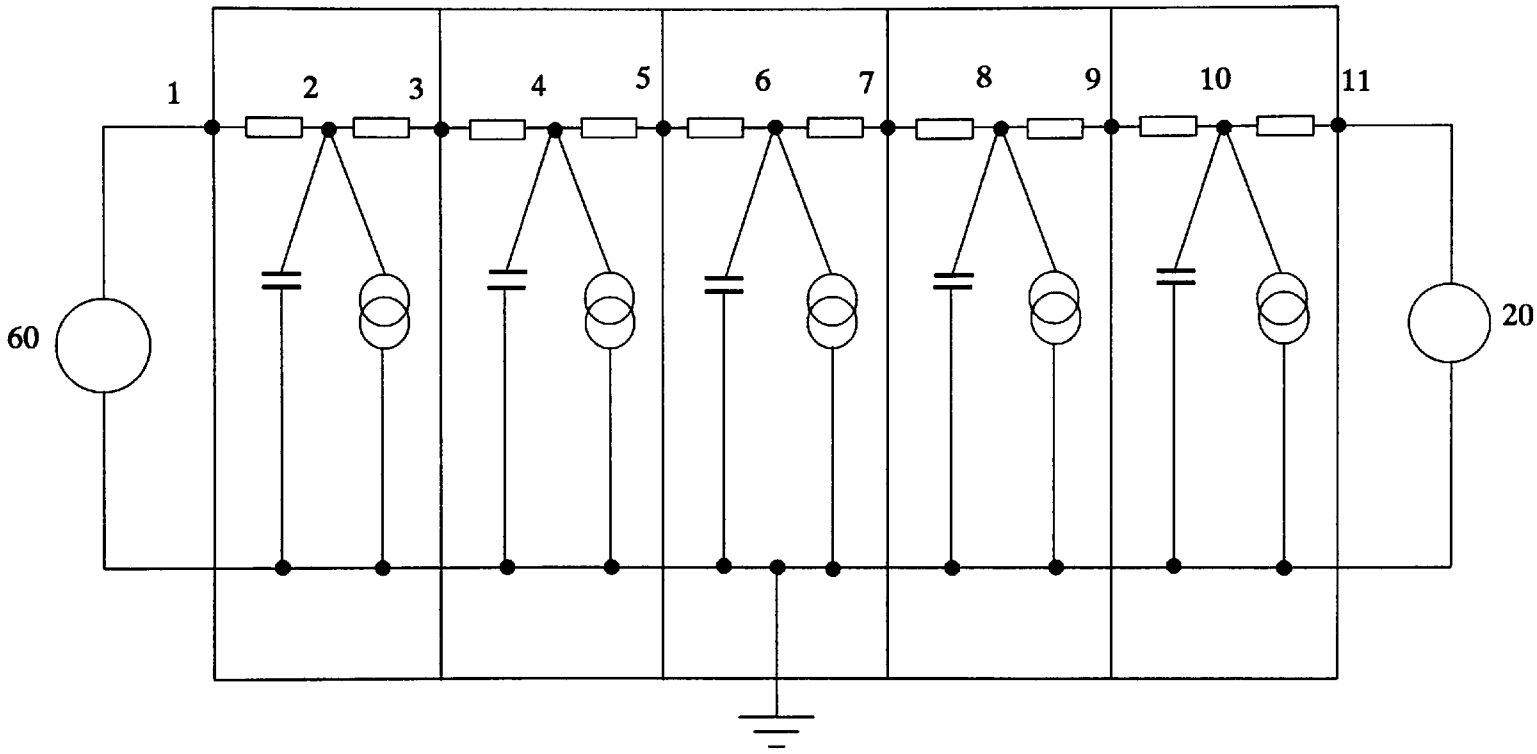

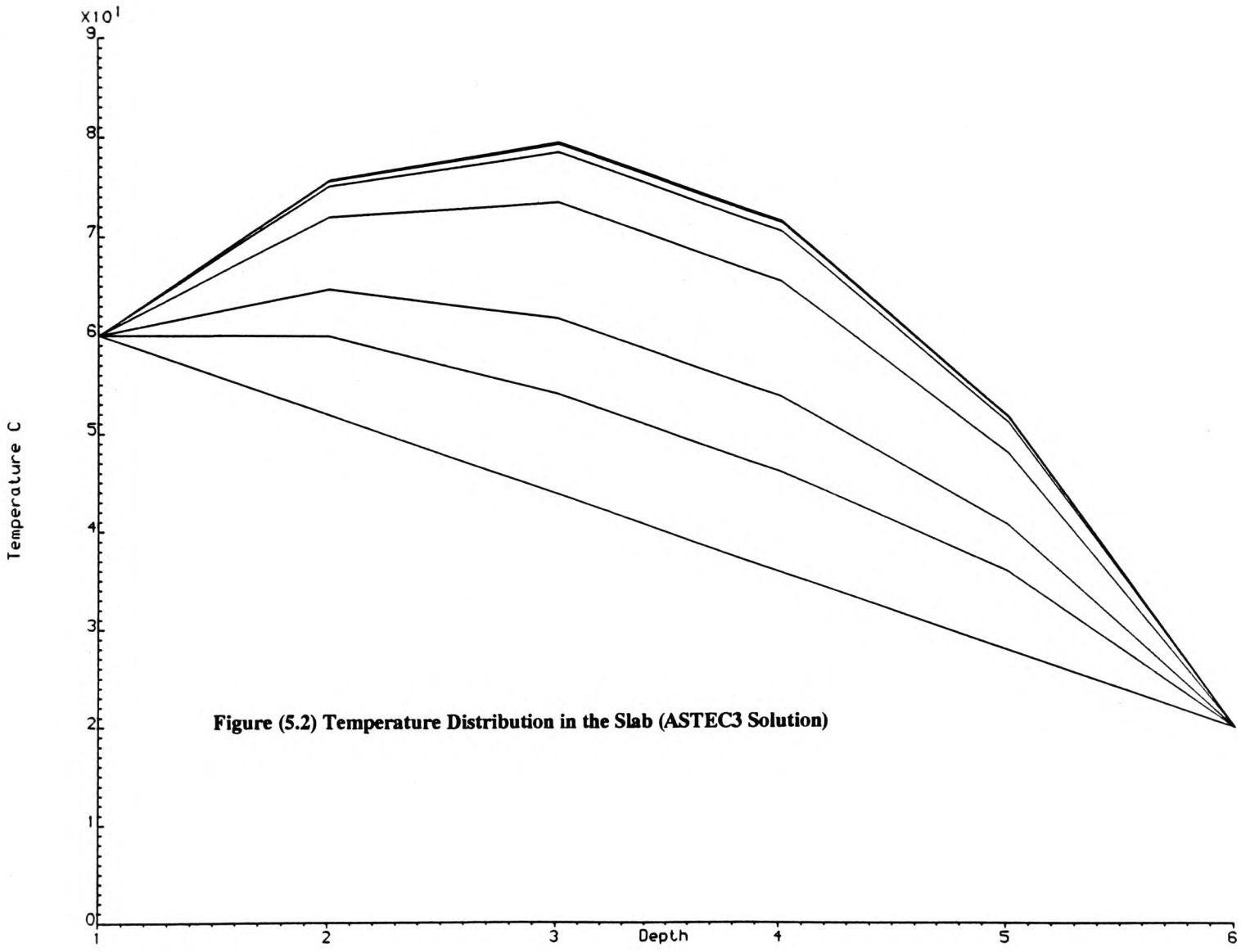

Figure (5.2) Temperature Distribution in the Slab (ASTEC3 Solution)

equations [1]. Results of these calculations are shown in figure (5.3) and a comparison of temperatures of identical nodes at equivalent times for both ASTEC3 and the finite-difference technique is given in Table (5.1).

c Analytical Solution

For the simple case studied above it is possible to obtain a more accurate assessment of the errors within ASTEC3 by comparing the results obtained with the analytical solution given in appendix (3). The steady-state solution to the one-dimensional conduction equation is in the form:

$$T = -1/2(q^{*}/K)x^{2} + Bx + C \qquad 5.1$$

where B and C are constants with values of 2176.88 and 60 respectively and x is the distance in meters from the left-hand edge of the slab. The values of constants were determined using the specified boundary conditions. Using these values and the values for q^{*} (2.06 MW/m^{3}) and K (17.3 W/mK) the temperatures are calculated at the points of interest which are also given in Table (5.1).

Table (5.1) Results of the 1-D Conduction only Problem

Node	Initial Temperature °C	Final Temperature °C		
		ASTEC3	Finite Difference	Analytical
1	60.0	60.0	60.0	60.0
3	52.0	75.815031	75.8150177	75.8150289
5	44.0	79.722541	79.7225266	79.7225433
7	36.0	71.722541	71.7225266	71.7225433
9	28.0	51.815027	51.8150215	51.8150289
11	20.0	20.0	20.0	20.0

Figure (5.3) Temperature Distribution in the Slab
(Finite Difference Technique)

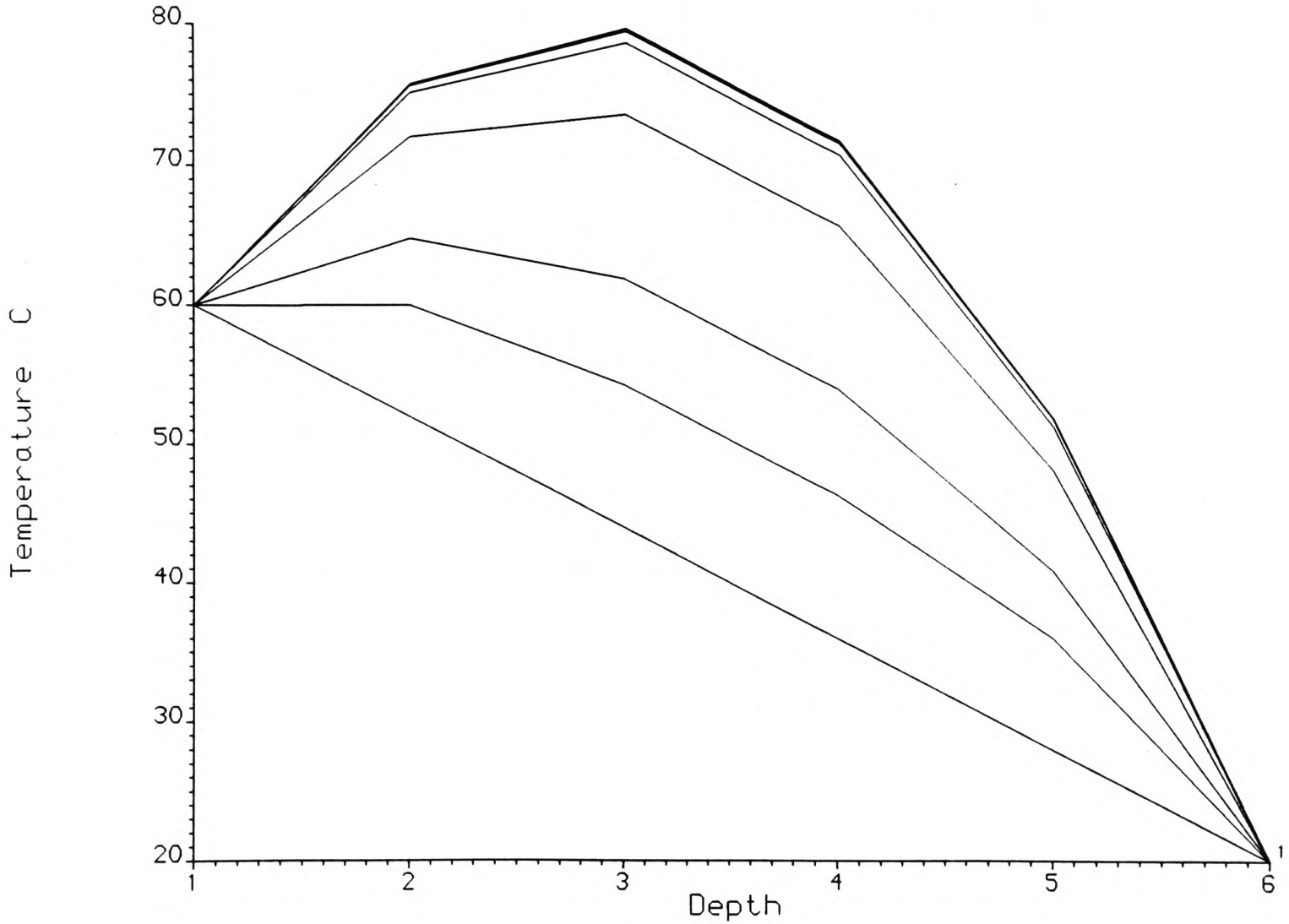

It can be seen from Table (5.1) that ASTEC3 has simulated the temperatures in the one-dimensional structure to within 3×10^{-6} °C of the analytical solution and to within 1.5×10^{-5} °C of a finite-difference solution. The latter is itself within 1.7×10^{-5} of the exact solution. The finite-difference technique should give errors of the order of $(\Delta x)^2$ [2] where Δx is the width of each division. For our example with a space increment of 0.01 *m* the errors should be of the order of 0.0001 °C, which can itself be seen from the table.

5.2.2 Conduction and Convection

The above problem can be considered with the addition of convection at the boundaries with a heat transfer coefficient of 5 kW/m^2K from both ends. Convection at the boundaries is incorporated into the network by adding resistors of values $1/h_c$ to the two outer nodes as shown in figure (5.4). The results obtained from ASTEC3 and finite-differencing are shown in figures (5.5) and (5.6) respectively. The steady-state temperatures are given in Table (5.2), showing maximum difference of 5×10^{-4} °C between the two techniques.

Table (5.2) Results of 1-D with Conduction and Convection

		Final Temperature °C	
Node	Initial Temp.°C	ASTEC3	Finite Difference
13	60.0	60.0	60.0
1	57.6	67.86851	67.86841
3	50.5	84.656107	84.65576
5	43.5	89.536205	89.53574
7	36.5	82.508798	82.50835
9	29.5	63.573893	63.57358
11	22.4	32.731485	32.73140
12	20.0	20.0	20.0

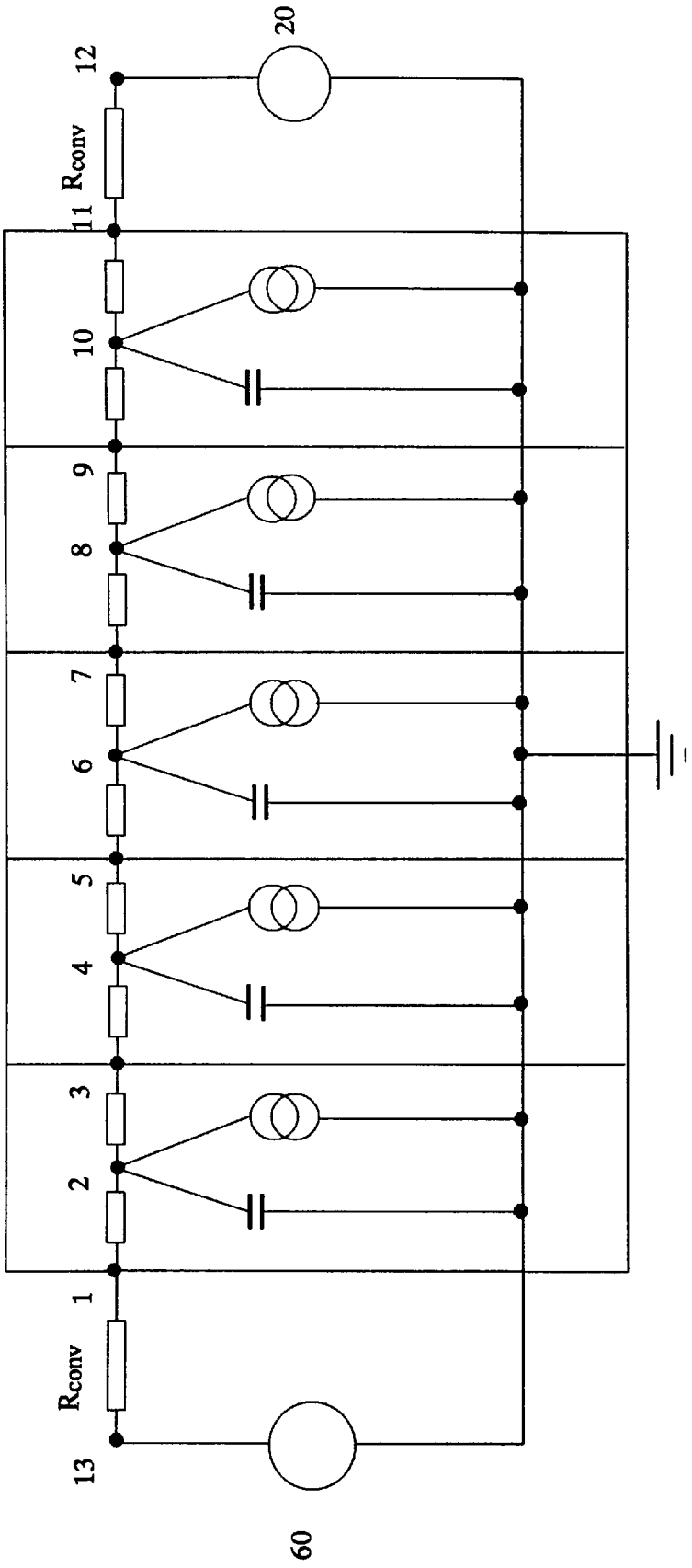

Figure (5.4) The Electrical Configuration for the One-dimensional Problem with Convection

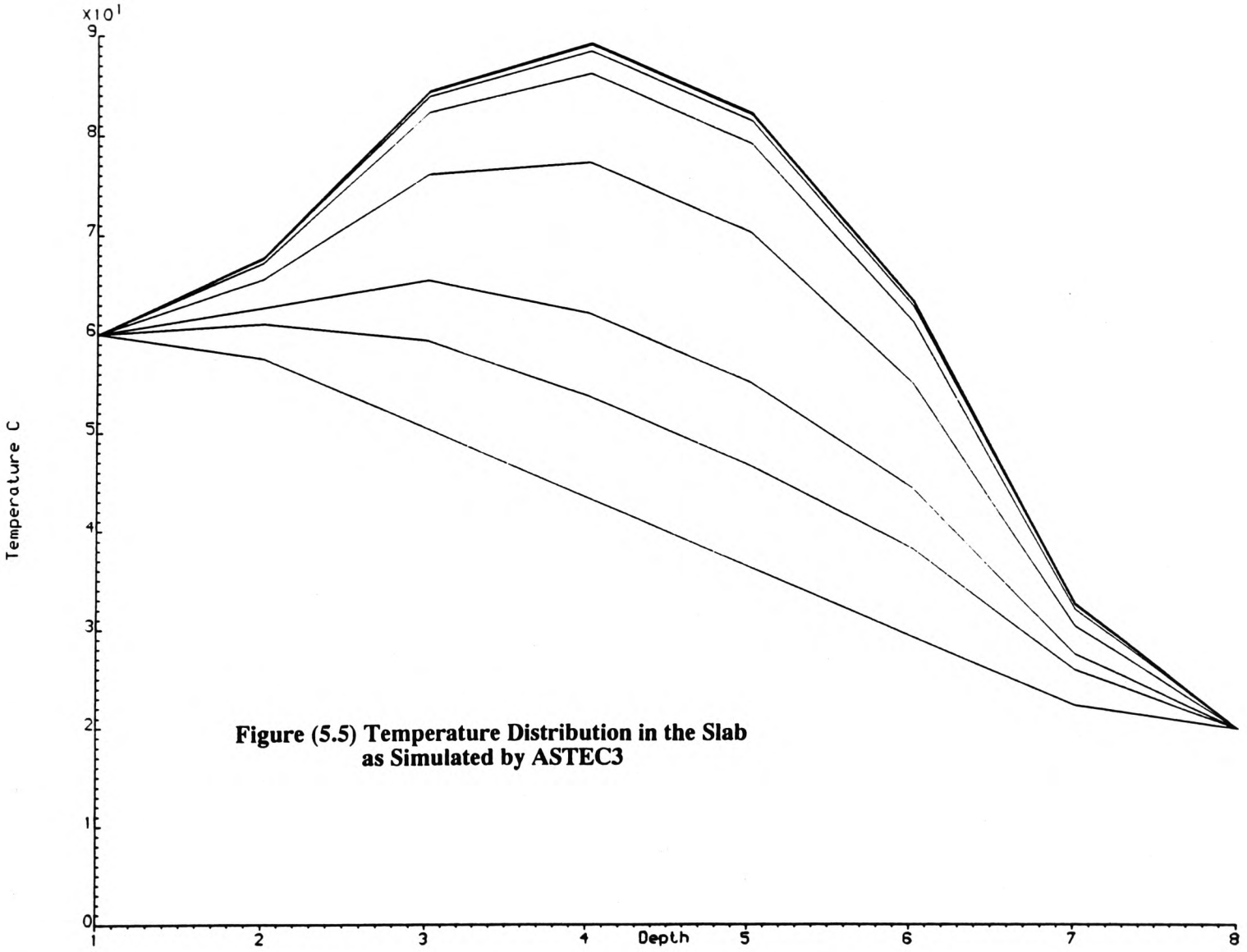

Figure (5.5) Temperature Distribution in the Slab as Simulated by ASTEC3

Figure (5.6) Temperature Distribution in the Slab Calculated via a Finite Difference Method

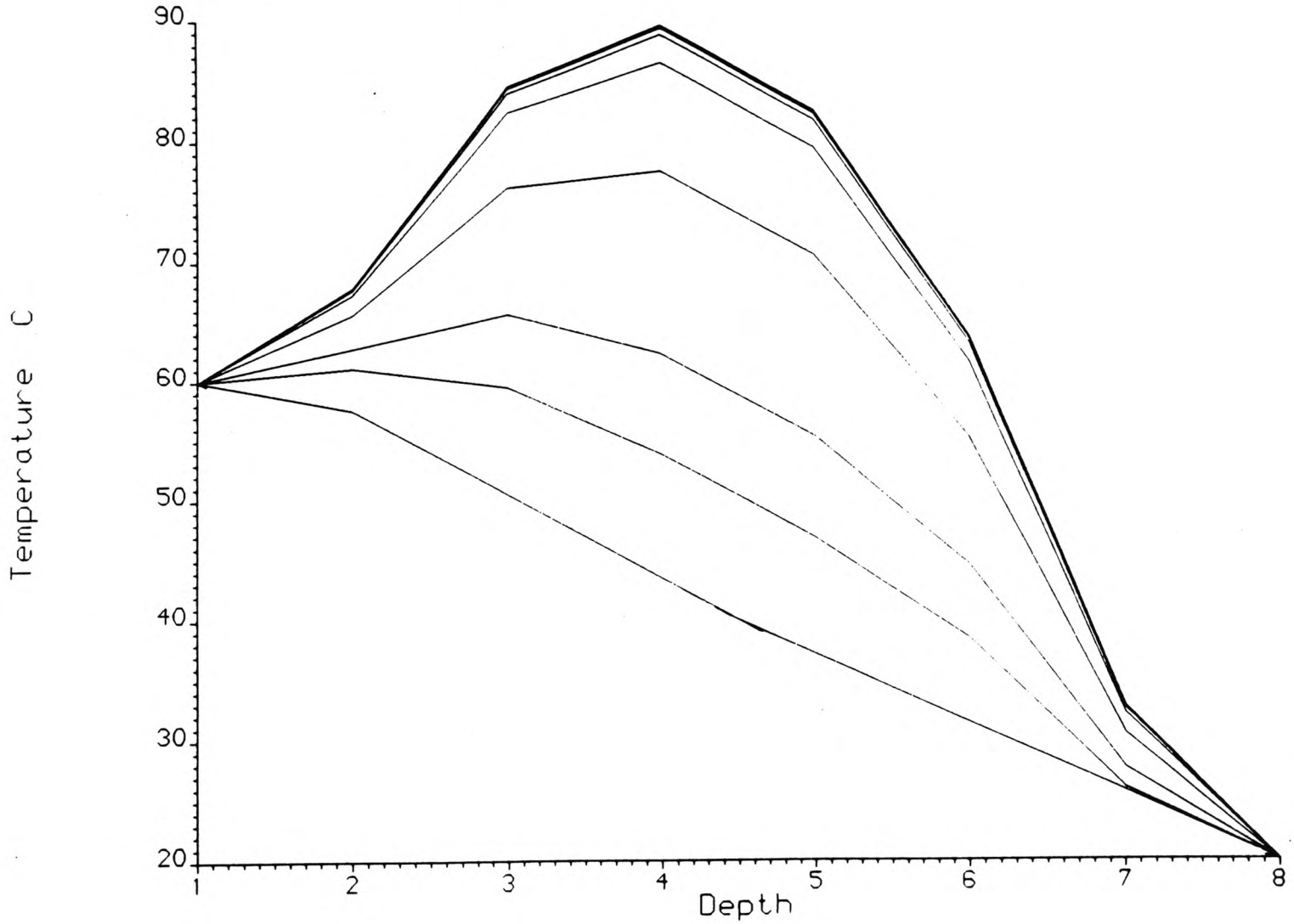

5.3 Two-dimensions

To assess the performance of ASTEC3 in the case of two-dimensional heat transfer problems, the heat flow in a thin rectangular plate as shown in figure (5.7) is simulated where the top and bottom faces of the plate are insulated so that the thermal gradient in a direction perpendicular to the plate is negligible and hence the temperature in the plate is only a function of x and y space coordinates. Three sides of the rectangular plate 50 *mm* wide and 30mm high are maintained at a constant temperature of 0 °C. The upper side has a sinusoidal temperature distribution with an amplitude T_m of 100 °C impressed upon it. The final steady-state temperature distribution in the plate is required. Values of 0.05 *W/mK*, 150 kg/m^3 and 1.88 *kJ/kgK* are taken for the thermal conductivity, density and specific heat of the solid respectively.

The general solution to this problem has been derived analytically [3,4] where a method of separation of variables is used to solve the 2-dimensional steady-state heat-conduction equation. The general solution is given below with reference to figure (5.7) showing the boundary conditions and other parameters.

$$T(x,y) = T_m \cdot \frac{\sinh(\pi y/L)}{\sinh(\pi b/L)} \cdot \sin(\pi x/L) \qquad 5.2$$

The above expression can be used to determine the final temperature of any point in the plate.

Throughout the document references have been made to coarse and fine meshes which are of course relative terms. Coarse mesh is used to denote a first approximation to the solution of the particular problem and fine mesh to denote simulation of the same structure at a higher resolution.

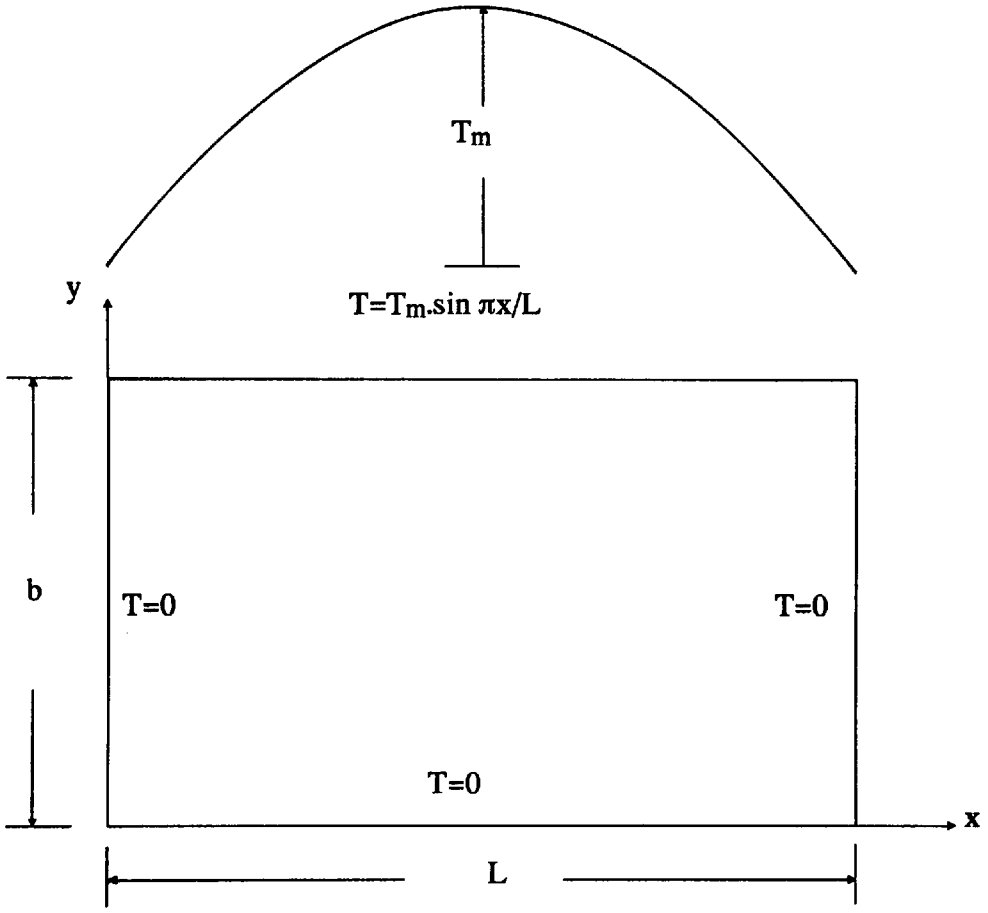

Figure (5.7) Block Diagram showing the Parameters and Symbols used in the General Solution to the 2-D Problem

5.3.1 ASTEC3 Solution

a Coarse Mesh

For ASTEC3 modelling, the plate is divided into 15 square cells of dimensions ($10\,mm \times 10\,mm$). R_{th} and C_{th} are calculated using expressions (4.5) and (4.6) and an electrical network is constructed by connecting 15 such cells as shown in figure (5.8). Average values are calculated for each segment of the sine function and applied as voltage sources to the 5 nodes on the upper side of the circuit and the outer nodes of the 3 remaining sides are tied to ground representing a temperature of 0°C. Figure (5.9) in page 84 shows a contour-map which is plotted using the steady-state temperatures of the mid-nodes of the cells. Note that figure (5.9) is plotted in such a way that the sinusoidal input to the plate is from the bottom face and not from the top as illustrated in figure (5.8).

A comparison between the temperatures of the mid-nodes of the cells obtained from the ASTEC3 and equation (5.2) is given in Table (5.3) in page 83 with reference to figure (5.8). The errors are in the range of 2.6 °C at the top of the plate to 0.16 °C at the bottom. The errors associated with these results appear to be higher in the areas where temperature gradients are relatively higher.

b Fine Mesh

It is postulated that a significant part of the divergence between the exact solution and that generated by the simulation is caused by the errors involved in approximating the system with a mesh. These errors should be reduced by using a finer mesh whereby the plate is divided into smaller cells. This is carried out here by dividing each square cell in the coarse mesh into 4 smaller ones. ASTEC3's modelling facility can be used here to write a model

Figure (5.8) The Electrical Equivalent Model of the Rectangular Plate as used in ASTEC3 Simulation

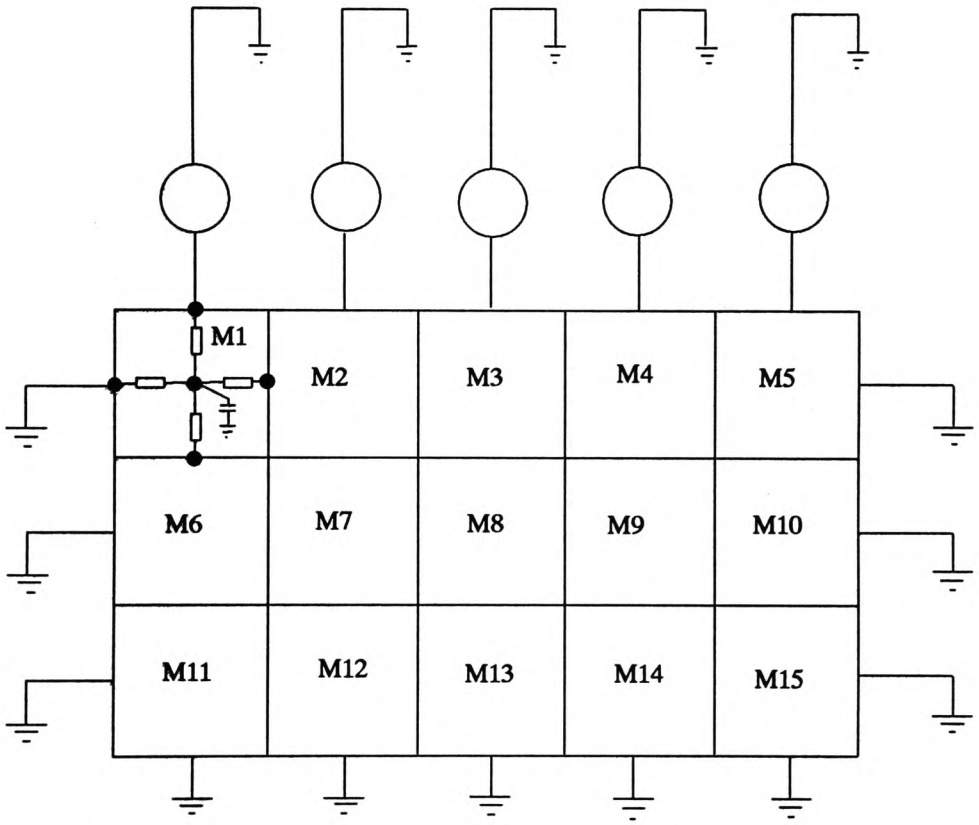

consisting of four 2-D cell-models with appropriate values of R_{th} and C_{th}, connected as shown in figure (5.10) in page 85. This model is then used to construct an electrical network in the same way as before. In this case the sinusoidal input is applied at 10 points instead of 5.

An isothermal map of the plate in the steady-state condition is given in figure (5.11) and a comparison of the ASTEC3 solution with the exact solution is shown in Table (5.4) in page 86 with reference to figures (5.8) and (5.10). The contour-map of figure (5.11) also shows a better and more accurate distribution compared to figure (5.9) since more data points were available for its description. The accuracy of the simulated temperatures in the fine mesh solution compared to that obtained via a coarse mesh model is also due to the sinusoidal input voltage (temperature) to the plate being applied at ten points rather than five. The ten point distribution is of course a more accurate representation of the sine input which in turn leads to more accurate simulated temperatures within the plate.

The fine mesh results show errors of 0.8 °C at the top to 0.01 °C at the bottom of the plate. These results, as anticipated, show a marked reduction in the errors observed with the coarse mesh model which varied from 2.6 °C at the top to 0.05 °C at the bottom of the plate. Similar to the coarse mesh model, the errors seem to be higher in the areas with higher temperature gradients.

Table (5.3) 2-D Problem Using a Coarse-Mesh Model			
Mid-Node of Cell	Final Temperature °C		Temperature Difference °C
	ASTEC3	Analytical	
M1	21.34	22.1	0.76
M2	55.8	57.84	2.04
M3	68.93	71.53	2.60
M4	55.8	57.84	2.04
M5	21.34	22.1	0.76
M6	10.22	10.45	0.23
M7	26.74	27.37	0.63
M8	33.05	33.82	0.77
M9	26.74	27.37	0.63
M10	10.22	10.45	0.23
M11	3.021	3.067	0.05
M12	7.91	8.03	0.12
M13	9.77	9.93	0.16
M14	7.91	8.03	0.12
M15	3.021	3.067	0.05

Figure (5.9) Contour Map of the Final steady-State Temperatures of the 2-D Problem Using a Coarse Mesh Model

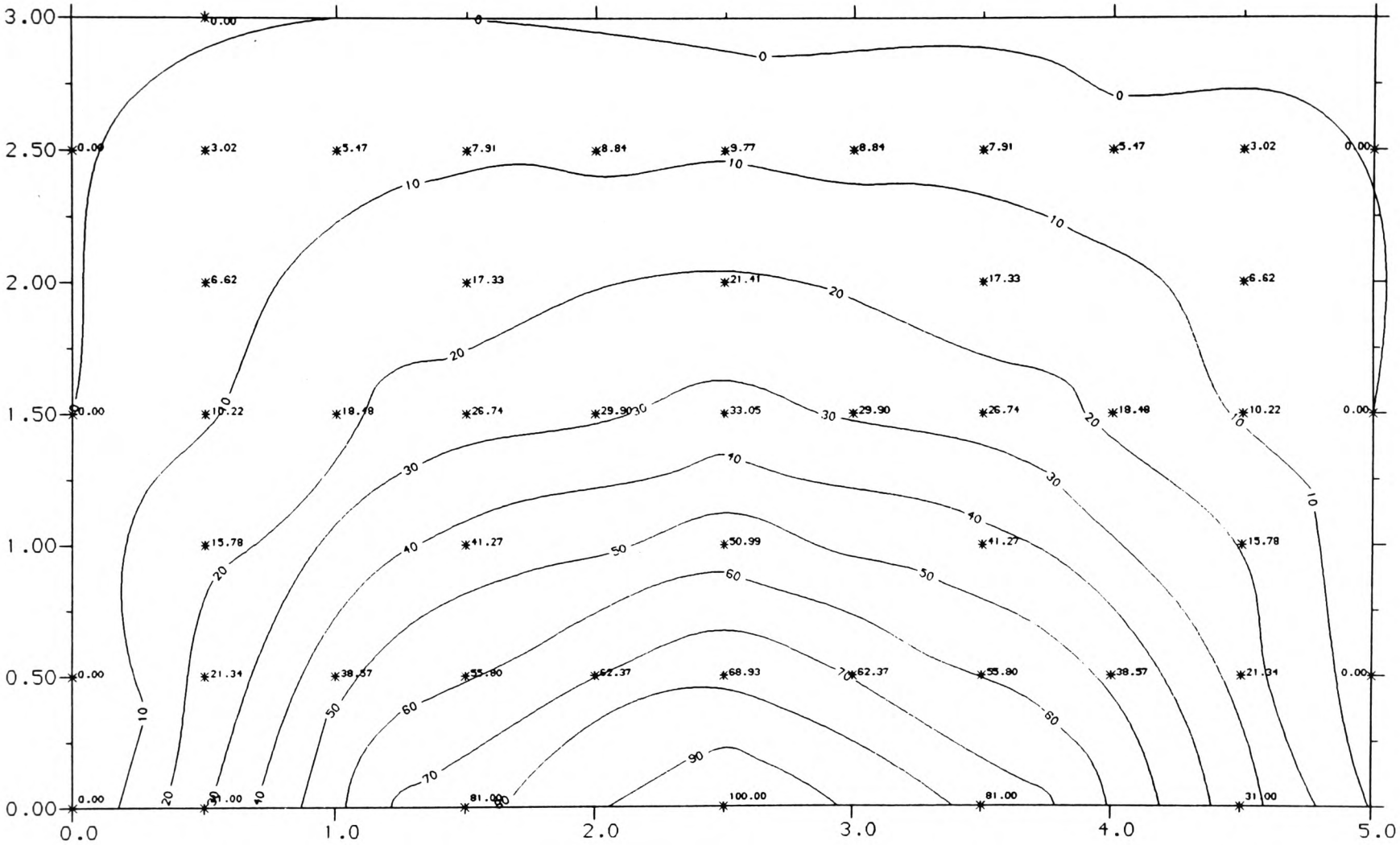

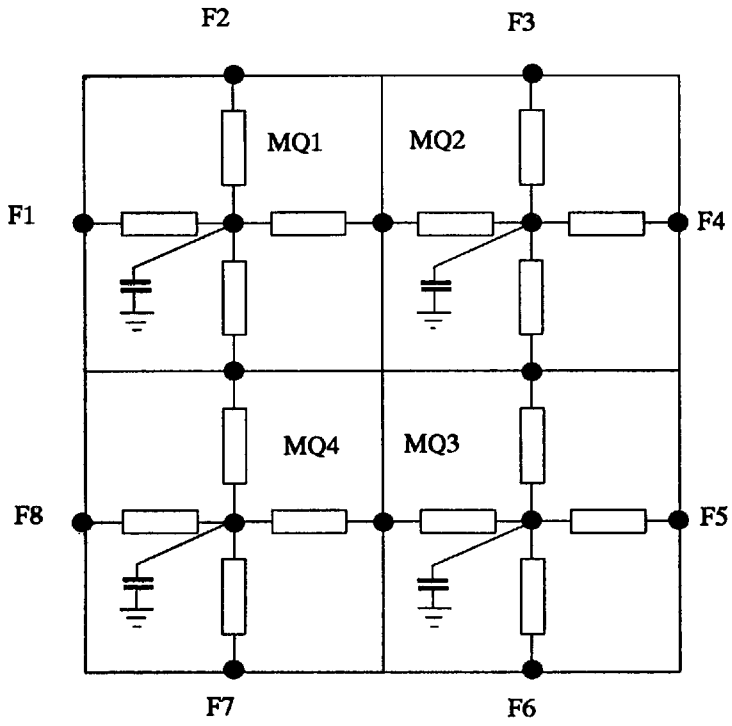

Figure (5.10) The Electrical Equivalent Model of a Fine Cell

Table (5.4) 2-D Problem using a Fine-Mesh Model			
Mid-Node of Cell	Final Temperature °C		Temperature Difference °C
	Analytical	ASTEC3	
M1.MQ1	13.25	13.0	0.25
M1.MQ2	38.46	38.0	0.46
M2.MQ1	59.91	59.2	0.71
M2.MQ2	75.49	74.7	0.79
M3.MQ1	83.68	82.8	0.88
M1.MQ4	9.40	9.30	0.10
M1.MQ3	27.29	27.0	0.29
M2.MQ4	42.51	42.1	0.40
M2.MQ3	53.56	53.1	0.46
M3.MQ4	59.38	58.8	0.58
M6.MQ1	6.49	6.44	0.05
M6.MQ2	18.83	18.7	0.13
M7.MQ1	29.31	29.1	0.21
M7.MQ2	36.97	36.7	0.20
M8.MQ1	40.97	40.7	0.27
M6.MQ4	4.22	4.20	0.02
M6.MQ3	12.28	12.2	0.08
M7.MQ4	19.09	19.0	0.09
M7.MQ3	24.04	23.9	0.14
M8.MQ4	26.65	26.5	0.15
M11.MQ1	2.38	2.37	0.01
M11.MQ2	6.89	6.86	0.03
M12.MQ1	10.74	10.7	0.04
M12.MQ2	13.54	13.5	0.04
M13.MQ1	15.0	14.9	0.10
M11.MQ4	0.76	0.76	0.00
M11.MQ3	2.22	2.22	0.00
M12.MQ4	3.46	3.45	0.01
M12.MQ3	4.37	4.35	0.02
M13.MQ4	4.84	4.82	0.02

Figure (5.11) Isothermal Lines for the Final Temperatures Simulated using a Fine Mesh Model

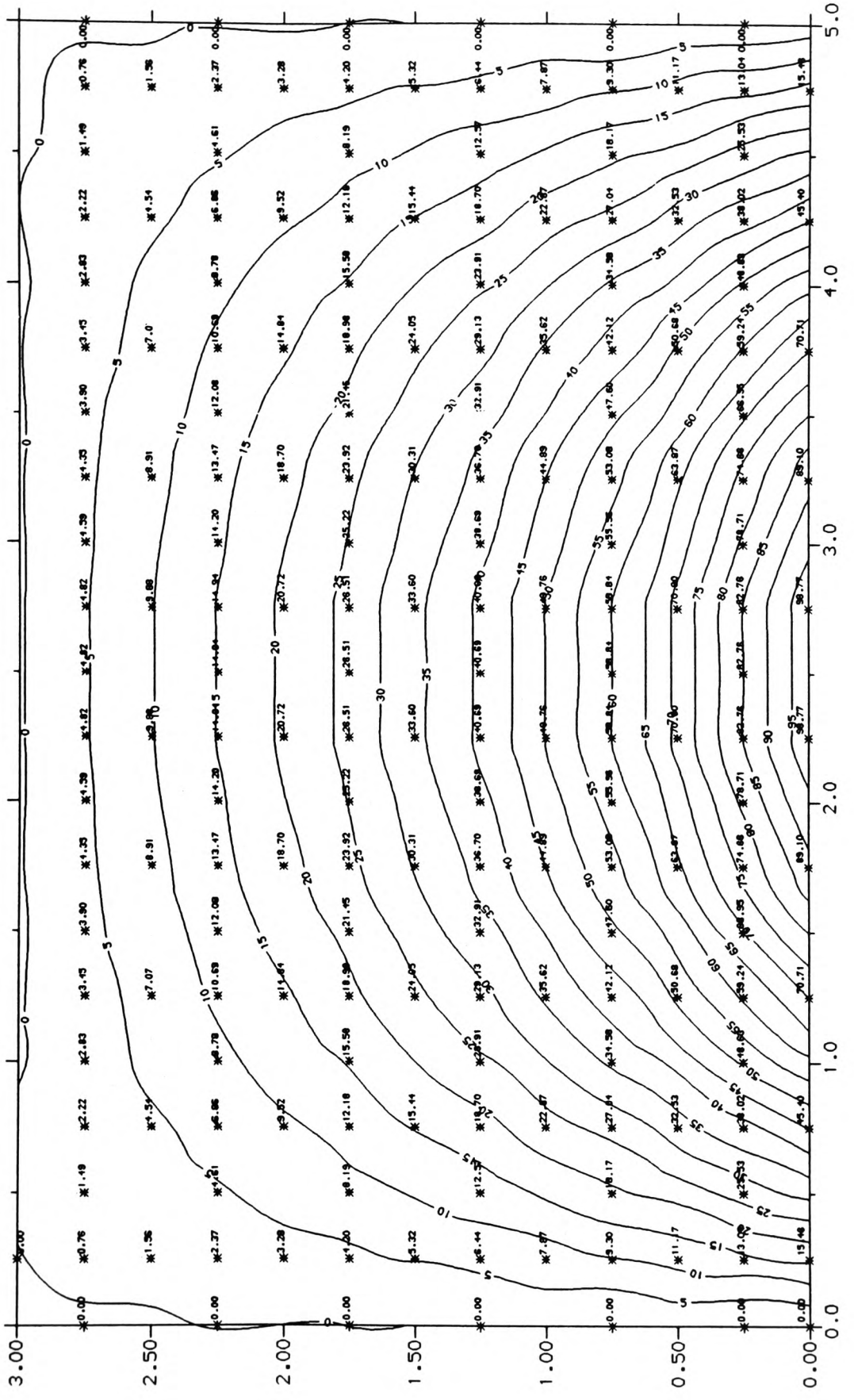

5.4 Three-dimensions

To verify that simulations can be performed on a three dimensional structure the following problem was envisaged. A block of material (50 *mm* × 30 *mm* × 20 *mm*) was assumed to have five of its faces perfectly insulated and a sinusoidal temperature profile impressed upon one of its (30 × 20) faces. The same thermal parameters as the 2-D problem were used. The block was divided into cubes of equal dimensions of 10 *mm* and an electrical network constructed in the same way as before. The temperature distribution plot of the final steady-state results for the top face is shown in figure (5.12). An analytical solution could not be found for this problem and hence no comparison was possible.

5.5 Efficiency: A combination of Coarse and Fine Mesh Models

Improving the resolution errors while maintaining a control of execution time can be achieved by mixing the coarse and fine meshes in the same simulation. This should reduce the computing time required for simulations. Of course this requires the introduction of an interface cell-model as shown in figure (5.13) in page 90.

In the interface model two resistors are connected from the mid-node to the two nodes on those faces shared with fine cells. These two resistors are in parallel in electrical terms and in order to keep the same total value, each is given a value of R_{th}. Figures (5.13) to (5.15) show models interfacing one, two and three fine cells.

To determine the effect of this approach on accuracy and on CPU time, the 2-D problem in section (5.2) was simulated first with only one cell, M3 in figure (5.8), and then 3 cells M2, M3 and M4 replaced by fine cells. The position of the fine cells was chosen to be in the areas with maximum error.

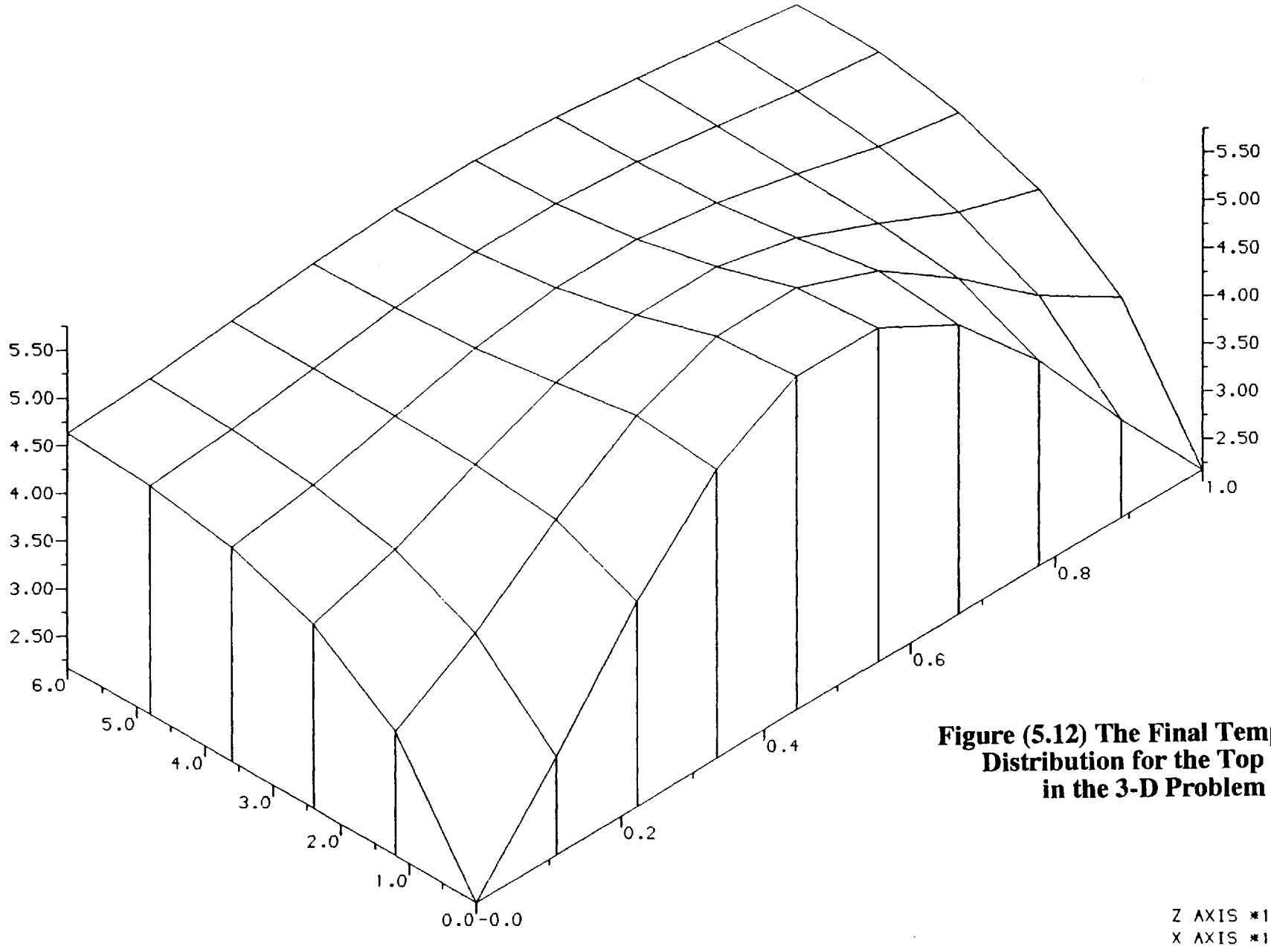

Figure (5.12) The Final Temperature Distribution for the Top Face in the 3-D Problem

Figure (5.13) The Electrical Equivalent Model of a Cell Interfacing One Fine Cell

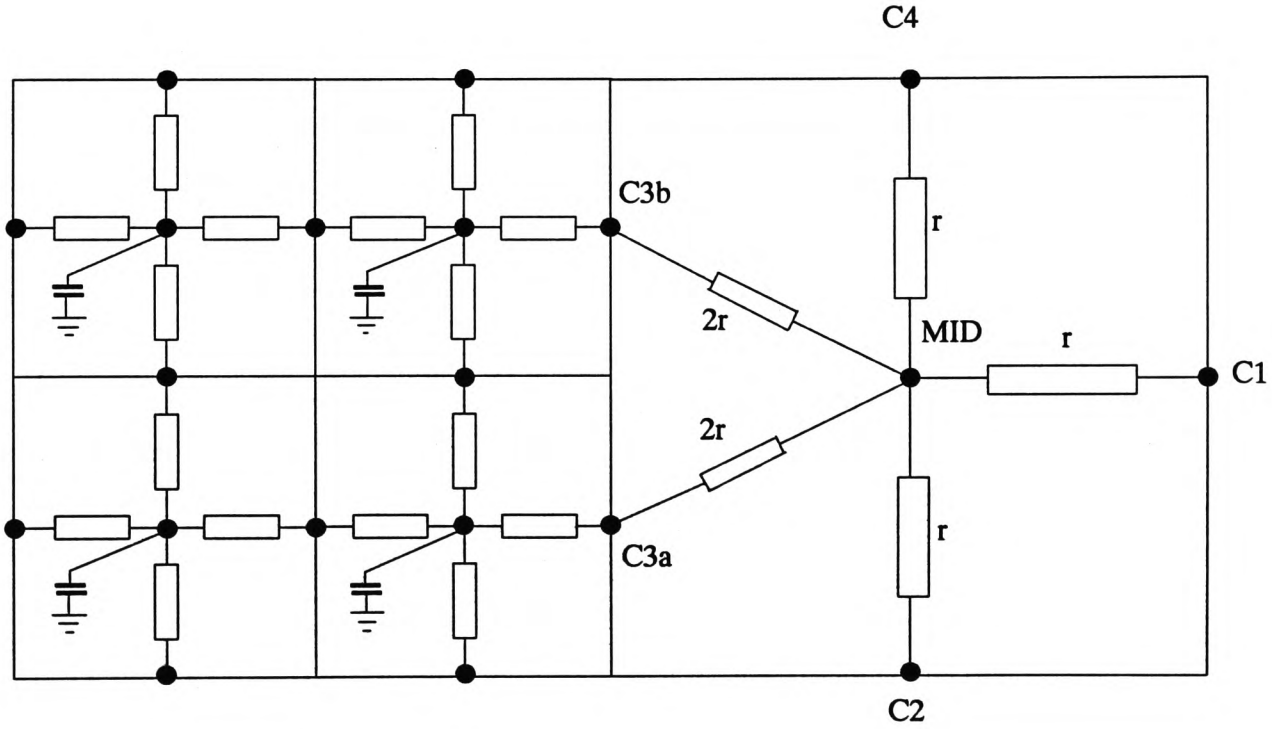

Figure (5.14) Electrical Equivalent Model for a Cell interfacing Two Fine Cells

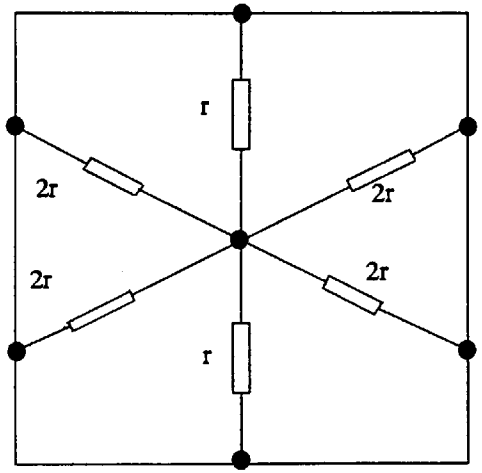

Figure (5.15) Electrical Equivalent Model for a Cell interfacing Three Fine Cells

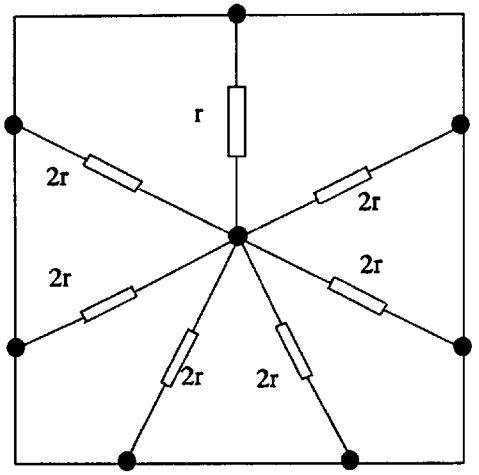

$r = 1/2\ R_{th}$

The results of these simulations are given in Tables(5.5) and (5.6) respectively and the subsequent CPU times are shown in Table (5.7). Tables (5.5) and (5.6) give the mid-node temperatures of all cells in the coarse and the fine meshes whichever is applicable. Reference is made to figures (5.8) and (5.10).

Table (5.5) 2-D Problem with one fine Cell			
Mid Node Of Cell	Final Temperature °C		Temperature Difference °C
	ASTEC3	Analytical	
M1	21.6	22.1	0.50
M2	57.2	57.84	0.63
M3.MQ1	80.8	83.68	2.88
M3.MQ2	80.8	83.68	2.88
M3.MQ3	60.54	59.38	1.10
M3.MQ4	60.54	59.38	1.10
M4	57.21	57.84	0.63
M5	21.6	22.1	0.50
M6	10.4	10.45	0.05
M7	27.3	27.37	0.07
M8	33.35	33.82	0.20
M9	27.3	27.37	0.07
M10	10.4	10.45	0.05
M11	3.075	3.067	0.008
M12	8.06	8.03	0.03
M13	9.927	9.93	0.003
M14	8.06	8.03	0.03
M15	3.075	3.067	0.008

Table (5.6) 2-D Problem with Three Fine Cells			
Mid-Node of Cell	Final Temperature °C		Temperature Difference °C
	ASTEC3	Analytical	
M1	22.17	22.10	0.07
M2.MQ1	58.73	59.91	1.18
M2.MQ2	74.66	75.49	0.83
M2.MQ3	53.11	53.56	0.45
M2.MQ4	43.30	42.51	0.79
M3.MQ1	82.82	83.68	0.86
M3.MQ2	82.82	83.68	0.86
M3.MQ3	59.15	59.38	0.23
M3.MQ4	59.15	59.38	0.23
M4.MQ1	74.66	75.49	0.83
M4.MQ2	58.73	59.91	1.18
M4.MQ3	43.30	42.51	0.79
M4.MQ4	53.11	53.56	0.45
M5	22.17	22.10	0.07
M6	10.40	10.45	0.05
M7	26.60	27.37	0.77
M8	32.70	33.82	1.12
M9	26.60	27.37	0.35
M10	10.40	10.45	0.35
M11	3.04	3.067	0.027
M12	7.86	8.03	0.17
M13	9.69	9.93	0.24
M14	7.86	8.03	0.17
M15	3.04	3.067	0.027

Table (5.7) Comparison of CPU Time Requirements for 2-Dimensional Transient Simulations	
Model	CPU Time (Seconds)
2-D Coarse Mesh (15 Cells)	0.88
2-D Fine Mesh (60 Cells)	4.41
2-D Mixed Mesh with 1 Fine Cell (18 Cells)	1.11
2-D Mixed Mesh with 3 Fine Cells (24 Cells)	1.32

The results of the simulations with one fine cell, show an excellent agreement with the analytical results with errors ranging from a maximum of 2.88 °C in the fine mesh area to 0.003 °C at the bottom of the plate. The errors in the simulated temperature in the fine cells M3.MQ1 and M3.MQ2 in Table (5.5) seem higher than M3 in Table (5.3). It should be noted however that these nodes are in a physically different position than M3 in Table (5.3), situated closer to the edge of the plate and hence see a higher temperature gradient leading to bigger errors. The results with three fine meshes also show excellent agreement with the analytical solutions with reduction of errors in the fine mesh areas to a maximum of 1.18 °C but with a maximum of 0.35 °C in the interface cell M8 at the bottom of the fine mesh areas. Similar argument to that given above applies to errors in cells M2.MQ1 and M4.MQ2 in Table (5.6) which are also in higher temperature gradient areas.

5.6 Computing-Time Considerations

In order to allow the user to forecast the computer time required for thermal simulations of the transient type, an attempt was made to derive a relationship between the number of cells and the CPU time. In the first instance this was only carried out for two-dimensional modelling.

To simplify the procedure, the equivalent fine-mesh-model already developed for the two-dimensional problem described in section (5.2) was itself written as a sub-model in the ASTEC3 library so that it could be repeated as many times as required. This model consisted of 60 cells which means a fairly rapid increase in the number of elements.

The results of the initial investigations using a Vax 11/785 computer are illustrated in figure (5.16) as a graph of CPU-time versus number of cells. The graph follows a fairly linear path up to 1200 cells and again from 1500, with a change of gradient, up to 2400. There exists a transition region between the two linear sections. Simulations were carried out to establish the nature of the curve in the region between the two sections which showed it to be real and not fictitious.

Investigations into the reasons for the unexpected increase in the gradient of the straight line have shown the *working-set size* to play an important role in this problem. This is the size of the memory space on the computer disk allocated to each user in a multi-user system. This fact has been verified by simulating the same circuits with a larger working set (equivalent to 10 MBytes of memory where the default setting was 2 MBytes for the Vax 11/785), the results of which are also shown in figure (5.16). This shows great improvements in the results since the CPU times for the larger circuits have been reduced showing a fairly linear relationship between the simulation time and the number of cells. By fitting the best straight line through all the points using a least-square fit method the functional relationship between the two parameters for the Vax 11/785 is found to be of the following form :

$$T_{Tran} = 4.276 + 0.09\,N \qquad 5.3$$

Figure (5.16) Transient Simulation Time for 2-D Modelling Vs Number of Cells

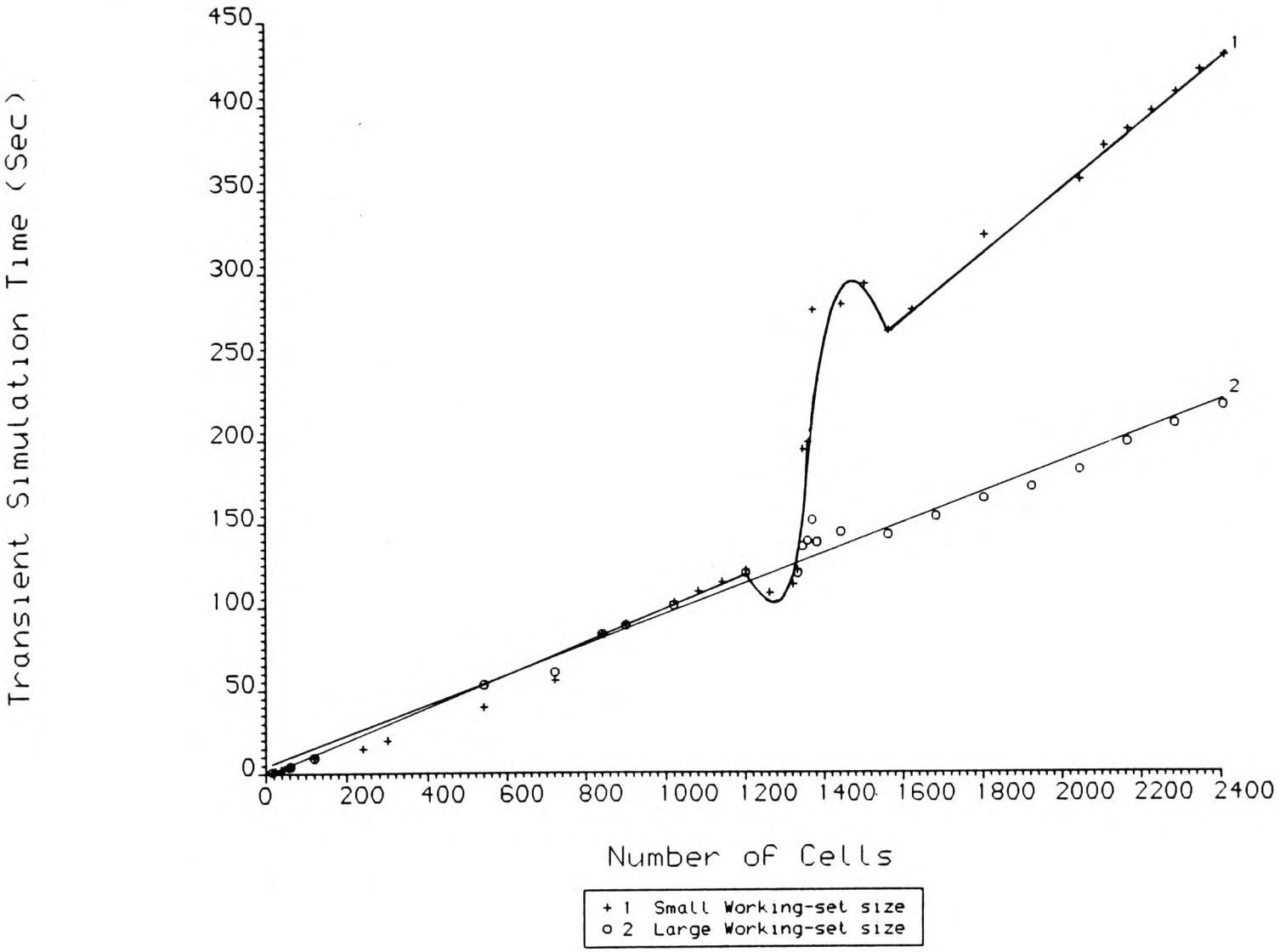

where T_{Tran} and N are the CPU time needed for transient simulations in seconds and the number of cells respectively.

The increase in the working-space size has also reduced the size of the scatter in the region between 1200 to 1500 cells. The variation is so small that its effect may be overlooked in the prediction of simulation times.

Further measurements were also made for Vax 8650 and MicroVax computers using the same circuits. The results of these computations are given in figure (5.17). The working-set size was kept the same (10 MBytes) for both Vax 8650 and Vax 11/785 machines. The MicroVax however has limited work-space and the maximum was used for these tests.

The equation defining the best straight line for the Vax 8650 machine is in the following form:

$$T_{Tran} = 1.59 + 0.024\,N \qquad 5.4$$

Further calculations were carried out to establish a relationship between the computers' power rating in MFLOPS (Millions of Floating Point Operations per second) and the number of cells which can be simulated per second. The results of these calculations are shown in figure (5.18) for three Vax machines. All the MFLOP ratings were taken from a survey [5] on the performance of various computers. A best straight line was fitted through the points giving a value of approximately 63.85 Cells/Seconds/MFLOPS.

For a hybrid circuit with minimum feature size of 0.1 mm and substrate size of 20 mm by 20 mm the maximum number of cells to be simulated is 40,000 although this could be

Figure (5.17) Transient Simulation Time Vs Number of Cells for Three Vax Computers

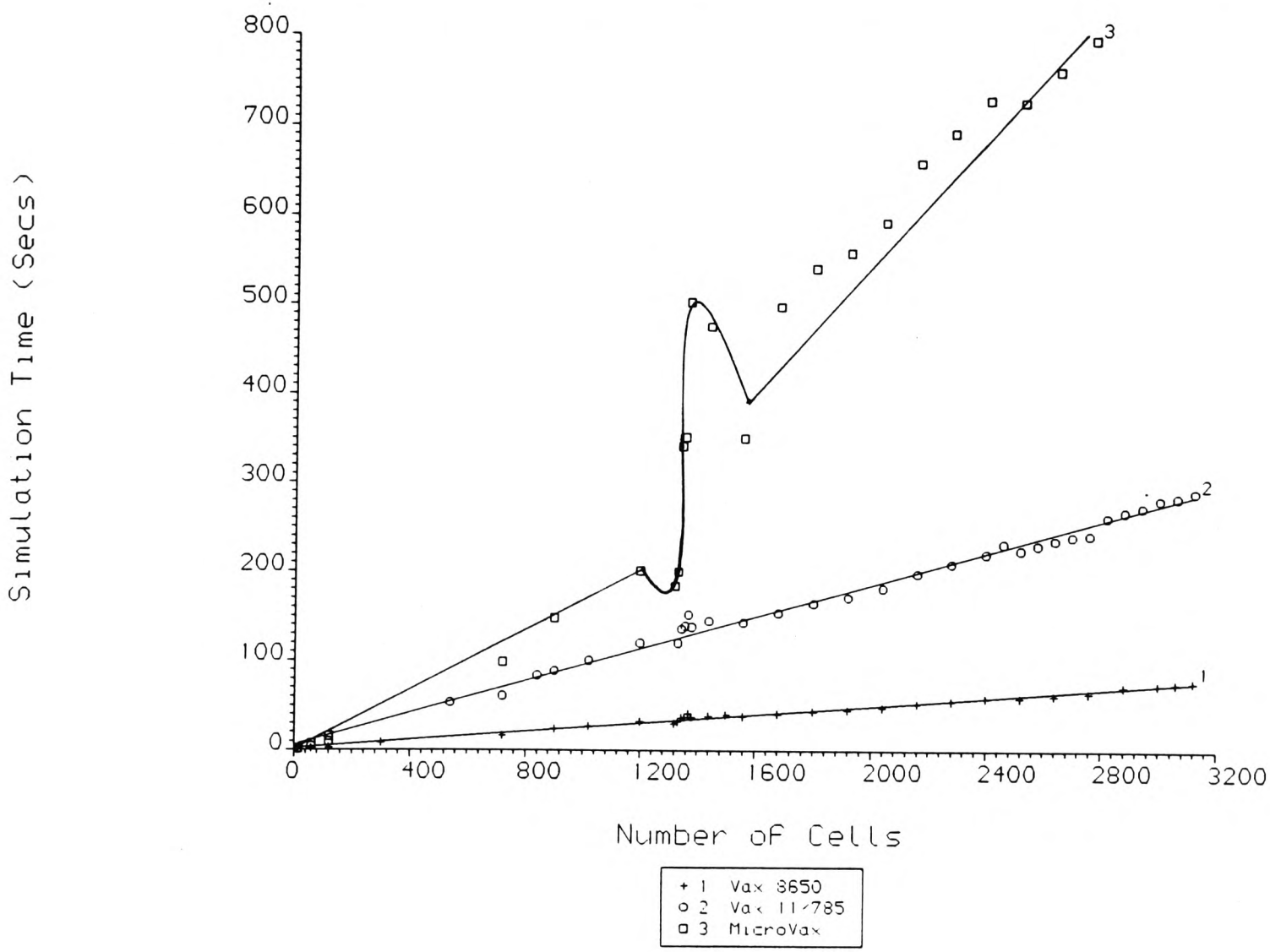

Figure (5.18) Cells/sec Vs MFLOPS for Three Vax Computers

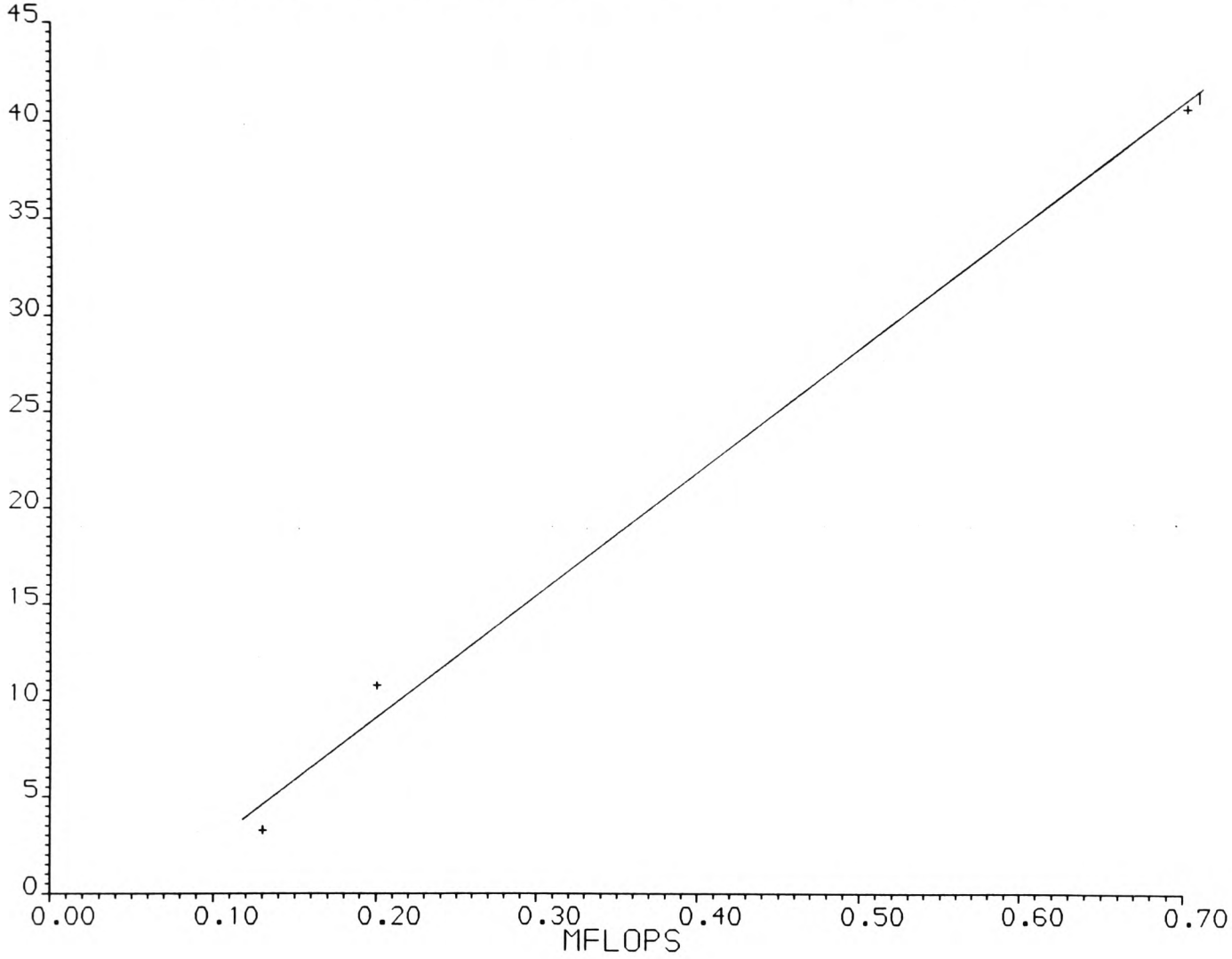

reduced if sensible use of coarse cells is employed in areas of low interest. The rating calculated above can be used to estimate the CPU simulation times needed by various computers as given below:

Computer	CPU Time
MicroVax II	1 hr 20.3 Mins
Vax 11/785	52.2 Mins
Vax 8650	16.5 Mins

A version of the ASTEC3 package has been released for the CRAY series of computers [6] which should reduce the simulation times drastically which will be important when dealing with extremely large circuits. The predicted CPU times for the example above are given below for two CRAY computers:

CRAY 1s	52.2 secs
CRAY XMP2	26.1 secs

So far in this section, the CPU time for the transient simulation stage has been dealt with. During the ASTEC3 run the CPU times needed for processing the $DESC (The circuit Description) section of the files (§ 2.1) were also recorded. A further graph was produced which illustrates the CPU description-time versus number of cells for the three Vax machines as shown in figure (5.19). The $DESC part of a simulation does not necessarily need repeating. Once the simulation of this section is carried out it may be saved via an option in ASTEC3 and called up for further analysis using different thermal parameters.

Figure (5.19) Description Time For 2-D Modelling Vs Number of Cells

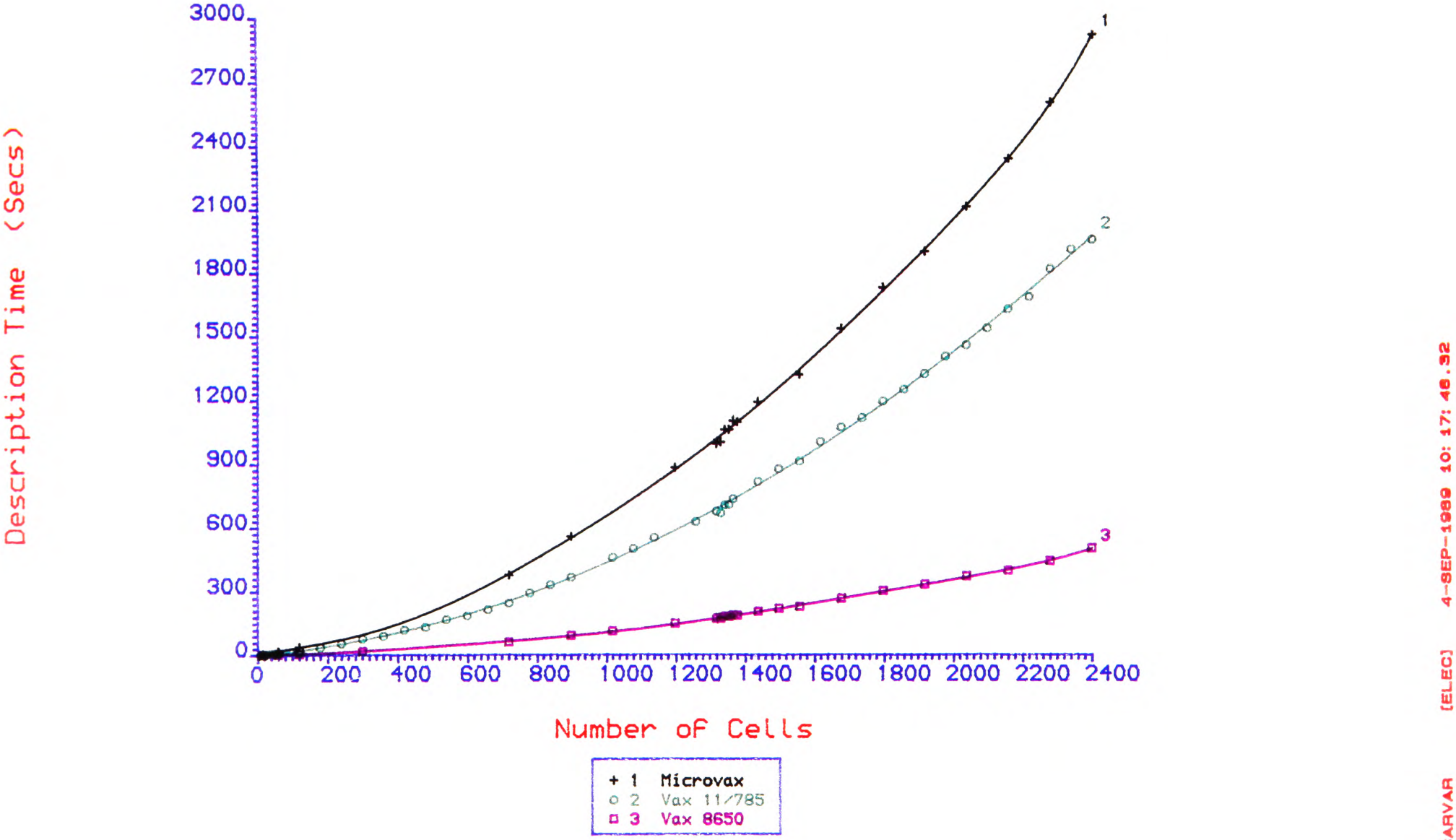

5.7 Conclusion

In this section, the ASTEC3 thermal modelling procedures were used for simulation and prediction of the temperature distributions in one and two-dimensional heat transfer problems. The numerical results presented for the one-dimensional problem with both conduction and convection were in excellent agreement with the analytical and finite difference solutions. The results for the two-dimensional problem using a coarse mesh showed very good agreement with the analytical solution. The small errors observed were reduced to negligible margins when a finer mesh was employed.

In order to minimise the computer time required for simulations and hence make it economically more acceptable, interface models were introduced allowing the mixing of coarse and fine cells. The tests on these models showed excellent agreement with the analytical solution and greatly reduced the CPU time when compared with the full-fine-mesh model.

A great number of simulations were carried out with increasing numbers of thermal cells using three Vax computers. This was to establish a relationship between the number of conduction cells and the CPU time needed for simulations. This would in turn enable a user to predict the CPU time in advance and the relationship between the MFLOPs and the CPU times. It has also been shown that the computing times are practical for real situations (Hybrid Circuits).

6 EXPERIMENTAL STUDIES IN MACRO-SCALE

In chapter (4), a modelling procedure was described whereby the temperature distribution in thermal systems involving conduction, convection and radiation could be predicted via a simulation using the ASTEC3 package. This was subsequently used to solve some standard heat flow problems as given in chapter (5) which showed excellent agreement with results obtained from alternative, more conventional techniques.

The ASTEC3 heat transfer modelling was used for the simulation of simple experimental structures. Initially, in order to avoid the problems of measuring surface temperatures of very small areas, a large scale physical model was used for the experiments. The nature of these models was similar to that of hybrid circuits with heat generating elements being mounted in good thermal contact with an insulating substrate.

Experiments will be described where surface temperatures of some copper cladding strips and plates which may be totally or partially heated were measured. These were then modelled and simulated using ASTEC3. This demonstrated the extent to which the idealised heat transfer models developed needed amendment for practical use.

6.1 Experimental Arrangement

In these experiments, a HEIMANN infrared radiation pyrometer type KT14, capable of measuring between ambient up to 300 °C to an accuracy of 1.5 °C was used to measure the temperature at various points on the surfaces of some heated samples made of copper cladding. This is the type of printed circuit board which consists of a very thin layer of

copper 15 μm or 35 μm thick (depending on the type of board used) on a fibre-glass base 1.6 mm thick. Electric currents were passed through the copper layer on top, causing a rise in the temperature of the specimen due to the conversion of electrical to thermal energy.

The apparatus was placed inside a chamber, a great deal larger than the test specimen. A larger enclosure was required for the following reason. The sample radiates an energy density which decreases with distance. The heat transfer coefficients are related to this energy density and altering the energy density of the immediate surroundings, by means of a reflected field (eg. from the walls), would change the heat transfer coefficient. To overcome this experimental problem the box was made many times larger than the sample size which allowed the field intensity to decrease proportionally to r^{-2} due to the spreading of the field and also by $e^{-\mu x}$ due to attenuation where μ is the absorption coefficient of air and x is the displacement through the air. The reflected radiation was kept to a minimum by coating the inside of the chamber with matt black paint.

Furthermore, the size of the box should be large enough for the enclosed ambient air temperature to be unaffected by the heat input as this would induce irregularities in the results. This may be checked by calculating the temperature rise in the box due to 6 Watts of input electrical power which was the maximum power generated within the samples used in these experiments. Taking a value of $718 J/kgK$ for C_v, the specific heat capacity of air and 1.15 kg/m^3 for its density, for a box with dimensions of ($0.9m \times 0.6m \times 0.6m$) the temperature rise for an experimental run may be determined from the following relationship:

$$Q = mC_v\Delta T$$

$$\Delta T = \frac{6}{(0.9 \times 0.6 \times 0.6 \times 1.15) \times 718} = 0.02°C$$

which is sufficiently small compared to the temperature of the strip to be ignored.

The box was also sealed very carefully in order to avoid any draughts from the room. This in turn allowed the occurrence only of natural convection which is rather simpler to account for in the calculations than a mixture of natural and forced convections.

A schematic diagram of the apparatus is presented in figure (6.1). A specially designed holder was used to accommodate the samples. Grooves were cut into two flat pieces of wood which were fixed parallel to each other onto another flat board. The distance between the parallel grooves was slightly greater than the length of the copper cladding samples. The above configuration allowed the specimen boards to be easily inserted into position. The width of the grooved pieces was made as small as possible to ensure the least contact between the sample and the rest of the holder assembly in order to minimise the amount of heat lost by conduction at the grooves.

Figure (6.1) shows a rectangular sample of copper cladding mounted horizontally and glass wool with thermal conductivity of less than 0.05 W/mK used to insulate the bottom surface of the strip thus restricting the heat losses by convection and radiation to the top surface. The sample was heated by passing an electric current through the connections at the ends of the heated sections.

Initially the current was supplied to the heated areas through fixed points at their ends. Measurements at various positions showed a non-uniform distribution of temperature over the surface being cooler towards the corners of the plate. This phenomenon is known as the *crowding effect* which occurs when the current is applied in the specific configuration.

Figure (6.1) The Schematic Diagram of the Heat Transfer Experiments

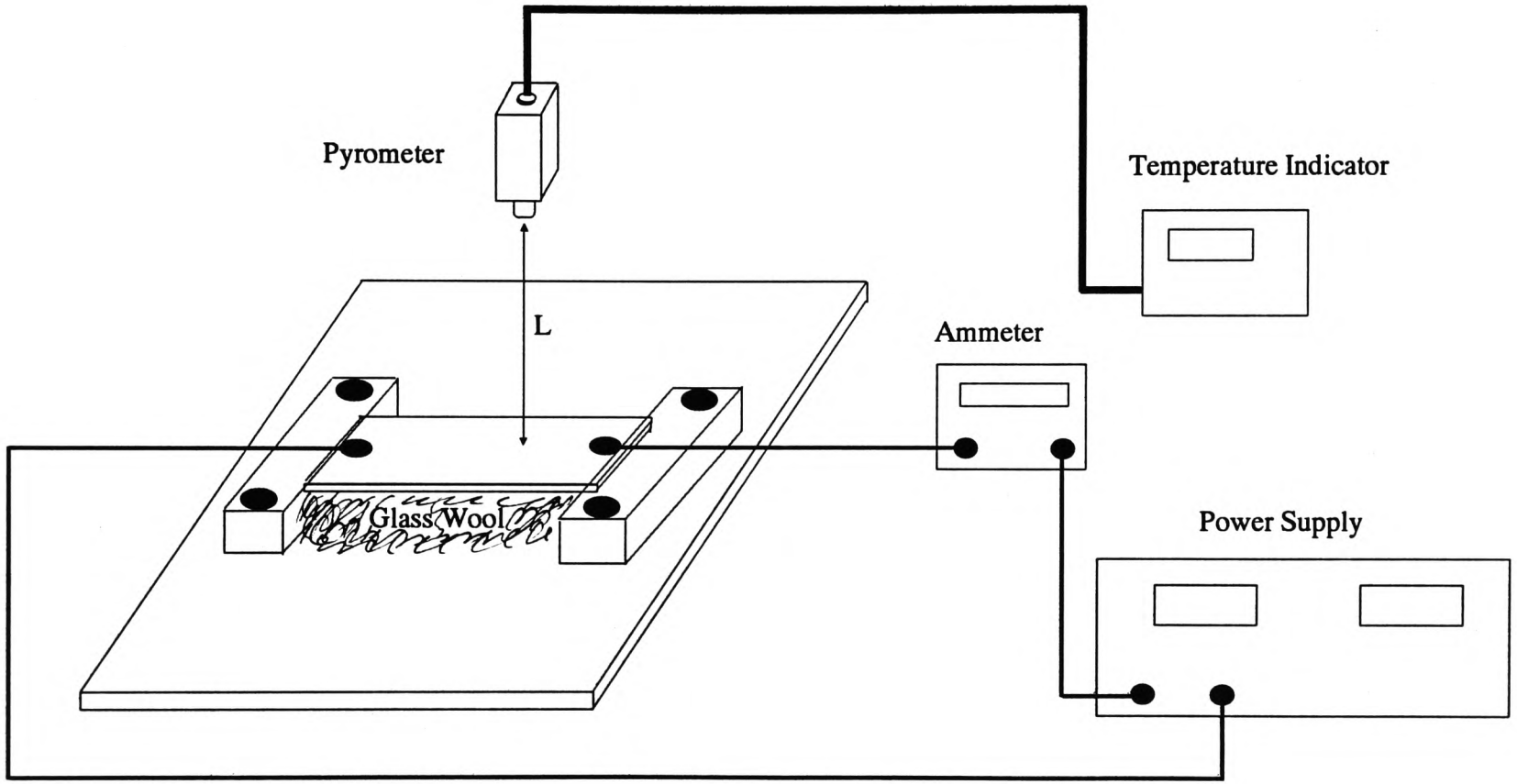

Since the current is entering the heated strips through a point terminal much smaller than its width, the electrons travel along the strip to the other terminal in a non-uniform fashion as shown in figure (6.2). In doing so, the current distribution may even miss parts of the strip which will not be heated at all. Improvements were therefore made by applying the current to the islands through a number of wires at each end. Six holes of each 1 *mm* in diameter were drilled along the width of each *resistor* evenly distributed. Wires of appropriate thickness capable of handling at least 5 amperes were inserted in these holes and soldered to the copper surface, figure (6.3). These wires were then bunched together and connected to the main supply line. The above arrangement should in turn establish a more uniform current distribution and hence a more uniform heating effect in the islands.

The infrared pyrometer was positioned with its axis perpendicular to the plane of the surface. The distance L between the edge of the lens barrel and the surface was set to exactly 80 *mm* as specified by the manufacturers. A specially designed insertion gauge, figure (6.4) consisting of a flat metal disc and a rod which screws into the centre of the disc was used for this purpose. The total height of the disc and the rod was adjusted to exactly 80 *mm*. The diameter of the rod was 4 *mm* which made it possible to aim quite accurately at a certain target position by sliding the flat surface of the disc onto the lens barrel. The tip of the rod marked the minimum target spot at the proper working distance of 80 *mm*.

The pyrometer is designed to respond accurately only for surfaces with emissivities of nearly 1. To overcome this problem when dealing with copper boards, at positions of interest, small circular patches of around 4 *mm* in diameter (focusing area of pyrometer) were coated with black velvet paint 2010 from 3M. This material is claimed to have an emissivity of 0.95 [1].

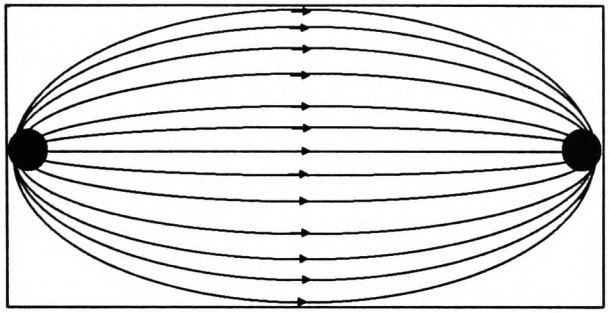

Figure (6.2) Crowding Effect

Figure (6.3) Uniform Current Distribution

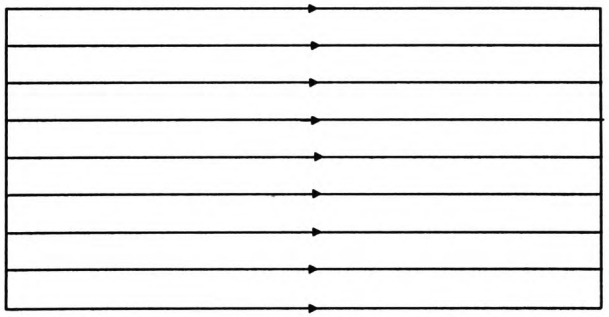

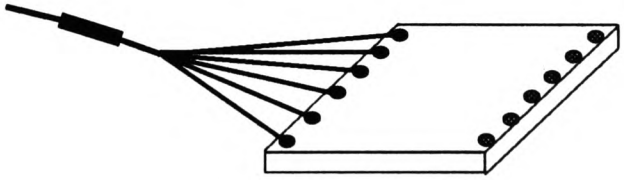

Figure (6.4) A Diagram Showing the Insertion-Gauge for Adjusting the Distance Between the Pyrometer and the Heated Surface

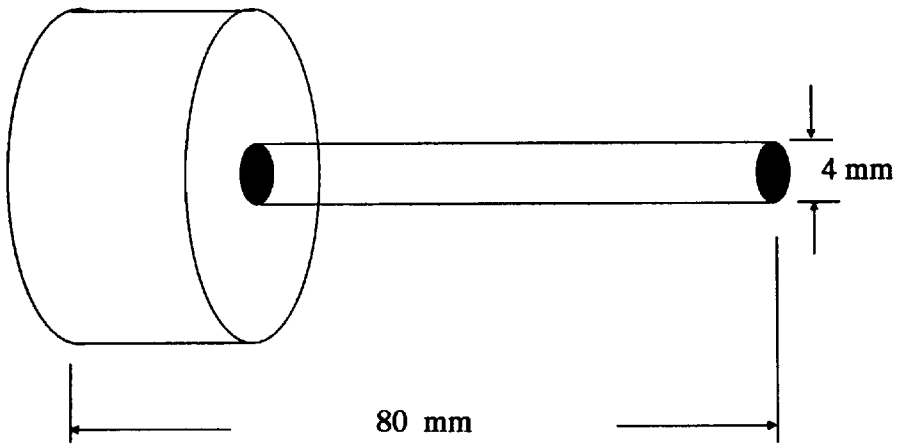

Prior to each experimental run, the focusing distance L was checked and the chamber was sealed carefully for a draft-free atmosphere. The desired currents were selected and after switching on, the set-up was left to reach a steady-state condition. At this point the surface and the ambient temperatures were recorded.

A number of confirmatory experiments were carried out as outlined below:

(i) Experiment (1) - A rectangular strip uniformly heated.

(ii) Experiment (2) - A rectangular plate with two electrically heated islands formed on its conducting layer by cutting grooves in its copper layer. These islands are electrically isolated from the rest of the plate but thermally connected via the glass fibre insulating board.

(iii) Experiment (3) - Rectangular plates with only one heated island. One smaller plate has an island symmetrically situated on it. Three other plates have a heated island in different positions.

The full details of the above experiments are given in the following sections.

6.1.1 Experiment 1

A rectangular strip of copper cladding ($140\,mm \times 26\,mm \times 15\,\mu m$) was used as the specimen. For a current of 30 amperes at an ambient temperature of 23.7 °C a uniform temperature of 125 °C was measured at all points along the strip.

The thermal characteristics of this experiment were simulated by applying the procedure described in chapter (4) for three dimensional conduction. The strip was divided into 15

equal segments, figure (6.5), each a cuboid of dimensions ($28mm \times 8.67mm \times 15\ \mu m$). The thermal resistances in the x, y and z directions and the thermal capacitance of each cell were calculated using the expressions given in chapter (4).

The rate of heat generation in the strip was calculated assuming that all the electric power supplied to the strip is converted into thermal energy. Under steady-state conditions then the total heat generation is simply given by I^2R, where I is the current in Amps and R the electric resistance of the copper plate in Ohms.

Using the values given in the experiment section the total power was calculated as 5.5 Watts. The rate of heat generation in each cell was then the total divided by the number of segments which in this case gives a value of 366 milliWatts/segment.

To estimate the convective heat transfer coefficient and subsequently the value of thermal resistance $R_{convection}$ for the ASTEC3 model, use was made of the correlations derived by other workers [2]. These correlations are non-dimensional and for natural convection from uniformly heated horizontal surfaces are of the form given in section (3.2).

Once the value of the Nusselt number was determined using equation (3.5) in conjunction with equations (3.7 and 3.8), it was then be used to calculate the value of h_c from equation (3.6) relating the convective heat transfer coefficient to Nusselt number.

Various values have been quoted [2-5] for constant C and the characteristic length l to be used in equation (3.5). The values of h_c arising from these would obviously be different. For C, values of 0.54 [3,5] and 0.59 [4] are given. For a rectangular plate, either an average of the two sides [3] or the ratio of the area A over the perimeter p [2,4,5] have been recommended for l. When tested in the ASTEC3 model however, the correlations

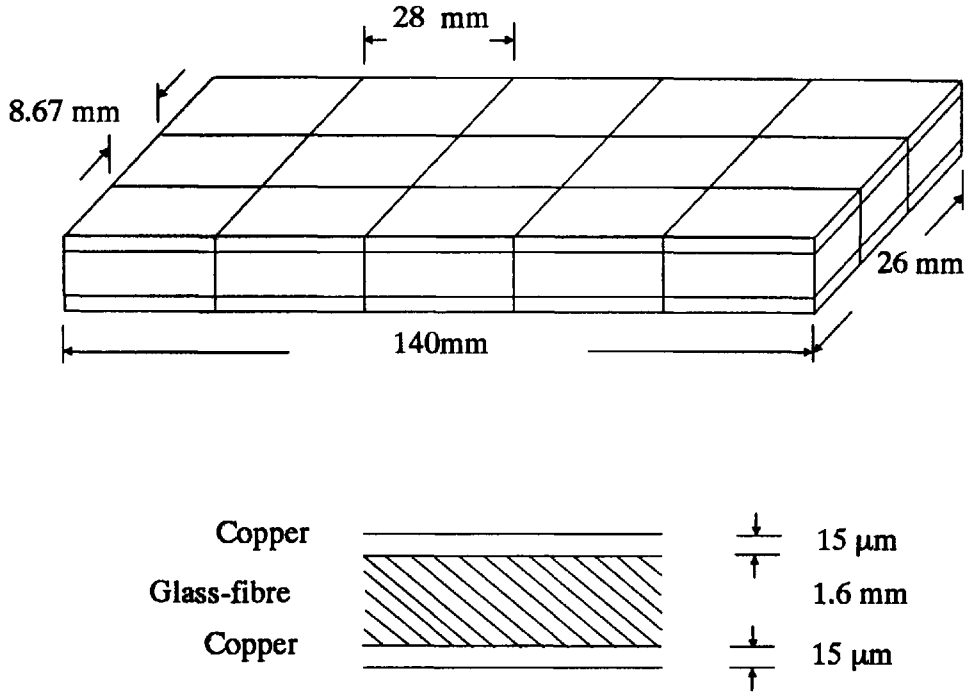

Figure (6.5) The Breakdown of the PCB Strip for use in ASTEC3 Modelling

recommended by Chapman [2] (C=0.54,l=A/p) appeared to yield a value of h_c which gave simulated temperatures closely matched to those measured experimentally. Details of the calculations are given in appendix (4).

For calculating the heat transfer coefficient of radiation h_r using the equations given in section (3.3), the emissivity of the copper surface was needed. This was estimated via a method utilising the infrared pyrometer as recommended by the manufacturers of the thermometer [6]. A set of experiments was carried out details of which are given in appendix (5). A value of 0.086 was obtained for the emissivity of the copper clad surface. This value was subsequently used in appendix (4) for determination of h_r.

Using a combined convective and radiative heat transfer coefficient of 13.85 W/m^2K, the simulated results showed a uniform temperature of 131 °C along the strip which is in good agreement and within 4.8% of the 125 °C measured experimentally.

6.1.2 Experiment 2

A more complicated system for experimentation was devised where use was made of the same experimental rig already described in section (6.1). This experiment was designed taking into account the type of thermal problem which may be encountered when simulating the thermal characteristics of hybrid microcircuit and semiconductor integrated circuits.

Hybrid microcircuits are types of device which normally consist of several separate component parts attached to a ceramic substrate [7] and interconnected either by wire bonds or suitable metallisation pattern. Considering a very simple case of a hybrid circuit with two resistors of different values on a substrate, the following specimen was designed

for experimentation. The copper cladding boards used here onwards were the pre-sensitised type manufactured by Mica & Micanite of Ireland [8] which can be used easily to form the required patterns very accurately. The copper layer thicknesses in these boards is given as 35 μm and the fibre glass is the type FR4 1.6 *mm* thick.

A rectangular plate of the above material was chosen with dimensions of 140 *mm* by 120 *mm*. Two islands were cut into the conducting layer of the board, figure (6.6) but not the insulation by chemically etching very thin, shallow grooves all the way round the islands, just enough to isolate them electrically from the rest of the copper. Subsequent checks were made for no electrical continuity.

Electric currents of 30 and 10 amps were supplied to the larger and the smaller islands respectively. The set-up was left to reach a steady-state condition and then the infrared pyrometer was used to measure the surface temperatures at selected points.

An electrical-equivalent circuit model of the system was developed using the procedure given in section (4) and figure (6.7). Each layer was divided into (6 × 7) three-dimensional cells. The fibre glass layer was assumed to be isotropic and a value of 0.343 *W/mK* was used for thermal conductivity to calculate the thermal resistances of conduction in this layer. This figure was experimentally determined via an electrically heated Lees' disc apparatus details of which will be given in chapter (7).

One major problem here was the estimation of the value of the convective heat transfer coefficient. Correlations used in section (6.2) are derived for horizontal plates which are uniformly heated and do not necessarily apply to non-uniform situations. However, for the first approximation, the plate was divided into six rows along the 120 *mm* edge and the same correlations used in experiment (1) were utilised to obtain an average value for

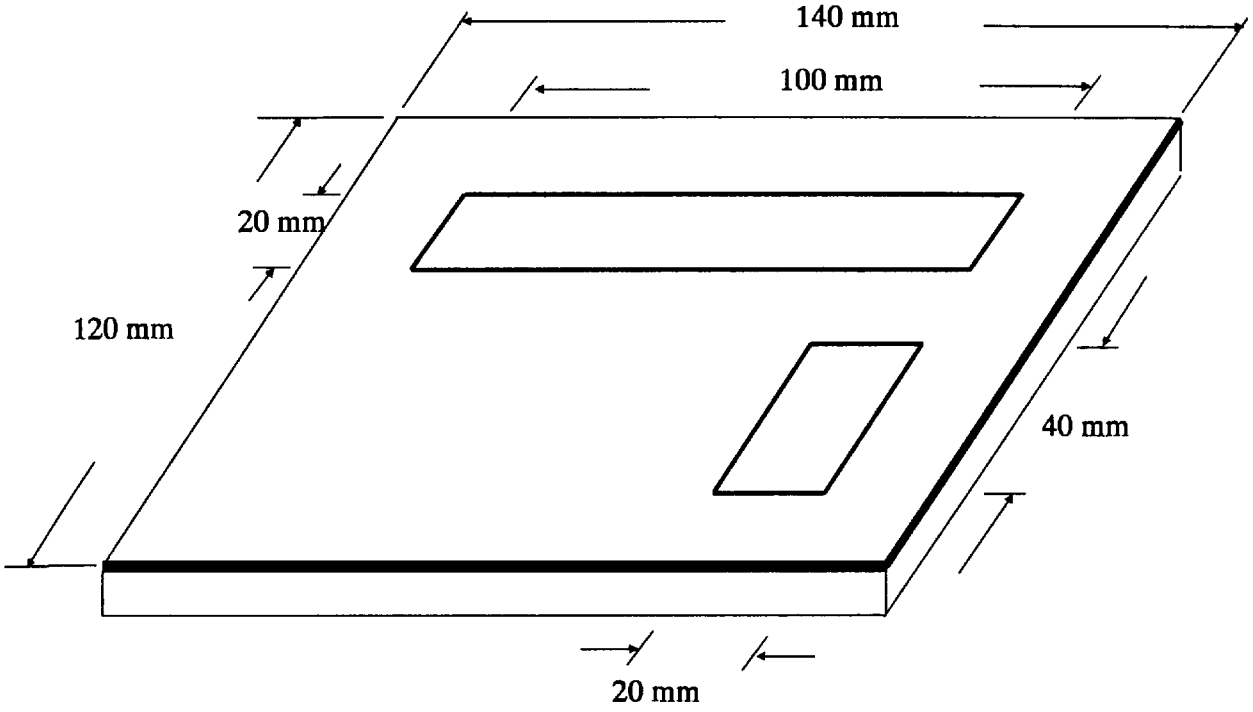

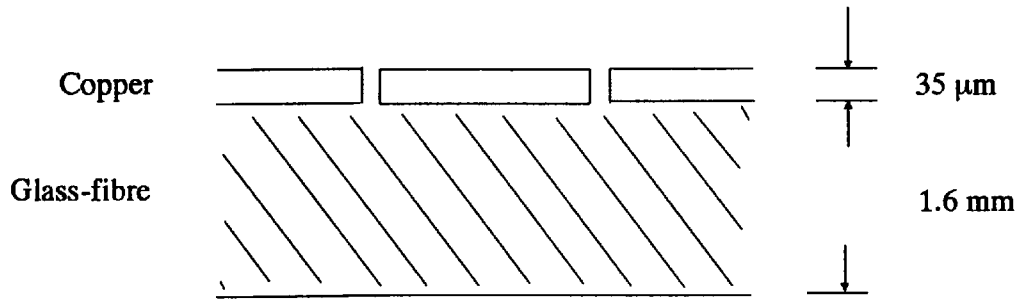

Figure 6.6 The Layout of the PCB Plate used in Experiment 2

Figure (6.7) The Grid Pattern used for Simulation of the Copper Plate in Experiment 2

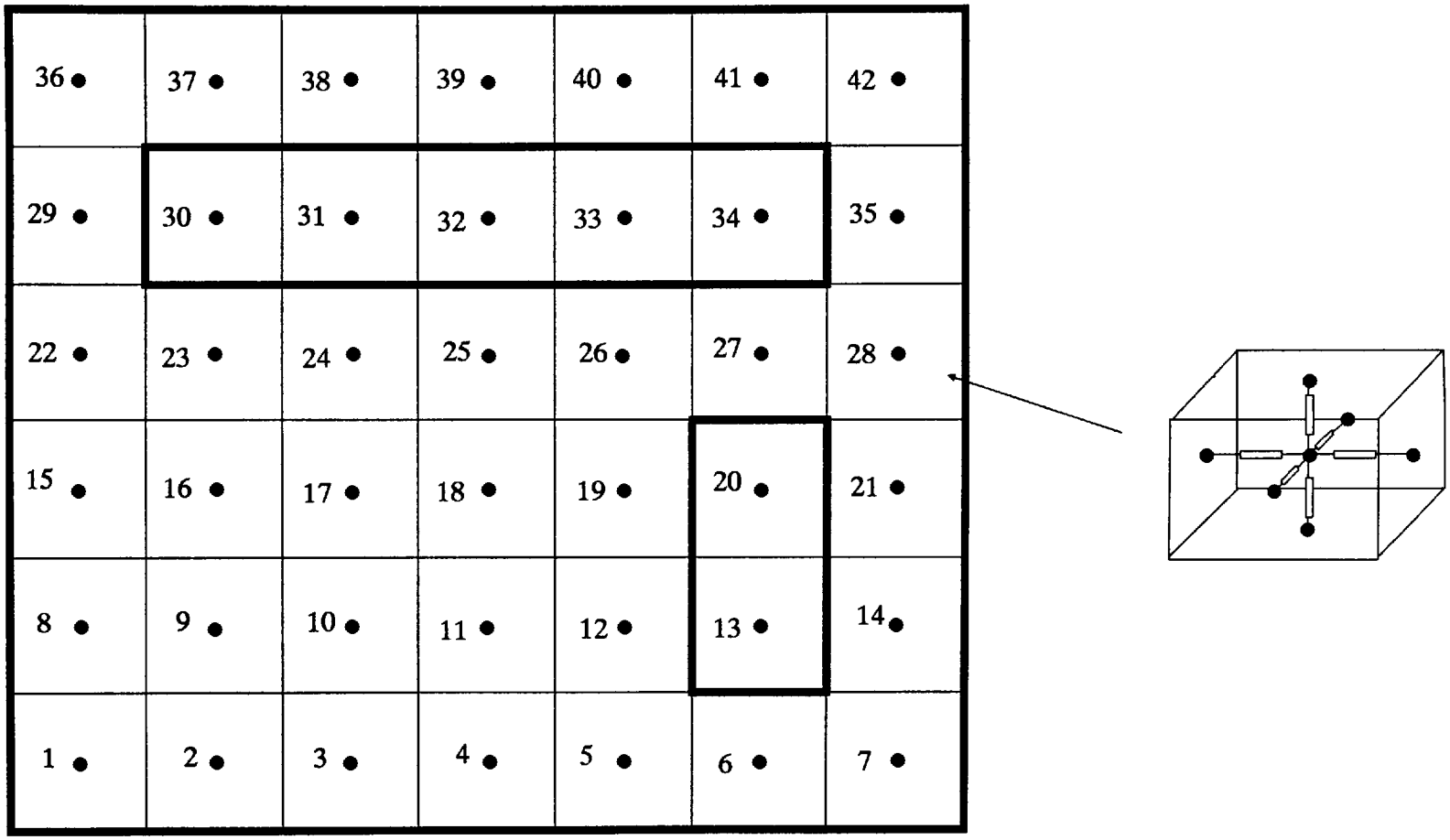

each of the six rows. The results of the simulations for temperatures of the top nodes of each three dimensional cell are given in figure (6.8) along with the experimental results. This is an overhead view of the plate with the heated islands shown as shaded areas. The top figure in each cell is the experimentally measured temperature and the lower one the simulated data for the same point. The blank squares are the areas where measurements were not possible because of the overlapping wires.

Figure (6.8) Simulation Results for the Plate with Two Heated Islands
$K_{FR4} = 0.343\ W/mK$

34.6 29.9	41.7 31.3	47.1 32.0	49.2 32.2	47.1 32.0	41.8 31.4	34.8 30.1
	66.7 97.1	70.6 98.2	74.9 98.6	71.7 98.2	65.2 97.1	
37.5 28.6	39.6 29.1	41.7 29.4	42.8 29.6	40.7 29.9		
33.4 27.7	34.3 27.9	35.3 28.1	36.4 28.2	34.3 28.4	31.1 36.5	30.0 28.3
31.0 27.2	32.0 27.3	32.1 27.4	32.3 27.5	31.0 27.7	30.0 36.6	29.9 27.7
29.8 26.9	29.8 27.0	29.9 27.0	29.9 27.1	29.9 27.2		29.8 27.3

Top Figure : Measured

Bottom Figure: Simulated

The results of this experiment showed good agreement with the simulated results at some points on the plate with greatest errors occuring inside the larger island.

The difference between the experimental and simulated results is less than 5°C for most positions on the plate although temperature differences in excess of 20 °C are observed

within the larger, hotter island. The greatest temperature gradients appear to induce the largest temperature differences between the observed experimental results and the simulated data.

6.1.3 Experiment 3

It was decided that before an understanding of composite geometries was attempted, the various factors affecting the heat losses from the samples should be studied on simpler structures. Further samples were designed with only one heated region which could possibly produce the required understanding of the physical processes involved with heat transfer coefficients. These were as follows:

a One heated island positioned symmetrically in between two unheated sections of the same width as shown in figure (6.9).

b The area of the heated section is kept constant but its position is changed on the plate, figure (6.10).

The dimensions of the heated section in *a* are the same as the larger *resistor* in the experiment with two heated sections (100*mm* × 20*mm*). The overall size of the plate is (140 *mm* × 60 *mm*).

The sizes of the plates in *b* are chosen to be the same as the one with two heated islands for possible comparisons of the results. The area of the plate is (140 *mm* × 120*mm*) and the size of the heated *resistor* is (100 *mm* × 20 *mm*).

a was the simplest situation following the uniformly heated strip in experiment (1) which

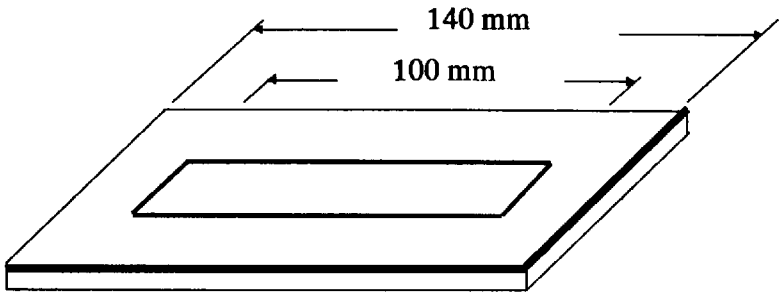

Figure (6.9) One Heated Island Symmetrically Situated on a PCB Plate

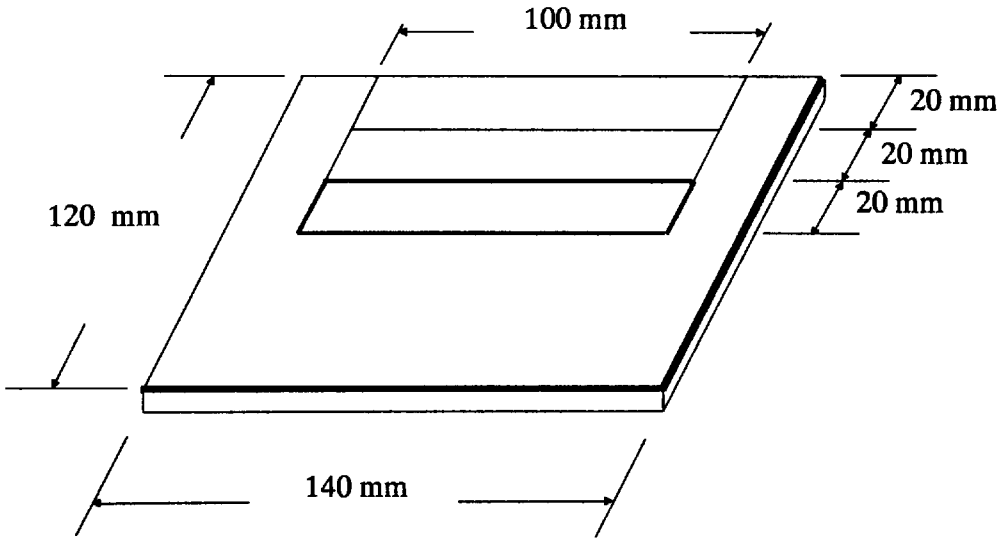

Figure (6.10) Diagram Showing the Three Positions for the Heated Island on the PCB Plates

should show the effect of introducing unheated areas adjacent to a heated *resistor*.

b may give an understanding of the effect of the location of heat source on temperatures at different points on the plate and the heat transfer by convection.

All the samples were heated by passing a current of 30 Amperes through the (20 *mm* × 100 *mm*) island. The ASTEC3 model of the plates was constructed by dividing the plate in *a* into (3×7) cells and the plates in *b* into (6×7) cells in each layer. The convection and radiation heat transfer coefficients were again obtained by dividing the samples into six rows and using the empirical relationships given previously. The results of the simulations for the surface nodes of copper layer are given in figures (6.11) to (6.14). The heated regions are shown as shaded rows in each figure.

Figure (6.11) Simulation Results for the Plate with One Heated Island symmetrically situated
$K_{FR4} = 0.343\ W/mK$

40.3 29.6	46.5 30.8	49.5 31.4	51.4 31.6	49.8 31.4	47.0 30.8	41.4 29.6
	71.0 96.4	73.7 97.6	76.0 97.9	74.7 97.6	72.1 96.4	
40.9 29.6	46.5 30.8	49.3 31.4	51.4 31.6	49.3 31.4	46.5 30.8	41.3 29.6

Figure (6.12) Simulation Results for
the Plate with One Heated Island
in the 1st row
K_{FR4} = 0.343 *W/mK*

	66.0 99.9	77.0 101	81.0 102	76.5 101	66.5 99.9	
35.3 26.1	39 26.6	43.4 26.8	44.9 26.8	43.4 26.8	38.5 26.6	34.3 26.1
31.6 25.0	33.7 25.2	35.3 25.3	35.8 25.3	34.8 25.3	33.7 25.2	31.6 25.0
28.9 24.4	30.0 24.5	31.0 24.5	31.0 24.5	30.5 24.5	30.0 24.5	28.9 24.4
28.4 24.0	28.9 24.0	28.9 24.1	29.5 24.1	28.4 24.1	28.9 24.0	28.9 24.0
27.8 23.9	27.8 23.9	27.9 23.9	28.4 23.9	27.8 23.9	27.9 23.9	27.9 23.9

Figure (6.13) Simulation Results for
The Plate with One Heated Islands
in the 2nd row
K_{FR4} = 0.343 *W/mK*

36.4 29.7	41.7 31.0	47.1 31.8	48.1 32.0	46.6 31.8	41.7 31.0	36.4 29.7
	58.6 97.3	67.4 98.5	71.1 98.8	68.5 98.5	60.6 97.3	
34.8 28.2	37.4 28.7	41.2 28.9	42.2 28.9	41.7 28.9	37.4 28.7	34.3 28.2
31.5 27.3	33.2 27.4	35.3 27.5	35.3 27.5	34.8 27.5	33.2 27.4	31.5 27.3
31.0 26.7	31.5 26.7	32.1 26.8	32.7 26.8	32.1 26.8	31.5 26.7	31.0 26.7
30 26.4	30.5 26.5	31.0 26.5	31.0 26.5	31.0 26.5	31.5 26.5	30.5 26.4

Figure (6.14) Simulation Results for the plate with one heated Island in the 3rd row
K_{FR4} = 0.343 *W/mK*

33.2 25.9	34.3 26.2	35.8 26.4	37.4 26.5	36.4 26.4	35.3 26.2	33.8 25.9
33.2 26.3	38.5 27.1	41.7 27.4	43.9 27.5	41.7 27.4	38.0 27.1	34.3 26.3
	59.6 96.2	66.3 97.4	70.6 97.7	66.3 97.4	59.6 96.2	
34.3 25.9	38.5 26.5	41.0 26.8	42.8 26.9	41.7 26.8	39.6 26.5	39.6 25.9
33.2 25.2	34.3 25.4	35.3 25.5	36 25.6	36.4 25.5	34.8 25.4	33.8 25.2
32.1 24.8	33.2 24.9	33.2 25.0	34.3 25.0	33.2 25.0	33.2 24.9	32.1 24.8

In all the experiments described so far, the temperature differences between the experimental and simulated results were in excess of 20 °C in the heated region (100 *mm* × 20 *mm*) and the temperatures simulated anywhere else in the plates were just above the ambient.

To arrive at a solution to this problem it is necessary to consider the parameters that affect the simulations. For conduction these parameters are the thermal conductivities of copper and FR4 insulating board which are used in the calculation of thermal resistances of conduction in the *x*, *y* and *z* directions. For radiation and convection, the heat transfer coefficients are the important quantities which have to be considered.

In chapter (7) techniques will be described which lead to accurate measurement of the thermal conductivity normal to and in the plane of the FR4 fibre-glass boards.

In chapter (8) an optical method will be described which allows the visual inspection of the thermal plumes forming over heated surfaces. This will therefore reveal the convection mechanism by which the heat is lost from the surface of the samples tested in this chapter. Using the results of the optics experiment and a large number of simulations it is then possible to estimate the *h* factor for convection. This leads to a revised simulation model in chapter (8) which gives a better agreement between simulation and practice.

6.2 Conclusions

In this chapter, experiments were described for testing the accuracy of the ASTEC3 thermal modelling procedure in practical situations. The subsequent simulated data have been compared with experimentally measured data.

The modelling has proved successful when applied to uniformly heated structures. In one experiment maximum errors of 4.8% were calculated for measured temperatures of 125 °C.

Experiments using PCB plates with heated islands have shown unexpectedly large errors when simulated. These errors were much higher within the heated islands. The parameters affecting the simulation are the thermal conductivities of the materials, convection and radiation heat transfer coefficients.

The PCB plates are made of a thin layer of copper deposited onto a glass-fibre base. Copper is an isotropic material and its thermal conductivity is well documented. No data were however found for the thermal conductivity of FR4 boards. These boards are fabricated using 8 layers of woven glass sheets bonded together under pressure using epoxy resin and it is therefore highly likely that the boards are anisotropic. If this is true and thermal

conductivity is higher in the plane of the boards than normal to it, then this could account for part of the excess temperatures simulated in the heated areas as the heat is obviously not conducted away. It is therefore crucial that these quantities are measured accurately.

The amount of radiative heat losses is a function of the emissivity of the copper surface which has already been measured quite accurately in appendix (5) and included in the ASTEC3 model. This then only leaves the convection losses to be considered.

The convective heat transfer coefficient is a multifunction variable of which position and temperature are the main factors. In experiments described in previous sections, the simplified methods used to determine these coefficients do not produce acceptable results and will therefore have to be modified for a more exact evaluation of the temperature profile. To produce a more closely matched simulation, a better understanding of the physical processes involved with heat transfer coefficients is required.

7 THERMAL CONDUCTIVITY MEASUREMENTS OF FIBRE-GLASS LAMINATES AND THEIR EFFECT ON SIMULATION

7.1 Introduction

It has been mentioned in chapter (6) that for accurate simulation of the thermal characteristics of the two layer PCB structures, precise values of thermal conductivity are required for both copper and fibre glass layers. Thermal conductivity of copper is well documented [1] and readily available. No data were however found for thermal conductivity of FR4 [2] or any other type of epoxy/glass boards and this had to be measured experimentally.

A rectangular PCB copper cladding board (14 *cm* × 12 *cm*) using FR4 epoxy/glass as the substrate was chosen to demonstrate the effect of thermal conductivity values in the simulations. This was one of the samples already described in chapter (6). One electrically isolated island resembling a resistor on a hybrid circuit was cut into the copper layer of the plate as shown in figure (7.1). This *resistor* was Joule heated by the passage of an electric current of 30 amps and the surface temperatures were measured at selected points along the surface using a HEIMANN infra red pyrometer type KT14 capable of temperature readings to an accuracy of 1.5 °C. As the island was electrically isolated heat conduction from the heated island to its surrounding board was through the fibre-glass substrate only.

An ASTEC3 model of the structure was constructed for simulation purposes using the procedures given in chapter (4). This was a three-dimensional, two layer model consisting of the copper and fibre-glass layers. Each layer was divided into (7 × 6) thermal cells of

Figure (7.1) The Heated Structure used in Thermal Conductivity Tests

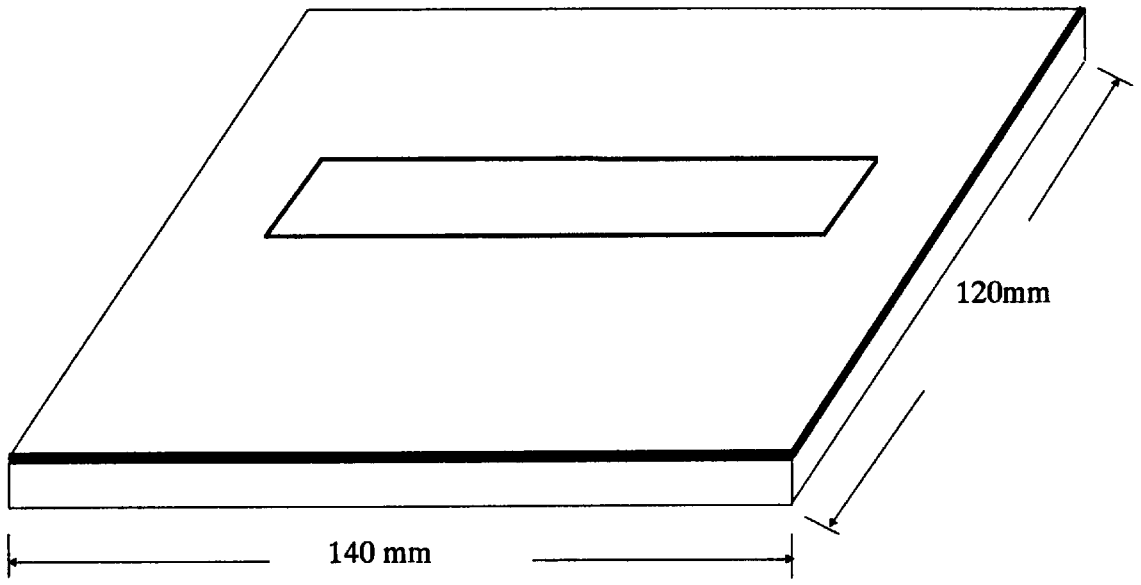

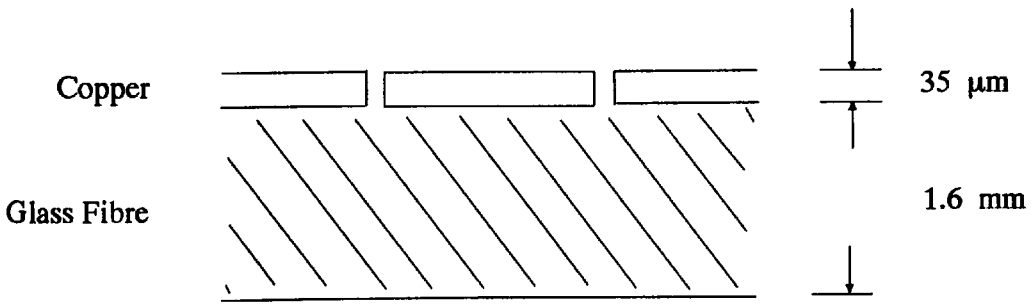

(2 *cm* x 2 *cm*) dimensions. The full description of the model is given in section (6.1.3). In the model, thermal conduction in the copper and fibre-glass layers was taken into account. Convection and radiation from the copper surface were also accounted for and were calculated using empirical relationships given by other workers [3]. These are very rough estimates for the heat transfer coefficients and will be dealt with in chapter (8). Their calculations will not be given in this section since at this stage their values are kept constant in all the simulations.

Initially the fibre-glass layer was assumed to be isotropic and its thermal conductivity was measured using a Lees' disc apparatus which will be described in section (7.2). A value of 0.343 *W/mK* was found which was subsequently used in the model. The results of the simulations are given in figure (7.2) along with the measured temperatures. This is an overhead view of the plate with the heated island in the third row surrounded by double lines. In each cell the top figure is the measured temperature and the bottom value represents the simulated top-node temperature.

These show simulated temperatures of greater than 38% above the experimental results inside the heated island. The temperatures computed anywhere else on the plate are just above ambient which was measured at 23 °C. These observations lead to the conclusion that the heat generated in the island was not conducted away and therefore resulted in excessive temperatures simulated in this area.

Figure (7.2) Simulation Results for
$K_{Isotropic} = 0.343\ W/mK$

	C1	C2	C3	C4	C5	C6	C7
R1	33.2 25.9	34.3 26.2	35.8 26.4	37.4 26.5	36.4 26.4	35.3 26.2	33.8 25.9
R2	33.2 26.3	38.5 27.1	41.7 27.4	43.9 27.5	41.7 27.4	38.0 27.1	34.3 26.3
R3		59.6 96.2	66.3 97.4	70.6 97.7	66.3 97.4	59.6 96.2	
R4	34.3 25.9	38.5 26.5	41.0 26.8	42.8 26.9	41.7 26.8	39.6 26.5	39.6 25.9
R5	33.2 25.2	34.3 25.4	35.3 25.5	36 25.6	36.4 25.5	34.8 25.4	33.8 25.2
R6	32.1 24.8	33.2 24.9	33.2 25.0	34.3 25.0	33.2 25.0	33.2 24.9	32.1 24.8

Top Figure : Experimental

Bottom Figure : Simulated

One possible reason for the observed results is anisotropy of thermal conductivity in the PCB. A matrix of simulated results was obtained by keeping the thermal conductivity normal to the plane K_{normal} constant at its measured value 0.343 *W/mK* and simulating the model with different values of thermal conductivity in the plane of the fibre-glass layer K_{plane}. The heat transfer coefficients were kept the same in all subsequent simulations. The results of these simulations are given in Table (7.1) for in-plane conductivities ranging between 0.7 to 1.5 *W/mK*. Only a selected number of results are shown for comparison. The rows and columns in the table are as shown in figure (7.2).

Table (7.1) Sample Results of the Simulations using Isotropic and Anisotropic Thermal Conductivities					
Position		Isotropic	Anisotropic		
Row	Column	$K_{isotropic}$= 0.343 *W/mK*	K_{normal}=0.343 *W/mK* K_{plane}=0.7 *W/mK*	K_{normal}=0.343 *W/mK* K_{plane}=1.0 *W/mK*	K_{normal}=0.343 *W/mK* K_{plane}=1.5 *W/mK*
R1	*C1*	33.2 25.9	33.2 27.7	33.2 28.8	33.2 30.0
R2	*C3*	41.7 27.4	41.7 30.2	41.7 31.7	41.7 33.4
R3	*C2*	55.6 96.2	55.6 84.6	55.6 78.1	55.6 70.6
R3	*C4*	70.6 97.7	70.6 86.9	70.6 80.8	70.6 73.6
R4	*C5*	41.7 26.8	41.7 29.2	41.7 30.5	41.7 32.0
R5	*C2*	34.3 25.4	34.3 26.9	34.3 27.8	34.3 28.9
R6	*C6*	33.2 24.9	33.2 26.2	33.2 26.9	33.2 27.8

It can be seen from Table (7.1) that a closer agreement between the experimental and simulated results may be obtained with a considerably higher thermal conductivity values along the plane of the substrate than normal to it. This suggests that the reinforced fibre-glass substrates are strongly anisotropic. An experiment was therefore proposed to determine the sensitivity of the results to change in the in-plane thermal conductivity, the normal conductivity having been measured experimentally.

A standard Lees' disc method [4,5] was used to measure the thermal conductivity of materials in the shape of thin flat discs in a direction normal to the plane of the boards (§7.2). This is a method where a disc of the sample and a heater are sandwiched between three metal slabs and the temperatures of the metal discs are measured. It is then possible to calculate the thermal conductivity of the sample by equating the amount of input electrical energy with the heat losses from the system.

A novel technique (§7.3) was devised for measuring the thermal conductivity of these materials in the plane of their surfaces. This technique involves heating rectangular samples of the material at one end and measuring temperatures at various points along the specimen. The experimentally measured temperature distribution is then matched to a distribution obtained from a finite-difference solution, in which only the thermal conductivity value is unknown, to determine the thermal conductivity of the material.

7.2 Thermal Conductivity Normal to the Plane of Glass-Fibre Laminates

An electrically heated Lees' disc apparatus was used to estimate the thermal conductivity in a direction normal to the glass fibre boards.

7.2.1 Apparatus and Equations

The apparatus consists of three flat circular metal discs of good thermal conductivity, figure (7.3), drilled radially where thermometers are inserted. A circular disc of the sample of exactly the same diameter as the metal slabs is sandwiched between discs 2 and 3 and a heating coil between discs 1 and 2. All these components are clamped firmly together and the outside surfaces are coated white to give them the same total emissivity.

In a steady state condition, all the electrical energy supplied to the heating coil is lost from the surfaces of the metal discs and the specimen exposed to ambient air. For a voltage V and current I the following equation applies [4,5]:

$$VI = e\left[A_1(T_1 - T_a) + A_2(T_2 - T_a) + A_x\left(\frac{T_2 + T_3}{2} - T_a\right) + A_3(T_3 - T_a)\right] \qquad 7.1$$

where T_1, T_2, T_3 and T_a are the temperatures of discs 1, 2, 3 and the ambient air respectively. A_1, A_2, A_3 and A_x are the emissive areas of discs 1, 2, 3 and of the specimen respectively. From this equation, e, the power loss per unit area per °C above the ambient is obtained.

The heat flowing into the sample from disc 2 is eventually lost from the surfaces of either the sample or disc 3. If the cross sectional area of the sample is A and its thickness t is very small then the thermal conductivity K may be obtained from the following equation [4,5] where e is calculated from equation (7.1):

$$KA\frac{(T_2 - T_3)}{t} = e\left[\frac{A_x}{2}\left(\frac{T_2 + T_3}{2} - T_a\right) + A_3(T_3 - T_a)\right] \qquad 7.2$$

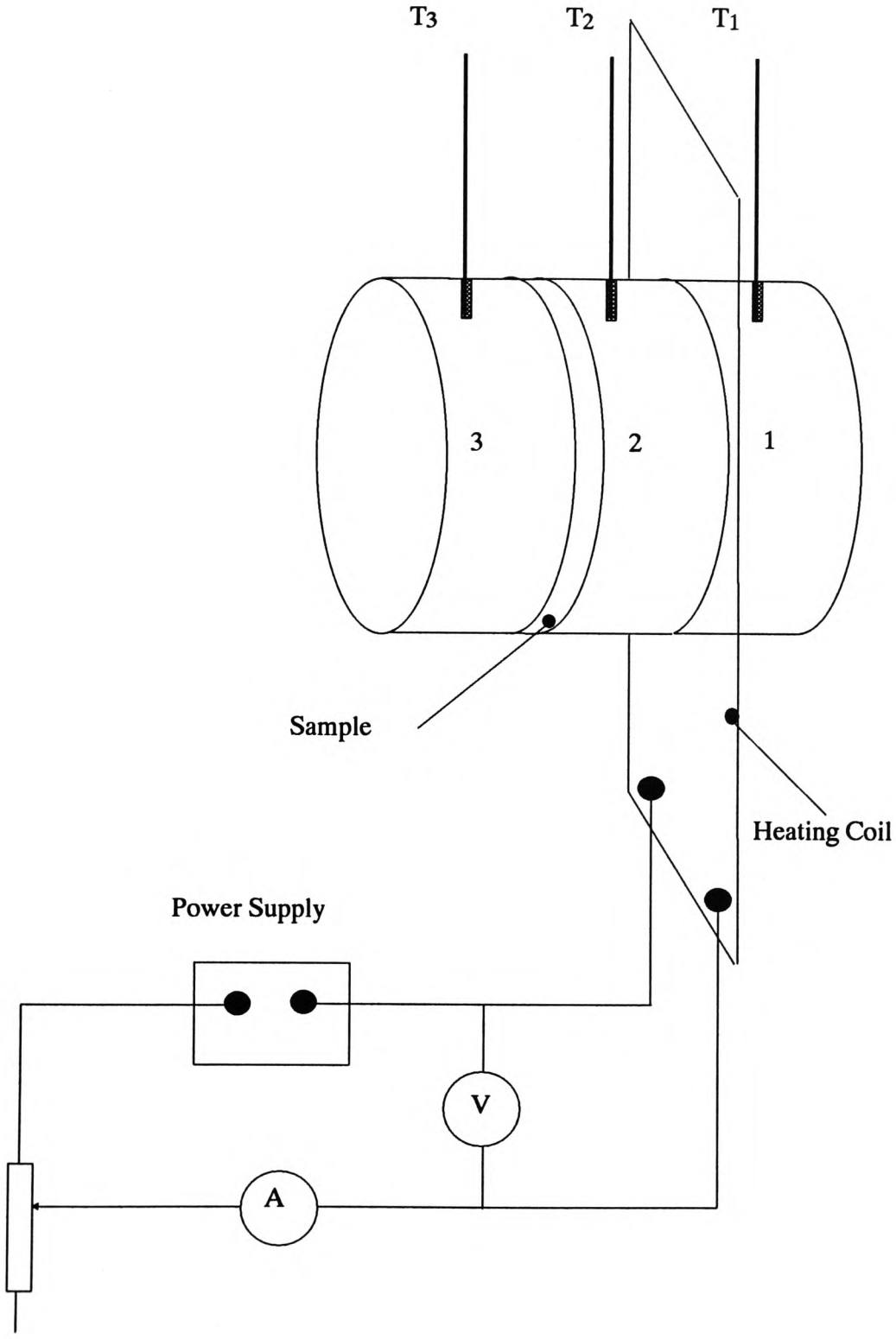

Figure (7.3) A Schematic Diagram of the Electrically Heated Lees' Disc Apparatus

7.2.2 Experimental Procedure

The whole of the Lees' disc apparatus is placed inside a draught-free enclosure to stop any temperature fluctuations that may occur due to the inevitable air currents in the room.

To establish the relationship between the thickness of the sample and its measured thermal conductivity for the particular apparatus and also to test the equipment's reliability, the initial experiments were carried out on a homogeneous material by using PTFE whose thermal conductivity is well-documented. Subsequent tests were then carried out on glass fibre reinforced substrates.

During the steady-state period observations were made at regular intervals as some variation was found in the equilibrium temperatures and the electrical input power. The mean and standard deviation of the mean were then calculated for the thermal conductivity of the particular sample.

The common parameters used in the calculations are given in Table (7.2).

Table (7.2)		
Diameters of all discs		$5.06\times10^{-2}m$
Thickness of all metal discs		$1.26\times10^{-2}m$
Emissive area of disc 1	A_1	$4.01\times10^{-3}\ m^2$
Emissive area of disc 2	A_2	$2.00\times10^{-3}\ m^2$
Emissive area of disc 3	A_3	$4.01\times10^{-3}\ m^2$

7.2.2.1 PTFE

These tests were carried out on samples made of solid sheets of PTFE with varying thicknesses. Tables (A6.1-A6.3) in appendix (6) give the input power, the various temperatures and the resulting thermal conductivities from the particular set of readings. The last row in the tables gives the mean and the error in the mean for the thermal conductivity at that sample thickness. These errors are calculated by using the recommendations given by Topping [6] for combination of errors when a parameter is a function of many variables. This is carried out by inserting in equations (7.1) and (7.2) the errors in each of the thermometer readings (±0.25 °C), voltage (±0.1%), current values (± 0.3%) and the error (±0.005 *mm*) in the micrometer readings of the length measurements. The No. 1 test results in Table (A6.2) given in appendix (6) were arbitrarily chosen for estimation of the errors associated with the thermal conductivity value. Details of these error calculations are given in appendix (7) and show a 5 per cent error in the thermal conductivity obtained via the Lees' disc apparatus.

The three measured thermal conductivities were then plotted against the thickness of the corresponding sample as shown in figure (7.4). A curve fitting program, which uses subroutines from the CAD package GINO for its plotting procedures, was used to best fit a straight line through the points which clearly shows a linear relationship between the two variables. At zero thickness a value of 0.25597 ± 0.013 *W/mK* is found which is in very good agreement and within 0.066% of the quoted value of 0.25586 *W/mK* [7]. The thermal conductivity was extrapolated to zero thickness in order to remove the errors associated with finite sample thickness. The equations are derived assuming that the sample is at a uniform temperature given by the average of the two adjacent metal discs. This assumption leads to errors which increase with thickness and it is reduced to a minimum for samples of negligible thicknesses.

Figure (7.4) Thermal Conductivity of PTFE as a Function of Thickness

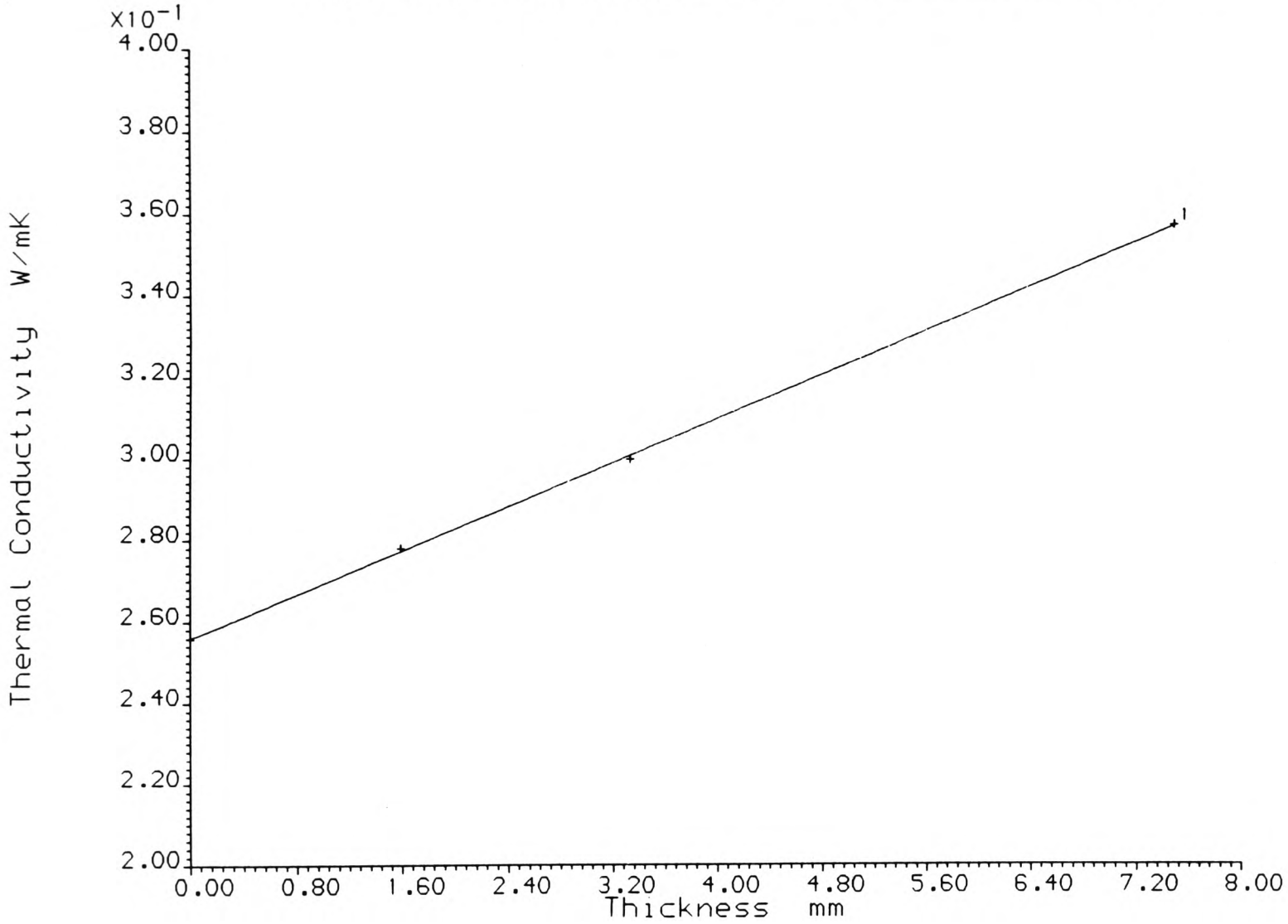

This has illustrated the reliability of the method which was then used to estimate the thermal conductivity of fibre glass boards in a direction normal to their plane.

7.2.2.2 Glass Fibre Boards

The same procedure was repeated to estimate the thermal conductivity of FR4 epoxy glass laminates. Because of the unavailability of glass fibre sheets in different thicknesses 1, 2, 3 and 4 discs of the PCB laminates were clamped together into position. All discs of the sample were cut from the same sheet of fibre glass to exactly the same diameter as the metal discs. These were cleaned with white spirit and polished prior to the experiment. The possible air gaps between the various discs were removed by tightening the clamp screws.

The results of these experiments are given in Tables (A8.1-A8.4) in appendix (8) in the same way as the PTFE results and shown graphically in figure (7.5).

Again by fitting a best straight line through the points and by extrapolation a value of 0.343 ± 0.017 W/mK was obtained for thermal conductivity of fibre glass at zero thickness.

7.3 Thermal Conductivity in the plane of the boards

The following experiment was set up for the measurement of thermal conductivity in-the-plane of the glass fibre laminates. Rectangular samples of FR4 board were heated at one end and temperatures were measured along their lengths. These measured temperatures were then matched with a finite-difference solution of the equation defining the flow along the specimen. The thermal conductivity value in the equation was varied

Figure (7.5) Thermal Conductivity of FR4 as a Function of Thickness

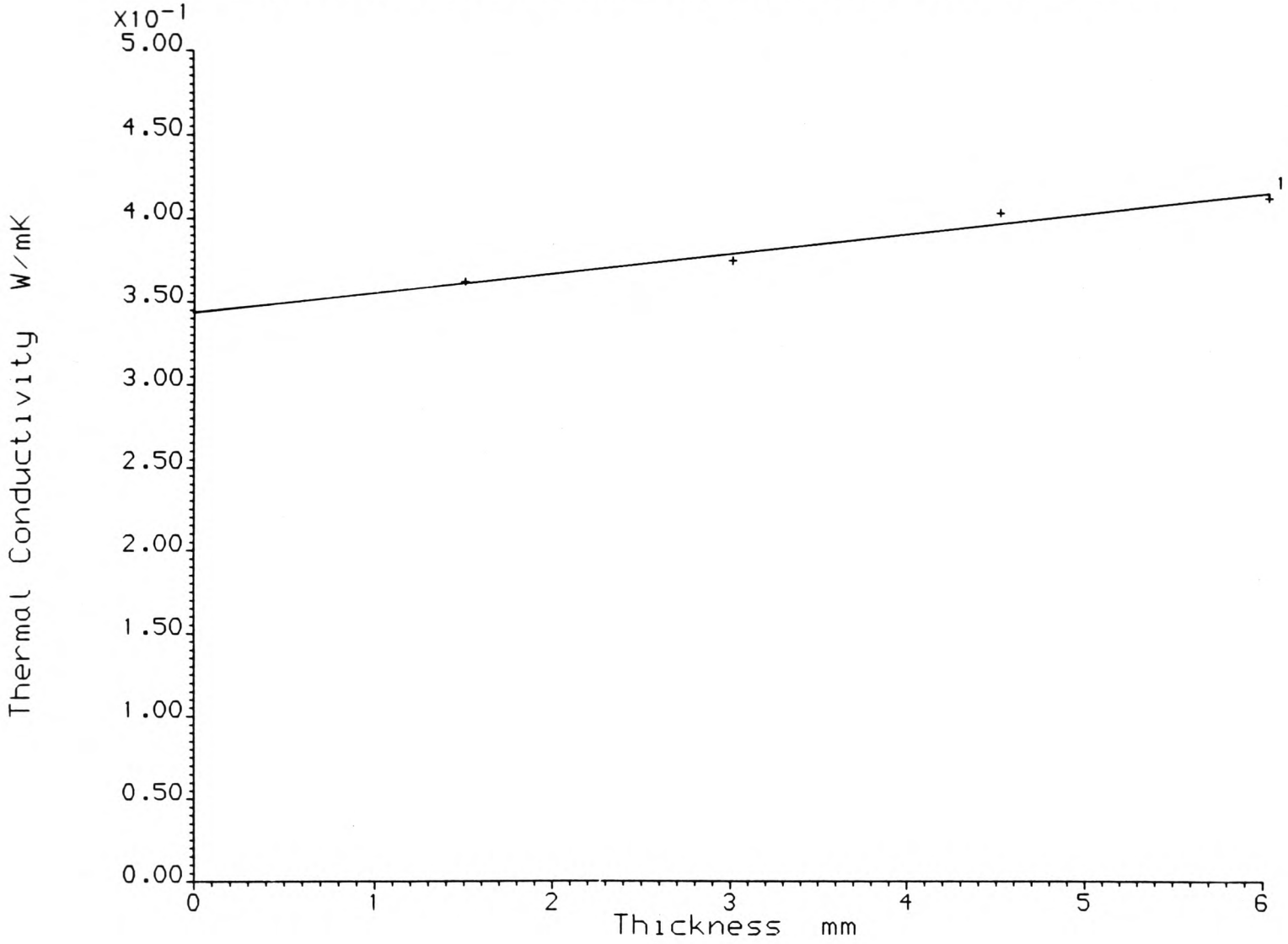

and the resulting temperatures were monitored until the square-root-error between the measured and the calculated values was minimised. This value of thermal conductivity was then taken to be that of the test sample. Finite-difference is a method where a particular structure is divided into small regions called "nodes" and heat balances are made on each of the nodes. This gives rise to a set of linear algebraic equations which can be solved simultaneously for the temperatures at the required points. Errors of the order of $(\Delta x)^2$ [8] are normally expected with the one-dimensional form of this technique, Δx being the space increment.

The experiment was designed in such a way that the heat flow situation was as simple as possible to analyse numerically. The samples were heated uniformly along their widths so that the heat would be travelling along their lengths in a parallel fashion with negligible flow in the direction normal to the main flow. The chosen samples were of small thickness and heated around their perimeter at one end to ensure minimal temperature gradients normal to the faces. Furthermore, the temperatures were determined assuming no convection or conduction from the surfaces. This was achieved experimentally by enclosing the specimen in a vacuum chamber and taking results at several pressures, then extrapolating to zero pressure (perfect vacuum). This left radiation as the only heat loss mechanism. As energy loss by radiation is a function of the surface emissivity the surface was coated with a paint of known emissivity.

Also to simplify the situation further all the temperatures were recorded at their steady-state value. This along with the criteria given above means that a one-dimensional steady-state heat flow equation with only a radiative heat loss term could be adopted.

Rectangular samples were prepared 15 centimetres long and with varying widths of 3, 4, 5 and 6 centimetres. The copper layer of the PCB boards was chemically etched off except

for very small circular patches of about 3 *mm* in diameter along the length of the samples as shown in figure (7.6). Thermocouples were trapped under a very small amount of solder at these positions. Solder does not adhere to the thermocouple tips and it is used here merely to hold the thermocouple tips in good thermal contact with the surface.

Since the emissivity of the boards was unknown, they were coated with *black velvet* paint 2010 with an emissivity of 0.95 made by 3M [9]. Heating wires were wrapped around the first 50 *mm* of each sample and connected to a power supply. The specimen was then clamped onto a holder and placed inside a steel pressure chamber as shown in figure (7.7). The inside walls of the vessel were blackened to stop any reflection. The system was evacuated in order to eliminate the effects of convection and to allow the calculation of the true value of temperature along the sample when radiation is the only heat loss mechanism. The thermocouple wires were taken out through a hole on top of the chamber which was carefully sealed to stop any leakage into the system while pumping down. The output signals of the thermocouples were fed into an AD595AQ thermocouple amplifier circuit with an internal cold junction (ice-point) compensator. A calibrated voltmeter capable of measuring microvolts was subsequently used to monitor the amplified signal and hence the temperatures along the specimen.

Since zero pressure is almost impossible to achieve the following procedure was carried out in order to determine the zero pressure temperatures along the samples.

For a constant electrical input power, the variation of steady-state temperatures with pressure was recorded for each thermocouple. Graphs were produced for temperatures of each point versus pressure in the vessel. By extrapolation, the values of temperature corresponding to zero pressure were obtained for each position.

Figure (7.6) A Block Diagram of the Samples used in Thermal Conductivity Measurements in the Plane of the Boards

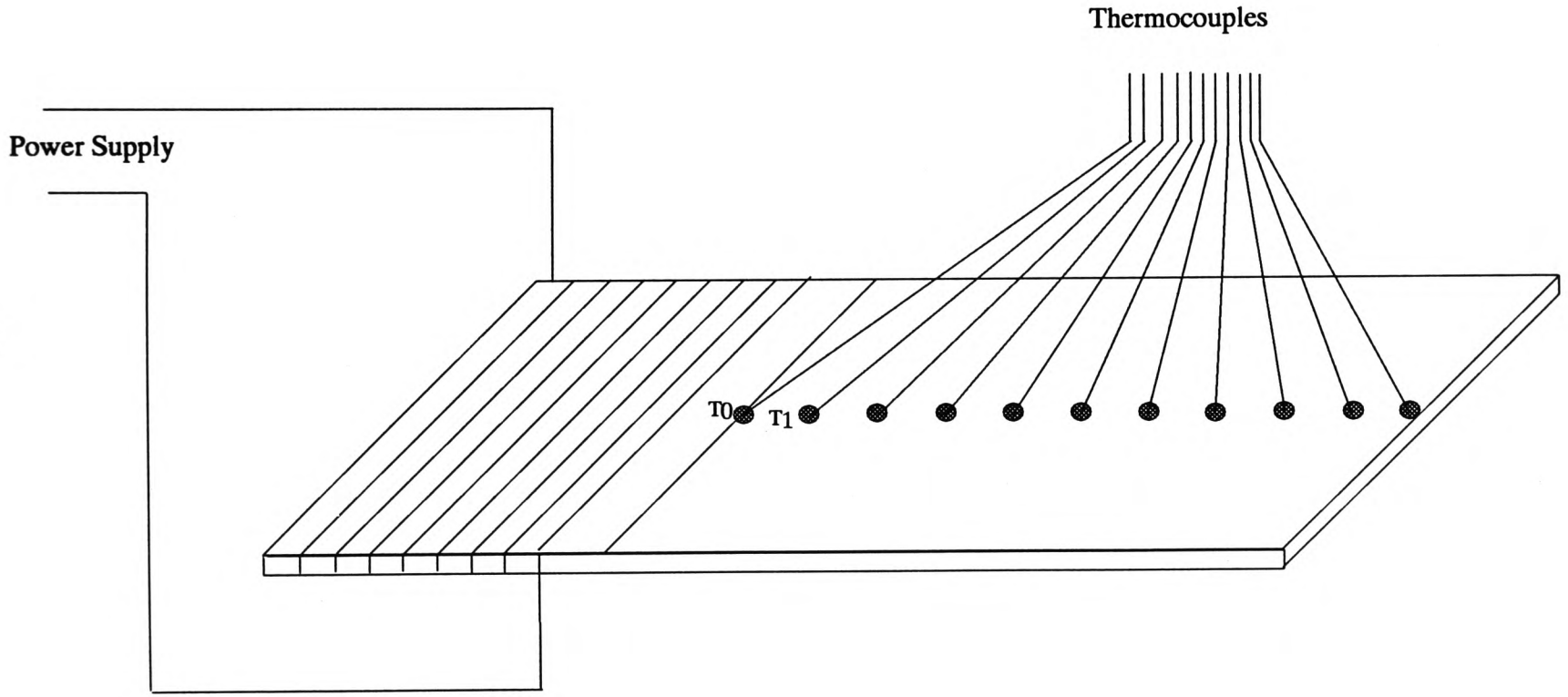

Figure (7.7) A Block Diagram Showing the Vacuum Chamber and the Sample used for Thermal Conductivity Measurements in the Plane of the Boards

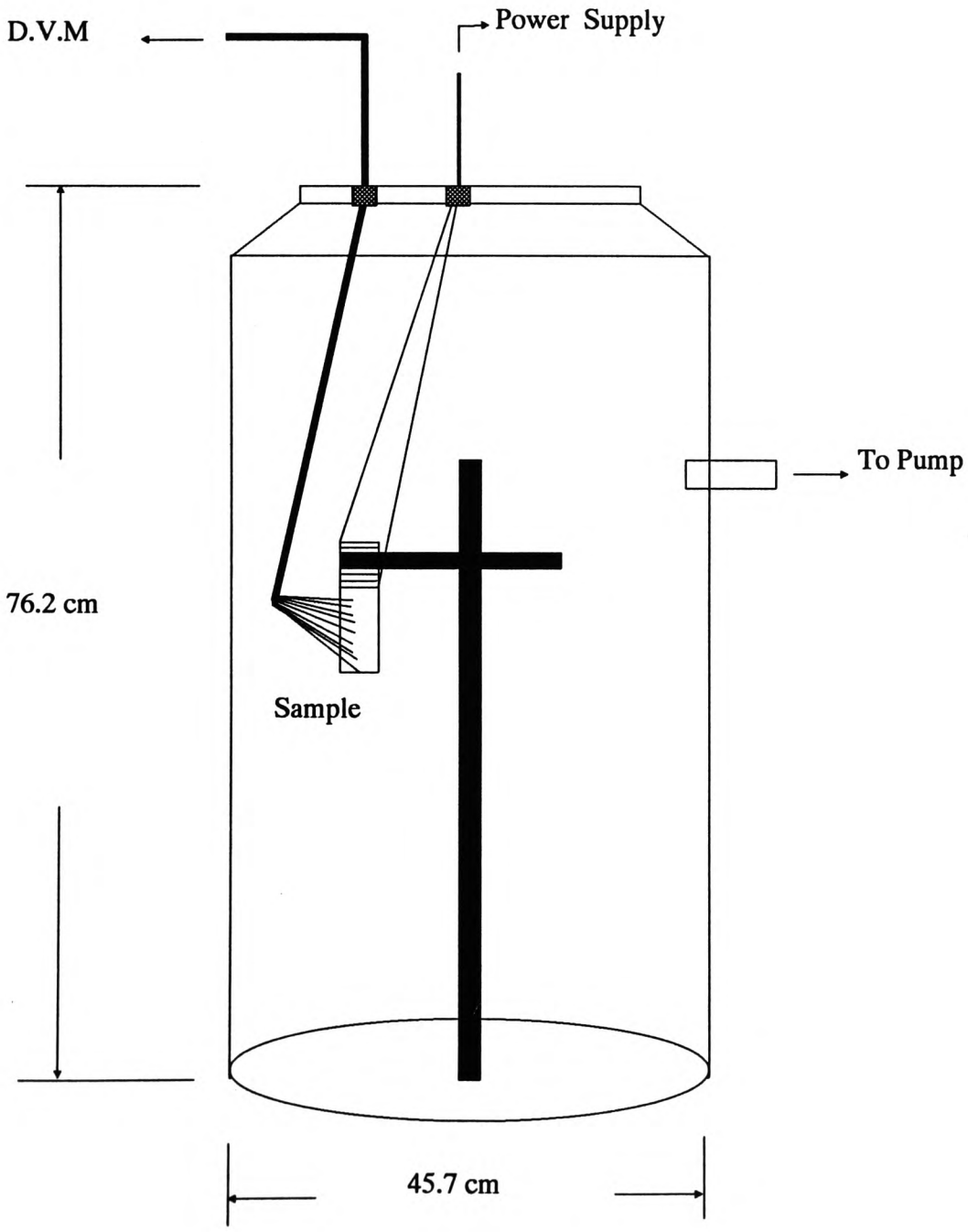

Two samples of each size were tested at different heating levels. A sample graph for a 10 *cm* by 5 *cm* specimen is given in figure (7.8), each line in the graph representing the temperature of each point as a function of pressure in the chamber. The position of each thermocouple for the particular specimen is given in the legend below the graph. The raw results for this sample are presented in Table (7.3) giving the measured temperatures for each specimen at various vessel pressures with reference to figure (7.6). The temperature of each position at zero pressure is given in Table (7.4) as determined from figure (7.8). Temperatures T_6 and T_8 in Table (7.4) correspond to positions 0.06 *m* and 0.08 *m* from the zero position (T_0) of the specimen. These two temperatures were not measured originally and therefore had to be calculated from a graph of zero pressure temperatures versus position. This was a very smooth curve which made it possible to read these two temperatures accurately.

The raw results and the graphical representation of the remaining sample are given in Tables (A9.1-A9.7) and figures (A9.1-A9.7) in appendix (9).

Table (7.3) Temperatures along 2nd 5 *cm* Sample as measured via Thermocouples at various Vessel Pressures

Pressure Torr Temperature °C	13	152	303	455	607	762
T_0	76.92	66.21	60.94	56.93	54.28	51.75
T_1	41.54	33.33	30.05	28.15	27.26	26.06
T_2	27.46	23.47	22.37	21.76	21.58	21.07
T_3	22.16	20.67	20.27	19.86	20.17	19.76
T_4	19.96	19.66	19.56	19.36	19.26	19.26
T_5	18.70	19.26	19.26	18.95	19.16	19.16
T_6	17.94	18.95	18.85	18.75	18.85	18.75
T_7	17.65	18.65	18.65	18.45	18.65	18.55

Figure (7.8) Temperature Vs Pressure For 2nd 10cmx5cm Sample

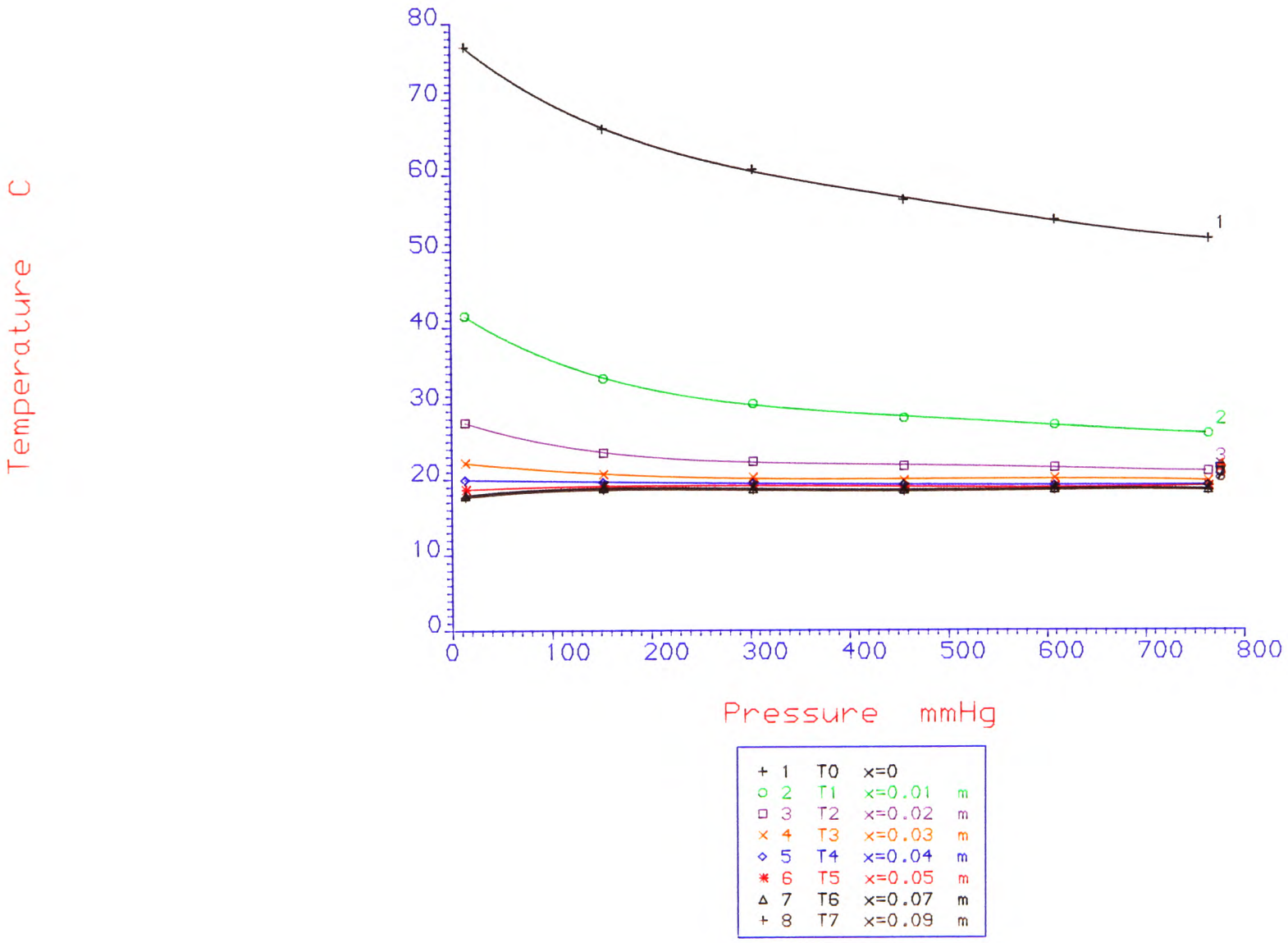

Table (7.4)	
Node	Temperature °C
T_0	78.29
T_1	42.64
T_2	28.02
T_3	22.33
T_4	19.97
T_5	18.67
T_6	18.21
T_7	17.75
T_8	17.60
T_9	17.45
T_V	17.35

A finite-difference method was used to solve the steady-state one-dimensional heat-conduction equation defining the heat flow in thin rectangular plates where heat is only lost by radiation. The resultant temperature distribution was then compared with that found in practice and the only unknown, in-plane thermal conductivity, varied to obtain a best fit.

Finite-difference is a technique whereby the partial differential equation of conduction is replaced by a system of linear algebraic equations for temperatures at a number of nodal points over the region [3]. This gives rise to a set of simultaneous equations which can

be solved for temperatures at the required points.

The fins were divided into ten intervals as shown in figure (7.9). The energy balance for an i^{th} node inside the fin is given by [3]:

$$KA\left(\frac{T_{i-1}-T_i}{\Delta x}\right)+KA\left(\frac{T_{i+1}-T_i}{\Delta x}\right)=\sigma\varepsilon(P\Delta x)(T_i^4-T_V^4) \qquad 7.3$$

where σ, ε, P and A are Stephan-Boltzmann constant, emissivity, perimeter and the cross sectional area of the sample respectively. K and Δx are thermal conductivity and space increment. T_V is the vessel temperature and T_i represents the temperature at the i^{th} node. The energy equation for the last half element is given by:

$$KA\left(\frac{T_9-T_{10}}{\Delta x}\right)=\sigma\varepsilon\left(A+P\frac{\Delta x}{2}\right)(T_{10}^4-T_V^4) \qquad 7.4$$

A set of ten equations were obtained and solved simultaneously by using T_0, the root temperature as measured experimentally. A BASIC program was developed to calculate the other nodal points by stepping through a range of T_1 values, figure (7.6). The program repeats this for thermal conductivity values ranging between 0.7 and 1.4 *W/mK*. In this way, all the nodal temperatures are determined for a range of thermal conductivities. A mean square error value between the extrapolated (zero pressure) and the calculated temperatures is then computed for each value of in-plane thermal conductivity. The program automatically selects the set of calculated results with the smallest error squared value and prints out the corresponding conductivity. This error minimisation technique gives a thermal conductivity value with the smallest sum of the errors squared.

This procedure was repeated for all eight samples, two for each size as given in Table (7.5).

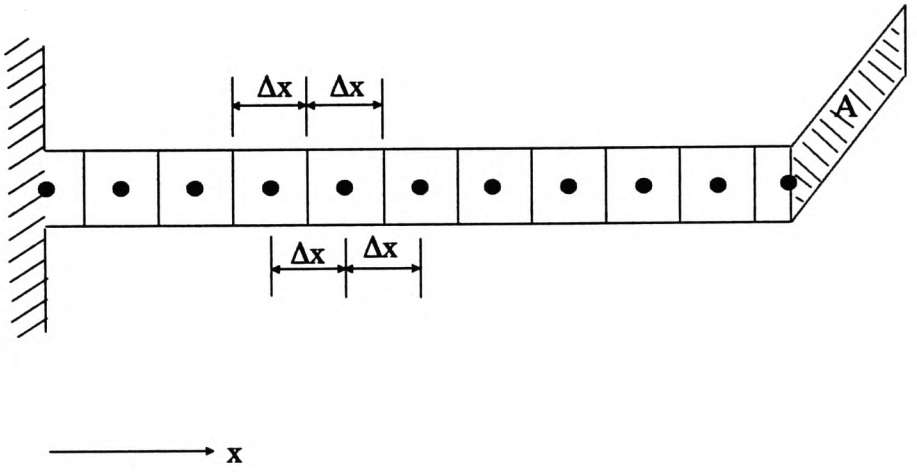

Figure (7.9) The Breakdown of the Rectangular Samples for Finite-Difference Solution

Table (7.5)		
Sample Width ***mm***	**Best-Fit Thermal conductivity** ***W/mK***	
	Sample 1	Sample 2
30	1.090	1.030
40	1.045	1.075
50	1.050	1.055
60	1.055	1.075

From the eight results an average value of 1.059 *W/mK* and standard deviation of 0.019 were obtained for the thermal conductivity in the plane of FR4 boards.

A temperature measured using a k-type thermocouple may have an error of ±0.75% associated with it. The calculated thermal conductivity would clearly have a certain amount of variation due to the uncertainty in the thermocouple readings. To estimate such variations, the following steps were added to the program to calculate the in-plane thermal conductivity within the ±0.75% error margins:

- The highest and lowest possible values were calculated for each data point (0.75% above and below the measured temperature).
- A random value was subsequently generated via the software within the calculated limits.
- These values were then used in an iterative process as explained before to calculate a best-fit thermal conductivity.
- The whole process was repeated 1000 times, each time with a different, randomly generated set of temperatures.
- The lowest and highest values of thermal conductivities calculated in this way for each set of experimentally measured data were recorded.

The maximum and minimum in-plane thermal conductivities calculated for FR4 boards within the error margins of the thermocouples are given for all eight samples in Table (7.6). As expected the conductivities obtained using the nominal temperature values shown in Table (7.5) fall within the range found by the above computations.

Table (7.6)

Sample Width *mm* ↓	**Best-Fit Thermal conductivity** *W/mK*			
	Sample 1		Sample 2	
	Min	Max	Min	Max
30	0.835	1.1	0.86	1.18
40	0.8	1.08	0.865	1.22
50	0.945	1.075	1.01	1.14
60	1.02	1.185	0.995	1.285

In order to verify the accuracy of the iterative technique described in this section, another independent approach was employed to estimate the in-plane thermal conductivity of the boards. This will involve a different calculation method for the parameter using the same temperature profiles as before. A simple conservation of energy criterion will be applied to each sample by which equations are derived relating the thermal conductivity to other known parameters. This is presented in detail in the following section.

7.3.1 Verification of the Technique for the In-Plane Thermal Conductivity Measurement

A simple *heat-in=heat-out* approach is also used to estimate the in-plane thermal conductivity of the FR4 boards. The plate is divided into ten intervals as shown in figure (7.10) and heat balances are written for each of the nodes. The heat conduction into or out of each node along the board is denoted by B and the radiation input by R. The only possible

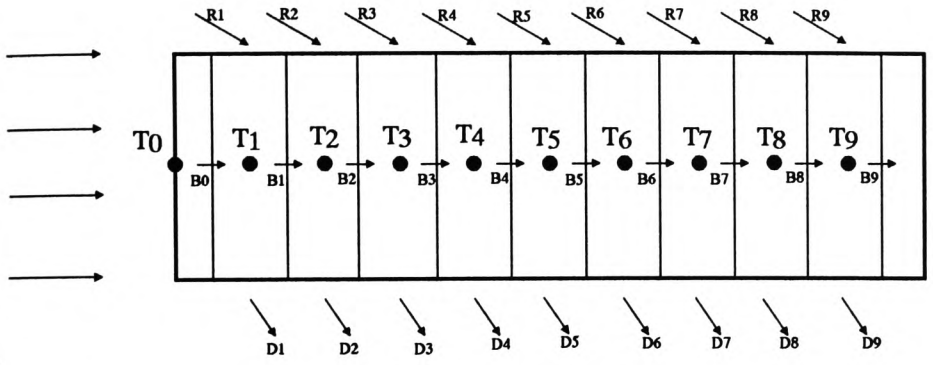

Figure 7.10 The Breakdown of the FR4 Boards for the "Heat Balance" Approach

radiation input to the sample is via the heater assembly. Heat losses are denoted by a collective term D which includes a radiation element out of the node and a conductive one to the vessel walls. At very low pressures convection is assumed to be negligible. The following equations are then developed for each node:

$$B_0 + R_1 = B_1 + D_1$$

$$B_1 + R_2 = B_2 + D_2$$

$$B_2 + R_3 = B_3 + D_3$$

$$B_3 + R_4 = B_4 + D_4$$

$$B_4 + R_5 = B_5 + D_5 \qquad 7.4$$

$$B_5 + R_6 = B_6 + D_6$$

$$B_6 + R_7 = B_7 + D_7$$

$$B_7 + R_8 = B_8 + D_8$$

$$B_8 + R_9 = D_9$$

assuming that the conduction term B_9 from node 9 to the edge of the strip is negligible.

Solving the equations for B_0, an expression is obtained in terms of the radiative input flux R to the strip and the heat loss D from it as follows:

$$B_0 = \sum_1^9 D_i - \sum_1^9 R_i \qquad 7.5$$

B_0 is the thermal conduction from the first node to the second as shown in figure (7.10) and is equal to:

$$B_0 = \frac{KA(T_0 - T_1)}{\Delta x} \qquad 7.6$$

where K is the in-plane thermal conductivity, A is the cross-sectional area and Δx is the space increment.

The first term on the right hand side of equation (7.5) is a collection of conductive and radiative heat losses from the body which may be written in the following form:

$$\sum_{1}^{9} D_i = \sum_{1}^{9} \left(\frac{K_A A_2 (T_i - T_V)}{\Delta x_2} + \varepsilon \sigma A_2 \left(T_i^4 - T_V^{\,4} \right) \right) \qquad 7.7$$

where K_A, A_2 and Δx_2 are the thermal conductivity of air, the surface area of the strip of width Δx and the distance between the sample and the vessel walls respectively. Equation (7.7) may be simplified by taking the constants out of the sums as follows:

$$\sum_{1}^{9} D_i = \frac{K_A A_2}{\Delta x_2} \left(\sum_{1}^{9} T_i - 9T_V \right) + \varepsilon \sigma A_2 \left(\sum_{1}^{9} T_i^4 - 9T_V^4 \right) \qquad 7.8$$

The second term on the right hand side of equation (7.5) is a collection of radiation fluxes received from the heater at different nodes :

$$\sum_{1}^{9} R_i = \sum_{1}^{9} F_{h \to i} \varepsilon \sigma A_2 (T_h^4 - T_i^4) \qquad 7.9$$

where T_i and T_V are the temperatures of node i and the vessel temperature respectively. In the conduction equations the temperatures are in °C and in the radiation ones in Kelvin. $F_{h \to i}$ is the geometrical factor (§3.3.1) for radiation from the heater to the i^{th} node and T_h is the absolute temperature of the heater walls.

$$\sum_{1}^{9} R_i = \varepsilon\sigma A_2\left(\sum_{1}^{9} F_{h\to i} T_h^4 - \sum_{1}^{9} F_{h\to i} T_i^4\right) \qquad 7.10$$

It was found that the majority of the generated heat was conducted away by the sample stand to the bottom of the vessel. The temperature of the exposed surfaces of the heater assembly was therefore small enough so that the radiation term R could be neglected. At zero pressure the air conduction from the sample to the chamber walls is negligible and this may also be omitted from the calculations. Substituting all the significant terms equation (7.5) is reduced to:

$$\frac{KA(T_0 - T_1)}{\Delta x} = \varepsilon\sigma A_2\left(\sum_{1}^{9} T_i^4 - 9T_V^4\right) \qquad 7.11$$

where K is given by:

$$K = \frac{\Delta x\, \varepsilon\sigma A_2}{A(T_0 - T_1)}\left(\sum_{1}^{9} T_i^4 - 9T_V^4\right) \qquad 7.12$$

A sample calculation is shown here for the 5 *cm* wide samples for which the nodal temperatures at zero pressure are shown in Table (7.4). This is as follows:

$$\sum_{1}^{9} T_i^4 - 9T_V = 6.907 \times 10^{10} - 9(7.121 \times 10^9) = 4.97873 \times 10^9$$

The values for the other parameters in equation (7.12) are as follows:

Δx=0.01 *m*

ε=0.95

$\sigma=5.67\times10^{-8}\ W/m^2K^4$

$A=7.5\times10^{-5}\ m^2$

$A_2=1.03\times10^{-3}\ m^2$

Substituting these values in equation (7.12) the in-plane thermal conductivity of the FR4 board is found to be $K_{plane}=1.033\ W/mK$. Similar calculations were carried out on the rest of the eight samples. The full results of these evaluations are given in Table (7.7) along with the values computed using the original technique.

Table (7.7)

Sample		K_{plane} in W/mK	
Width *mm*	No.	Best Fit	Heat Balance Approach
30	1	1.090	0.851
	2	1.030	0.89
40	1	1.045	1.01
	2	1.075	0.908
50	1	1.050	1.033
	2	1.055	1.085
60	1	1.055	1.18
	2	1.075	1.26
Average ± SD		1.059 ± 0.019	1.027 ± 0.144

It can be seen from Table (7.7) that the average in-plane thermal conductivity obtained from the simple approach is in good agreement and within 3% of the iterative technique. The values are very close to thermal conductivity of glass reported as 1.1 W/mK [1] which suggests that along the plane of the boards the majority of the heat is conducted by the woven glass-fibre sheets.

7.3.2 Improved Experiment for the In-Plane Thermal Conductivity Measurements

An improved experimental set-up was also used to measure the in-plane thermal conductivity of FR4 boards as shown in figure (7.11). A vacuum chamber capable of reaching pressures much lower than the original experiment was used for this purpose. Pressures of lower than 5×10^{-2} Torr were made possible using a two-stage rotary pump followed by an oil diffusion pump. To avoid the great amount of heat loss through the stand, the sample/heater assembly was suspended vertically as shown in figure (7.11). The samples were prepared in the same way as before by wrapping heater wires around the first 5 *cm* of the strips. Thermocouples were then attached along the samples using the technique described in section (7.3). Thermocouples were bundled together and led out of the system from a hole in the bottom plate of the vessel. Epoxy resin was used at this point to seal the chamber from the atmosphere. The inside surface of the glass bell-jar was coated with the 2010 black velvet paint as before and subsequently baked in an oven for 2 hours at 150 °C to minimise the outgassing rate. The pressure was measured by a McLeod gauge capable of measuring accurately in the range 10 to 10^{-2} Torr. Temperatures were measured at atmospheric and various pressures below 10 Torr. No measurements were taken in the intermediate range because of the unavailability of an accurate pressure gauge in that range. The results of such measurements are given in Table (7.8).

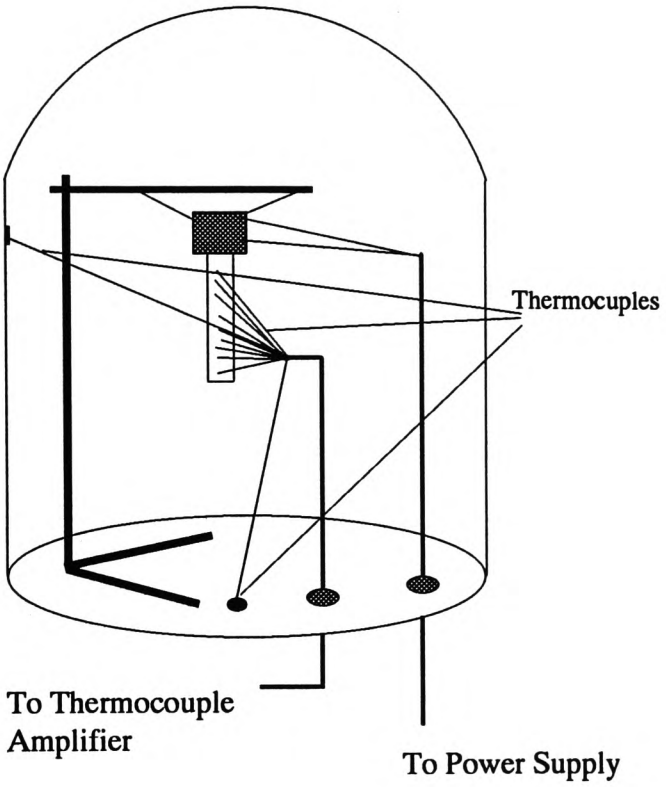

Figure (7.11) The Experimental Set-up for thermal Conductivity Measurements using a High -Vacuum Chamber

Table (7.8)					
Pressure Node	1.5×10^{-2} Torr	0.12 Torr	1.9 Torr	6.5 Torr	760.25 Torr
T_0	75.10	72.51	61.83	58.03	38.68
T_1	52.71	50.46	45.48	43.42	30.83
T_2	43.32	41.33	38.55	37.21	28.69
T_3	38.91	34.13	35.22	34.01	27.86
T_4	36.29	34.59	33.17	32.37	27.40
T_5	34.95	33.32	32.15	31.38	27.10
T_6	33.96	32.37	31.3	30.58	26.84
T_7	32.97	31.58	30.56	29.89	26.59
T_8	32.215	30.88	29.99	29.34	26.37
T_9	31.62	30.29	29.45	28.82	26.08

In order to measure the vessel temperature, thermocouples were attached to the bottom plate of the chamber and to the inside surface of the bell-jar at the heater height. The temperatures recorded from the two thermocouples were different. The thermocouple attached to the bell-jar showed a temperature of 37 °C whereas the one at the bottom plate measured only 26.5 °C. This could only be attributed to the radiated heat from the heater assembly. This was further justified by calculating the total power generated by the heater wires which amounted to 9.15 watts (voltage=12.07 Volts, current=758 *mA*). Simple

calculations show that only a fraction of this power was conducted and radiated away by the sample (0.9 Watts). At pressures as low as 1.5×10^{-2}, the remaining 8 watts can only be lost to the bell-jar by radiation and heating of the inside surface.

The calculations of the in-plane thermal conductivity were carried out at the lowest pressure possible with the current system (ie. 1.5×10^{-2} Torr). Even at such high vacuum levels there may exist some heat losses by convection and conduction through the surrounding air to the vessel. Therefore calculations are carried out in the following sections to estimate the thermal conductivity and convection coefficient for the sample. Calculations will also be presented for the radiation received at the specimen from the heater assembly. This may be significant, as it was found, by measurement, that the surface of the heater assembly exposed to the sample was at a temperature of 120 °C.

Thermal Conductivity of Air at Low Pressure

The thermal conductivity K of any gas may be determined from the kinetic theory in the form [10]:

$$K = \frac{1}{3} n m \lambda C_v \qquad 7.13$$

where n, m and λ are the number of molecules per unit volume (molecular density), mass and mean free path of molecules respectively. C_v is the specific heat capacity of the gas at constant volume.

n and λ at a pressure of 10^{-2} Torr are given as [10] 3.3×10^{20} molecules per m^3 and 5×10^{-3} m respectively. It is known [11] that atmospheric air is a mixture of Nitrogen (78.09%),

Oxygen (20.95%), Argon (0.93%) and Carbon Dioxide (0.03 %). This yields an average molecular weight of 28.96 for air. According to Avogadro there are 6.022×10^{23} molecules per mole of a gas and since there are 28.96 *grammes* of air per mole, the mass of a molecule of air may be found by dividing the former to the latter as follows:

$$m = \frac{28.96 \quad g/mole}{6.022\times10^{23} \quad molecules/mole} = 4.809\times10^{-23} \quad g/molecule = 4.809\times10^{-26} \quad kg/molecule$$

The specific heat capacities of a gas at constant pressure C_p and at constant volume C_v are related by [11]:

$$\gamma = \frac{C_v}{C_p} \qquad 7.14$$

where γ is 1.4 [11] for diatomic gases such as Nitrogen N_2 and Oxygen O_2 which are the largest constituents in a volume of air. The specific heat capacity of air at constant pressure is 1.005×10^3 *J/kgK* and therefore C_v is found from equation (7.14) as 717.85 *J/kgK*.

Substituting all the values in equation (7.13), a value of 1.9×10^{-5} *W/mK* is calculated for the thermal conductivity of air at a pressure of 10^{-2} Torr.

Heat Transfer Coefficient of Convection

An average value for convection coefficient may be estimated using the simplified empirical equations of the type shown below [12] recommended for laminar natural convection from a vertical plate:

$$h_c = 1.42\left(\frac{\Delta T}{L}\right)^{1/4} \qquad 7.15$$

where ΔT and L are the temperature difference between the plate and the ambient and the height of the plate respectively. For convection at lower pressures equation (7.15) may be multiplied by the factor $(P/1.0132)^{1/2}$ [12] where P is the pressure in bars. For a vertical plate with a height of 0.01 metres at an average temperature of 42 °C and an ambient temperature of 26.5 °C in a chamber at a pressure of 10^{-2} Torr (1.333×10^{-5} bars), the convection coefficient may be computed as follows:

$$h_c = 1.42\left(\frac{1.333\times10^{-5}}{1.0132}\right)^{1/2}\left(\frac{15.23}{0.1}\right)^{1/4} = 0.018 W/m^2K$$

which is very small compared to typical values of 5-25 W/m^2K [3] for natural convection and it may therefore be omitted from the calculations.

Input Radiation

The heat transfer by radiation from the heater assembly to the sample may be estimated using the procedure given in section (3.2.1.1). The calculations are carried out with reference to figure (7.12). The configuration is of two rectangular plates at right angles sharing a common edge. The shape factors for such arrangements have been given in the form of plots for a range of (L_1/W, L_2/W) values [12] where L_1, L_2 and W are the lengths of the plates and the width of their common edge. In this case, shape factors will be determined for each division as shown in figure (7.12). The height of the heater assembly exposed to the specimen is denoted by L_h and the shape factor to a cell i as $F_{h\rightarrow i}$. $F_{h\rightarrow 1}$

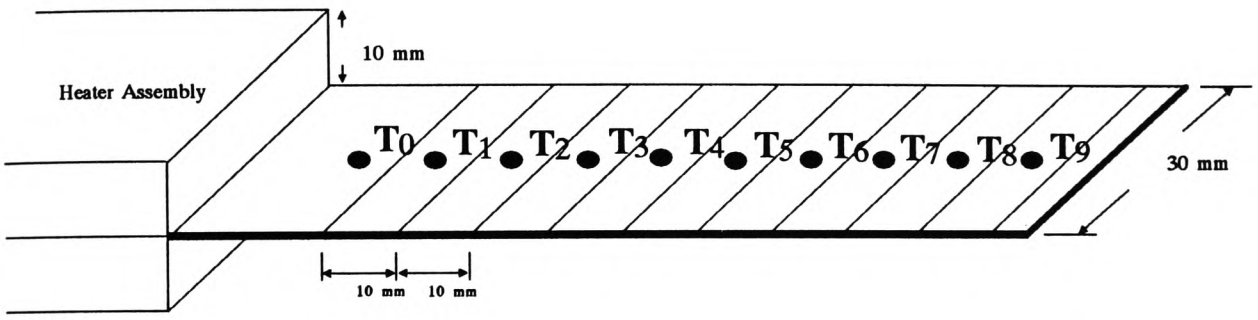

Figure (7.12) The Configuration used for Calculation of the View Factor for the Radiation Received by the Specimen fom the Heater Assembly

is calculated as follows:

$$\frac{L_h}{W} = \frac{0.01}{0.03} = 0.333$$

and:

$$\frac{L_1}{W} = \frac{0.01}{0.03} = 0.333$$

for which the shape factor is read as [12]:

$$F_{h \to 1} = 0.27$$

for division number 2 the following procedure is used (§ 3.2.1.1):

$$\frac{L_{(1+2)}}{W} = \frac{0.02}{0.03} = 0.667$$

for which :

$$F_{h \to (1+2)} = 0.32$$

using relationship (3.29):

$$F_{h \to 2} = F_{h \to (1+2)} - F_{h \to 1} = 0.32 - 0.27 = 0.05$$

The same procedure may be carried out for the rest of the divisions which shows that $F_{h\to 3}=0.02$ and $F_{h\to 4}=0.01$ and so on approximately halving each time. These are subsequently used in the calculations of the radiation received at each space increment.

Calculation of the in-plane Thermal Conductivity

Substituting equations (7.6), (7.8) and (7.9) into equation (7.5) the following relationship is arrived at:

$$\frac{KA(T_0-T_1)}{\Delta x}=\sum_{1}^{9}\left(\frac{K_A A_2(T_i-T_{v_i})}{\Delta x_2}+\varepsilon\sigma A_2\left(T_i^4-T_{v_i}^4\right)\right)-\sum_{1}^{9}F_{h\to i}\varepsilon\sigma A_2(T_h^4-T_i^4) \qquad (7.16)$$

The parameters for the equations are as follows:

$K_A = 1.9\times10^{-5}\ W/mK$

$A_2 = 0.01\times0.63=6.3\times10^{-4}\ m^2$

$\Delta x_2 = 0.15\ m$

$\varepsilon = 0.95$

$\sigma = 5.67\times10^{-8}\ W/m^2K^4$

$F_{h\to i}$ = As calculated in previous section

$A = 4.5\times10^{-5}\ m^2$

$\Delta x = 0.01\ m$

These values are substituted in the individual terms in the right and left hand sides of equation (7.16) as follows:

$$\frac{KA(T_0 - T_1)}{\Delta x} = \frac{K \times 4.5 \times 10^{-5}(75.1 - 52.71)}{0.01} = 0.1K$$

$$\frac{K_A A_2}{\Delta x_2}\left(\sum_1^9 T_i - \sum_1^9 T_{v_i}\right) = \frac{1.9 \times 10^{-5} \times 6.3 \times 10^{-4}}{0.15}(336.945 - 314) = 1.831 \times 10^{-6}$$

$$\sum_1^9 \varepsilon\sigma A_2\left(T_i^4 - T_{v_i}^4\right) = 0.95 \times 5.67 \times 10^{-8} \times 6.3 \times 10^{-4}(8.03465 \times 10^{10} - 8.397 \times 10^{10})$$

$$= 0.122963$$

Substituting these values in equation (7.16) we get:

$$0.1K = 1.831 \times 10^{-6} + 0.122963 - 0.0181$$

from which the thermal conductivity K along the plane of the boards is computed as:

$$K = 1.0486\ W/mK$$

The results from the new apparatus capable of a high level of vacuum are in very good agreement with the results obtained from the previous set-up. It has been demonstrated that the technique by which the zero pressure temperature along the specimen is determined is valid. Therefore a very good vacuum chamber is not essential for thermal conductivity measurements although if such a vessel is available, the sequence for determining the zero pressure temperatures may be omitted from the calculations hence simplifying the procedure.

7.4 Simulation of original Test configuration using the measured Thermal Conductivities

The computer model of the PCB structure shown in figure (7.1) was modified to account for the anisotropic thermal conductivity. This was carried out by calculating thermal resistances using the measured anisotropic thermal conductivities in-the-plane and in normal directions. The results of the steady state simulations are given in figure (7.13) which shows a marked reduction in the errors between the simulated and measured temperatures compared with earlier simulations, which assumed isotropy. For example, this error is 12.88% at the centre point of the heated island compared to 38.4% simulated previously.

Figure (7.13) Simulation Results using the Measured Anisotropic Thermal Conductivities
$K_{plane} = 1.059\ W/mK$
$K_{normal} = 0.343\ W/mK$

33.2 29.0	34.3 29.6	35.8 30.0	37.4 30.2	36.4 30.0	35.3 29.6	33.8 29.0
33.2 29.8	38.5 31.2	41.7 31.9	43.9 32.2	41.7 31.9	38.0 31.2	34.3 29.8
	59.6 77.0	66.3 79.1	70.6 79.7	66.3 79.1	59.6 77.0	
34.3 29.1	38.5 30.2	41.0 30.8	42.8 30.9	41.7 30.8	39.6 30.2	39.6 29.1
33.2 27.6	34.3 28.0	35.3 28.3	36.0 28.4	36.4 28.3	34.8 28.0	33.8 27.6
32.1 26.9	33.2 27.1	33.2 27.2	34.3 27.3	33.2 27.2	33.2 27.2	32.1 26.9

7.5 Conclusions

In this chapter the anisotropic thermal conductivity of FR4 epoxy/glass laminates used for printed circuit boards has been measured. A technique has been described for measuring thermal conductivity in the plane of a thin flat board. This technique may be used in other areas of research where thermal conductivity of materials in the form of thin flat boards is required. An electrically heated Lees' disc apparatus is also used to determine this quantity in a direction normal to their plane.

PTFE was used as a standard sample to evaluate the reliability of the Lees' disc apparatus. A value of 0.25597 $W/mK \pm 0.013$ was measured which is very close to the quoted value of 0.25586 W/mK. The subsequent measurements on samples of FR4 laminates yielded an average value of 0.343 ± 0.017 W/mK for the thermal conductivity in a direction normal to the plane of the boards.

The thermal conductivity in the plane of the boards was measured using a novel technique involving the use of a vacuum chamber. Two different vacuum vessels were employed for this purpose. Values of 1.059 W/mK and 1.048 W/mK were obtained using a moderate vacuum (around 10 Torr) and a much better vacuum (1.5×10^{-2} Torr) respectively.

These experiments have demonstrated that the thermal conductivity of these reinforced boards in a direction tangential to their surfaces is almost three times greater than that normal to their planes.

The sensitivity of the simulated temperatures to thermal conductivity and heat transfer coefficients of convection and radiation has been mentioned before. It has been demonstrated that using the correct values of thermal conductivity of fibre glass the

simulation errors of nearly 40% have been reduced to around 12%. The remainder of the discrepancies between the experimental and the simulated temperatures may be due to the wrong values of heat transfer coefficients. These factors will be investigated in detail in chapter (8).

8 SCHLIEREN EXPERIMENT FOR VISUALISATION OF NATURAL CONVECTION PLUMES

8.1 Introduction

As previously mentioned in chapter (6), the simplified procedure for calculation of heat transfer coefficient of convection h_c has proved unsuccessful. Using the particular method used in that section a higher value of h_c was obtained for the heated island than in the unheated cooler regions. This of course may not necessarily be true.

From the boundary layer theory the convection mechanism from a surface occurs in two stages, first via conduction in a thin layer near the surface and then by advection in the main fluid. The conductive heat loss at any point in the layer adjacent to the surface is a function of the temperature gradient at that point [1]. Thermal boundary layer thickness increases as the flow develops inwards from the edge of the plate and accordingly the magnitude of the temperature gradient and hence the heat transfer by conduction decrease. The convective heat losses would therefore be higher near the edge of a plate decreasing towards the centre of the plate.

To investigate the nature of the plumes forming over the composite structures used in the experiments described in chapter (6) and hence the heat loss mechanism, an optical technique was utilised. This was a Schlieren method which is used for examination of refractive index variations in a medium caused by density gradients in that region.

8.2 Theory of Operation

A Schlieren apparatus is an optical device which was originally developed for observing the shock waves that form around aerofoils in jet aircraft and bullets in ballistics [2,3]. These shock waves normally form when the flight of these objects is at supersonic speeds.

The Schlieren method allows the observation of the density gradients as variations in the intensity of illumination. For instance, an increase or decrease in temperature around a body alters the density of the fluid surrounding that body as a result of which the refractive index of the fluid in that region changes. This phenomenon then causes a change in the direction of any light that is passing through the medium and due to variations in the directions of the light rays, more or less light will pass a knife-edge (cut-off) in the apparatus and hence lighter/darker regions appear on a viewing screen.

The arrangement of the Schlieren system may be explained by referring to figure (8.1). A beam of parallel light is obtained by passing the light from a source, *s*, through a lens L1. The source is in form of a rectangular cut-out placed at the focus of a lens as shown in figure (8.1a). After passing through the test section, the beam of light is focused by a second lens L2. An image of the source is obtained at the focal plane, p, of lens L2. A portion of the light is then cut off and the remainder passes through this plane and is directed onto a screen via an objective lens L3.

The focusing mechanism may be explained in the following fashion considering beams of projection from given points rather than individual rays. For example, a point, *a*, in the source emits a projected beam *abc* which is focused on, *a'*, at the image plane, *p*. In the same way all the other points in the source are focused onto their corresponding points

(8.1)

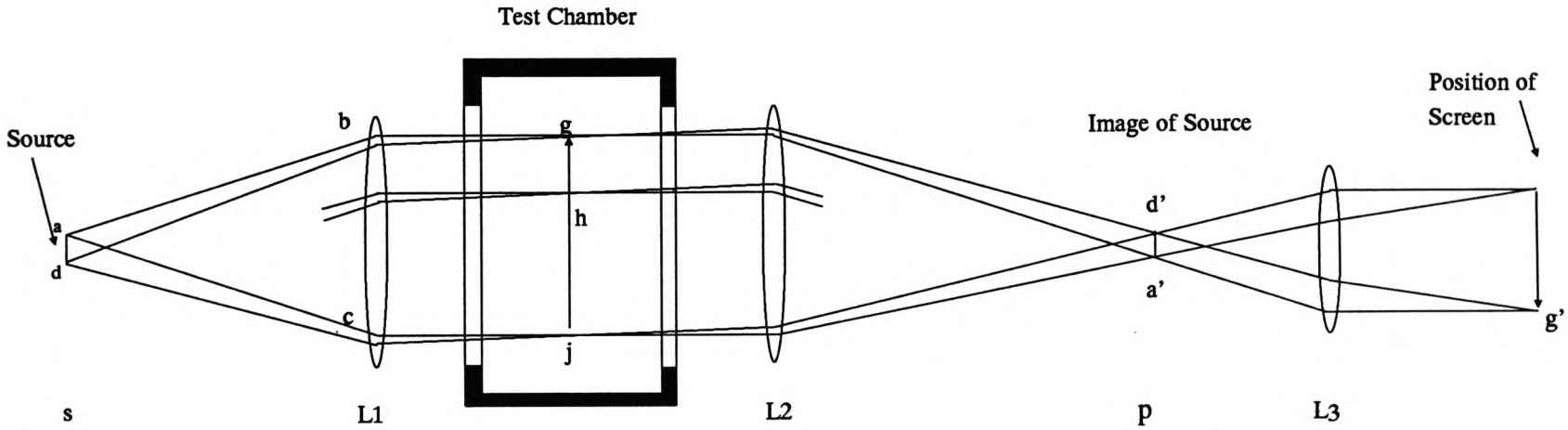

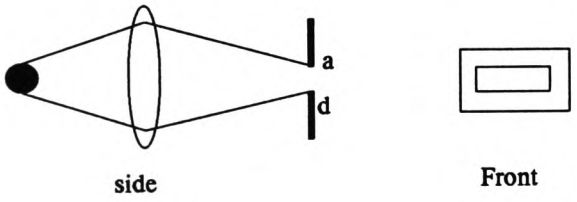

(8.1.a)

Figure 8.1 Schlieren System With Lenses

in *p*. It should be noted however that each projected beam of light completely fills the whole of the test section and hence each point in the image receives light from every portion of the test section.

Furthermore, the light reaching a point, *g*, in the test section via projection from *a* and *d* namely *adg*, is transmitted within *gd'a'*, which is focused at, *g'*, on the viewing screen. This beam passes through the image plane, *p*, and completely fills it. Other beams from the test section are also focused at their image points on the screen and can subsequently an image of the test section is produced there.

As described and shown in figure (8.1) all the beams of light overlap in plane, *p*. Therefore if part of the light is obscured at this plane, only the intensity of the illumination of the final screen is reduced. All parts are however darkened at the same rate since all the beams are affected equally.

Now if one of the beams is deflected by a linear angle θ at the test section due to a refractive index change, figure (8.2), then it would not overlap the other beams at the focal plane of L2 and its image point on the screen will be darkened by a different amount which will result in a darker or lighter point compared with the rest of the field [4]. This of course depends on the position of the displaced image at the knife edge.

Assuming that the distance along the pencil is f_2, the focal length of lens L2, then the displacement Δh, figure (8.2), due to angular displacement θ can be approximated for small angles as [4,5] :

$$\Delta h = f_2\theta \qquad 8.1$$

Considering a perpendicular axis, ΔI, as shown in figure (8.2) could be calculated in a similar manner.

The knife edge is set parallel to the long side of the slit and hence its image at the plane, p is as shown in figure (8.3). This leaves a portion h_1 of the image uncovered. The intensity of illumination of the screen, I, is therefore proportional to h_1. If a point on the screen then has an additional illumination ΔI imposed upon it (due to the deflected beam) then ΔI would be proportional to the displacement Δh. A contrast may then be defined as [4,5] :

$$c = \frac{\Delta I}{I} = \frac{\Delta h}{h_1} \qquad 8.2$$

by substituting for Δh in terms of f_2 and θ, c becomes:

$$c = \frac{f_2 \theta}{h_1} \qquad 8.3$$

Considering interactions across a test area L it has been shown [4] that for a plane flow (ie. where conditions are the same in all x-planes), the angle of deflection θ after a ray has passed through a box with density variation in the y direction, figure (8.4), may be given by the following relationship:

$$\theta = \frac{L\beta}{\rho_s}\left(\frac{d\rho}{dy}\right) \qquad 8.4$$

L represents the total interaction length and is given by the width of the box which is the distance the rays travel before emerging from the box. β and ρ_s are parameters which determine the refractive index and according to:

$$n = 1 + \beta\frac{\rho}{\rho_s} \qquad 8.5$$

ρ is the actual density and ρ_s is a reference density [4] for the particular gas in the medium measured at standard conditions which for a temperature of 0 °C, pressure of 760 *mmHg* and at a wavelength of 5893 *Å*. β is a dimensionless quantity [4] which for example for

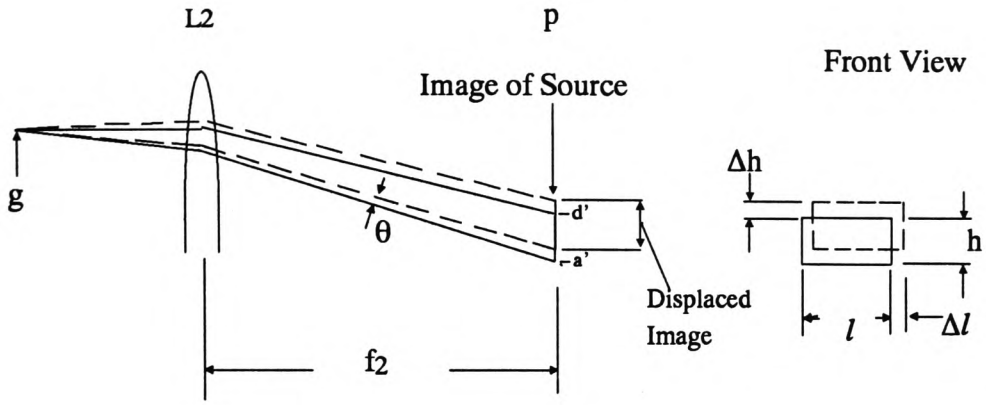

(8.2)

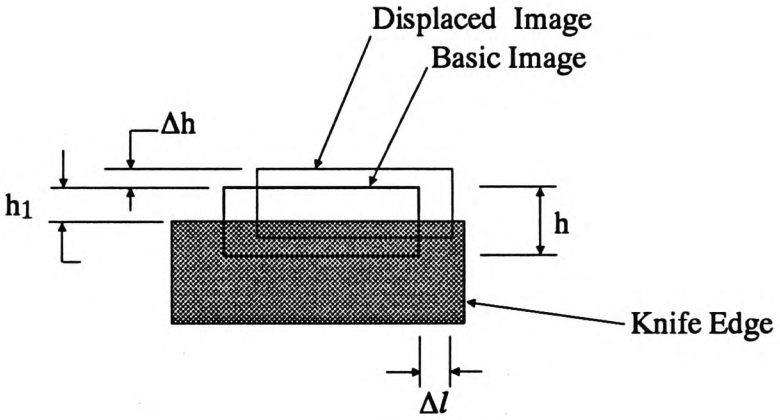

(8.3)

Figure (8.2) Displacement of Part of the Light due to Refraction
Figure (8.3) Interception of Source Image by an Opaque Cut-off

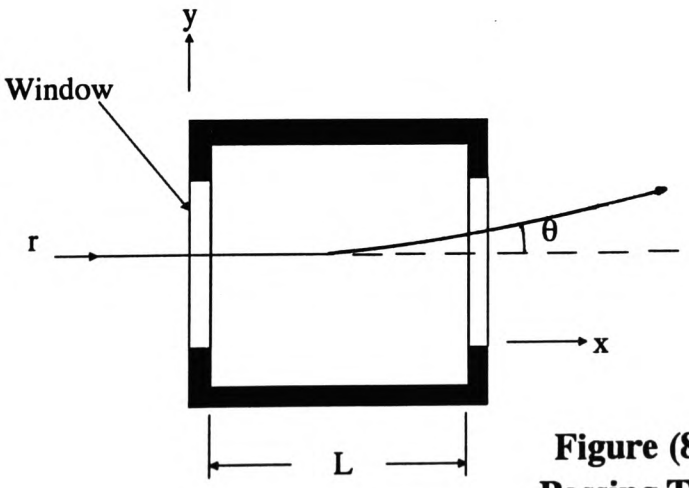

Figure (8.4) Refraction of a Ray Passing Through a Chamber with interactions throughout the length L

air at 5893 $\AA$ is equal to 2.92×10^{-5}. It can therefore be seen that the contrast on the screen is a function of density gradients, density and refractive index in the test section given by:

$$c = \frac{f_2 L(n-1)}{h_1 \rho}\left(\frac{d\rho}{dy}\right) \qquad 8.6$$

An increase or decrease in the intensity of illumination at the viewing screen is directly proportional to the density changes in the flow.

In order to obtain a large field of view, a large aperture lens would be required [6]. Designers have therefore developed Schlieren apparatus where lenses are replaced by a system of mirrors which are cheaper to produce. The internal quality of glass is also not of great importance in mirrors and at the same time less light is lost in a mirror than in a lens [5]. Of course by using mirrors the chromatic errors normally associated with lenses are avoided [6].

8.3 Experiments for the Estimation of the Convection Coefficients

A Schlieren apparatus was used to examine the convection plumes forming over the partially heated PCB boards. This was done in order to ascertain the variation of the convection coefficient over the surface and how it is possible to simplify the definition of this parameter in the ASTEC3 thermal model of the structure.

8.3.1 Apparatus

The apparatus used in this experiment also utilised mirrors. A schematic layout of the system is shown in figure (8.5). The various components of the apparatus were as follows:

Mirrors

These were very high quality spherical mirrors which were vacuum deposited with very thin layer of metallic aluminium.

Light source

The light source was a 36 Watt bulb with a single straight axial filament. This is important since bulbs with V-shaped filaments cannot be used for this application. A condenser lens and a collimating slit were used to ensure that the bundle of rays passing the cut-off at the focus of mirror M1 was truly rectangular.

The Cut-off

A razor blade was used for the knife-edge. It was mounted such that it could be positioned accurately in the focus of mirror M2 using micrometer screws.

Projector Lens and Viewing Screen

A projecting lens L2 was used to direct the image from the cut-off onto a ground glass screen. A tube between the lens and the screen prevented stray light falling onto it and also provided a focusing adjustment.

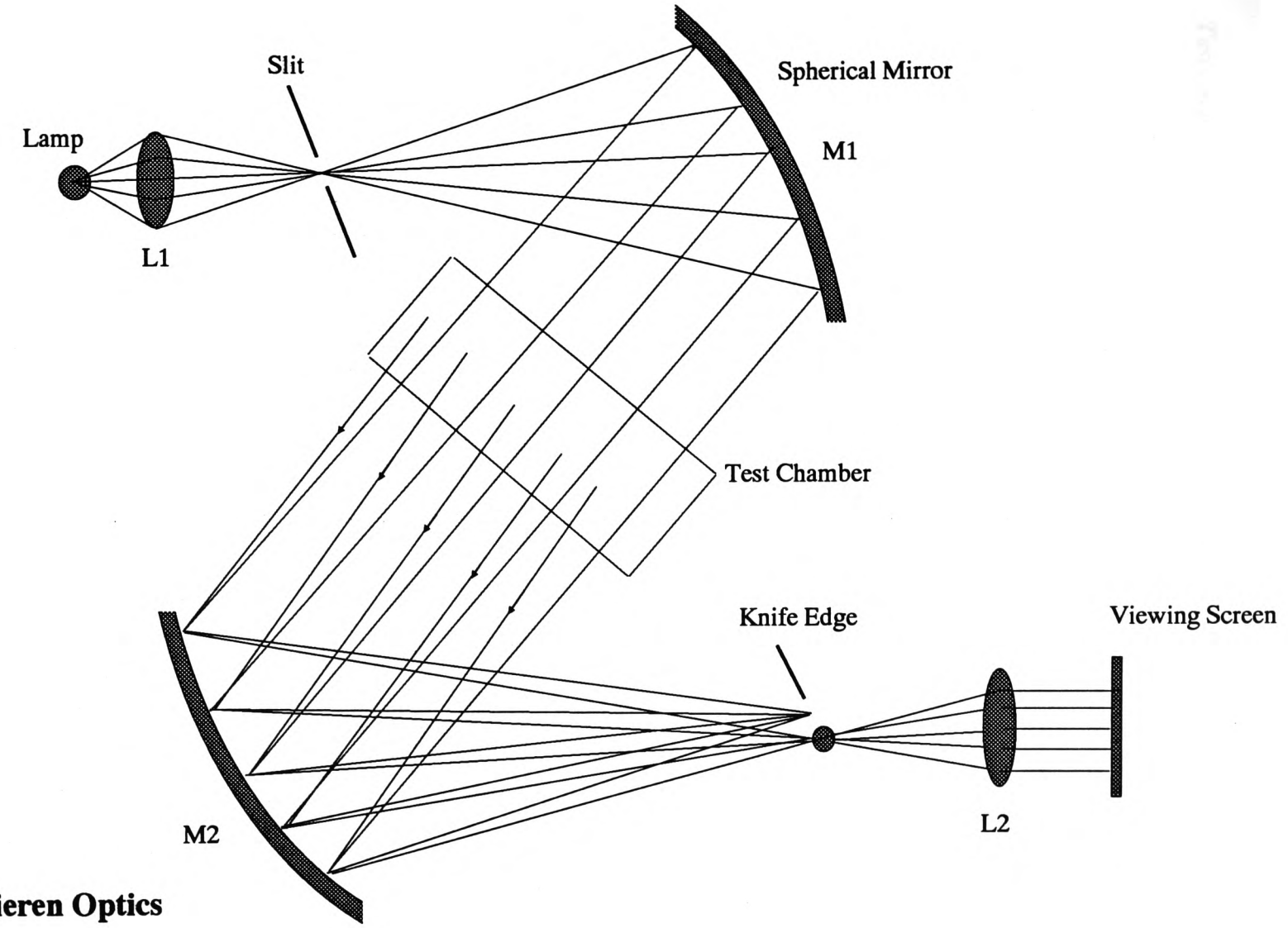

Figure (8.5) Schlieren Optics

Test Section

A box was made almost the same size as the one used for temperature measurements in chapter (6). It was large enough to stop the plume being affected by reflected fields from the walls of the chamber. Two square holes were cut into two opposite vertical faces of the box large enough to allow the parallel beam of light to pass through it. Unused photographic plates were fixed at these positions and the test chamber was sealed very carefully to avoid any draughts from the room.

8.3.2 Experimental Procedure

The following steps were taken to set up the system [7]:

a The position of the condenser lens L1 with respect to the bulb was adjusted until a sharp image of the filament was observed on the knife edges of the slit. Micrometer screws were then used to centralise the slit within the image of the filament.

b The light source assembly was tilted and rotated on its base until the beam emerging from the slit was horizontal and filled the mirror M1. The distance between the centre of the mirror and the slit was then adjusted to the focal length of the mirror.

c The height of mirror M1 was adjusted so that the beam of light deflected was parallel and passed through the windows of the test box. To check if the beam was parallel and horizontal, a piece of paper was placed on the window and the attitude of the mirror adjusted until the disc of light on the paper was circular. The slit assembly was then moved very slightly backwards and forwards until the diameter of the disc of light was the same as the mirror.

d The height of the second mirror at the other side of the test chamber was adjusted so that the beam of light just filled it.

e The lens L2/screen assembly was positioned so that a clear and bright image could be viewed on the screen.

f The focal plane of mirror M2 was found using a piece of paper and the knife-edge assembly was placed in this position. The cut-off was then used to obscure a portion of the image at the plane *p*. When the set-up was carried out correctly, the illumination of the picture on the viewing screen was uniform and no matter what proportion of light rays were obscured it stayed uniform.

8.3.3 Tests and results

The results from the Schlieren apparatus were in the form of photographs which were taken from the ground-glass viewing screen. A 35 *mm* Single Lens Reflex (SLR) camera fitted with a macro-lens was used for this purpose. The camera was mounted onto a sturdy tripod to reduce the risk of camera-shake during the long exposures needed for photographing the fairly dark screen. Furthermore, 400 ASA Black & White films were chosen as a compromise between the film speed and the subsequent grain size in the final prints.

Some of the enlarged photographs were found to be very faint and in order to enhance the shape of the plume in the photographs, further processing was carried out on the prints. A Desk Top Publishing Package called PUBLISHS PAC™ was used for this purpose. This is a software package which allows any form of print or text to be scanned via a line scanner. The scanner breaks the image into a number of pixels which can be preset by the user with a maximum of 300 dpi (Dots Per Inch) as used here. A Black & White bit-map

representation of the image is then produced on a VDU screen with continuous shades of grey. By adjusting brightness and contrast controls, it was possible to improve the quality of the displayed image. A Polaroid instant camera with a large hood was then used to photograph the VDU screen.

The Schlieren apparatus was used to view the plumes formed over a few of the samples already described in chapter (6). Details of the samples, the current input and the viewing directions are as follows:

Case 1 The (140 *mm* × 60 *mm*) copper clad board was positioned horizontally with its 140mm edge parallel to the direction of the light beam. The sample was heated by passing currents of 20, 30 and 40 amperes through the central island. At each current level the system was left to stabilise and to reach a steady-state condition. Final adjustments were made for the best possible image as viewed on the screen and then photographs were taken from the screen. The results of this experiment are given in figures (8.6) to (8.8), which are the photographs taken directly from the ground-glass screen.

Case 2 The same plate was heated in the same way and viewed in a direction perpendicular to the 140 *mm* edge. No photographs are presented here since there were no natural convection plumes visible as viewed from this direction. This was perhaps because of the small temperature gradients which exist along the length of the sample.

Case 3 The (140 *mm* × 120 *mm*) plate with an island in position 3 in figure (6.10), heated with a current of 30 amperes. The sample was viewed in a direction parallel to the length of the heated island. Figures (8.9) and (8.9a) show the plume, the former being the actual photograph and the latter the processed image.

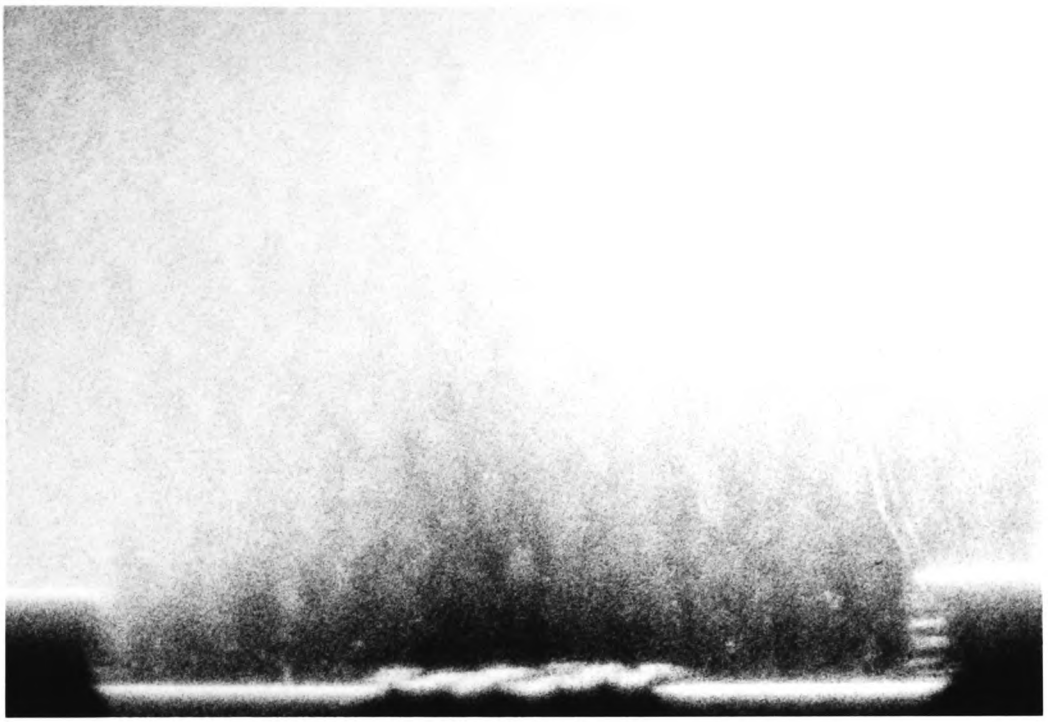

Figure (8.6) The Schlieren Image of the plume over the Plate (140mmx60mm) Current=20 Amps

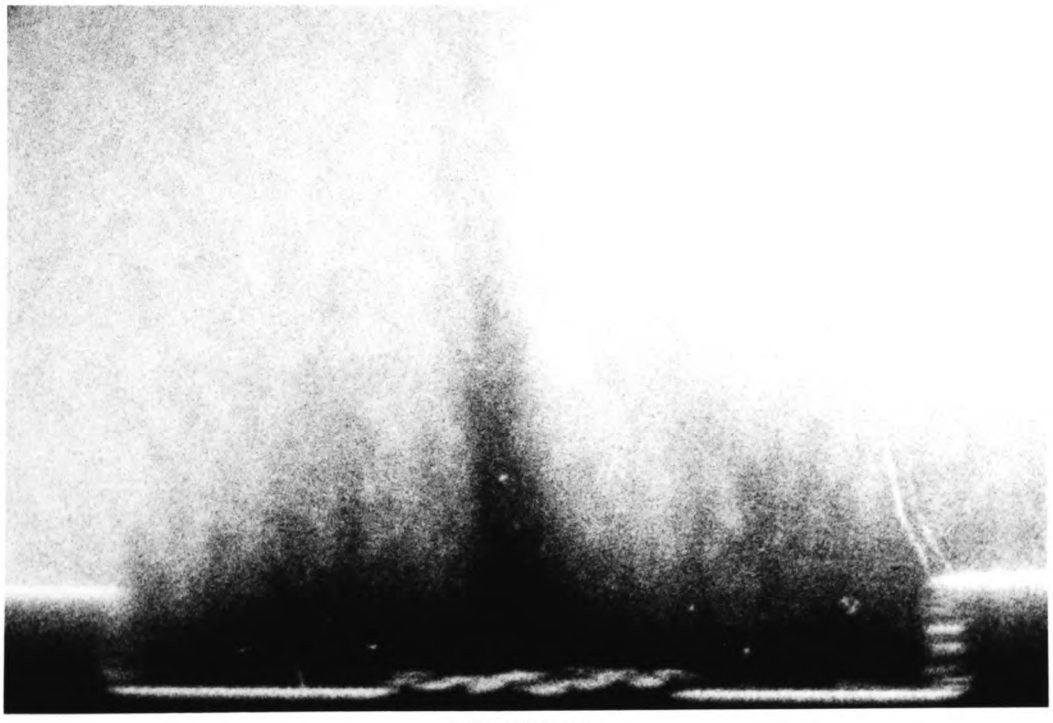

Figure (8.7) The Schlieren Image of the plume over the Plate (140mmx60mm) Current=30 Amps

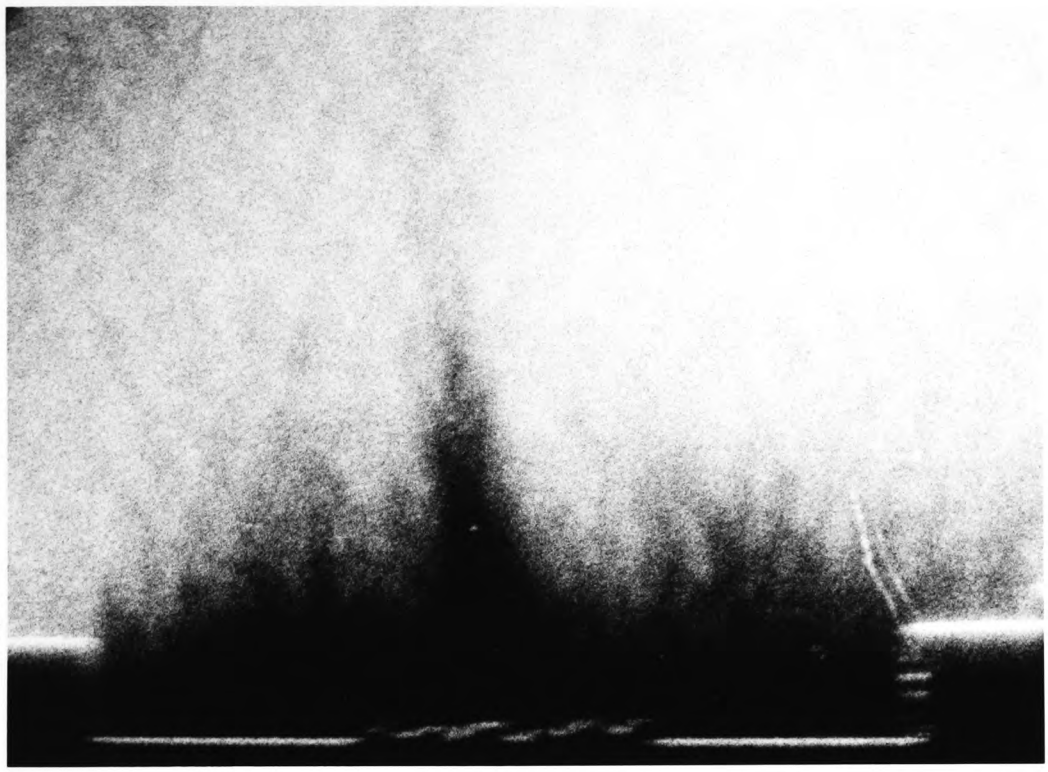

Figure (8.8) The Schlieren Image of the plume over the Plate (140mmx60mm) Current=40 Amps

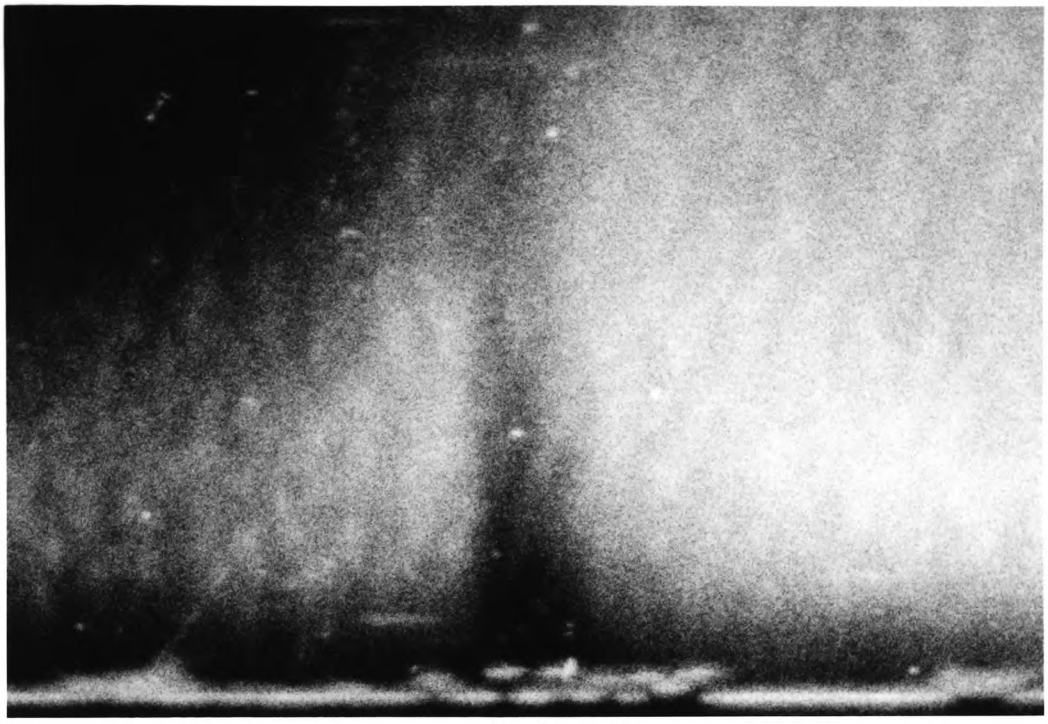

Heated Area

Case 3

Figure (8.9) The Schlieren Image of the Plume over the Plate (140mmx120mm) heated with a Current of 30 Amps

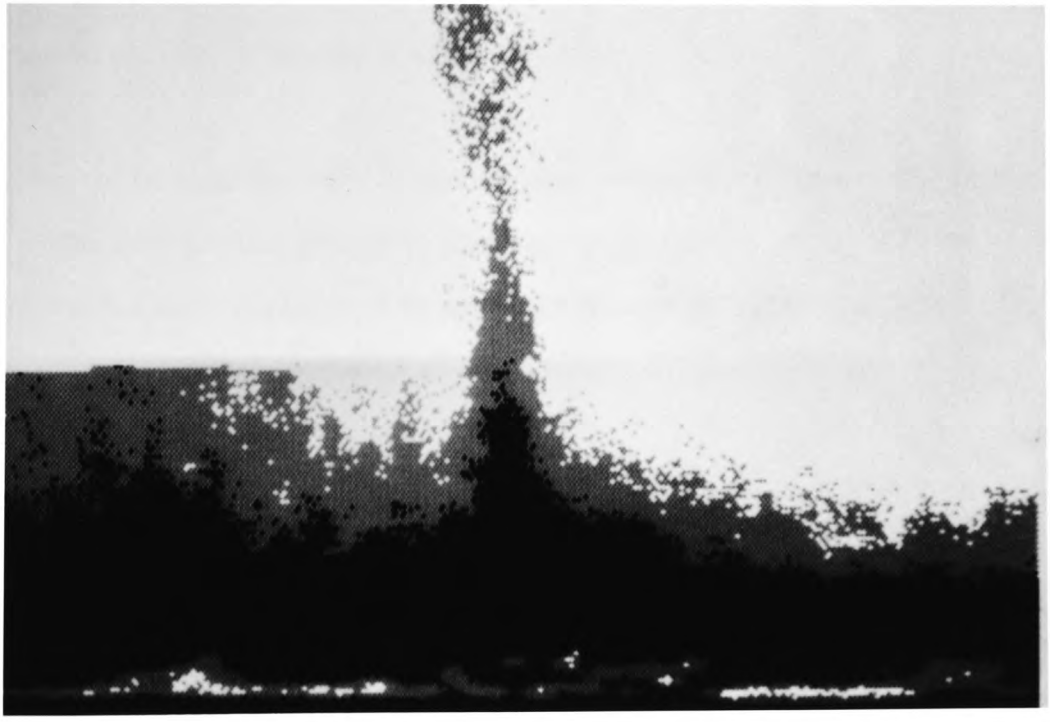

Figure (8.9a) The Processed Image of Figure (8.9)

Case 4 The plate with two heated islands as shown in figure (6.6) was heated by passing currents of 30 and 10 amperes through the (100 *mm* × 20 *mm*) and (40 *mm* × 20 *mm*) islands respectively. The corresponding images are given in figures (8.10) and (8.10a).

In *case 1* as the current was increased an increase in the thickness of the boundary layer was observed thought to be due to the increase in the surface temperature. The steady-state photographs were however similar in that they could all be divided into three main sections. Two almost horizontal boundary layers extended from the edges of the plates along the unheated, cooler areas to the edges of the *resistor* region. The two boundary layers then met in the middle section and rose in the form of a chimney.

The absence of plume in *case 2* seems to be due to the lack of an appreciable temperature gradient along the plate and hence an observable density gradient.

The observed plume in *case 3* above was very similar in nature to that described for *case 1* with thinner boundary layers due to lower surface temperatures. These layers met at the hot *resistor* and rose in the form of a chimney.

The shape of the boundary layer in *case 4* was of similar form to the rest of the samples. The plume seemed to stay parallel to the plate over the smaller (40 *mm* × 20 *mm*) island which was due to the small size of the island and the corresponding small joule heating in that region. This was not producing enough heat for a distinct plume rise.

These observations lead to a very important conclusion that for the ASTEC3 simulation of the thermal behaviour of the heated plates, it is necessary to define only two values of heat transfer coefficient, one for the unheated areas and one for the *resistor* area. This will of course simplify the modelling of the convection part of the heat flow problems.

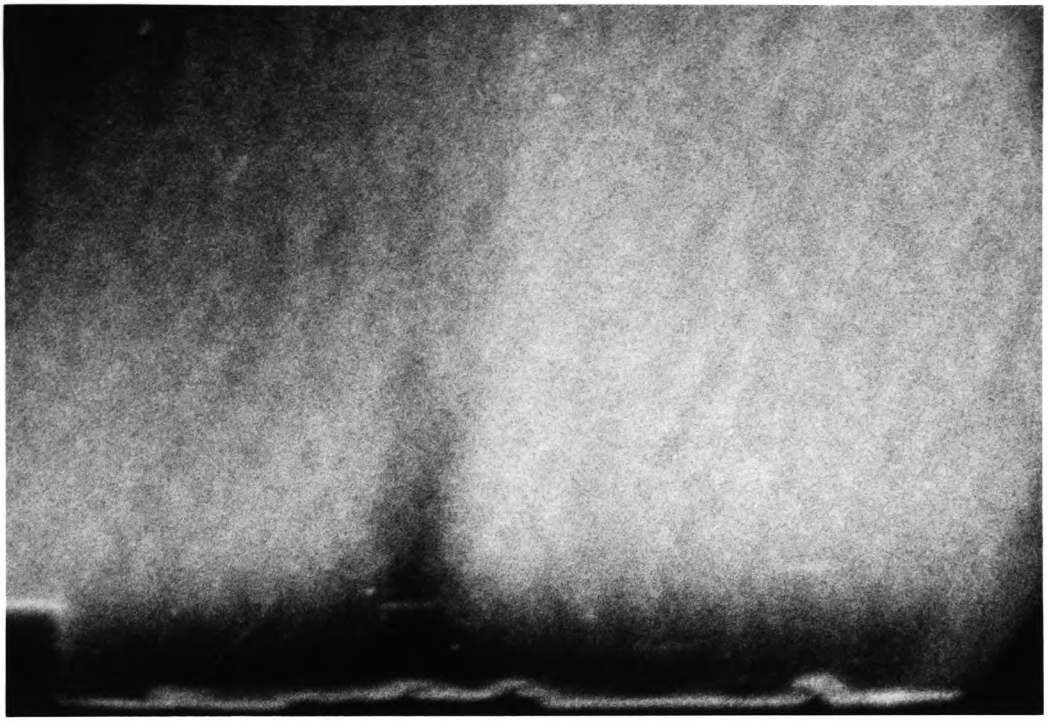

Heated Area

Case 4

Figure (8.10) The Schlieren Image of the Plate with two Heated Islands

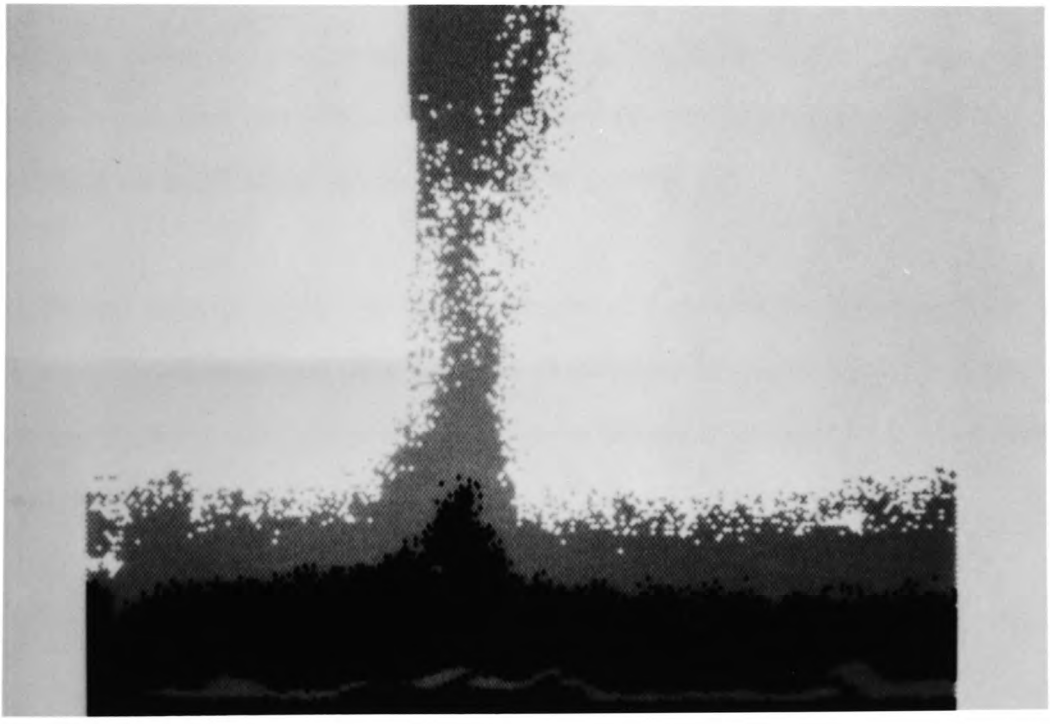

Figure (8.10a) The Scanned Image of the Plume in Figure (8.10)

8.4 Determination of the Optimum Mesh Resolution

A further study was carried out to establish the effect of reducing the size of the thermal cell used in the modelling of the structure and hence increasing the model resolution. The (60 *mm* × 140 *mm*) plate shown in figure (6.11) with a heated island of dimensions (20 *mm* × 100 *mm*) was used for this purpose. The heat transfer coefficients for the losses from the surface due to convection and radiation were kept the same as those calculated in the preliminary experiments described in section (6.1.3). These values were acceptable for this particular test since only the effect of resolution was being studied.

The structure was divided into seven increments in each of the two layers, along the length of the specimen. The width of the layers (60 *mm* edge) however was divided into more and more increments namely 3, 9, 27 and finally 81 strips. The meshes with 3 and 9 divisions are shown in (a) and (b) respectively in figure (8.11).

The temperatures of two points were simulated: that of the middle point of the heated strip, T_2, and also the adjacent unheated section, T_1 as shown in figure (8.11). The simulated temperatures of these two points were then plotted against the corresponding number of strips along the width of the sample as shown in figure (8.12).

It can be seen from the graph that the temperatures of these two points vary considerably as the resolution is increased from very low (3 strips) up to around 27 strips. They then become asymptotic and around 81 strips the variations in the simulated temperatures become negligible.

Furthermore, the percentage errors in the simulated temperatures compared with the experimental results were calculated for the two points T_1 and T_2 in figure (8.11) at each

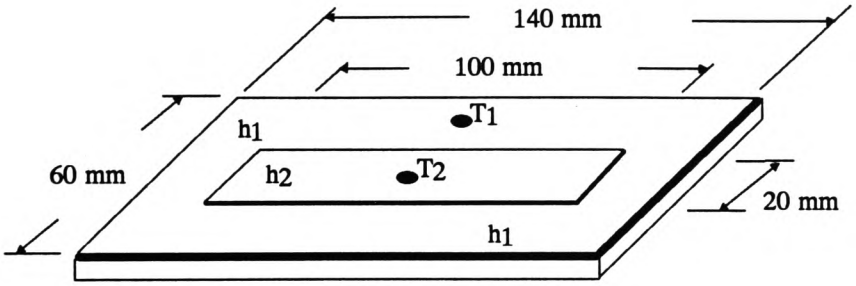

(a)

3 Divisions

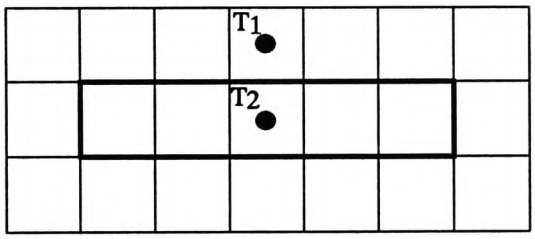

(b)

9 Divisions

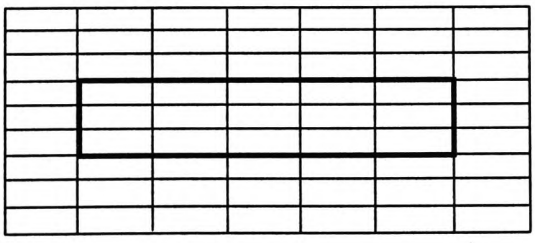

Figure (8.11) Block Diagram of the Sample used for Simulation Tests at Different Resolutions

Figure (8.12) Simulated Temperatures Vs Number of Strips

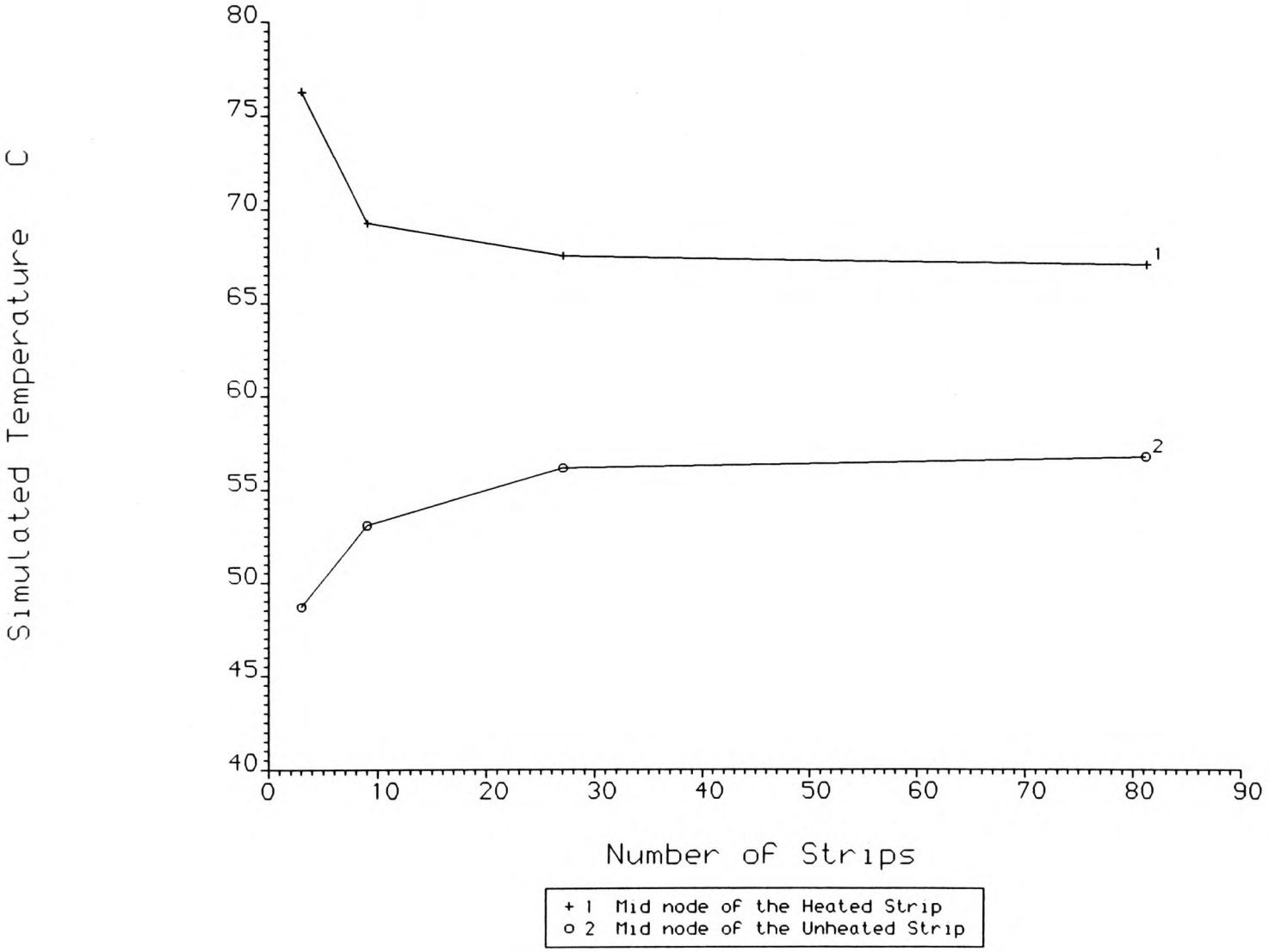

resolution. The results are shown in figure (8.13) as the percentage error in the results versus the total number of strips along the 60 *mm* edge of the plate. These results show very clearly that the resolution induced errors are reduced to negligible levels when the number of strips exceeds 27 per island. This is the near optimum resolution which was used for further experiments.

8.5 Determination of heat transfer coefficient values

Using the optimum resolution level, further tests were carried out to obtain the best values of heat transfer coefficient for the least error in the simulated results compared to the experimentally measured temperatures. In all these simulations a value h_1 is used for the combined convective and radiative coefficients from the heated region and h_2 for the remaining unheated areas. This approach is justified from the Schlieren experimental results which show an almost laminar flow over the unheated areas of the plate and a sharp rise in the central heated region leading to the suggestion that the convection coefficients may be approximated by two values over the surface of the plate. After each simulation a value was calculated for $\sqrt{\%\Delta T_1^2 + \%\Delta T_2^2}$ where $\%\Delta T_1$ and $\%\Delta T_2$ are the percentage errors in T_1 and T_2 compared with experimentally measured values of 76.0 °C and 51.4 °C respectively for an input current of 30 amps.

The simulations were carried out for h_1 and h_2 values ranging from 0 to 26 W/m^2K and a matrix of error results was obtained for each combination of h_1/h_2. In the first instance, the range was divided into coarse steps of h_1/h_2 values and using the square-root error as a guide, the steps were then reduced in the portion of the range where this error was smallest. This was carried out until the square-root error was reduced to near zero.

The results of the above tests are plotted as shown in figure (8.14) where the x and y axes

Figure (8.13) Errors in the Simulated Temperatures Vs Number of Strips

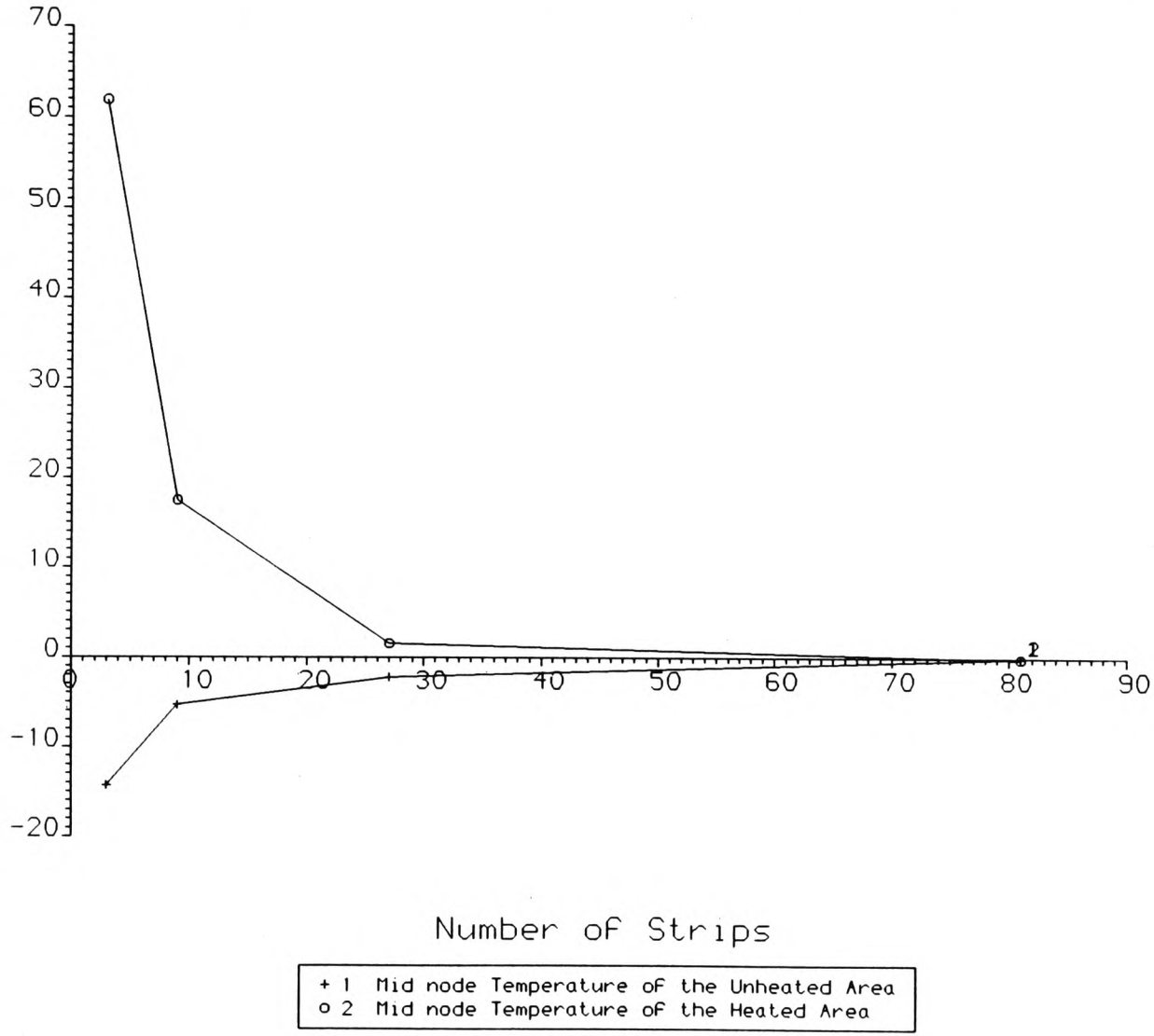

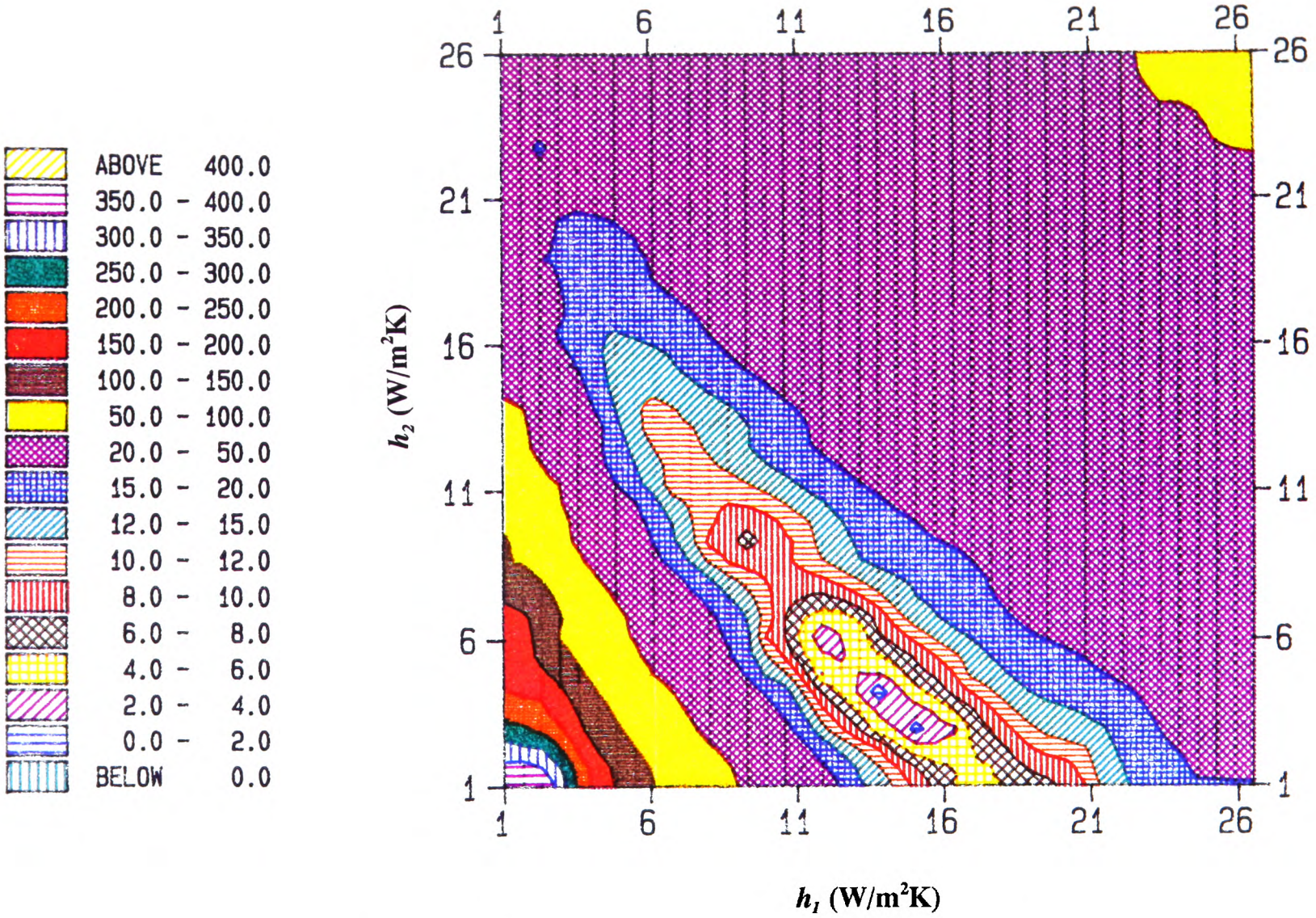

Figure (8.14) Contour Map Showing the Variation of Errors ($\sqrt{\%\Delta T_1^2 + \%\Delta T_2^2}$) with h_1 and h_2

are the h_1 and h_2 values and the z axis is the error. These plots were obtained using a graphics package called UNIRAS which is available on the Vax computers. This is a *state-of-the-art* graphics system which consists of various subroutine libraries, capable of producing contour maps and three-dimensional distribution plots. These may be colour-coded plots with each colour representing a range of values for the parameter in the z axis.

The h_1 and h_2 values of 13.5 and 4 W/m^2K respectively were found to reduce the square-root of the sum of the percentage errors to 0.33. This suggests that the heat transfer rate from the unheated, cooler region in the plate is 3.375 times greater than from the central heated island.

8.6 Simulation of the Original Test Configuration using the Optimised Convection Coefficients

An ASTEC3 model of the plate was developed to include the anisotropy in the thermal conductivity of the fibre glass laminate as found in chapter (7), the optimum resolution level (81 strips along the width of the plate) and the convection coefficients obtained in the previous section. A selected number of simulation results are shown in figure (8.15) relating to the same data points as the original test in figure (6.11). These are the centre points of the cells if the plate was divided into a (7×3) mesh as in figure (6.11). The top figure represents the experimentally measured temperature and the bottom figure the simulated value. The figure in bold gives the percentage error between the measured and the corresponding simulated temperature for each individual data point.

Figure (8.15) Simulation Results using Anisotropic Thermal Conductivity (K_{normal}=0.343 *W/mK* & K_{plane}=1.059 *W/mK*) and Optimised Convection Coefficients (h_1=13.5 W/m^2K & h_2=4 W/m^2K)

Measured	40.3	46.5	49.5	51.4	49.8	47.0	41.4
% Error	**4.96**	**2.58**	**2.02**	**0.19**	**1.40**	**1.49**	**2.17**
Simulated	42.3	47.7	50.5	51.3	50.5	47.7	42.3
		71.0	73.7	76.0	74.7	72.1	
		2.96	**1.90**	**0.26**	**0.53**	**1.39**	
		73.1	75.1	75.8	75.1	73.1	
	40.9	46.5	49.3	51.4	49.3	46.5	41.3
	3.40	**2.58**	**2.43**	**0.19**	**2.43**	**2.58**	**2.42**
	42.3	47.7	50.5	51.3	50.5	47.7	42.3

It is evident from figure (8.15) that great improvement has been accomplished in the simulated temperatures compared to those in the original simulation shown in figure (6.11). Excellent agreement is obtained towards the centre of the plate as expected since minimisation of the errors in the two hottest areas was used as the criterion for the optimisation tests. The errors however increase towards the edges of the plate with a maximum value of 4.96% which is still in acceptable margins.

8.7 Conclusions

The Schlieren photographs show that the plume, as observed from a direction parallel to the longer edge of the (100 *mm* × 20 *mm*) resistor consists of two main parts. An almost horizontal layer covers the cooler unheated region. This is a boundary layer via which heat is transferred by conduction to the main fluid part. Over the heated region there is a sharp rise in the height of the plume which appears in the shape of a chimney. There seems to

be no boundary layer present in this section of the plume and no reference has been found to any work investigating the nature of the flow in the region close to the surface at the bottom of the chimney.

It may be suggested that the heat loss from the hot region occurs via the particles gaining energy from the hot surface and bouncing off due to buoyancy forces. This is almost like pieces of burnt paper and wood in the middle of a bonfire being thrown into the air. The rate at which this phenomenon may occur is dependent on the number of particles of air present near the surface which is in turn a function of the density of air in that region. The air density is of course dependent on the temperature of the air close to the plate which being high, reduces the number of particles in that vicinity.

From the above analysis it may be concluded that the heat transfer rate and hence the convective heat transfer coefficient in the central region are much smaller than in the unheated section which has a conductive boundary layer.

Further evidence has been gained by simulating the original experimental structure (§6.4) with varying heat transfer coefficient values. It has been shown for instance that for the (140 *mm* × 60 *mm*) plate it is very plausible that a difference may exist between the convection coefficients in the heated island and the outer unheated region. It is also shown that a ratio of 3.375 to 1 (unheated:heated) is a possible ratio for the two coefficients. Application of this ratio to the original test configuration has produced excellent agreement with the experimentally measured temperatures. A combination of anisotropic thermal conductivity, reduction in the thermal cell size and the optimised convection coefficients has reduced the errors to a minimum of 0.19% around the centre of the plate and a maximum of 4.96% at one edge.

9 EXPERIMENTAL MEASUREMENTS AND SIMULATION TESTS ON HYBRID CIRCUITS

9.1 Introduction

Following the detailed investigations on large scale structures and the successful simulation results, it was necessary to use the ASTEC3 modelling procedure to study the thermal characteristics of small scale devices.

In order to investigate the effect of reducing the size of the test structures on simulations, it was decided to design the hybrid resistor samples using the same patterns as the macro scale but reduced in size. Royal Signals and Radar Establishment (R.S.R.E) agreed to manufacture the required samples. The test specimens were designed by using the standard thick film resistor width of 0.040 inches (1.016 *mm*) as specified by R.S.R.E. The equivalent width in macro scale 20 *mm*. The ratio of these two figures, ie. 1.016/20, was used to scale all the other dimensions in the reduced case. For example, the hybrid device resembling the PCB plate (140 *mm* × 60 *mm*) with a symmetrically situated island of (100 *mm* × 20 *mm*) was scaled to (7.112 *mm* × 3.048 *mm*) with a resistor size of (5.08 *mm* × 1.016 *mm*). All the samples (A to E) are illustrated in figure (9.1) with their dimensions.

9.2 Sample Preparations

The resistor samples produced by R.S.R.E were all prepared using the materials given below. The relevant parameters and production techniques are included where applicable.

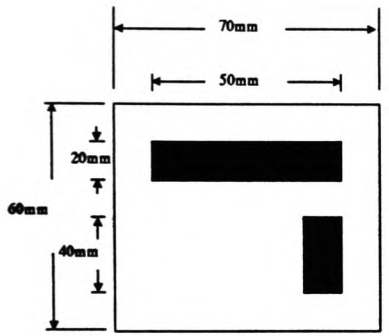

A

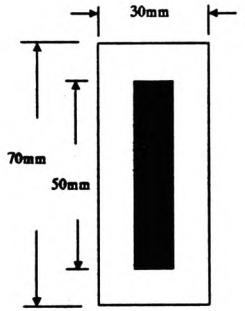

B

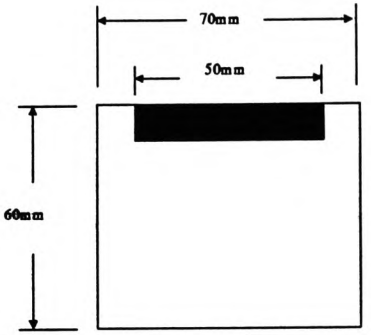

C

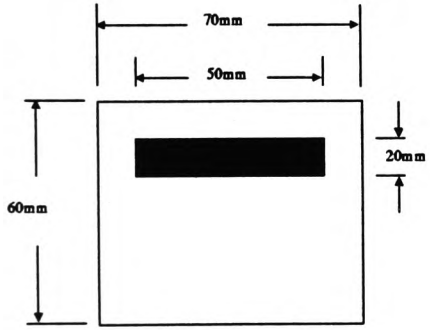

D

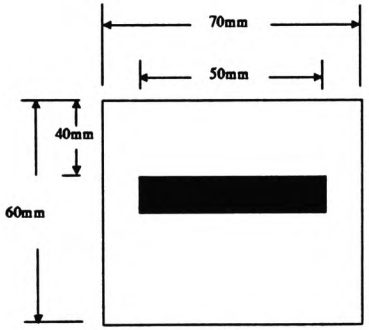

E

Figure (9.1) Resistor Samples

Substrate

White alumina ceramic substrates (Code No. ADS-96R PER CPC-STD-49) were used as the base for the resistors [1]. The substrates were 0.025 inch (635 μm) thick with 96% concentration of Al_2O_3 and a thermal conductivity of 20 *W/mK* at 100 °C [1].

Resistor

Thick film resistor material from the BIROX 1400 series resistor composition made by Du Pont Electronic Materials [2] was used for this purpose. These materials are produced with resistivities ranging from 10 Ω/square to 1 *M*Ω/square. The 1 *k*Ω/square type was chosen by R.S.R.E to match the design specifications. The thermal conductivity of the 1400 series resistor material is related to its resistance varying from 2 *W/mK* for sheet resistance of 10 Ω/square to 1 *W/mK* for sheet resistance of 10 MΩ/square [3]. The two parameters have a fairly linear relationship between these two extremes [3] yielding a thermal conductivity of 1.999 for the 10 *k*Ω/square resistor.

The resistors were printed onto the substrate to 25 ± 3 μ*m* dried print thickness using a 200-mesh stainless steel screen. The prints were allowed to level for 5 to 10 minutes at room temperature and dried for 15 minutes at 150 °C. The printing was followed by a 60 minute firing cycle with 10 minutes at a peak temperature of 850 °C.

Package

The packages used were of 24-pin type made of black ceramic with 90 % Al_2O_3 purity and with a thermal conductivity of 24.29 *W/mK* [4]. The substrates were adhered to the package using a very thin layer of electrically insulating adhesive made by Ablestic Laboratories.

This was the Ablebond 41-4 type with a thermal conductivity of 0.52 *W/mK* at 121 °C [5].

Electrical connections to the chip were made via gold bonding wires which were attached to the contact pads at the ends of the resistors. Each bond wire was then connected to another pad on the package using a standard ball-joint bonding technique which was subsequently routed internally to one of the pins. A typical carrier assembly is shown in figure (9.2) with the substrate in position.

9.3 Temperature Measurement System

The samples were tested using thermal imaging equipment manufactured by AGEMA. The particular model was from their Thermovision 800 series comprising an 880 infrared scanner unit [6] which has an In-Sb liquid Nitrogen-cooled infrared detector. The unit can be fitted with a wide range of bayonet-mount lenses which make it possible to adapt the system to different measurement situations. A 38 *mm* lens with a 20 ° field of view was found to adequately cover the size of the samples used here.

The Thermovision 880 system is a real-time thermal imaging device capable of surface temperature measurements and analysis of dynamic and static thermal patterns. The infrared radiation emitted by the object is detected by the scanner and subsequently converted into an electrical video signal. The surface of the object is scanned 25 times per second which produces a real-time TV-like thermal image of the object. A temperature accuracy of ± 2 % or ± 2 °C is guaranteed by the manufacturers [6].

The thermograms were displayed on a colour video monitor with a colour chart alongside the image displaying temperature readings in 3 °C intervals as detailed later. If a more

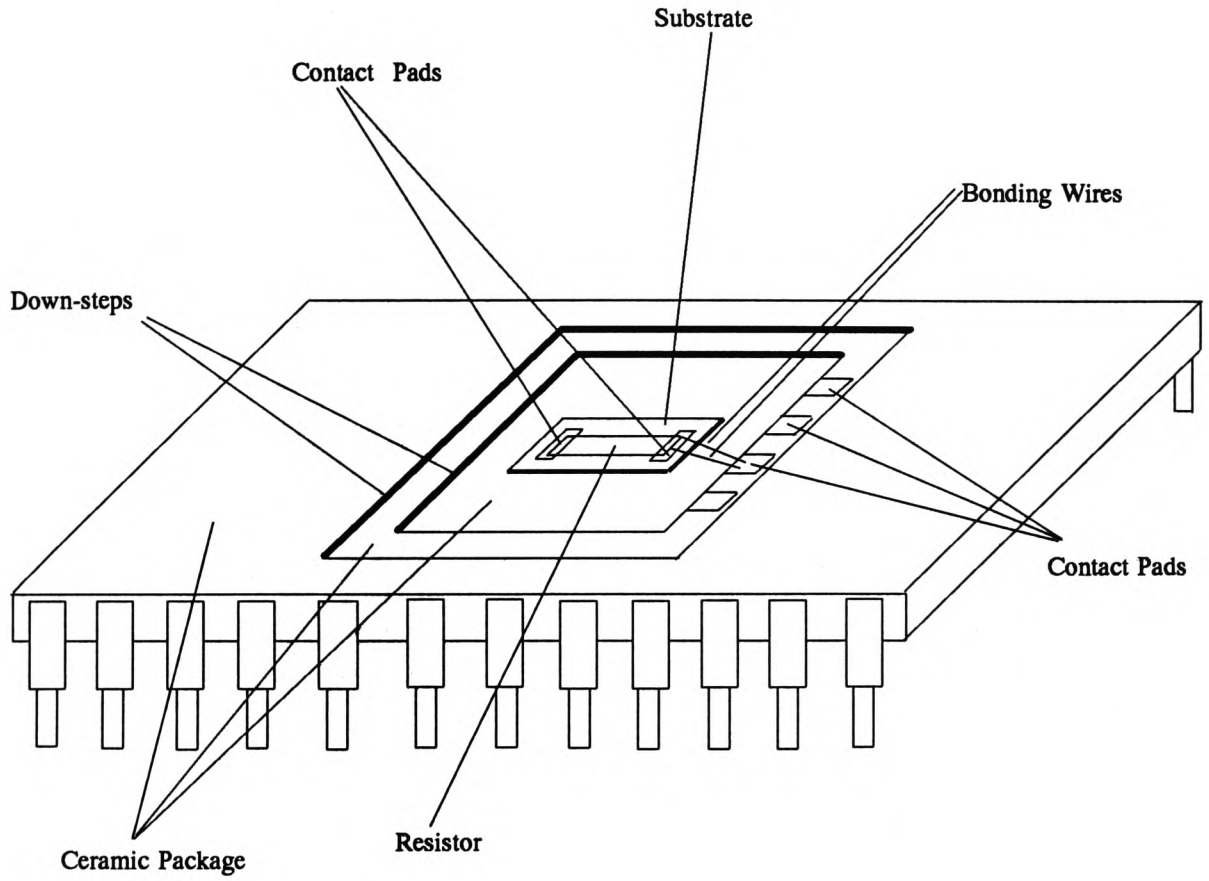

Figure (9.2) The Carrier Assembly

accurate measurement is needed there is a facility provided whereby a cursor can be positioned at any point of interest for which a more exact temperature value is required and the value is displayed on the screen.

9.3.1 Emissivity Considerations

Accurate non-contact surface temperature measurements are complicated due to the varying emissivities of surfaces of different materials. There is a facility within the AGEMA infrared system which allows predefined areas of the object surface to take up different emissivities chosen here to be the areas covered by the resistors.

The emissivities were calculated using a heating stage supplied with the system. The legs were cut from one of the carriers which then made it possible to mount the sample flat onto the stage. A small amount of conductive paste was used to enhance the thermal contact between carrier and the heating plate. A calibrated electrical heater was used to raise the temperature of the specimen to a fixed steady-state temperature. The scanner was focused onto the assembly and the radiation emitted from the object was measured. This value was then used via an option in the software to calculate the emissivities in different areas. Because of the company's sensitivity in protecting their new product the exact nature of the calculations was not disclosed by AGEMA. For the samples described in the beginning of this chapter the emissivity of the white ceramic substrate was found to have a value of 0.95. For the black resistor material however, values of 0.88 and 0.9 were calculated at reference temperatures of 60 and 80 °C respectively. An average value of 0.89 was therefore taken for the emissivity which is in good agreement and within 2 per cent of the value of 0.87 measured experimentally by other workers [7]. The calculated emissivities were subsequently programmed into the software for the temperature measurements when the

devices were powered up.

The emissivity of the carrier itself was also determined by the same experiment as 0.95. This parameter was needed for calculations of the radiation coefficient in the ASTEC3 model of the structure.

9.3.2 Experiments and Results

In an attempt to simplify the physical situation to be modelled and to make the results comparable to the macro scale experiments, it was decided to maintain the design of the sample holder very similar to that of the large scale structures.

The packaged devices were mounted onto pieces of standard matrix board with the device facing upwards. Terminal pins were inserted into the boards in appropriate positions to which a few of the substrate-carrier legs were soldered. The number of connections was kept to a minimum possible of 4 to reduce the conductive heat losses from the carrier via the pins and at the same time stabilise the sample in the parallel position with the board. The legs were conveniently chosen to be the resistor terminals so that electric power could be applied from the same points. The configuration for a one resistor sample is shown in figure (9.3).

As in the large scale experiments, the same glass-wool material was used here to insulate the lower face of the ceramic package by loosely packing the insulating material between the carrier and the matrix boards. This was done to minimise any heat losses from the back face of the carrier and to restrict the convective and radiative heat losses to its top face.

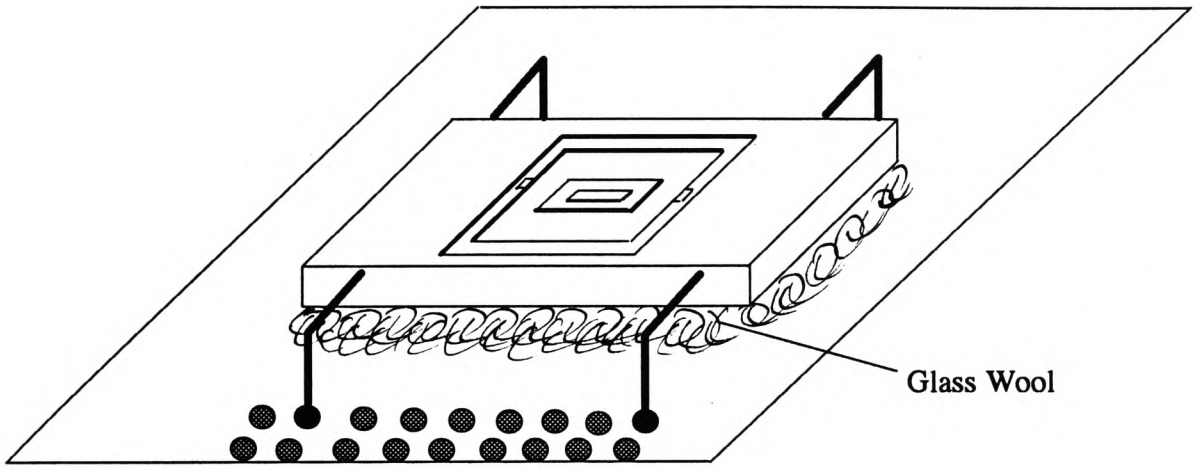

Figure (9.3) A Diagram Showing the Mounted Resistor Sample for Temperature Measurements

The AGEMA system was used to obtain the surface thermal patterns for all the devices described in the beginning of this chapter. Each sample was in turn powered using four Farnell E30/1 power supplies cascaded to give the required voltage range of around 100 volts and currents of 20 *mA*. A preliminary set of tests was carried out to determine approximate values for current and voltage needed for the experiment. A K-type thermocouple with an accuracy of ±0.75% was used for temperature measurements and it was found that a potential of 100 V and a current of 20 *mA* would give rise to temperatures of around 135 °C in the resistor area of the samples.

The system was left to stabilise and then a thermal image of the surface was recorded onto the computer hard disc for further investigation. The result of the experiment are given in the form of a colour print in figure (9.4) corresponding to sample B in figure (9.1). The power input corresponding to the particular thermogram is shown in the bottom right-hand side of the image as 1.95 Watts.

9.4 ASTEC3 Simulation Model

The modelling of one of the hybrid resistor samples is considered here for simulation purposes. This is sample B in figure (9.1) with one resistor of dimensions (1.016 *mm* × 5.08 *mm*) symmetrically printed onto a substrate of dimensions (3.048 *mm* × 7.112 *mm*). A Wheatstone Bridge manufactured by PYE Scientific Instruments Serial No. 39822 was used to measure the electrical resistance of the sample. A resistance of 6.198 *kΩ* was measured at a room temperature of 24 °C. This value was subsequently used to calculate the total input power when a current of 17.72 *mA* was passed through the resistor corresponding to thermogram given in figure (9.4).

Figure (9. 4) The Temperature Distribution of the Resistor Sample as obtained via the AGEMA Infra-red thermal Imaging Equipment

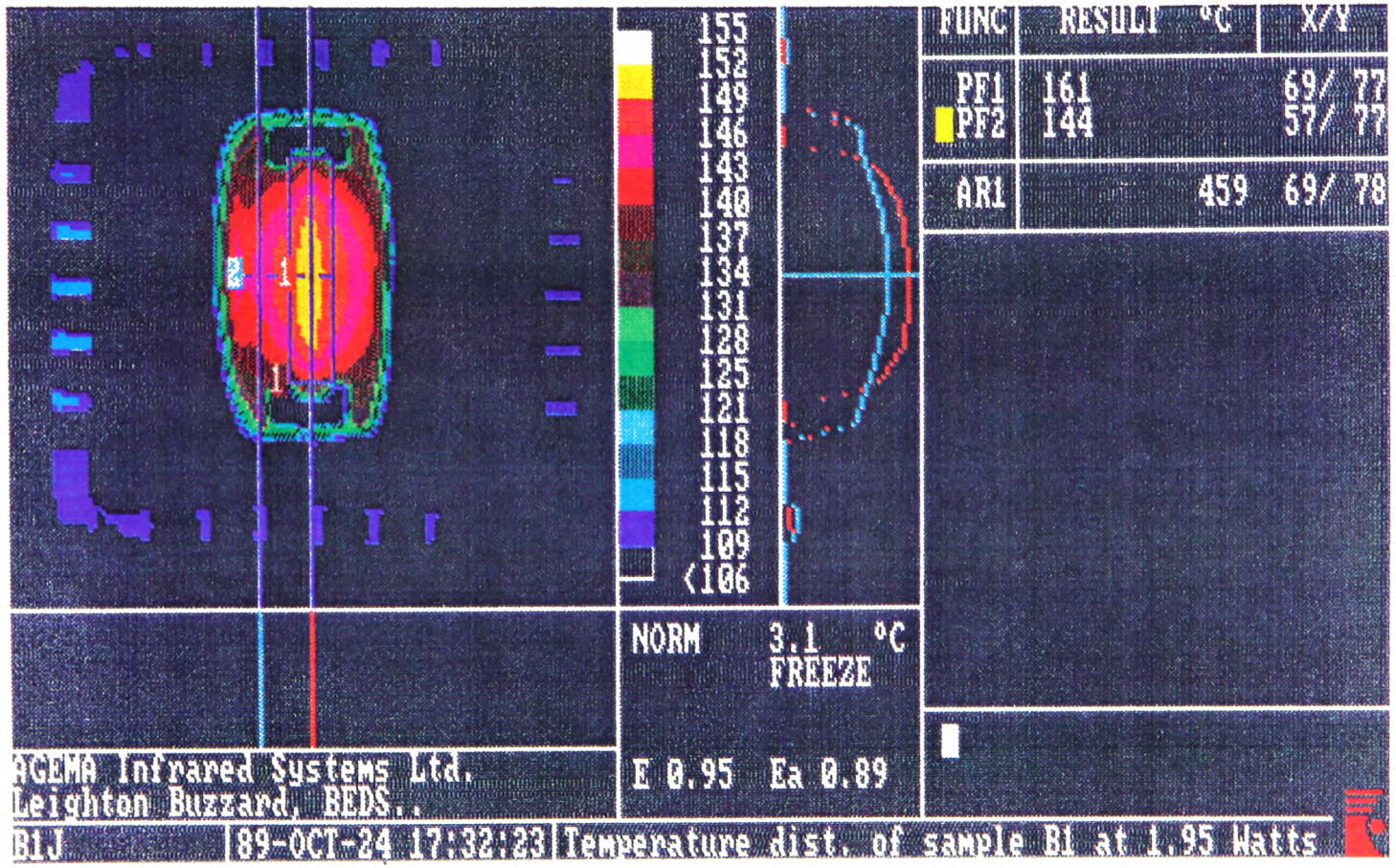

An electrical equivalent circuit description of the thermal structure was constructed in ASTEC3 syntax taking account of the following:

The resistor/substrate combination was modelled using the optimum resolution level obtained when dealing with the macro scale structure of the same pattern (§ 8.4). ie. 81 and 7 strips along the 3.048 *mm* and 7.112 *mm* edges respectively. The arrangement is shown in figure (9.5) where the resistor layer is modelled as (5×27×1) and the substrate as (7×27×1) thermal cells. Both layers are modelled as single layers.

Since a very accurate simulation of the carrier was not required it was decided to model this section of the assembly in the coarsest possible resolution. This would reduce the number of thermal cells which would in turn reduce the computing-time needed for the simulations. An ASTEC3 model was therefore generated by constructing a three-dimensional interface cell (§ 5.4) immediately below the substrate as shown in figure (9.6). This is effectively a 3-dimensional thermal cell with single resistors (of value $1/2R_{th}$) connected from all the faces to the centre-point of the cell apart from the resistor connection from the top face. This resistor was replaced by 567 resistors joining all the bottom nodes of the substrate to the centre-node of the interface cell. In electrical terms these resistors are parallel to each other and hence the value of each resistor was simply calculated by multiplying the single thermal resistor value ($1/2R_{th}$) by the number of resistors which was 567 in this case.

The model for thermal conduction within the rest of the carrier was then developed using normal 3-dimensional cells keeping their sizes as large as possible. Figure (9.7) shows a top view of the carrier illustrating the break-up of the assembly into thermal conduction cells. For each cell in the model the conduction resistances were calculated using the equations given in section (4.2) and the corresponding thermal conductivities.

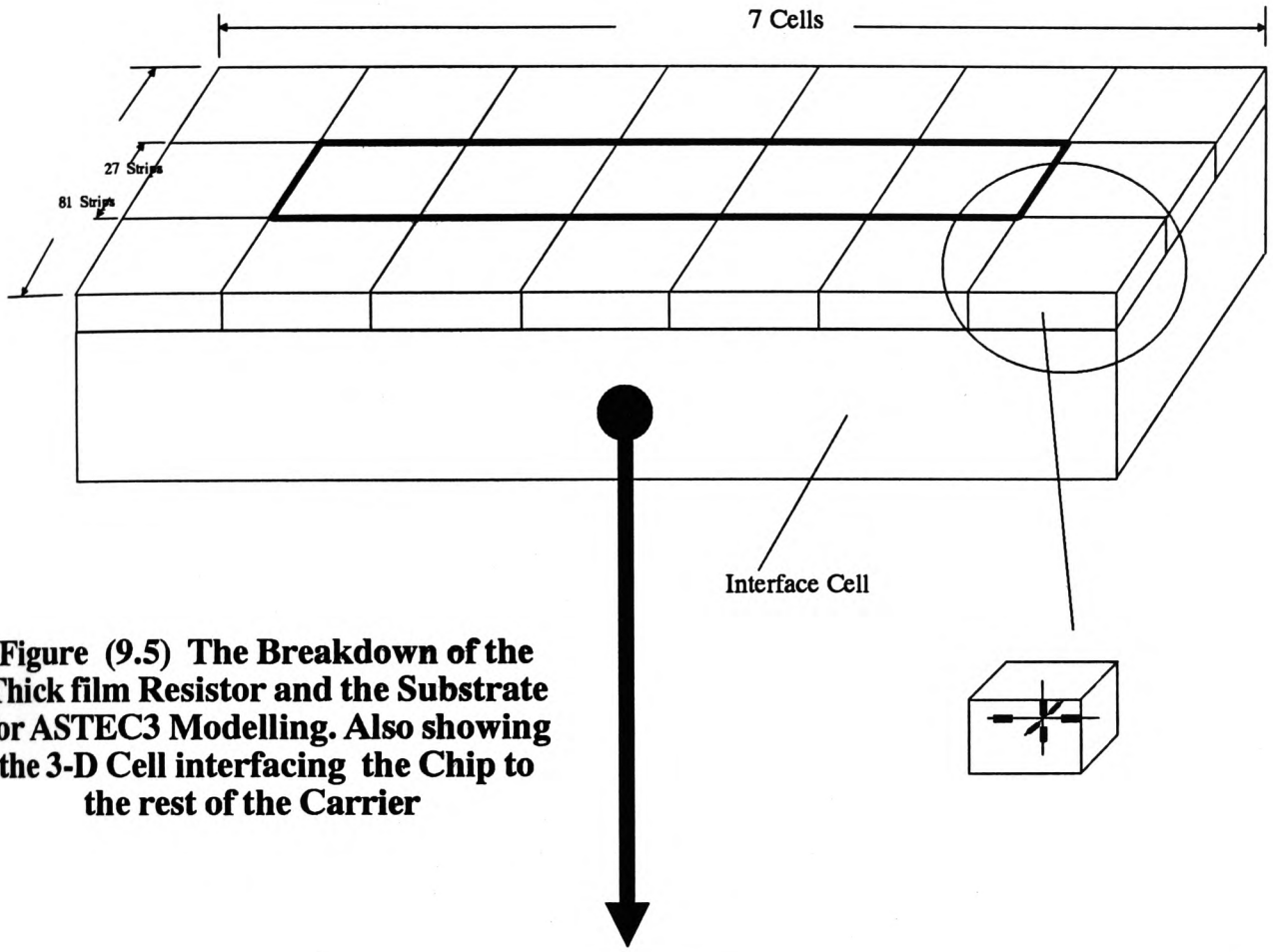

Figure (9.5) The Breakdown of the Thick film Resistor and the Substrate for ASTEC3 Modelling. Also showing the 3-D Cell interfacing the Chip to the rest of the Carrier

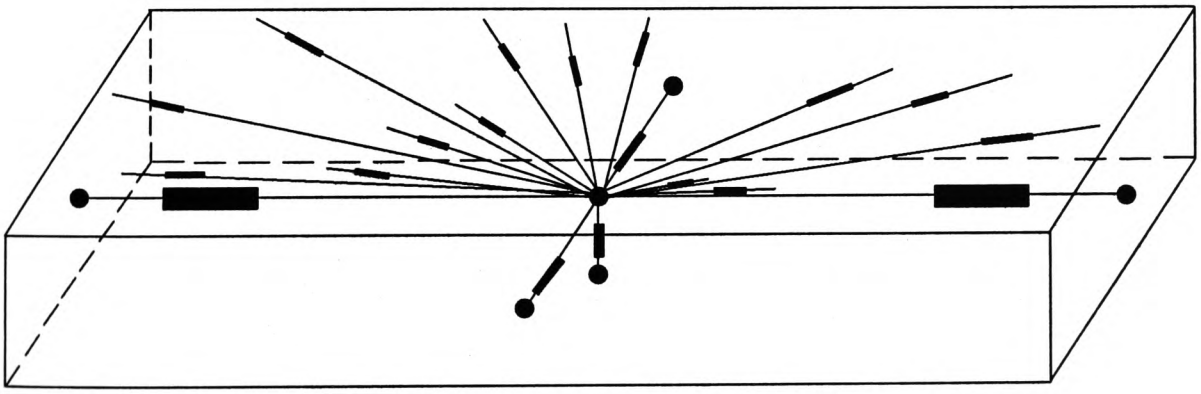

Figure (9.6) The Resistor Model of the Interface Cell

Figure (9.7) Top View of Sample B as used for ASTEC3 Modelling.
Thin Lines Represent the Thermal Cell Boundaries

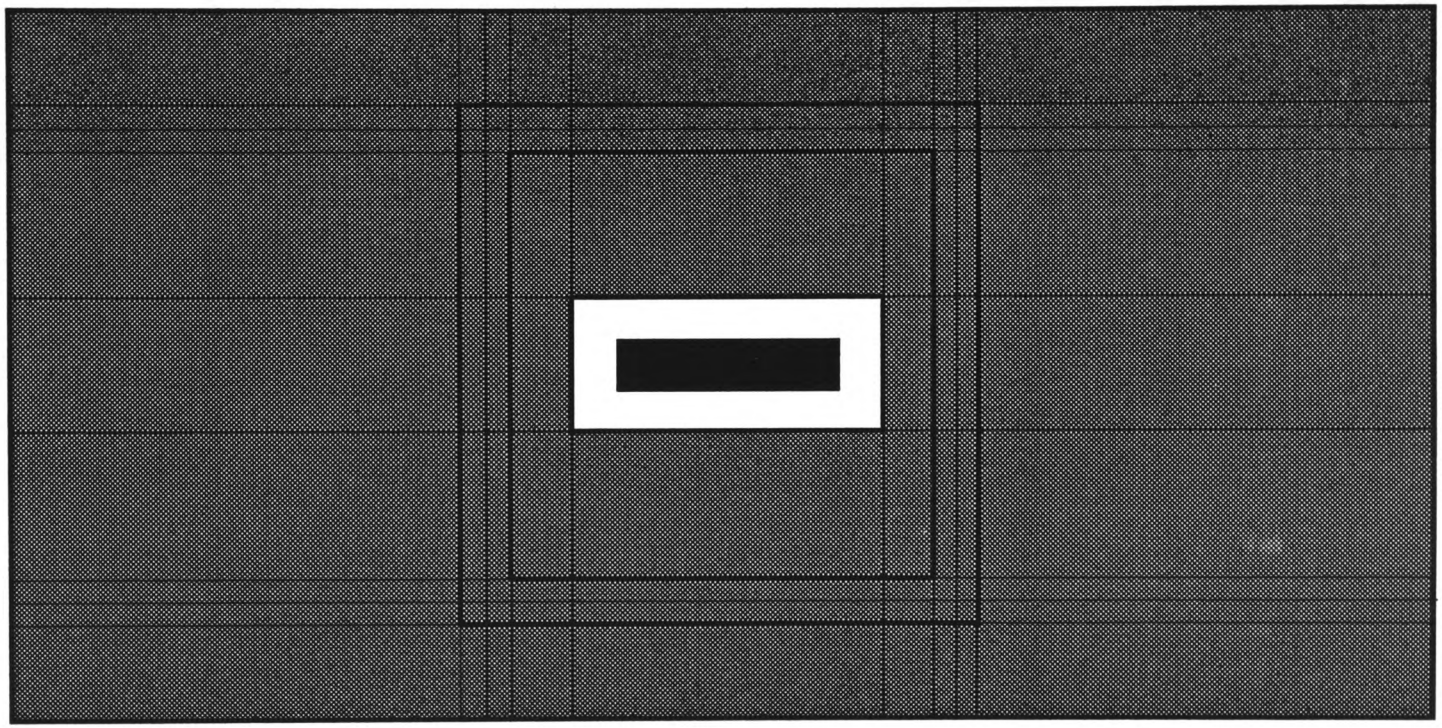

Convection and radiation losses were also accounted for in the model. For the substrate/resistor section of the structure, in the first instance, values of 13.5 and 4 W/m^2K were used for the convective losses as determined from the large scale model (§8.4.1). Emissivities of 0.89 and 0.95 were used to calculate the radiative heat transfer coefficients for the resistor and the ceramic substrate respectively as determined by the AGEMA system. Values of 10.19 W/m^2K and 10.017 W/m^2K were subsequently obtained for the resistor and substrate areas respectively.

Assuming that the exposed surfaces of the carrier assembly were all at the same steady temperature and using an emissivity of 0.95 for the matt-black alumina material as determined in section (9.3.1), a radiative heat transfer coefficient, h_r, of 9 W/m^2K was calculated. Convection from the package was also accounted for by using the empirical relationships given in section (3.2.2) to calculate an average value of h_c of 15.72 W/m^2K. Details of these calculations are given in appendix (10). A combined radiation and convection heat transfer coefficient of 24.7 was therefore incorporated into the ASTEC3 model by connecting resistors of appropriate sizes (§ 4.1) from the nodes at the top face of the structure to ambient air temperature.

The subsequent thermal simulation of the structure yielded surface temperatures of 235 °C and 223 °C in the mid-point of the resistor and the adjacent ceramic substrate respectively. These are 74 °C and 79 °C above the temperatures measured via the thermal imaging technique. Further investigation was required to reduce the simulation errors as described in the following sections.

9.5 Heat Transfer Coefficient of Convection

It has been shown that the average heat transfer coefficient calculated for convection heat losses from the hybrid resistor samples did not produce the correct simulation results. It was therefore necessary to investigate the heat losses in a similar manner to the large scale models. That is to use the Schlieren apparatus to observe the heat flow mechanism giving a possible indication of where on the surface the losses by convection are greater. A subsequent set of simulations using a matrix of heat transfer coefficient values should give the optimum values of convection coefficient which reduce the simulation errors to acceptable margins.

9.5.1 Schlieren Experiment

The Schlieren apparatus (§ 8) was used to obtain an image of the density variations over the top surface of the hybrid samples. The experiment was carried out to visualise the pattern from two directions, first with the longer edge of the resistor parallel to the beam of light and second perpendicular to it.

The device was powered by applying 1.95 Watts of electric power and it was left to reach a steady-state temperature. An image of the density pattern was obtained on the screen which was subsequently photographed for inspection.

The photographic results of the experiment are presented in figures (9.8) and (9.9). Figure (9.8) is with the longer edge of the resistor in the direction of the light rays and figure (9.9) normal to it. Figure (9.8) shows two boundary layers which extend from the two edges of the chip carrier to the substrate. These two boundary layers then meet at the hot substrate and rise in the form of a chimney. The loss from the boundary layer is higher than the

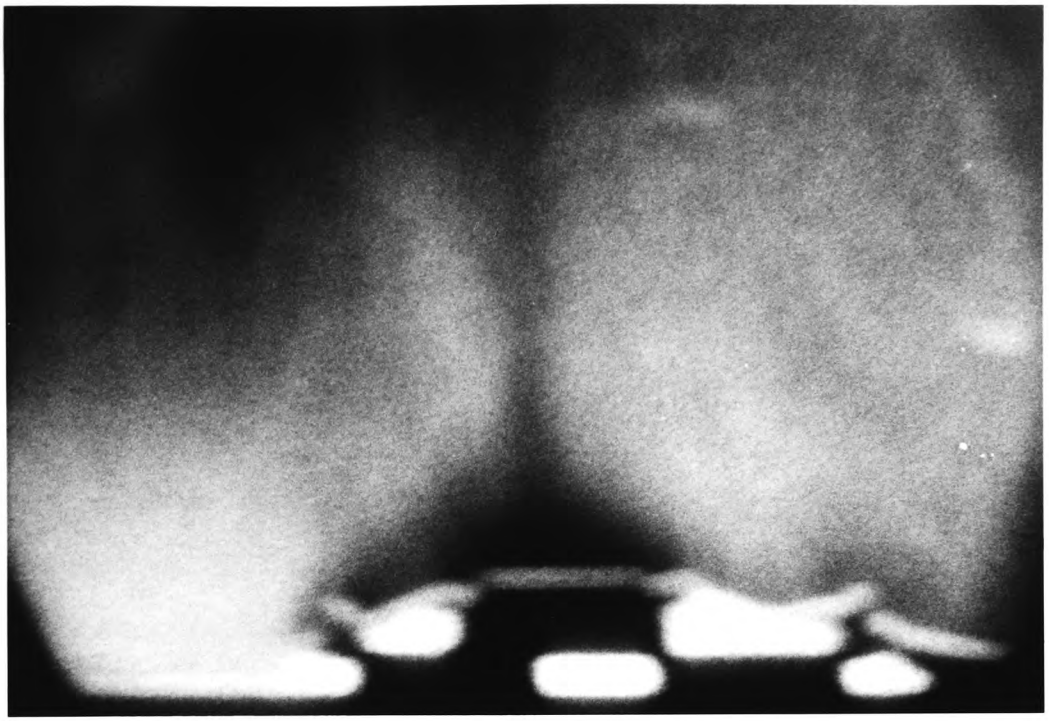

Figure (9.8) A Schlieren Image of the Plume Over the Carrier as Observed from a Direction Along the Length of the Resistor

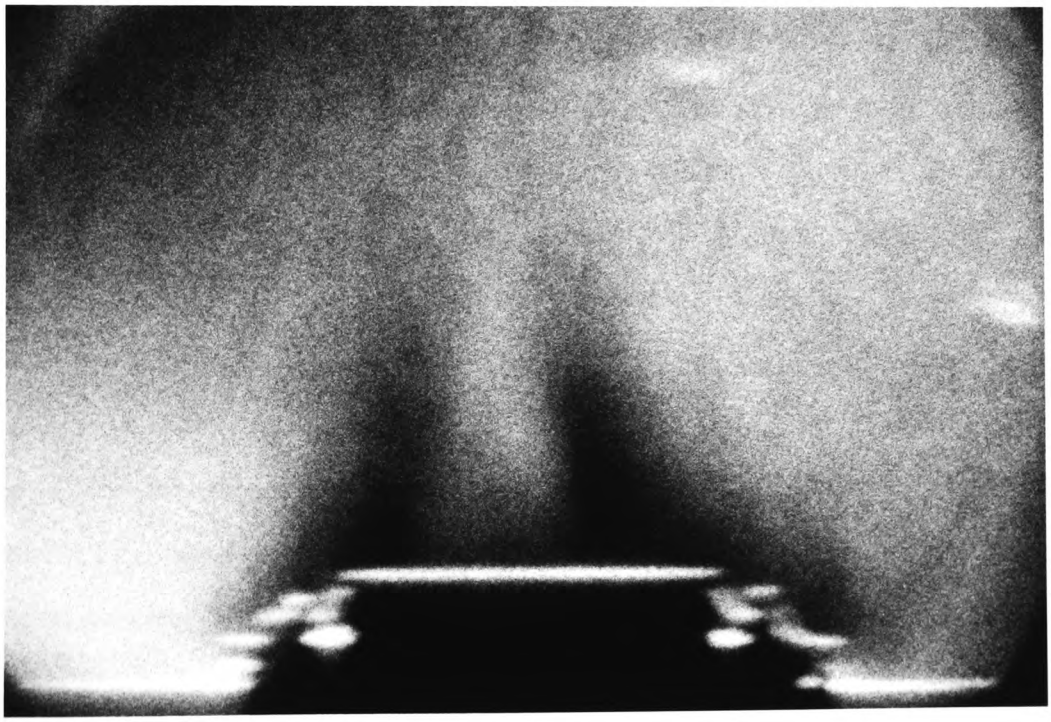

Figure (9.9) The Plume Observed from the Direction Normal To the Longer Edge of the Carrier

central region due to conduction within the layer which is essentially nonexistent in the centre of the plume.

It must be stressed here that the Schlieren apparatus gives an indication of the variation in the air density seen by the light rays passing through the medium. The image is therefore not necessarily the flow pattern over the surface. This leads to the suggestion that the double plume observed in figure (9.9) is in fact one plume similar to figure (9.8) starting from the two edges meeting in the middle to rise in the form of a chimney.

The variations in the air density observed inside the chimney may be due to the construction of the substrate carrier. The carriers are designed in such a way that there exists a square area (11.5 *mm* × 11.5 *mm*) which is at a lower level (1.01 *mm*) than the rest of the carrier surface. The hybrid samples are mounted centrally in this lower surface which may subsequently be covered for protection.

The break-up of the plume seems to occur at around these down-steps. It may therefore be suggested that the steps cause the irregularity in the plume as shown in figure (9.10). Initially the air inside the chimney is hotter than the outer regions. As the flow develops the cool air which is drawn from the edges meets the down step which depending on the flow velocity could cause some mixing of hot and cold air. This in turn reduces the temperature of the air in the central region of the chimney and a subsequent change in its density.

These observations lead to the conclusion that the flow is similar in shape to the macro scale models. The heat transfer coefficient of convection is therefore smaller in the regions inside the chimney than outside it. Its value decreases as one moves towards the middle

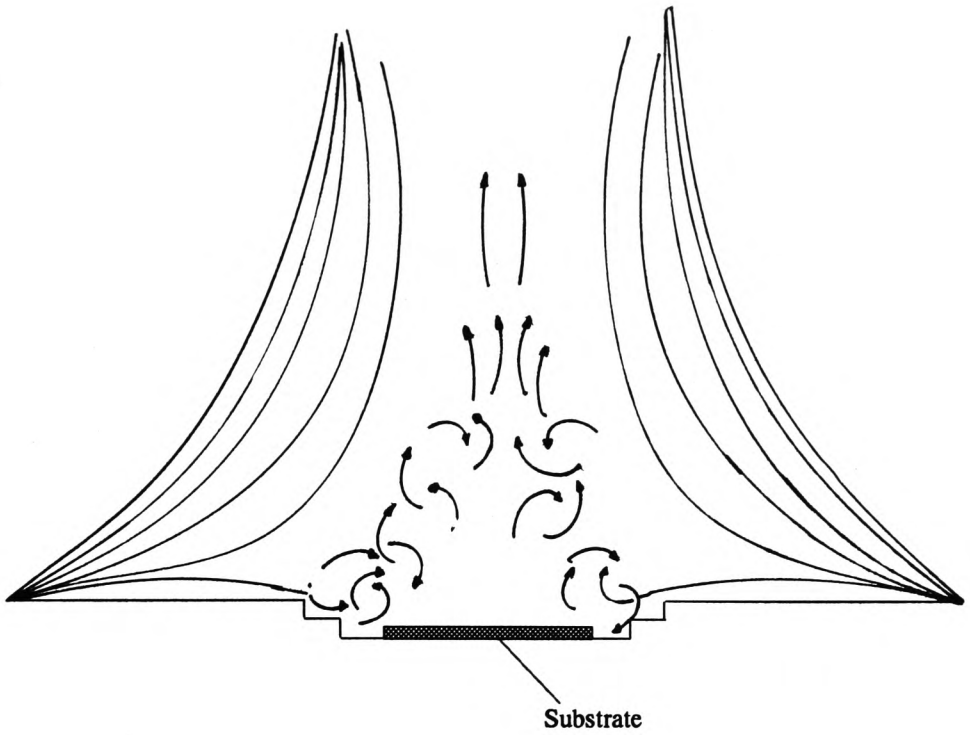

Figure (9.10) Diagram Showing the development of the Plume

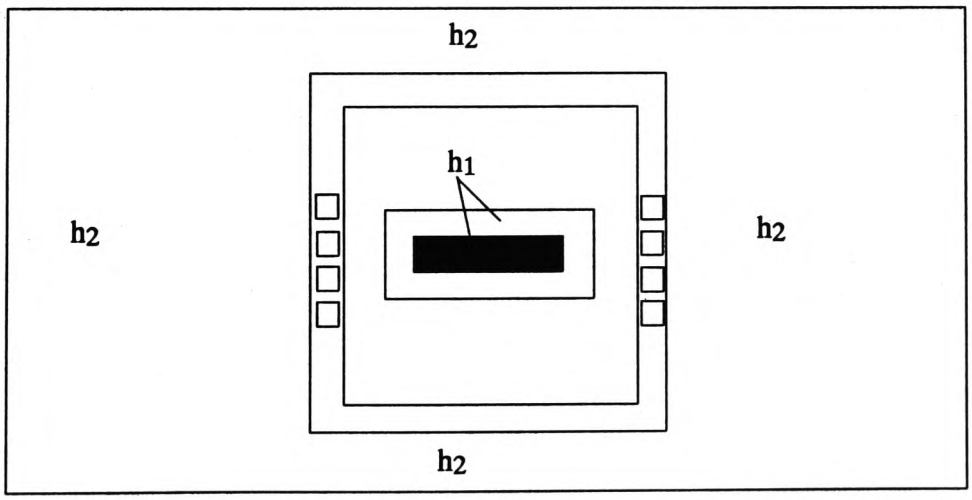

Figure (9.11) Diagram showing the h Values Attributed to different Sections of the Carrier Surface

of the carrier as the thickness of the boundary layer increases. For the sake of simplicity, it will be assumed that the convection coefficient takes an average value over the boundary layer section and assumes a smaller rate in the chimney area.

9.5.2 Optimisation Tests

Similar to the large scale model of the same structure, a large number of ASTEC3 simulations were carried out to determine the optimum values of heat transfer coefficients over the surface which would reduce the difference between the simulated and experimentally obtained temperatures to a minimum.

The surface of the carrier was divided into two regions as shown in figure (9.11). It was assumed that the heat transfer coefficient of convection stays constant within these two areas. These assumptions may be justified from the Schlieren observations which showed the substrate/resistor area to fall within the chimney of the plume and the rest of the carrier in the outer region. A value of h_1 was therefore allocated to the central region over the substrate and a value of h_2 over the rest of the carrier assembly.

A matrix of convection coefficient values was chosen ranging from 1 W/m^2K to 40 W/m^2K. For each set of h_1/h_2 values the simulated temperatures corresponding to the mid-points of the resistor area T_1 and the adjacent substrate section T_2 were recorded. The percentage errors $\%\Delta T_1$ and $\%\Delta T_2$ in the two temperatures when compared to the experimentally measured values were combined as $\sqrt{(\%\Delta T_1)^2 + (\%\Delta T_2)^2}$ [8]. The square root errors were then plotted as a function of h_1 and h_2 as shown in figure (9.12).

Close inspection of the results revealed that the optimum value of h_2 lies in the range 36 to 38.7 W/m^2K within which, the square root of the sum of the errors for T_1 and T_2 reduces

Figure (9.12) The Square Root Errors ($\sqrt{\%\Delta T_1^2 + \%\Delta T_2^2}$) plotted as a Function of h_c over the Substrate and h_c over the rest of the Carrier

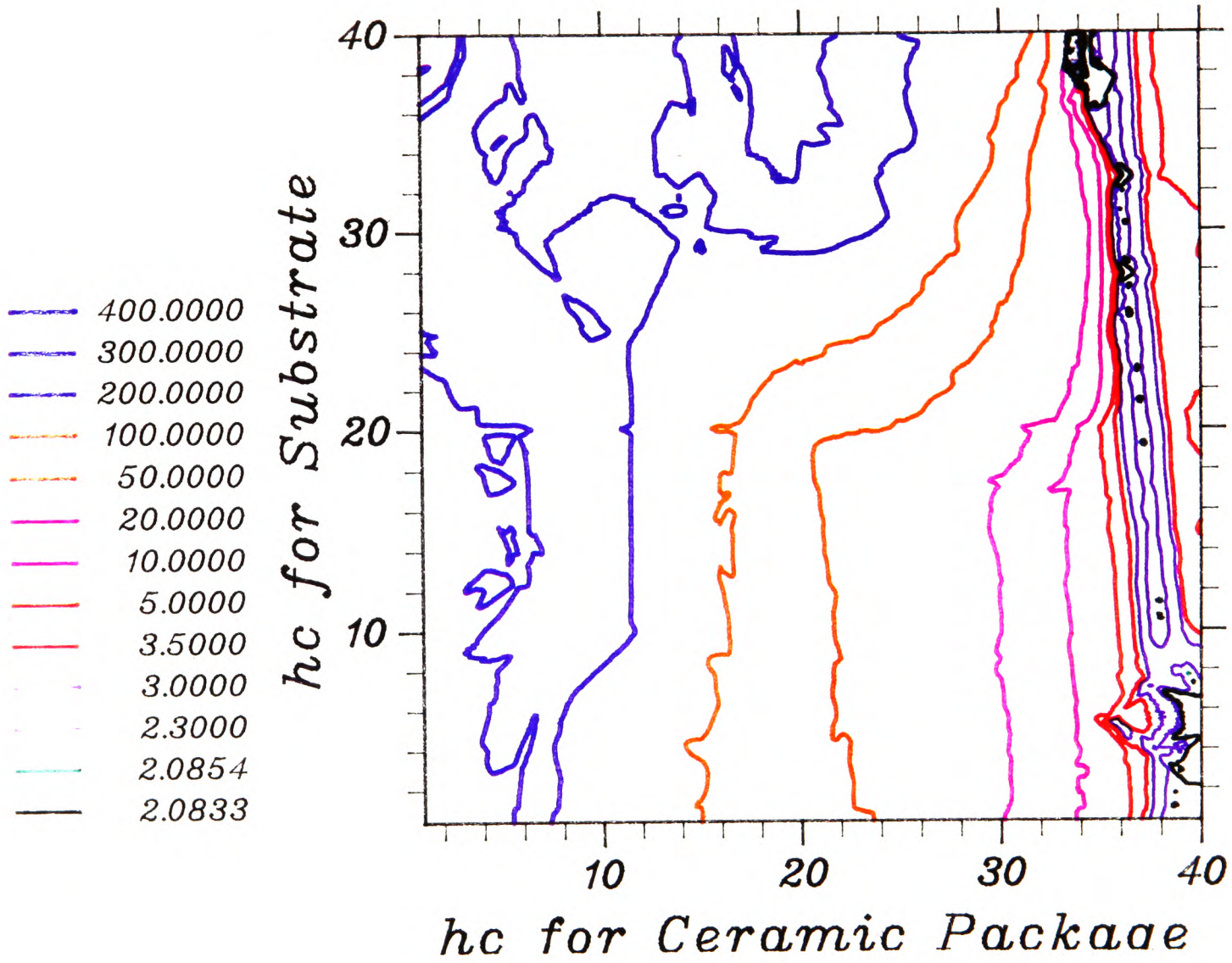

to a minimum value of 2.083. Further simulations showed that this minimum value could not be reduced any more by reducing the step sizes for h_1 and h_2 (below 0.1). These minima correspond to temperatures of 158.5 and 146 °C compared to experimentally obtained values of 161 and 144 °C. A number of such minima occur at various values of h_1 in the h_2 range mentiond above. A selected set of error results is given in Table (9.1) in which the error results are also presented for the h_1/h_2 values surrounding the minimum. These show similar error patterns appearing around each minimum point. The results indicate that at lower values of h_1 the minimum value is sustained in a larger range of h_1 values. For instance when h_2=38.6 W/m^2K the minimum occurs in the h_1 range of 0.9-1.2 W/m^2K whereas for h_2=36.1 W/m^2K the minimum only occurs at h_1=36.2 W/m^2K. No further minima were found for higher values of h_1.

These observations show that the simulation results are insensitive to the convection losses from the substrate/resistor (chip) section of the carrier. The important parameter for thermal analysis of the hybrid resistor is therefore the convection coefficient used for the outer section (surrounding ceramic) of the carrier where the convection losses are greater due to the formation of a boundary layer. This can be justified from the Schlieren photograph in figure (9.8) showing that the substrate is situated in the middle of the plume within the *chimney*. The transmission of heat by convection and conduction is restricted in this part of the plume because of a lack of a boundary layer and a reduced molecular density. The bulk of the heat generated in the resistor is therefore conducted through the ceramic carrier and subsequently convected away from the outer section of the carrier. Thus the process is relatively insensitive to the value of the convection coefficient over the chip. An ASTEC3 thermal simulation of a model of the package was therefore carried out using one set of h_1/h_2 values from which an output of all the steady-state nodal temperatures on the resistor/substrate surface was obtained. Figure (9.13) is a contour plot of the top surface of the device generated using the program described in section (2.3).

$h_1 \rightarrow$ $h_2 \downarrow$	0.8	0.9	1.0	1.1	1.2	1.3
38.5	2.143	2.143	2.092	2.092	2.092	2.092
38.6	2.13	2.083	2.083	2.083	2.083	2.13
38.7	2.134	2.092	2.092	2.092	2.092	2.14

(a)

$h_1 \rightarrow$ $h_2 \downarrow$	10.5	10.6	10.7	10.8	10.9
37.7	2.134	2.092	2.092	2.092	2.134
37.8	2.13	2.083	2.083	2.083	2.13
37.9	2.092	2.092	2.092	2.142	2.142

(b)

$h_1 \rightarrow$ $h_2 \downarrow$	21.4	21.5	21.6	21.7
36.8	2.092	2.143	2.092	2.092
36.9	2.13	2.083	2.083	2.13
37.0	2.092	2.092	2.142	2.142

(c)

h_1 & h_2 in W/m^2K

$h_1 \rightarrow$ $h_2 \downarrow$	30	30.1	30.2	30.3
36.1	2.143	2.092	2.092	2.134
36.2	2.13	2.083	2.13	2.13
36.3	2.092	2.142	2.142	2.142

(d)

Table (9.1) The Errors in the Simulation Results obtained Using a Combination of h_1/h_2 Values in the ASTEC3 Model of the Hybrid Resistor

Figure (9.13) The Steady-State Temperature Distribution over the Resistor Sample as Simulated by ASTEC3

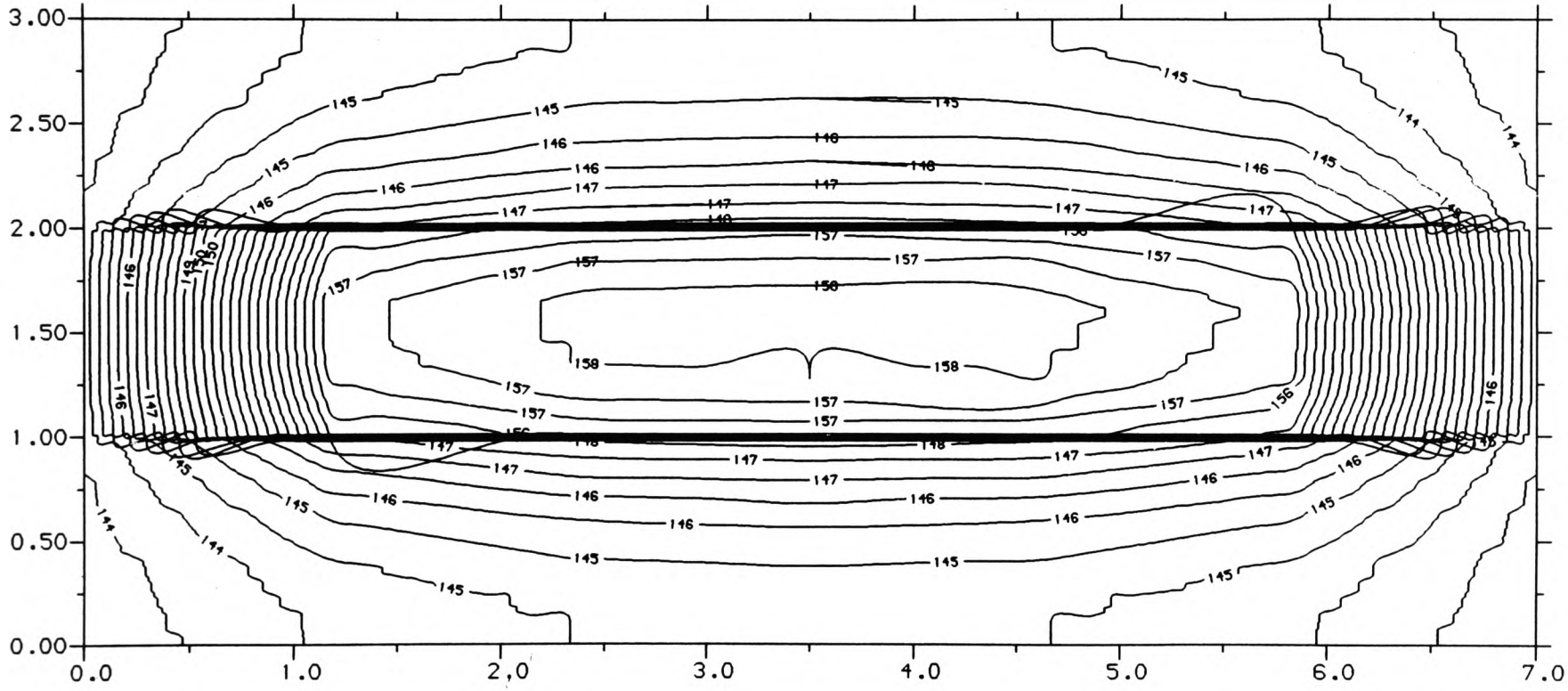

9.6 Conclusions

The ASTEC3 thermal modelling technique has been applied here for simulation of the heat flow in a hybrid resistor sample. This was the specimen with a (20 *mm* × 100 *mm*) resistor printed symmetrically onto a (60 *mm* × 140 *mm*) substrate. The AGEMA thermal imaging equipment was used to capture an image of the temperature distribution over the surface of the device. This showed steady-state temperatures of 161 ± 2 °C at the mid-points of the resistor and 144 ± 2 °C at the adjacent substrate areas when an electric power of 1.95 Watts were applied to it.

The sample was subsequently modelled and simulated via ASTEC3 package. It was found that the simulated temperatures were very sensitive to the convective heat transfer coefficient values. The value of this parameter varies considerably over the surface of the heated structures. Initial simulations using the average heat transfer coefficients obtained from the macroscopic case showed temperatures of 235 °C and 223 °C in the resistor and substrate areas respectively which were evidently excessive. A study of the convective heat flow over the whole of the carrier assembly using the Schlieren apparatus showed that the convective losses over the substrate area were much smaller than that of the rest of the carrier. This was thought to be due to the boundary layer forming over and covering the large area extending from the edge of the carrier to the substrate causing a great amount of heat loss by convection. The boundary layers from the two edges meet in the central region over the substrate rising in the shape of a chimney with a reduced heat loss rate due to the lack of a boundary layer.

An extensive number of ASTEC3 simulations revealed that the value of convection coefficient for the outer carrier section lies in a range extending from 36.2 and 38.6 W/m^2K within which the square root error is reduced to 2.083%. The simulation results were found

to vary very little with the value of the convection coefficient used for the thick film/substrate section in the ASTEC3 model suggesting that the generated heat is conducted through the bottom of the substrate and then convected into the atmosphere, thus variation in the direct chip to atmosphere path has minimal effect on the results.

10 DISCUSSIONS AND CONCLUSIONS

This thesis has been dealing with one of the major problem areas in the electronic industry. This is the thermal dissipation problem which is the result of the growing increase in the packing density of devices fabricated on ceramic substrates namely hybrid circuits. The initial objectives of the project was to develop a fully interactive computer modelling tool capable of simultaneous simulation of the electrical and thermal characteristics of hybrid and semiconductor device. The initial investigation using a macro-scale model however showed that a better understanding of the heat transfer mechanisms was needed. It was also found that the thermal conductivity of PCB reinforced laminates was required which meant that a great deal of effort was concentrated on determination of the conductivity of FR4 boards and convective heat transfer processes from the plates. A brief outline of the achievements within the context of the project will be given first and a more detailed discussion of these will be included later in the section.

• A novel experiment was designed which allowed the measurement of the tangential thermal conductivity of materials in the shape of a thin flat board. This was subsequently used to estimate the in-plane conductivity of FR4 insulating boards.

• It was demonstrated, using a Schlieren apparatus and optimisation techniques that the natural convection coefficient for partially heated boards in a horizontal position with the heated side facing upwards was much larger on the outside than in the heated region and that the coefficient may be approximated by two values for thermal analysis. The convection mechanism from the type of structures described in this thesis has not been treated by other workers and the results for convection coefficients not presented before.

• The Schlieren optical apparatus was used to observe the natural convection plumes forming over a horizontally positioned packaged hybrid resistor sample. It was found that:

a Convection *is* an important heat transfer mode in the analysis of electronic devices.

b The convection coefficient may be approximated by two values one for the area over the chip and the surrounding well and another one for the rest of the assembly.

c The simulation results are quite insensitive to the coefficient value used over the chip and the well but it is important and high over the ceramic package area.

The Schlieren technique has not in the past been used for the observation of convection plumes over packaged devices and no account of such analysis is published elsewhere.

• Interface cells have been introduced which make it possible to model via ASTEC3 the more important sections of a circuit in finer detail reducing computing time and hence saving resources.

• Software has been developed for producing thermal contour maps from the simulated temperature data.

• Programs are developed to facilitate the automatic generation of an error-free net-list of a particular structure.

• CPU time calculations have been carried out to allow the prediction of simulation times. It has been demonstrated that the simulation times are feasible for hybrid and VLSI circuits.

A more detailed account of the above statements is given below:

A modelling system has been used which makes use of the analogy between thermal and electrical systems. A thermal structure is divided into a number of thermal *cells* and an electrical equivalent model of the structure is constructed by connecting together the appropriate number of thermal cells. The circuit is subsequently simulated using ASTEC3 electronic simulation software.

Procedures have been proposed which allow the modelling of the more important areas of a device in finer details hence giving a more accurate temperature values at such positions. The connection between the *coarse* and *fine* mesh areas is accomplished using special thermal cells so-called *interface cells*. This optional facility reduces the computing time required for a simulation, clearly saving resources when dealing with very large circuits. Tests have been carried out showing that the introduction of fine mesh areas to a structure originally simulated via a full coarse mesh model greatly improves the accuracy of the simulated results.

The most tedious task in the modelling of a structure is the editing of the data file which includes the net-list for the particular device in ASTEC3 language. Software has therefore been devised to generate the ASTEC3 codes for a two or three dimensional structure divided into a uniform mesh. The user is asked a few simple questions such as the output file name, the number of thermal cells in the x, y and z directions. The type of simulation (transient or steady-state) and the length of a transient simulation is also inquired. Upon receiving the answers from the keyboard, the software automatically generates the listing for the particular structure. This is an important tool for any modelling system since it not only reduces the cumbersome task of inputting a large amount of data, it also produces an error-free circuit description which is virtually impossible to create manually for very large circuits.

Plotting routines have been developed which make it possible to draw temperature maps of a heated surface. The nodal temperatures are simulated and stored in a data-file. These are subsequently read by the program and routines from the GINO CAD package are called to produce contour-maps or three dimensional temperature distribution plots. The plotting routines and the ASTEC3 simulations are linked together via a master command file. The software is designed such that the transient thermal behaviour of a surface can also be studied by plotting the distributions at the required time steps. At each time step the screen is cleared and a new plot is generated.

It was important for a user to be able to predict the simulation time needed for thermal analysis of a particular device. It was also imperative that these simulation times were realistic. For this reason, tests were carried out which yielded a set of simple relationships which allow the prediction of the CPU time with a knowledge of the number of thermal cells. These equation were subsequently used to demonstrate that the CPU time was feasible for the analysis of a hybrid circuit.

Experiments were designed using Printed Circuit Boards (PCBs) resembling thick film resistors on ceramic substrates. The specimen were prepared by forming islands in the copper layer of the PCB plates. These were produced by etching grooves in the copper layer so that they were electrically isolated from the rest of the copper film but thermally connected via the insulator. The islands were heated electrically and an infrared pyrometer was used to measure surface temperatures at selected points. Assuming that the insulating board was isotropic, the thermal conductivity was measured using a Lees' disc apparatus which gives this parameter in a direction normal to the plate. The subsequent simulation of a model of the heated plates showed excessive temperatures within the islands. Further consideration of the method of fabrication and simulation tests using different values for the in-plane thermal conductivity of the boards revealed that the thermal conductivity of

the boards was in fact anisotropic. In the view of the fact that there were no apparatus available commercially or otherwise capable of measuring the thermal conductivity in the plane of such boards, an experiment was designed to carry out this task. In brief, the experiment is carried out in a vacuum chamber where long rectangular samples of the insulating board are heated. The heating is applied at one end and steady temperatures are measured along the length of the specimen. Temperatures of each position are recorded at various pressures and graphs are produced relating the pressure and the corresponding temperatures. By extrapolation to zero pressure, a temperature profile is obtained for the specimen at zero pressure. This is in order to simulate a situation where radiation would be the only heat loss mechanism from the sample and convection can be ignored since this is a very difficult process to account for. A finite difference representation of the structure is then derived in which the thermal conductivity is left as a variable. This is used to calculate the temperature profiles using a range of thermal conductivities. These are compared with the measured set of data until a best-match profile is found. The thermal conductivity yielding the particular temperature distribution is then taken as the thermal conductivity of the boards. A value of 1.059 ± 0.019 W/mK was obtained for the in-plane thermal conductivity of the FR4 boards compared to 0.343 ± 0.017 W/mK in a normal direction. The subsequent ASTEC3 simulation of the plates displayed a great reduction in the errors. The devised experiment is a novel one which can be used in other areas of research where thermal conductivity of materials in the form of a thin board is required. The final results of the experiment are of course invaluable for anyone dealing with the thermal aspects of PCB design.

Although the anisotropic conductivities reduced the simulation errors, there were still errors in the results due to the averaged convection coefficients used in the model which were calculated using empirical relationships. A Schlieren optical apparatus was therefore used to study the natural convection plumes forming over these plates. This is a technique

whereby a slit/lens combination is used to produce a parallel beam of light which is focussed to a point via another concave lens. The medium whose refractive index variation is to be investigated is located in the path of the light beam between the lenses. The variation in optical path causes the wavefront to be distorted and focussed as such. A knife edge is then used at the focus to obstruct part of the image and the remainder of is imaged on a ground-glass screen. The shadows reveal an angular displacement of the rays and it indicates the rate of change of index across the region concerned. Using this method it was demonstrated that the heat transfer coefficient of convection over a plate with a centrally heated island could be approximated to two values. One coefficient value over the heated island and another over the rest of the plate, the latter being much larger than the former. Tests also revealed that a ratio of 3.375 to 1 would reduce the simulation errors over two selected points on the surface to a minimum.

Hybrid resistor samples which resembled the PCB plates were also tested. These were manufactured by RSRE and temperature measurements were carried out using an AGEMA thermal imaging equipment. The Schlieren apparatus was again employed to view the heat flow over the packaged devices. The tests over the resistor sample similar to that used in macro scale experiment displayed that the convection coefficients could again be approximated to two values. One coefficient value could be used for convection from the chip (resistor/substrate) region and another for the rest of the carrier assembly. This was different from the macro scale situation where the two sections were the heated island and the unheated surrounding areas of the PCB plate. It was found that a value for the outer section of the carrier in the range 36.2-38.6 W/m^2K reduced the errors in the simulated temperatures to a minimum. The simulated results and hence the square root errors were however found to be insensitive to the convection coefficient used in the model for the resistor/substrate section of the carrier.

ASTEC3 package is now almost ten years old and with the availability of advanced circuit analysis packages, it is perhaps advisable for a future user to investigate the possibility of replacing ASTEC3 with a more user-friendly *successor*. Such a simulation program should ideally have the following capabilities:

- It should be an analogue circuit simulator capable of performing AC small signal, DC steady-state and transient simulations.
- The simulation technique should be fast, efficient and also very accurate.
- The model generation should be simple and possibly automated.
- There should be no restrictions in the variables allowed and also the number of circuit components.
- It should be possible to store the final results of a simulation so that the circuit may be analysed again later using different parameter values without the need for repeating the whole simulation.
- The user should be able to monitor the simulation so that the state of the analysis can be checked.
- It should have a built-in facility for plotting contour-maps which is important for thermal modelling.

10.1 Future Work

The code generation software so far developed can only produce the electrical equivalent circuit of a device if it was divided into a uniform rectangular mesh. It is not capable of producing the necessary syntax for cases where a mixture of fine and coarse mesh areas is used. This would have to include the necessary routines for generating the code for the interface cells. This is an area which needs further development in order to make the modelling more user-friendly.

The contour-plotting programs may be extended in the future to display a three-dimensional temperature map of a device growing with time rather than at each time-step. It may also be possible to use another plotting package such as UNIRAS which is capable of producing colour maps making it easier to distinguish between different temperature areas.

The future development of the ASTEC3 thermal modelling software could include building of a library of thermal modules for typical component structures. These can then be called up within the description file of more complex circuit arrangements without the need for generating the code for the particular components. Further tests could also be carried out to establish whether or how the 2-D simulation times can be used to estimate the simulation times for a 3-D model.

The coupling of the electrical and thermal analysis of packaged devices was an area which was not dealt with within the project as was originally intended. This is an avenue which should be explored fully in the future especially if the transient behaviour of circuits is to be considered. The description section ($DESC) of the ASTEC3 data file in this case will have two *layers*, one describing the electronic components of the circuit and the other will include the thermal model of the same device. Of course the layer dealing with the thermal aspect of the device will consist of the thermal model of the chip and that of the package. The simulation of the circuit would calculate the essential parameters at each time step which will then be input into the thermal layer for temperature calculations. The heat transfer coefficients of convection and radiation would be re-adjusted according to the simulated temperature distribution. Further work should be carried out to establish the manner by which these coefficients vary over the surface in a transient situation.

Further work could also be carried out to develop a fully interactive structure placement facility with continuous update of the thermal simulation, thus allowing a user to optimise

the layout for thermal performance.

So far in this investigation the analysis has been on very simple hybrid resistor sample. This should be extended to a more complex circuit arrangement and simulation results verified accordingly. Hybrid microcircuits normally consist of several separate components attached to a ceramic substrate and interconnected by wire bonds or suitable metallisation pattern. The individual parts may consist of diffused or thin film components or one or more monolithic integrated circuits. In dealing with the thermal analysis of such devices various approaches may be taken depending on the requirements of the design. If the reliability of the individual microcircuit (an operational amplifier for example) on the hybrid chip is not in question, then these components may be treated as single point sources and modelled as such. However if the temperature details of the individual integrated circuits is required which may be a Medium Scale Integration (MSI) or Large Scale Integration (LSI) device then these parts may be modelled using a suitable fine grid and the rest of the hybrid chip modelled using an appropriate coarse mesh, the different grids connected together via interface cells of the correct type.

Further tests will also be needed to explore the modelling situation in the case of devices fabricated on semiconducting substrates. These would initially be on MSI circuits and extended further to higher density circuits. In dealing with VLSI circuits because of the very small feature sizes and a very large number of components the model would contain an extremely large number of thermal cells if a full fine grid was used. In order to save computer resources, investigations should be carried out to explore the mixing of fine and coarse mesh areas. To ascertain where on the device finer grids may be needed it would perhaps be practical to carry out a full coarse mesh simulation to reveal the hotter, more important sections of the chip. This would then then be followed by a mixed grid simulation.

To allow temperature measurements from the surface of the resistor samples, the covers had been removed from the top of the carrier. In the real situations these covers would of course be in position protecting the chip from possible damage. With the lid in position, there will be a very small gap of about 1 mm between the chip and the cover. The gap is so small that when the device is operating, the boundary layers discussed for the de-lidded situation cannot develop. What can happen is that the generated heat will be conducted through the trapped air (or whatever the filling) and cause a temperature rise of the cover and the surrounding carrier sections. The heat is then convected and radiated to the surroundings. Further work can be carried out to investigate the effect of the lid on the chip surface temperature. The ceramic lid may be replaced in these investigations with a material transparent to infrared radiation such as polyethylene [transparent in the range 1.8-5.5 μm] which would allow the measurement of the chip temperature profile with the lid in position. The Schlieren apparatus could subsequently be used to examine the heat flow over the carrier with the simulated lid leading to a better understanding of the convection losses. Further tests can be carried out to determine the heat transfer coefficients of convection for various devices specified possibly by the geometry, total input power, etc. Charts may be produced in this way which will allow the thermal designer to select the optimum values for a new circuit.

11 REFERENCES

CHAPTER 1

1. KINNIMENT D J, EDWARDS D A: 'Thermal Design in a Hybrid System with High Packing Density', *IEEE Transactions on Components, Hybrids, and Manufacturing Technology*, Volume CHMT-1, No. 2, June 1978, pp. 176-181.
2. HASKARD M R: *An Introduction to Application Specific Integrated Circuits*, Prentice Hall, Australia, 1990.
3. WITTING P A, SARVAR F, POOLE N J: 'Electro-Thermal Simulation of Hybrid and VLSI Circuits', *Digest of NASECODE Software Forum*, Dublin, 1989.
4. DE MEY G: 'Thermal Analysis in CAD of Hybrid Circuits', *Hybrid Circuits (UK)*, No.22, May 1991, pp.16-17.
5. MAHLINGAM M : 'Thermal Management in Semiconductor Device Packaging', *Proceedings of the IEEE*, Volume 73, No. 9, September 1985, pp. 1396-1405.
6. KLINGER D J, NAKADA Y, MENENDEZ M A: *AT & T Reliability Manual*, Van Nostrand Reinhold, New York, 1990.
7. PECK D S: 'The Analysis of Data from Accelerated Tests', *Proceedings of the 9th Reliability Physics Conference*, 1971, pp. 69-78.
8. BASLER M: 'Hybrid Thermal Analysis: A Design Tool', *Hybrid Circuit Technology*, pp. 79-84, September 1987.
9. BOYLSTEAD R, NASHELSKY L: *Electronic Devices and Circuit Theory*, Prentice-Hall Inc., N.J., Third Edition, 1982.
10. SAVANT C J, RODEN M S, CARPENTER G L: *Electronic Circuit Design, an Engineering Approach*, The Benjamin/Cummings Publishing Company Inc., 1987.
11. SMITH R J: *Circuits Devices and Systems*, John Wiley & Sons Inc., New York, Third Edition, 1977.
12. MILLMAN J: *Microelectronics: Digital and Analog Circuits and Systems*, McGraw-Hill Book Company, Singapore, 1986.
13. HODGES D A, JACKSON H G: *Analysis of Digital Integrated Circuits*, McGraw-Hill, 1983.
14. CARR W N, MIZE J: *MOS/LSI Design and Application*, New York, McGraw-Hill, 1972.
15. HEIN V L, LENZI V D: 'Thermal Analysis of Substrates and Integrated Circuits', *Proceedings of Electronic Component Conference*, May 1969, pp. 166-177.
16. SZEKELY Y, SZIRANYI T: 'On the Simulation of IC Chip Temperature Distribution', *Period. Polytech. Electron. Eng. (Hungary)*, Volume 30, No. 1, 1986, pp. 49-53.

17. DAVID R F: 'Computerised Thermal Analysis of Hybrid Circuits', *IEEE Transactions on Parts, Hybrids and Packaging*, Vol. PHP-13, No. 3, September 1977 pp. 283-289.
18. GREGORY P: 'Thermal Characteristics of a Hybrid Microcircuit', *11th Seminex Conference on Advances in Electronic Components and Systems*, 1982 pp.347-57.
19. WEHRHAHN E: 'Temperature Distribution on Substrate of Hybrid Integrated Circuits', *5th European Microelectronics Conference*, 1985 pp. 288-295.
20. KIP A F: *Fundamentals of Electricity and Magnetism*, 2nd Edition, McGraw-Hill Kogakusha Ltd., Tokyo.
21. SPROUL R L: *Modern Physics*, second Edition, Wiley &Sons, New York, 1966.
22. WHITE O M: *Essentials of Electricity and Magnetism*, McMillan, 1965.
23. NOAKES G R: *A Text Book of Electricity and Magnetism*, McMillan & co. Ltd., London, 1950.
24. ZIMMER C R: 'Computer Simulation of Hybrid Integrated Circuits Including Combined Electrical and Thermal Effects', *3rd European Hybrid Microelectronics Conference*, Avignon, 1981, pp.44-50.
25. ARKIN O: 'Practical Computer Program for Improved Hybrid Thermal Analysis', *Hybrid Circuit Technology*, pp. 37-39, November 1986.
26. REED D L, GARTNER B W: 'Thermal Modelling of Hybrid Microelectronics', *Spanning the Peaks of Electrotechnology, IEEE Region 5 Conference*, pp. 235-239, 1988.
27. SIBERGOVIC S, BOSNJAK K.M.: 'Computer Application in Thermal Analysis of Microelectronic Circuits', *International Colloquium on New Orientations of Passive Components*, 1982 pp. 415-418.
28. CASSELMAN G, DE MAY G : 'A Thermal Model for Hybrid Circuits', *Hybrid Circuits*, No. 10, May 1986, pp.9-13.
29. ROTTIERS L, DE MEY G : 'Hot Spot Effects in Hybrid Circuits', *IEEE Transactions on Components, Hybrids, and Manufacturing Technology*, Vol. 11, No. 3, September 1988, pp. 274-278.
30. HAMBLING P G, DEAN D J: 'Microcircuit Thermal Design Tables and Computer Program for Two-Dimensional Layouts', *Conference on Hybrid Microelectronics*, England, September 1975, pp. 191-204.
31. DE MEY G, SCHOOR L V: 'Thermal Analysis of Hybrid Circuits with Mounted Components', *Hybrid Circuits*, No. 15, January 1988, pp. 28-32.
32. POGSON J T, FRANKLIN J L: 'Analysis and Temperature Control of Hybrid Microcircuits', *Transactions of the ASME, Journal of Engineering for Industry*, November 1973, pp. 1048-1052.
33. WENTHEN F T: 'Computer Aided Thermal Analysis of Power Semiconductor Devices', *IEEE Transactions on Electronic Devices*, Volume ED-17, No. 9, September 1970, pp. 765-770.

34. BILSON R T, ALLEN R W, McCARTHY J P, STANLEY A J: 'Thermal Management Evaluation of Large Size Thick Film Hybrids', *Hybrid Circuits*, No. 10, May 1986, pp. 65-67.
35. WEHRHAHN E: 'Temperature Distribution on Multilayer Substrates', *Proceedings of the 6th European Microelectronics Conference*, pp. 264-280, England, June 1987.
36. BARBOU R, MENOZZI G and MOULIN G: 'Temperature Prediction on Hybrid Microelectronics', *Proceedings of the 6th European Microelectronics Conference*, pp. 332-339, England, June 1987.
37. BAYLEY F J, OWEN M J, TURNER A B: *Heat Transfer*, Nelson & Sons Ltd., London, 1972
38. KREYSZIG E: *Advanced Engineering Mathematics*, Fourth Edition, John Wiley & Sons, New York, 1979.
39. LINDSTED R D, SURTY R J: 'Steady-State Junction Temperature of Semicinductor Chips', *IEEE Transactions on Electron Devices*, Volume ED-19, No. 1, January 1972, pp. 41-44.
40. LEE C C, PALISOC A L: 'Thermal Analysis of GaAs IC Devices', *IEEE Gallium Arsenide Integrated Circuit Symposium*, Technical Digest, 1986, pp. 115-118.
41. CASTELLO R, ANTOGNETTI P: 'IC Thermal Modelling', *IEEE Journal of Solid State Circuits*, June 1978, pp. 146-147.
42. ANTOGNETTI P, BISIO G R, CURATELLI F, PALARA S: 'Three Dimensional Transient Thermal Simulation: Application to Delayed Short Circuit Protection in Power IC's.', *IEEE Journal of Solid-State Circuits*, Volume SC-15, No.3, pp. 277-281, June 1980.
43. RAMAKRISHNA K: 'Thermal Analysis of Composite Multilayer Structures with Multiple Heat Sources', *Proceedings of the 2nd IEPS Conference*, 1982, 281-295.
44. FERRARIS G P, TUDANCA M: 'The Solution of Two-Dimensional Heat Conduction Problems to Predict Operating Temperature and Power Handling Capabilities of Hybrid Circuits', *European Hybrid Microelectronics Conference*, Ghent, pp. 61-74, 1979.
45. ZIMMER C R: 'Electrothermal Analysis of Hybrid Integrated Circuits Using the SPICE II Computer Program', *Proceedings of the 32nd Electronic Components Conference*, New York, 1982, pp. 24-25.
46. SAULINER J B: 'Description of a Thermal Model Library for Use in Electrical C.A.D. Programs', *Proc. Spacecad 79 Computer aided design of Electronics for Space Applications*, Bologna, pp. 65-76, 19-21 September 1979.

CHAPTER 2

1. 'ASTEC3 User Manual', SIA Computer Services, London, England, 1984
2. WITTING P A: 'Electronic Circuit and System Simulation with ASTEC3', *Computer Aided Engineering Journal*, 1985, 2,(6), pp. 186-191.

3. 'Analogue Simulation- ASTEC3 Improves on SPICE', SIA Computer Services, London, England.
4. DWYER P: 'ASTEC3 - An Alternative To SPICE', *Electronic Design Products*, October 1984 pp. 89-90.
5. MILLER I, FREUND J E: *Probability and Statistics for Engineers*, New Jersey, Prentice Hall, 1985.
6. SMITH R J: *Circuits, Devices, and Systems*, 3rd edition, 1976, Wiley and Sons, p. 516.

CHAPTER 3

1. KITTEL C: *Introduction to Solid State Physics*, New York, Wiley and Sons, 5th edition, 1976.
2. BACKHURST J R, HARKER J H, PORTER J E: *Problems in Heat and Mass Transfer*, London, Arnold, 1974, P.84.
3. DEKKER A J: *Solid State Physics*, London, Macmillan & Co, 1st edition, 1967.
4. SPROULL R L: *Modern Physics*, London, Wiley & Sons, 2nd Edition, 1966.
5. CHAPMAN A J: *Heat Transfer*, New York, McGraw-Hill, 1984.
6. HOLMAN J P: *Heat Transfer*, New York, McGraw-Hill,1981.
7. BAYLEY F J, OWEN J M, TURNER A B: *Heat Transfer*, London, Nelson, 1972.
8. OZISIK M N: *Basic Heat Transfer*, New York, McGraw-Hill, 1977.
9. INCORPERA F P, DEWITT D P: *Fundamentals of Heat and Mass Transfer*, New York, Wiley and Sons, 1985.
10. KREITH F: *Principles of Heat Transfer*, New York, Harper and Row, 1973.
11. OZISIK M N: *Heat Transfer: A Basic Approach*, McGraw-hill Book Company, 1985.
12. JAKOB M: *Heat Transfer*, Volume 1, Wiley and sons, 1967.
13. EASTOP T D, McCONKEY A: *Applied Thermodynamics for Engineering Technologists*, New York, Longman, 2nd Edition, 1974.
14. ROGERS G F C, MAYHEW Y R: *Engineering Thermodynamics Work and Heat Transfer*, 2nd Edition, Longman, 1976.

CHAPTER 4

1. CHAPMAN A J: *Heat Transfer*, New York, McGraw-Hill, 1984.

CHAPTER 5

1. CHAPMAN A J: *Heat Transfer*, New York, McGraw-Hill, 1984.
2. BAYLEY F J, OWEN J M, TURNER A B: *Heat Transfer, London*, Nelson, 1972, pp. 90-92.
3. HOLMAN J P: *Heat Transfer*, New York, McGraw-Hill, 5th edition, 1981, pp. 61-65.
4. KREITH F: *Principles of Heat Transfer*, Harper & Row, 3rd edition, 1976, pp. 87-89.

5. DONGARRA J J: 'Performance of Various Computers Using Standard Linear Equations Software in a FORTRAN Environment', *Proceedings of the 3rd conference on Multiprocessors and Array Processors*, Jan 1987, pp. 15-32.
6. *Proceedings of the Reunion of the ASTEC Users Club*, France, Oct. 1988.

CHAPTER 6

1. 'Nextel 2010 Coating' Product Performance Bulletin and Application Instructions, 3M Industrial Chemical Products, 3M Head Office, Bracknell, Berks, England.
2. CHAPMAN A J: *Heat Transfer*, New York, McGraw-Hill, 1984.
3. OZISIK M N: *Basic Heat Transfer*, New York, McGraw-Hill, 1977.
4. GOLDSTEIN R J, SPARROW E M, JONES D C: 'Natural Convection Mass Transfer Adjacent to Horizontal Plates', *Int. Journal of Heat and Mass Transfer*, May 1972 pp. 1025-1034.
5. LLOYD J R, MORAN W R: 'Natural Convection Adjacent to Horizontal Surface of Various Planforms', *ASME Journal of Heat Transfer*, 1974 pp. 1-5.
6. HEIMANN Radiation Thermometer KT14 Instruction Manual, HEIMANN Gmbh, Infrared Measurements, D-6200 Wiesbaden-Dotzheim, West Germany.
7. BOYLSTAD R, NASHELSKY L: *Electronic Devices and Circuit Theory*, New Jersey, Prentice-Hall Inc., 1982, p. 488.
8. Private Communication, Mica and Micanite (Ireland) Limited, Mallow, Co. Cork, Ireland.

CHAPTER 7

1. KAY G W C, LABY T H: *Tables of Physics and Chemical Constants*, 15th Edition, Longman Group Limited, 1986, p. 69.
2. Private Communication, Mica and Micanite (Ireland) Limited, Mallow, Co. Cork, Ireland.
3. CHAPMAN A J: *Heat Transfer*, 4th Edition, McGraw-Hill, New York, 1984, p. 131.
4. STARLING A J, WOODALL A J: *Physics*, 2nd Edition, Longmans, 1964, pp.320-321.
5. Equipment Notes No. P28030/1 for Lees' Disc Apparatus from Philip Harris Ltd. Shenstone, England.
6. TOPPING J: *Errors of Observation and Their Treatment*, 4th Edition, Chapman and Hall, 1975.
7. Data Sheet No. PD4/7/82, Polypenco Engineering Plastics Materials Limited, 76 Bridge Road East, Welwyn Garden City, Herts, England.
8. BAYLEY F J, OWEN J M and TURNER A B: *Heat Transfer*, Nelson and sons Limited, 1972, pp 90-92.
9. 'Nextel 2010 Velvet Coating' *Product Performance Bulletin and Application Instructions*, 3M Head Office, Bracknell, Berks, England.

10. WARD L, BUNN J P: *Introduction to the Theory and Practice of High Vacuum Technology*, Butterworths & Co. Limited, London, 1967.
11. EASTOP T D, McCONKEY A: *Applied Thermodynamics for Engineering Technologists*, second Edition, Longman Group Limited, London, 1974.
12. OZISIK M N: *Basic Heat Transfer*, McGraw-Hill Book Company, New York, 1977.

CHAPTER 8

1. INCORPERA F P, DEWITT D P: *Fundamentals of Heat and Mass Transfer*, Wiley & Sons, Second Edition, 1981.
2. JENKINS F A, WHITE H E: *Fundamentals of Optics*, McGraw-Hill Kogakusha Limited, Fourth Edition, 1976, p. 604.
3. HECHT E: *Optics*, Addison-Wesley Pub. Co., Second Edition, 1987, p. 577.
4. LIEPMANN H W, ROSHKO A: *Elements of Gasdynamics*, Wiley and Sons Inc., New York, 1957, pp. 153-162.
5. PANKHURST R C, HOLDER D W: *Wind-Tunnel Techniques*, Pitman & Sons, London, 1952, pp. 162-167.
6. LONGHURST R S: *Geometrical and Physical Optics*, Longmans, second Edition, 1968, pp. 336-337.
7. 'The SCHLIEREN Apparatus' Instructions Manual No. TE65/A, Plint and Partners Limited, Fishpond Road, Wokingham, Berkshire, England.

CHAPTER 9

1. Thick Film Substrates Data Sheet, Design Standard 49, COORS Ceramics Electronics Limited, 64 Cavendish Way, Southfield Industrial Estate, Glenrothes, Fife, Scotland.
2. Birox* 1400-Series Resistor Compositions for High Performance Hybrid Microcircuits and Resistor Networks. Data Sheet No. E13361. Du Pont Electronics, Du Pont (UK) Limited, Wedgwood Way, Stevenage, Herts.
3. Private Communication: Du Pont Electronics, Microcircuit & Printed Circuit Materials, Wedgwood Way, Stevenage, Herts, SG1 4QN.
4. Ceramic Packages Data Sheet No. 87C04, SHINKO Electric Industries Co. Limited, Supplied by: Dage (GB) Limited, Rabans Lane, Aylesbury, Bucks, England.
5. Data Sheet for Ablebond 41-4, electrically Insulating Adhesive For Microelectronics, Ablestic Laboratories, 833 West 182nd Street, Gardena, CA 90248, USA.
6. Thermovision 880 SWB Specifications, Publication No. 556556875 Ed. II Eng., AGEMA Infrared Systems Limited, Arden House, Leighton Buzzard, Beds, England.
7. PITT K E G: 'The Emissivity of Thick Film Resistor Materials', *Proceedings of the Int. Electronic Packaging and Production Conf.*, U.K., 1980, pp 258-260.
8. CHAPMAN A J: *Heat Transfer*, New York, McGraw-Hill, 1984.
9. TOPPING J: *Errors of Observation and Their Treatment*, 4th Edition, Chapman and Hall, 1975.

12 APPENDIXES

APPENDIX 1: Contour Plotting Programs

Program 1

```
c
c     This program reads the output file of an ASTEC3 simulation and
c     creates another file containing only the tables of results.
c


      CHARACTER*80 INLINE

10    READ(50,100)INLINE
      IF (INLINE(2:3).NE.'&T') GOTO 10
20    WRITE(51,100)INLINE
      READ (50,100,END=999)INLINE
      IF (INLINE(2:5).NE.'EDIT') GOTO 20
100   FORMAT(A)
999   END
```

Program 2

```
c
c     This program makes use of the tabular form of ASTEC3 output to plot
c     contour maps at each time interval. This is limited to centre nodes
c     of the cells.
c

c
c     All the arrays , strings etc. are defined as used within the program.
c

      IMPLICIT INTEGER*4 (A-Z)
      REAL X(200),Y(200),Z(200),X_INC,Y_INC,START_Y,START_X
      REAL AZ(30,50),W(2000),XLOW,XHIGH,YLOW,YHIGH
      REAL   INPUT_TIME(5)
      REAL   INPUT_VAR1(15)
      REAL   INPUT_VAR2(15)
      REAL   INPUT_VAR3(15)
      REAL   INPUT_VAR4(15)
      REAL   INPUT_VAR5(15)
      CHARACTER*80 FILE_NAME,TIME_STRING*30
      REAL STORE_ARRAY(15,500),MIN_DIFF
      REAL STORE_TIME(500)
      INTEGER*4  ARRAY_NUM,ADD_ON

c
c     ASTEC3 output file ir OPENed, READ and the data is stored in arrays
c     input_var
c

20    FORMAT(14X,F9.3,4(3X,F9.3))
      OPEN(UNIT=1,FILE=FILE_NAME)
      ARRAY_NUM=1
      ADD_ON=5
100   READ(51,20,ERR=100,END=999)(INPUT_TIME(I),I=1,5)
      DO J=ARRAY_NUM,ARRAY_NUM+4
      STORE_TIME(J)=INPUT_TIME((J-ARRAY_NUM)+1)
      ENDDO
      DO I=1,15
      READ(51,20,ERR=100,END=999)INPUT_VAR1(I),INPUT_VAR2(I),
     1INPUT_VAR3(I),INPUT_VAR4(I),INPUT_VAR5(I)
      IF (INPUT_VAR1(I).NE.0 .OR. INPUT_VAR2(I).NE.0) THEN
      STORE_ARRAY(I,ARRAY_NUM)=INPUT_VAR1(I)
      IF (INPUT_VAR2(I).NE.0 ) THEN
      STORE_ARRAY(I,ARRAY_NUM+1)=INPUT_VAR2(I)
      IF (INPUT_VAR3(I).NE.0 ) THEN
      STORE_ARRAY(I,ARRAY_NUM+2)=INPUT_VAR3(I)
      IF (INPUT_VAR4(I).NE.0 ) THEN
      STORE_ARRAY(I,ARRAY_NUM+3)=INPUT_VAR4(I)
```

```
      IF (INPUT_VAR5(I).NE.0 ) THEN
      STORE_ARRAY(I,ARRAY_NUM+4)=INPUT_VAR5(I)
      ELSE
      ADD_ON=4
      ENDIF
      ELSE
      ADD_ON=3
      ENDIF
      ELSE
      ADD_ON=2
      ENDIF
      ELSE
      ADD_ON=1
      ENDIF
      ELSE
      ADD_ON=0
      ENDIF
      ENDDO
      ARRAY_NUM=ARRAY_NUM+ADD_ON
      ADD_ON=5
      READ(51,11,END=999)
11    FORMAT(/)
      GOTO 100
999   CONTINUE
      I=0


c
c     The starting point, the number of grid points in the x and y directions
c     and the x and y increments are inquired to set up the grid.
c

      PRINT *,'Please give base value of X'
      READ(*,*)X(1)
      PRINT *,'Please give base value of Y'
      READ(*,*)Y(1)
      PRINT *,'Please give number of grids in X'
      READ(*,*)NUM_X
      PRINT *,'Please give number of grids in Y'
      READ(*,*)NUM_Y
      PRINT *,'Please give X increment'
      READ(*,*)X_INC
      PRINT *,'Please give Y increment'
      READ(*,*)Y_INC


c
c     A uniform mesh is generated comprising the centre nodes of all the cells
c

      START_Y=Y(1)
      START_X=X(1)
      COUNT=1
```

```
      DO I=1,NUM_Y
      DO J=1,NUM_X
      Y(COUNT)=START_Y
      IF (J.NE.1) X(COUNT)=X(COUNT-1)+X_INC
      COUNT=COUNT+1
      ENDDO
      START_Y=START_Y+Y_INC
      Y(COUNT)=START_Y
      X(COUNT)=START_X
      ENDDO

      DO I=1,COUNT
      ENDDO

      PRINT 6
6     FORMAT(1X,'Please give minimum time difference between plots ')
      READ(*,*)MIN_DIFF


c
c     All the necessary GINO subroutine are initialised for plotting purposes.
c

      CALL SETDEV(K)
      J=-1
      CALL ERRSWI(J)
      J=-1
      CALL ERRMAX(J)
      DO IZ=1,ARRAY_NUM
      IF (ILAST_PLOT.EQ.1.OR.
     1        ABS(STORE_TIME(ILAST_PLOT)-STORE_TIME(IZ)).GE.MIN_DIFF)
THEN
      ILAST_PLOT=IZ

      WRITE(TIME_STRING,1100)STORE_TIME(IZ)
1100FORMAT(1X,F10.0,'Seconds')
      DO I=1,15
      Z(I)=STORE_ARRAY(I,IZ)

      ENDDO
      NW=2000
      CALL PICCLE
      NP=NUM_X*NUM_Y

      XLOW=0
      YLOW=0
      XHIGH=NUM_X*X_INC
      YHIGH=NUM_Y*Y_INC
      CALL TITSTR(TIME_STRING)
      CALL RANGRD(NP,X,Y,Z,NUM_X,XLOW,XHIGH,NUM_Y,YLOW,
     1 YHIGH,AZ,NW,W)

      NCONT=10
      ISM=1
      NSYM=-8
      CALL RANPTS(NSYM)
      CALL DRACON(NUM_X,XLOW,XHIGH,NUM_Y,YLOW,YHIGH,
     1  AZ,NCONT,ISM,NW,W)
```

```
      CALL CHAMOD
      CALL WAIT

      ENDIF
      ENDDO
      END

c
c     Subroutine 'wait ' allows 3 seconds delay between each plot.
c

      SUBROUTINE WAIT
      IMPLICIT INTEGER*4 (A-Z)
      INCLUDE  '($IODEF)'
      LOGICAL FIRST/.TRUE./
      CHARACTER TERM*3 /'TT:'/,BUFF*1
      IF (FIRST) STATUS=SYS$ASSIGN(TERM,CHAN,,)
      FIRST=.FALSE.
      FUNC=IO$_READVBLK.OR.IO$M_TIMED
      STATUS= SYS$QIOW(,%VAL(CHAN),%VAL(FUNC)
     1 ,,,,BUFF,%VAL(1),%VAL(3),,,)
      RETURN
      END
```

Program 3

```
c
c     This program is designed to make use of the tabular form of ASTEC3 output
c     for a particular two-dimensional thermal simulation to plot contour maps
c     at each time interval. It generates three uniform grids in 2-D models to
c     carry out this task. It uses subroutines from GINO CAD package for
c     plotting.
c


c
c     All the various strings, arrays etc. used in the program are defined.
c

      IMPLICIT INTEGER*4 (A-Z)
      REAL X(200),Y(200),Z(200),X_INC,Y_INC,START_Y,START_X
      REAL AZ(30,50),W(2000),XLOW,XHIGH,YLOW,YHIGH
      CHARACTER CHAR*100,BUFFERS*1
      LOGICAL PLOTTER/.FALSE./
      REAL INPUT_TIME(5)
      REAL   INPUT_VAR(5)
      CHARACTER*80 FILE_NAME,TIME_STRING*30,ANS*80
      REAL STORE_ARRAY(5000,0:200),MIN_DIFF
      REAL STORE_TIME(5000),START_YN,START_XN
      CHARACTER*15 STRING
      INTEGER*4  ARRAY_NUM,ADD_ON
      COMMON STORE_TIME,LAST_TIME

c
c     ASTEC3 output file is OPENed, READ and the temperature data is stored in
c     arrays input_var for each time-interval.
c

      LAST_TIME=0
20    FORMAT(A14,F9.3,4(3X,F9.3))
      OPEN(UNIT=1,FILE=FILE_NAME)
      ARRAY_NUM=1
      ADD_ON=5
100   READ(51,20,END=999)STRING,INPUT_VAR(1),INPUT_VAR(2),
     1INPUT_VAR(3),INPUT_VAR(4),INPUT_VAR(5)
      IF (STRING(2:3).EQ.'&T') THEN
      DO ITIME=1,5
      INPUT_TIME(ITIME)=INPUT_VAR(ITIME)
      ENDDO
      ELSE IF (STRING(2:3).EQ.'  ') THEN
      ELSE
      IF (INPUT_TIME(1).NE.0 .OR. INPUT_TIME(2).NE.0) THEN
      WHERE_I=FIND_ARRAY(INPUT_TIME(1))
      STORE_ARRAY(WHERE_I,0)=STORE_ARRAY(WHERE_I,0)+1
      STORE_ARRAY(WHERE_I,STORE_ARRAY(WHERE_I,0))=INPUT_VAR(1)
      IF (INPUT_TIME(2).NE.0 ) THEN
      WHERE_I=FIND_ARRAY(INPUT_TIME(2))
```

```
      STORE_ARRAY(WHERE_I,0)=STORE_ARRAY(WHERE_I,0)+1
      STORE_ARRAY(WHERE_I,STORE_ARRAY(WHERE_I,0))=INPUT_VAR(2)
      IF (INPUT_TIME(3).NE.0 ) THEN
      WHERE_I=FIND_ARRAY(INPUT_TIME(3))
      STORE_ARRAY(WHERE_I,0)=STORE_ARRAY(WHERE_I,0)+1
      STORE_ARRAY(WHERE_I,STORE_ARRAY(WHERE_I,0))=INPUT_VAR(3)
      IF (INPUT_TIME(4).NE.0 ) THEN
      WHERE_I=FIND_ARRAY(INPUT_TIME(4))
      STORE_ARRAY(WHERE_I,0)=STORE_ARRAY(WHERE_I,0)+1
      STORE_ARRAY(WHERE_I,STORE_ARRAY(WHERE_I,0))=INPUT_VAR(4)
      IF (INPUT_TIME(5).NE.0 ) THEN
      WHERE_I=FIND_ARRAY(INPUT_TIME(5))
      STORE_ARRAY(WHERE_I,0)=STORE_ARRAY(WHERE_I,0)+1
      STORE_ARRAY(WHERE_I,STORE_ARRAY(WHERE_I,0))=INPUT_VAR(5)
      ELSE
      ADD_ON=4
      ENDIF
      ELSE
      ADD_ON=3
      ENDIF
      ELSE
      ADD_ON=2
      ENDIF
      ELSE
      ADD_ON=1
      ENDIF
      ELSE
      ADD_ON=0
      ENDIF
      ENDIF
      GOTO 100
999   CONTINUE
      I=0

c
c     The program inquires if the user wishes the acquired data to be displayed
c     for checking the correct operation.
c

      PRINT *,'Do you wish the values to be displayed and filed'
      PRINT *,'Give filename or return for No'
      READ(*,1010)ANS
1010FORMAT(A80)
      IF (ANS(1:10).NE.'          ') THEN
      OPEN(UNIT=3,FILE=ANS,RECL=132)
      DO IOUT=1,LAST_TIME-1
      WRITE(3,*)' time ',STORE_TIME(IOUT)
      WRITE(3,*) 'Temperature :-'
      ILINE=1
      DO WHILE (ILINE.LT.STORE_ARRAY(IOUT,0))
      START=ILINE
      END=ILINE+6
      ILINE=END+1
      IF (END.GT.STORE_ARRAY(IOUT,0)) END=STORE_ARRAY(IOUT,0)
```

```
      WRITE(3,*)(STORE_ARRAY(IOUT,IS),IS=START,END)
      ENDDO
      ENDDO
      ENDIF

c
c     The program inquires the starting point; as in a cartesian coordinate
c     system, the number of grid points in x and y directions and the (x and y)
c     space-increments. Theses are for the uniform mesh comprising the centre
c     nodes of the cells.
c

      PRINT *,'Please give base value of X'
      READ(*,*)X(1)
      PRINT *,'Please give base value of Y'
      READ(*,*)Y(1)
      PRINT *,'Please give number of grids in X'
      READ(*,*)NUM_X
      PRINT *,'Please give number of grids in Y'
      READ(*,*)NUM_Y
      PRINT *,'Please give X increment'
      READ(*,*)X_INC
      PRINT *,'Please give Y increment'
      READ(*,*)Y_INC

c
c     Three uniform meshes are generated.
c
      START_Y=Y(1)
      START_X=X(1)
      COUNT=1

      start_yN=start_Y
      start_xn=start_X

      DO I=1,NUM_Y
      DO J=1,NUM_X
      Y(COUNT)=START_Y
      IF (J.NE.1) X(COUNT)=X(COUNT-1)+X_INC
      COUNT=COUNT+1
      ENDDO
      START_Y=START_Y+Y_INC
      Y(COUNT)=START_Y
      X(COUNT)=START_X

      ENDDO

      start_Y=start_yn
      start_x=start_xn-(x_inc/2)
      x(count)=start_x

      DO I=1,NUM_Y
      DO J=1,NUM_X+1
      Y(COUNT)=START_Y
      IF (J.NE.1) X(COUNT)=X(COUNT-1)+X_INC
      COUNT=COUNT+1
      ENDDO
```

```
      START_Y=START_Y+Y_INC
      Y(COUNT)=START_Y
      X(COUNT)=START_X
      ENDDO
      start_Y=start_yn-(y_inc/2)
      start_x=start_xn
      x(count)=start_x
      DO I=1,NUM_Y
      DO J=1,NUM_X
      Y(COUNT)=START_Y
      IF (J.NE.1) X(COUNT)=X(COUNT-1)+X_INC
      COUNT=COUNT+1
      ENDDO
      START_Y=START_Y+Y_INC
      Y(COUNT)=START_Y
      X(COUNT)=START_X
      ENDDO
      DO I=1,COUNT
      ENDDO
      PRINT 6
6     FORMAT(1X,'Please give minimum time difference between plots ')
      READ(*,*)MIN_DIFF
c
c     Various GINO subroutines are initialised for plotting purposes.
c
1     CALL SETDEV(K)
      J=-1
      CALL ERRSWI(J)
      J=-1
      CALL ERRMAX(J)
      ILAST_PLOT=1
      DO IZ=1,LAST_TIME-1
      IF (ILAST_PLOT.EQ.1.OR.
     1ABS(STORE_TIME(ILAST_PLOT)-STORE_TIME(IZ)).GE.MIN_DIFF)
THEN
      ILAST_PLOT=IZ
      WRITE(TIME_STRING,1100)STORE_TIME(IZ)
1100FORMAT(1X,F10.0,'Seconds')
      DO I=1,STORE_ARRAY(IZ,0)
      Z(I)=STORE_ARRAY(IZ,I)
      ENDDO
2     NW=2000
      CALL PICCLE
      NP=NUM_X*NUM_Y+((NUM_X+1)*NUM_Y)+(NUM_X*(NUM_Y+1))
      XLOW=0.0
      YLOW=0.0
      XHIGH=NUM_X*X_INC
      YHIGH=NUM_Y*Y_INC
      CALL TITSTR(TIME_STRING)
```

```
      CALL RANGRD(NP,X,Y,Z,NUM_X,XLOW,XHIGH,NUM_Y,
     1 YLOW,YHIGH,AZ,NW,W)
      NCONT=10
      ISM=1
      CALL DRACON(NUM_X,XLOW,XHIGH,NUM_Y,YLOW,YHIGH,
     1 AZ,NCONT,ISM,NW,W)
      CALL CHAMOD

c
c     WAIT subroutine is called to allow the user a few seconds to decide if a
c     printout of the particular plot is required.
c

      IF (.NOT.PLOTER) CALL WAIT(BUFFERS)

c
c     By pressing the letter 'p' on the keyboard a plot of the contour map is
c     automatically sent to the printer
c

      IF (BUFFERS.EQ.'P'.OR.BUFFERS.EQ.'p') THEN
      IF (PLOTER) THEN
      CALL DEVEND
      CALL SETDEV(k)
      CALL ERRSWI(J)
      CALL ERRMAX(J)
      PLOTER=.FALSE.
      GOTO 2
      ELSE
      PRINT *,'Doing output to the printer'
      CALL DEVEND
      KI=9
      CALL SETDEV(KI)
      CALL ERRSWI(J)
      CALL ERRMAX(J)
      PLOTER=.TRUE.
      GOTO 2
      ENDIF
      ENDIF
      ENDIF
      ENDDO
      END


c
c     Subroutine 'wait' allows 3 second delay between each plot
c

      SUBROUTINE WAIT(BUFFER)
      IMPLICIT INTEGER*4 (A-Z)
      INCLUDE  '($IODEF)'
      LOGICAL FIRST/.TRUE./
      CHARACTER TERM*3 /'TT:'/,BUFFER*1
      IF (FIRST) STATUS=SYS$ASSIGN(TERM,CHAN,,)
      FIRST=.FALSE.
```

```
      BUFFER = ' '
      FUNC=IO$_READVBLK.OR.IO$M_TIMED
      STATUS= SYS$QIOW(,%VAL(CHAN),%VAL(FUNC)
     1 ,,,,%REF(BUFFER),%VAL(1),%VAL(3),,,)
      RETURN
      END


c
c     This function looks through the output file and locates the various
c     blocks of data for the same time interval.
c

      INTEGER FUNCTION FIND_ARRAY(TIME)
      IMPLICIT INTEGER*4 (A-Z)
      REAL TIME
      REAL STORE_TIME(5000)
      COMMON STORE_TIME,LAST_TIME
      I=1
      DO WHILE (I.LE.LAST_TIME.AND.STORE_TIME(I).NE.TIME)
      I=I+1
      ENDDO
      IF (I.LE.LAST_TIME) THEN
      FIND_ARRAY=I
      ELSE
      LAST_TIME=LAST_TIME+1
      STORE_TIME(LAST_TIME)=TIME
      FIND_ARRAY=LAST_TIME
      ENDIF
      END
```

a Two-Dimensional Code-Generation Program

```
c
c     This program can generate the uniform mesh for a thermal structure with
c     conduction in 2-dimensions.
c


c
c     Type and lengths and type of all the various characters and strings used
c     in the program are defined.
c
      CHARACTER*1 LEFT,RIGHT,TOP,BOTTOM,CENTRE,TMP*180,TMP1*50,
     1 FILENAME*20,STR1*30,STR2*50,STR3*50,STR4*30,STR5*70,STR6*70,
     1  TYPE*20,MODEL*20,STR10*100,STR11*100,STR20*50,STR21*50,
     1  STR31*50,STR32*50,STR25*50,STR26*50
      INTEGER LEFTN,RIGHTN,TOPN,BOTTOMN,CENTREN,TIME

c
c     The output file name, the ASTEC3 sub-model and the !TYPE of the sub-model
c     are requested.
c
      WRITE(6,5)
5     FORMAT('$Enter file name for output :')
      READ(5,11)FILENAME
11    FORMAT(A20)
      OPEN(20,FILE=FILENAME,STATUS='NEW',IOSTAT=IO)
      WRITE(6,8)
8     FORMAT('$Please give the ASTEC3 sub_model : ')
      READ(5,11)MODEL

      WRITE(6,7)
7     FORMAT('$Enter the type_extension for the sub_model
     1 followed by a semicolon :')
      READ(5,11)TYPE

c
c     The number of 2-dimensional cells in the x and y directions are requested.
c
      WRITE(6,1)
1     FORMAT('$Enter number of cells in X - Direction :')
      READ(5,200)M
200   FORMAT(I5)
      WRITE(6,3)
3     FORMAT('$Enter number of cells in Y - Direction :' )
      READ(5,200)M1
```

```
c
c     The codes for $DESC section of ASTEC3 circuit description file are
c     generated.
c


      WRITE(20,*)'$DESC'
      WRITE(20,*)' '
      WRITE(6,*)'$DESC'
      WRITE(6,*)' '


c
c     The codes are generated for the !LIB sequence which calls up the models
c     from the ASTEC3 library and start the CIRCUIT section.
c

      WRITE(STR10,*)'!LIB: ',MODEL,';',MODEL,'.',TYPE
      J=1
      STR11=' '
      DO I=1,LEN(STR10)
      IF (STR10(I:I).NE.' ') THEN
      STR11(J:J)=STR10(I:I)
      J=J+1
      ENDIF
      ENDDO
      WRITE(20,*)STR11
      WRITE(6,*)STR11
      WRITE(20,*)' '


      WRITE(20,*)'!CIRCUIT(G):'
      WRITE(6,*)' '
      WRITE(6,*)'!CIRCUIT(G):'
      WRITE(6,*)' '


c
c     The node names in the model and the numbering order are specified.
c     (eg. cell number 1 has nodes LEFT1 (L1), RIGHT1 (R1), TOP1 (T1) etc.).
c

      RIGHT='R'
      TOP='T'

c
c     Start a loop to generate the code for a 2-D model with M and M1 cells in
c     the X and Y directions respectively.
c

      DO N=1,M*M1
      J=MOD(N-1,M)
      RIGHTN=N
      TOPN=N
      IF (J.EQ.0) THEN
      LEFT='L'
```

```
      LEFTN=N
      ELSE
      LEFT='R'
      LEFTN=N-1
      END IF
      IF (N .LE. M) THEN
      BOTTOM='B'
      BOTTOMN=N
      ELSE
      BOTTOM='T'
      BOTTOMN=N-M
      END IF

      WRITE(TMP,1000)N,LEFT,LEFTN,RIGHT,RIGHTN,TOP,TOPN,
      1BOTTOM,BOTTOMN,N,MODEL,TYPE

1000FORMAT(' M',I,'(',A1,I,'-',A1,I,'-',A1,I,'-',A1,I,'-C',I,
      1   '-G)',A10,'.',A10)

      J=1
      TMP1=' '
      DO I=1,LEN(TMP)
      IF (TMP(I:I).NE.' ') THEN
      TMP1(J:J)=TMP(I:I)
      J=J+1
      ENDIF
      ENDDO

      WRITE(20,*)TMP1
      WRITE(6,*)TMP1
      END DO
      PRINT *
      PRINT *


c
c     The code for the !output sequence of ASTEC3 file is generated
c

      WRITE(20,*)'!OUTPUT:'
      WRITE(20,*)' '
      WRITE(6,*)'!OUTPUT:'
      WRITE(6,*)' '



c
c     A loop to generate the voltages (temperatures) at the CENTRE nodes of each
c     cell in the model to be outputed.
c

      DO NUM=1,M*M1
      WRITE(STR1,*)'VNC',NUM,';'
```

```
      J=1
      STR2=' '
      DO I=1,LEN(STR1)
      IF(STR1(I:I).NE.' ')THEN
      STR2(J:J)=STR1(I:I)
      J=J+1
      ENDIF
      ENDDO
      WRITE(20,*)STR2
      WRITE(6,*)STR2
      END DO
c
c     A loop to generate the voltages (temperatures) at the LEFT nodes of each
c     cell in the model to be outputed.
c

      WRITE(STR3,*)'VNL',NUM2,';'
      J=1
      STR4=' '
      DO I=1,LEN(STR3)
      IF(STR3(I:I).NE.' ')THEN
      STR4(J:J)=STR3(I:I)
      J=J+1
      ENDIF
      ENDDO
c
c     A loop to generate the voltages (temperatures) at the RIGHT nodes of each
c     cell in the model to be outputed.
c

      WRITE(STR31,*)'VNR',NUM2,';'
      J=1
      STR32=' '
      DO I=1,LEN(STR31)
      IF(STR31(I:I).NE.' ')THEN
      STR32(J:J)=STR31(I:I)
      J=J+1
      ENDIF
      ENDDO
      K=MOD(NUM2-1,M)
      IF (K.EQ.0) THEN
      WRITE(20,*)STR4
      WRITE(6,*)STR4
      ELSE
      WRITE(20,*)STR32
      WRITE(6,*)STR32
      ENDIF
      END DO
      DO NUM3=1,M*M1
```

```
c
c     A loop to generate the voltages (temperatures) at the BOTTOM nodes of each
c     cell in the model to be outputed.
c

      WRITE(STR20,*)'VNB',NUM3,';'
      STR21=' '
      J=1
      DO I=1,LEN(STR20)
      IF(STR20(I:I).NE.' ')THEN
      STR21(J:J)=STR20(I:I)
      J=J+1
      ENDIF
      ENDDO

c
c     A loop to generate the voltages (temperatures) at the TOP nodes of each
c     cell in the model to be outputed.
c

      WRITE(STR25,*)'VNT',NUM3,';'
      STR26=' '
      J=1
      DO I=1,LEN(STR25)
      IF(STR25(I:I).NE.' ')THEN
      STR26(J:J)=STR25(I:I)
      J=J+1
      ENDIF
      ENDDO

      IF (NUM3.LE.M) THEN
      WRITE(20,*)STR21
      WRITE(6,*)STR21

      ELSE
      WRITE(20,*)STR26
      WRITE(6,*)STR26
      ENDIF
      END DO


      WRITE(20,*)' '
      WRITE(6,*)' '

      WRITE(20,*)'!EXEC'
      WRITE(20,*)' '
      WRITE(6,*)'!EXEC'
      WRITE(6,*)' '


c
c     The program inquires whether a steady-state or transient simulation is
c     required and generates the appropriate codes.
c
```

```
      WRITE(20,*)' '
      PRINT *,'Do you require a transient or steady-state simulation'
      PRINT *,'Type 1 for transient or 2 for steady-state'
      READ(*,*)SIM

      IF (SIM.EQ.1) THEN
      PRINT *,'Please give the simulation time required'
      READ(*,*)TIME

      WRITE(20,*)'$TRAN'
      WRITE(20,*)'!INIT RESET'
      WRITE(6,*)' '
      WRITE(6,*)'$TRAN'
      WRITE(6,*)'!INIT RESET'

      WRITE(STR5,*)'!PARAM: TMAX=',TIME,';'
      STR6=' '
      J=1
      DO I=1,LEN(STR5)
      IF(STR5(I:I).NE.' ')THEN
      STR6(J:J)=STR5(I:I)
      J=J+1
      ENDIF
      ENDDO
      WRITE(20,*)STR6
      WRITE(6,*)STR6

      ELSE IF (SIM.EQ.2) THEN
      WRITE(20,*)'$DCAN'
      WRITE(6,*)'$DCAN'
      ENDIF

      WRITE(20,*)'!EXEC'
      WRITE(20,*)' '
      WRITE(6,*)'!EXEC'


c
c     The codes for the $EDIT part of the file is generated containing the
c     output results in and order needed for the contour-plotting program.
c

      WRITE(20,*)'$EDIT'
      WRITE(20,*)' '
      WRITE(20,*)'!PRINT.SIMUL1,VERSUS &T:'
      WRITE(6,*)' '
      WRITE(6,*)'$EDIT'
      WRITE(6,*)' '
      WRITE(6,*)'!PRINT.SIMUL1,VERSUS &T:'
      IC=16
      ICOUNT=0
      DO NUM=1,M*M1
```

```
      ICOUNT=ICOUNT+1
      IF(ICOUNT.EQ.IC)THEN
      WRITE(20,*)' '
      WRITE(20,*)'!PRINT.SIMUL1,VERSUS &T:'
      WRITE(20,*)' '
      WRITE(6,*)' '
      WRITE(6,*)'!PRINT.SIMUL1,VERSUS &T:'
      WRITE(6,*)' '
      ICOUNT=1
      ENDIF
c
c     generate the code for CENTRE-node temperatures. (eg. VNC1).
c
      WRITE(STR1,*)'VNC',NUM,';'
      J=1
      STR2=' '
      DO I=1,LEN(STR1)
      IF(STR1(I:I).NE.' ')THEN
      STR2(J:J)=STR1(I:I)
      J=J+1
      ENDIF
      ENDDO
      WRITE(20,*)STR2
      WRITE(6,*)STR2
      END DO

      DO NUM2=1,M*M1

      ICOUNT=ICOUNT+1
      IF(ICOUNT.EQ.IC)THEN
      WRITE(20,*)' '
      WRITE(20,*)'!PRINT.SIMUL1,VERSUS &T:'
      WRITE(20,*)' '
      WRITE(6,*)' '
      WRITE(6,*)'!PRINT.SIMUL1,VERSUS &T:'
      WRITE(6,*)' '
      ICOUNT=1
      ENDIF

c
c     generate the code for LEFT-node temperatures. (eg. VNL1).
c
      WRITE(STR3,*)'VNL',NUM2,';'

      J=1
      STR4=' '
      DO I=1,LEN(STR3)
      IF(STR3(I:I).NE.' ')THEN
      STR4(J:J)=STR3(I:I)
```

```
      J=J+1
      ENDIF
      ENDDO
c
c     generate the code for RIGHT-node temperatures. (eg. VNR1).
c
      WRITE(STR31,*)'VNR',NUM2,';'
      J=1
      STR32=' '
      DO I=1,LEN(STR31)
      IF(STR31(I:I).NE.' ')THEN
      STR32(J:J)=STR31(I:I)
      J=J+1
      ENDIF
      ENDDO
      K=MOD(NUM2-1,M)
      IF (K.EQ.0) THEN
      WRITE(20,*)STR4
      WRITE(6,*)STR4
      ELSE
      WRITE(20,*)STR32
      WRITE(6,*)STR32
      ENDIF
      END DO
      ICOUNT=ICOUNT
      DO NUM3=1,M*M1
      ICOUNT=ICOUNT+1
      IF(ICOUNT.EQ.IC)THEN
      WRITE(20,*)' '
      WRITE(20,*)'!PRINT.SIMUL1,VERSUS &T:'
      WRITE(20,*)' '
      WRITE(6,*)' '
      WRITE(6,*)'!PRINT.SIMUL1,VERSUS &T:'
      WRITE(6,*)' '
      ICOUNT=1
      ENDIF
c
c     generate the code for BOTTOM-node temperatures. (eg. VNB1).
c
      WRITE(STR20,*)'VNB',NUM3,';'
      STR21=' '
      J=1
      DO I=1,LEN(STR20)
      IF(STR20(I:I).NE.' ')THEN
      STR21(J:J)=STR20(I:I)
```

```
      J=J+1
      ENDIF
      ENDDO
c
c     generate the code for TOP-node temperatures. (eg. VNT1).
c
      WRITE(STR25,*)'VNT',NUM3,';'
      STR26=' '
      J=1
      DO I=1,LEN(STR25)
      IF(STR25(I:I).NE.' ')THEN
      STR26(J:J)=STR25(I:I)
      J=J+1
      ENDIF
      ENDDO
      IF (NUM3.LE.M) THEN
      WRITE(20,*)STR21
      WRITE(6,*)STR21
      ELSE
      WRITE(20,*)STR26
      WRITE(6,*)STR26
      ENDIF
      END DO
      WRITE(20,*)' '
c
c     The codes for executing the $EDIT section and ending the
c     simulation are generated.
c
      WRITE(20,*)' '
      WRITE(20,*)'!EXEC'
      WRITE(20,*)' '
      WRITE(20,*)'$END'
      WRITE(20,*)' '
      WRITE(6,*)' '
      WRITE(6,*)'!EXEC'
      WRITE(6,*)' '
      WRITE(6,*)'$END'

      END
```

b An example of the ouput of the 2-D Code-Generation Program

Questions and Answers for generating a (5×3) mesh

Enter file name for output : F2.DES
Please give the ASTEC3 sub_model : 2D
Enter the type_extension for the sub_model followed by a semicolon :S;
Enter number of cells in X - Direction :5
Enter number of cells in Y - Direction :3

Do you require a transient or steady-state simulation
Type 1 for transient or 2 for steady-state
1
Please give the simulation time required
2000

The Contents of The Output File F2.DES

$DESC

!LIB:2D;2D.S;

!CIRCUIT(G):

M1(L1-R1-T1-B1-C1-G)2D.S;
M2(R1-R2-T2-B2-C2-G)2D.S;
M3(R2-R3-T3-B3-C3-G)2D.S;
M4(R3-R4-T4-B4-C4-G)2D.S;
M5(R4-R5-T5-B5-C5-G)2D.S;
M6(L6-R6-T6-T1-C6-G)2D.S;
M7(R6-R7-T7-T2-C7-G)2D.S;
M8(R7-R8-T8-T3-C8-G)2D.S;
M9(R8-R9-T9-T4-C9-G)2D.S;
M10(R9-R10-T10-T5-C10-G)2D.S;
M11(L11-R11-T11-T6-C11-G)2D.S;
M12(R11-R12-T12-T7-C12-G)2D.S;
M13(R12-R13-T13-T8-C13-G)2D.S;
M14(R13-R14-T14-T9-C14-G)2D.S;
M15(R14-R15-T15-T10-C15-G)2D.S;

!OUTPUT:

VNC1;
VNC2;
VNC3;
VNC4;
VNC5;
VNC6;
VNC7;
VNC8;

```
VNC9;
VNC10;
VNC11;
VNC12;
VNC13;
VNC14;
VNC15;
VNL1;
VNR2;
VNR3;
VNR4;
VNR5;
VNL6;
VNR7;
VNR8;
VNR9;
VNR10;
VNL11;
VNR12;
VNR13;
VNR14;
VNR15;
VNB1;
VNB2;
VNB3;
VNB4;
VNB5;
VNT6;
VNT7;
VNT8;
VNT9;
VNT10;
VNT11;
VNT12;
VNT13;
VNT14;
VNT15;

!EXEC


$TRAN

!INIT RESET
!PARAM:TMAX=2000;

!EXEC


$EDIT

!PRINT.SIMUL1,VERSUS &T:

VNC1;
VNC2;
```

```
VNC3;
VNC4;
VNC5;
VNC6;
VNC7;
VNC8;
VNC9;
VNC10;
VNC11;
VNC12;
VNC13;
VNC14;
VNC15;

!PRINT.SIMUL1,VERSUS &T:

VNL1;
VNR2;
VNR3;
VNR4;
VNR5;
VNL6;
VNR7;
VNR8;
VNR9;
VNR10;
VNL11;
VNR12;
VNR13;
VNR14;
VNR15;

!PRINT.SIMUL1,VERSUS &T:

VNB1;
VNB2;
VNB3;
VNB4;
VNB5;
VNT6;
VNT7;
VNT8;
VNT9;
VNT10;
VNT11;
VNT12;
VNT13;
VNT14;
VNT15;

!EXEC

$END
```

c Program for Generating the ASTEC3 code for Three-Dimensional Conduction

```
c
c     This program generates the electrical equivalent circuit description of
c     a uniform thermal structure. It takes into account conduction in 3
c     directions and in this case convection and radiation from the top surface.
c
c
c     The type and sizes of all strings and arrays used within the program are
c     defined.
c
      CHARACTER*1 LEFT,RIGHT,TOP,BOTTOM,CENTRE,TMP*180,TMP1*70,
     1 FILENAME*20,END*1,FRONT*1,
     1 STR1*55,STR2*50,STR3*50,STR4*50,STR5*50,STR6*50,
     1 TYPE*20,MODEL*20,STR10*100,STR11*100,STR20*20,STR21*20,
     1 STR22*20,STR23*20,CTYPE(3000)*4,SP*1,EXT*4,LINE*70,LIN*5,
     1 SP1*1,LINE1*70,LIN1*6
      DIMENSION HC(1000)

      INTEGER LEFTN,RIGHTN,TOPN,BOTTOMN,CENTREN,FRONTN,ENDN,
      TIME,X1,X2


c
c     The output filename is inquired and opened.
c
      WRITE(6,5)
5     FORMAT('$Enter file name for output :')
      READ(5,11)FILENAME
11    FORMAT(A20)
      OPEN(20,FILE=FILENAME,STATUS='NEW',IOSTAT=IO)
      WRITE(6,8)


c
c     ASTEC3 name for the single cell model and the type of the cell are
c     inquired. These are as saved in the user's personal library.
c
8     FORMAT('$Please give the ASTEC3 sub_model : ')
      READ(5,11)MODEL

      WRITE(6,7)
7     FORMAT('$Enter the type_extension for the sub_model followed by a
     1 semicolon :')
      READ(5,11)TYPE
      DO 199 I=1,1000
199   CTYPE(I)=TYPE
      WRITE(20,*)'$DESC'
      WRITE(20,*)' '
```

```
      WRITE(6,*)'$DESC'
      WRITE(6,*)' '
c
c     The !LIB sequence of the ASTEC3 file is generated.
c
      WRITE(STR10,*)'!LIB: ',MODEL,';',MODEL,'.',TYPE
      J=1
      STR11=' '
      DO I=1,LEN(STR10)

      IF (STR10(I:I).NE.' ') THEN
      STR11(J:J)=STR10(I:I)
      J=J+1
      ENDIF
      ENDDO
      WRITE(20,*)STR11
      WRITE(6,*)STR11


c
c     The file name containing the cell numbers with different parameter values
c     or heat generation are inquired.It is subsequently opened and the data is
c     read. This includes the EXTension of the !TYPE of cell.
c
      WRITE(6,111)
111   FORMAT('$Enter file name containing the changes :')
      READ(5,11)FILENAME

      OPEN(22,FILE=FILENAME,STATUS='OLD',IOSTAT=IO)

202   READ(22,256,END=999)EXT
256   FORMAT(A4)

      IF(EXT(1:1).EQ.'*')GOTO 999
      TYPE *,EXT

c
c     The model names are written as given in the CIRCUIT description section of
c     ASTEC3 file as read from the above file.
c
      WRITE(STR10,*),MODEL,'.',EXT
      J=1
      STR11=' '
      DO I=1,LEN(STR10)
      IF (STR10(I:I).NE.' ') THEN
      STR11(J:J)=STR10(I:I)
      J=J+1
      ENDIF
      ENDDO
      WRITE(20,*)STR11
      WRITE(6,*)STR11
```

```
      READ(22,267)LINE
267   FORMAT(A70)
      TYPE *,LINE
      I=1

203   LIN=LINE(I:I+4)
      READ(LIN,1020)INDEX,SP
1020FORMAT(I4,A1)
      I=I+5
      TYPE *,LIN,'---> ',INDEX,SP
      CTYPE(INDEX)=EXT
      IF(SP.EQ.';')GOTO 202
      GOTO 203

c
c     The number of conduction cells in the three directions are inquired.
c

999   WRITE(6,1)
1     FORMAT('$Enter number of cells in X - Direction :')
      READ(5,200)NUM_X
200   FORMAT(I5)
      WRITE(6,3)
3     FORMAT('$Enter number of cells in Y - Direction :' )
      READ(5,200)NUM_Y
      WRITE(6,4)
4     FORMAT('$Enter number of cells in Z - Direction :' )
      READ(5,200)NUM_Z

      WRITE(20,*)' '
      WRITE(20,*)'!CIRCUIT(G):'
      WRITE(20,*)' '
      WRITE(6,*)' '
      WRITE(6,*)'!CIRCUIT(G):'
      WRITE(6,*)' '

c
c     The 3-D mesh is generated by sharing the appropriate nodes between the
c     adjacent cells.
c

      RIGHT='R'
      TOP='T'
      END='E'

      DO K=1,NUM_Z
      DO K1=1,NUM_X*NUM_Y
      N=K1+(K-1)*NUM_X*NUM_Y
      J=MOD(N-1,NUM_X)

      RIGHTN=N
      ENDN=N
      TOPN=N

      IF (J.EQ.0) THEN
      LEFT='L'
      LEFTN=N
      ELSE
```

```
      LEFT='R'
      LEFTN=N-1
      END IF
      IF ((N-(K-1)*NUM_X*NUM_Y) .LE. NUM_X) THEN
      BOTTOM='B'
      BOTTOMN=N
      ELSE
      BOTTOM='T'
      BOTTOMN=N-NUM_X
      END IF
      IF(N .LE. NUM_X*NUM_Y) THEN
      FRONT='F'
      FRONTN=N
      ELSE
      FRONT='E'
      FRONTN=N-NUM_Y*NUM_X
      ENDIF

      WRITE(TMP,1000)N,LEFT,LEFTN,RIGHT,RIGHTN,TOP,TOPN,BOTTOM,
      1 BOTTOMN,FRONT,FRONTN,END,ENDN,N,MODEL,CTYPE(N)

1000FORMAT('M',I,'(',A1,I,'-',A1,I,'-',A1,I,'-',A1,I,'-',A1,I,
     1 '-',A1,I,'-C',I,'-G)',A10,'.',A10)
      J=1
      TMP1=' '
      DO I=1,LEN(TMP)
      IF (TMP(I:I).NE.' ') THEN
      TMP1(J:J)=TMP(I:I)
      J=J+1
      ENDIF
      ENDDO
      WRITE(20,*)TMP1
      WRITE(6,*)TMP1
      END DO
      ENDDO
      WRITE(20,*)' '
c
c     The file name containing the heat transfer coefficients of convection and
c     radiation is inquired. It is OPENed, READ and the data is processed.
c
      WRITE(6,211)
211   FORMAT('$Enter file name containing heat transfer coeffs:')
      READ(5,11)FILENAME
      OPEN(23,FILE=FILENAME,STATUS='OLD',IOSTAT=IO)
357   READ(23,367)LINE1
367   FORMAT(A70)
      TYPE *,LINE1
1090I=1
      DO NUM=1,NUM_Z
```

```
      X1=(NUM_X*(NUM_Y-1)+1)+(NUM_X*NUM_Y)*(NUM-1)
      X2=NUM_X*NUM_Y*NUM
303   DO N1=X1,X2

      LIN1=LINE1(I:I+5)
      READ(LIN1,1030,END=1031)HC1,SP1
1030FORMAT(F5.0,A1)
1031TYPE *,LIN1,'---> ',HC1,SP1
      TYPE *,N1
      HC(N1)=HC1
      TYPE *,HC(N1),HC1
      I=I+6
      IF(SP1.EQ.';')THEN
      READ(23,367)LINE1
      I=1
      ENDIF
      ENDDO
      ENDDO
c
c     The codes are genearted for a series of resistances which connect the
c     appropraiate nodes at the top surface of the structure to the ambient air.
c

1999DO NUM=1,NUM_Z
      X1=(NUM_X*(NUM_Y-1)+1)+(NUM_X*NUM_Y)*(NUM-1)
      X2=NUM_X*NUM_Y*NUM
      DO NUM_2=X1,X2
      WRITE(STR1,*)'RT',NUM_2,'(T',NUM_2,'-COM)',HC(NUM_2),';'
      J=1
      STR2=' '
      DO I=1,LEN(STR1)
      IF(STR1(I:I).NE.' ')THEN
      STR2(J:J)=STR1(I:I)
      J=J+1
      ENDIF
      ENDDO
      WRITE(20,*)STR2
      WRITE(6,*)STR2
      END DO
      ENDDO

      WRITE(20,*)' '
      WRITE(6,*)' '
      WRITE(6,2000)
2000FORMAT('$Please give the ambient temperature :' )
      READ(*,*)AMB
      WRITE(STR1,*)'ECOM(COM-G)',AMB,';'
```

```
      J=1
      STR2=' '
      DO I=1,LEN(STR1)
      IF(STR1(I:I).NE.' ')THEN
      STR2(J:J)=STR1(I:I)
      J=J+1
      ENDIF
      ENDDO

      WRITE(20,*)STR2
      WRITE(6,*)STR2


      PRINT *
      PRINT *

c
c     The !OUTPUT sequence of ASTEC3 file is generated. The codes for voltages
c     (temperatures) of the nodes at the top surface are generated.
c


      WRITE(20,*)' '
      WRITE(20,*)'!OUTPUT:'
      WRITE(20,*)' '

      WRITE(6,*)' '
      WRITE(6,*)'!OUTPUT:'
      WRITE(6,*)' '

      DO NUM=1,NUM_Z

      X1=(NUM_X*(NUM_Y-1)+1)+(NUM_X*NUM_Y)*(NUM-1)
      X2=NUM_X*NUM_Y*NUM
      DO NUM_2=X1,X2

      WRITE(STR1,*)'VNT',NUM_2,';'

      J=1
      STR2=' '
      DO I=1,LEN(STR1)
      IF(STR1(I:I).NE.' ')THEN
      STR2(J:J)=STR1(I:I)
      J=J+1
      ENDIF
      ENDDO


      WRITE(20,*)STR2
      WRITE(6,*)STR2
      END DO
      ENDDO

      WRITE(20,*)' '
      WRITE(6,*)' '

      WRITE(20,*)'!EXEC'
      WRITE(20,*)' '
      WRITE(6,*)'!EXEC'
      WRITE(6,*)' '
```

```
c
c     The type of simulation (Steady-state or Transient) is inquired and the
c     appropriate code in ASTEC3 syntax is generated.
c

      WRITE(20,*)' '
      WRITE(6,*)' '
      PRINT *,'Do you require a transient or steady-state simulation'
      PRINT *,'Type 1 for transient or 2 for steady-state'
      READ(*,*)SIM

      IF (SIM.EQ.1) THEN
      PRINT *,'Please give the simulation time required'
      READ(*,*)TIME

      WRITE(20,*)'$TRAN'
      WRITE(20,*)'!INIT RESET'

      WRITE(6,*)'$TRAN'
      WRITE(6,*)'!INIT RESET'

      WRITE(STR5,*)'!PARAM: TMAX=',TIME,';'

      STR6=' '
      J=1
      DO I=1,LEN(STR5)
      IF(STR5(I:I).NE.' ')THEN
      STR6(J:J)=STR5(I:I)
      J=J+1
      ENDIF
      ENDDO
      WRITE(20,*)STR6
      WRITE(6,*)STR6

      ELSE IF (SIM.EQ.2) THEN
      WRITE(20,*)'$DCAN'
      WRITE(6,*)'$DCAN'
      ENDIF
      WRITE(20,*)'!EXEC'
      WRITE(6,*)'!EXEC'

c
c     The $EDIT section of the file is generated which tabulates the required
c     output results in blocks of fifteen as require by ASTEC3 software. The
c     following sequence generates the voltages (temperatures) of the top
c     surface nodes.
c

      WRITE(20,*)' '
      WRITE(20,*)'$EDIT'
      WRITE(20,*)' '

      WRITE(20,*)'!PRINT.SIMUL1,VERSUS &T:'

      WRITE(6,*)' '
      WRITE(6,*)'$EDIT'
      WRITE(6,*)' '

      WRITE(6,*)'!PRINT.SIMUL1,VERSUS &T:'
```

```
      IC=16

      DO NUM_5=1,NUM_Z
      X1=(NUM_X*(NUM_Y-1)+1)+(NUM_X*NUM_Y)*(NUM_5-1)
      X2=NUM_X*NUM_Y*NUM_5
      ICOUNT=0

      DO NUM_6=X1,X2
      ICOUNT=ICOUNT+1
      Z=NUM_X*(NUM_5-1)+ICOUNT
      IF(Z.EQ.IC)THEN

      WRITE(20,*)' '
      WRITE(20,*)'!PRINT.SIMUL1,VERSUS &T:'
      WRITE(20,*)' '

      WRITE(6,*)' '
      WRITE(6,*)'!PRINT.SIMUL1,VERSUS &T:'
      WRITE(6,*)' '

      IC=IC+15
      ENDIF


      WRITE(STR22,*)'VNT',NUM_6,';'

      J=1
      STR23=' '
      DO I=1,LEN(STR22)
      IF(STR22(I:I).NE.' ')THEN
      STR23(J:J)=STR22(I:I)
      J=J+1
      ENDIF
      ENDDO

      WRITE(20,*)STR23
      WRITE(6,*)STR23
      END DO
      ENDDO

c
c     The !EXEC and $END sequences are generated.
c

      WRITE(20,*)' '
      WRITE(20,*)'!EXEC'
      WRITE(20,*)' '
      WRITE(20,*)'$END'
      WRITE(6,*)' '
      WRITE(6,*)'!EXEC'
      WRITE(6,*)' '
      WRITE(6,*)'$END'

      END
```

d Format of Data Files

Format of the file containing the changes in the cell '!type's

```
NJ;
  8,  9, 10, 11, 12, 13, 14, 22, 28, 36, 37, 38, 39, 40, 41, 42;
J;
 23, 24, 25, 26, 27;
*
```

Format of the file containing the combined thermal resistances for heat transfer coefficients of convection and radiation

```
19000,19000,19000,19000,19000,19000,19000,19000;
2000,2000,2000,2000,2000,
19000,19000,19000,19000,19000,19000,19000,19000;
```

e An example of the output of 3-Dimensional Code-Generation program

Questions and Answers for Generating a (7×2×3) 3-D Mesh

Enter file name for output : F3.DES
Please give the ASTEC3 sub_model : CUB
Enter the type_extension for the sub_model followed by a semicolon : F;

Enter file name containing the changes : F3.CHAN

Enter number of cells in the X - Direction : 7
Enter number of cells in the Y - Direction : 2
Enter number of cells in the Z - Direction : 3

Enter file name containing heat transfer coeffs: F3HEAT.DAT

Please give the ambient temperature :25

Do you require a transient or steady-state simulation?
Type 1 for transient or 2 for steady-state
1

Please give the simulation time required
2000

The Contents of The Output File F3.DES

$DESC

!LIB:CUB;CUB.F;CUB.NJ;CUB.J;

!CIRCUIT(G):

M1(L1-R1-T1-B1-F1-E1-C1-G)CUB.F;
M2(R1-R2-T2-B2-F2-E2-C2-G)CUB.F;
M3(R2-R3-T3-B3-F3-E3-C3-G)CUB.F;
M4(R3-R4-T4-B4-F4-E4-C4-G)CUB.F;
M5(R4-R5-T5-B5-F5-E5-C5-G)CUB.F;
M6(R5-R6-T6-B6-F6-E6-C6-G)CUB.F;
M7(R6-R7-T7-B7-F7-E7-C7-G)CUB.F;
M8(L8-R8-T8-T1-F8-E8-C8-G)CUB.NJ;
M9(R8-R9-T9-T2-F9-E9-C9-G)CUB.NJ;
M10(R9-R10-T10-T3-F10-E10-C10-G)CUB.NJ;
M11(R10-R11-T11-T4-F11-E11-C11-G)CUB.NJ;
M12(R11-R12-T12-T5-F12-E12-C12-G)CUB.NJ;
M13(R12-R13-T13-T6-F13-E13-C13-G)CUB.NJ;
M14(R13-R14-T14-T7-F14-E14-C14-G)CUB.NJ;
M15(L15-R15-T15-B15-E1-E15-C15-G)CUB.F;
M16(R15-R16-T16-B16-E2-E16-C16-G)CUB.F;

```
M17(R16-R17-T17-B17-E3-E17-C17-G)CUB.F;
M18(R17-R18-T18-B18-E4-E18-C18-G)CUB.F;
M19(R18-R19-T19-B19-E5-E19-C19-G)CUB.F;
M20(R19-R20-T20-B20-E6-E20-C20-G)CUB.F;
M21(R20-R21-T21-B21-E7-E21-C21-G)CUB.F;
M22(L22-R22-T22-T15-E8-E22-C22-G)CUB.NJ;
M23(R22-R23-T23-T16-E9-E23-C23-G)CUB.J;
M24(R23-R24-T24-T17-E10-E24-C24-G)CUB.J;
M25(R24-R25-T25-T18-E11-E25-C25-G)CUB.J;
M26(R25-R26-T26-T19-E12-E26-C26-G)CUB.J;
M27(R26-R27-T27-T20-E13-E27-C27-G)CUB.J;
M28(R27-R28-T28-T21-E14-E28-C28-G)CUB.NJ;
M29(L29-R29-T29-B29-E15-E29-C29-G)CUB.F;
M30(R29-R30-T30-B30-E16-E30-C30-G)CUB.F;
M31(R30-R31-T31-B31-E17-E31-C31-G)CUB.F;
M32(R31-R32-T32-B32-E18-E32-C32-G)CUB.F;
M33(R32-R33-T33-B33-E19-E33-C33-G)CUB.F;
M34(R33-R34-T34-B34-E20-E34-C34-G)CUB.F;
M35(R34-R35-T35-B35-E21-E35-C35-G)CUB.F;
M36(L36-R36-T36-T29-E22-E36-C36-G)CUB.NJ;
M37(R36-R37-T37-T30-E23-E37-C37-G)CUB.NJ;
M38(R37-R38-T38-T31-E24-E38-C38-G)CUB.NJ;
M39(R38-R39-T39-T32-E25-E39-C39-G)CUB.NJ;
M40(R39-R40-T40-T33-E26-E40-C40-G)CUB.NJ;
M41(R40-R41-T41-T34-E27-E41-C41-G)CUB.NJ;
M42(R41-R42-T42-T35-E28-E42-C42-G)CUB.NJ;


RT8(T8-COM)19000.00;
RT9(T9-COM)19000.00;
RT10(T10-COM)19000.00;
RT11(T11-COM)19000.00;
RT12(T12-COM)19000.00;
RT13(T13-COM)19000.00;
RT14(T14-COM)19000.00;
RT22(T22-COM)19000.00;
RT23(T23-COM)2000.000;
RT24(T24-COM)2000.000;
RT25(T25-COM)2000.000;
RT26(T26-COM)2000.000;
RT27(T27-COM)2000.000;
RT28(T28-COM)19000.00;
RT36(T36-COM)19000.00;
RT37(T37-COM)19000.00;
RT38(T38-COM)19000.00;
RT39(T39-COM)19000.00;
RT40(T40-COM)19000.00;
RT41(T41-COM)19000.00;
RT42(T42-COM)19000.00;

ECOM(COM-G)25.00000;

!OUTPUT:

VNT8;
```

```
VNT9;
VNT10;
VNT11;
VNT12;
VNT13;
VNT14;
VNT22;
VNT23;
VNT24;
VNT25;
VNT26;
VNT27;
VNT28;
VNT36;
VNT37;
VNT38;
VNT39;
VNT40;
VNT41;
VNT42;

!EXEC


$TRAN

!INIT RESET
!PARAM:TMAX=2000;

!EXEC


$EDIT

!PRINT.SIMUL1,VERSUS &T:

VNT8;
VNT9;
VNT10;
VNT11;
VNT12;
VNT13;
VNT14;
VNT22;
VNT23;
VNT24;
VNT25;
VNT26;
VNT27;
VNT28;
VNT36;

!PRINT.SIMUL1,VERSUS &T:

VNT37;
```

```
VNT38;
VNT39;
VNT40;
VNT41;
VNT42;

!EXEC

$END
```

A solution to this problem may be obtained for the steady state conditions by solving the differential equation describing conduction in one-dimensions as follows:

$$K\frac{d^2T}{dx^2}+q^* = 0 \qquad A4.1$$

where q^* and K are the heat generation per unit volume and thermal conductivity of the material as given in the problem description. The solution to above equation can be obtained by rearranging it in the following form and integrating twice :

$$\frac{d^2T}{dx^2} = -(q^*/K) \qquad A4.2$$

integrating both sides with respect to x:

$$\frac{dT}{dx} = -(q^*/K)x + B \qquad A4.3$$

where B is a constant. By separating the variables and performing a second integration we get:

$$T = -1/2(q^*/K)x^2 + Bx + C \qquad A4.4$$

Where C is also a constant. The values of B and C can be determined by applying the following boundary conditions :

$T = 60\ ^{\circ}C$ at $x = 0$

$T = 20\ ^{\circ}C$ $x = 0.05\ m$

which gives : $B = 2176.8786$ and $C = 60$. The above expression may be used to calculate final steady-state temperature of any point in the plate.

APPENDIX 4: Estimation of the Convective and Radiative Heat Transfer Coefficients for Experiment 1 (§6.1.1)

Two techniques are presented here for calculating the coefficients of convection h_c and radiation h_r. For the first method use is made of empirical relationships (§3.2.2) to estimate an average coefficient of convection over the surface and radiation coefficient is calculated using equation (3.44). The second technique uses a simple *heat generated=heat lost* approach where heat losses from the top of the plates and through the insulator is taken into account. This approach yields a combined convetion/radiation coefficient value.

Method 1

Convection

The convective heat transfer coefficient is calculated here for the copper strip in experiment 1. This is carried out using the recommendations given in Chapman [2] for natural convection from horizontal surfaces with the heated surface facing upwards. As recommended, the properties of air are taken at the mean film temperature defined by the average of the surface and the ambient temperature.

ie. $T_f = (T_a + T_s)/2 = 74.35\ ^\circ C$

$= 347.5\ ^\circ K$

The air properties at this temperature are as follows [2]:

$\nu = 20.41\ \mu m^2/sec$

$K = 29.565\ mW/mK$

$Pr = 0.7065$

where K, ν and Pr are the thermal conductivity, kinematic viscosity and the Prandtl number respectively. A characteristic length of $l = A/P$ is used where A and P are the area and perimeter of the strip which gives a value of $0.011m$. The above figures are then used to evaluate the Rayleigh number defined by the product of Grashof and Prandtl numbers defined in section (3.2):

$Ra = Gr.Pr = l^3 \beta g \Delta T.Pr/\nu^2 = 6456$

This Rayleigh number is in the range for a laminar flow for which the following correlation is recommended:

$Nu = 0.54\ Ra^{1/4}$

and since $h_c = Nu.K/l$ then

$h_c = 13.01\ W/m^2K$

Radiation

The radiative heat transfer coefficient h_r as defined in section(3.3) can be determined for steady-state conditions with values of 23.7 °C and 125 °C for the ambient and surface temperatures respectively and 0.086 for the emissivity of the surface as calculated previously. Thus:

$h_r = 0.84\ W/m^2K$ and therefore the total heat transfer coefficient (§4.4) is:

$h = h_c + h_r = 13.85\ W/m^2K$

Method 2

The average heat transfer coefficient over the area of the plate can also be estimated from the simple equation relating the heat generated and the heat lost in the system. Assuming that all the electric power is converted into Jule heat it may be written that:

Heat Generated = Heat lost by Convection and Radiation + Heat lost through the insulator

which is:

$q = (h_c + h_r)A\ (T_s - T_f) + KA\ (T_s - T_f)/x$

where K and x are the thermal conductivity and thickness of the glass wool insulation material. Substituting values of 0.05 W/mK [2] and 0.035 m for these parameters, a value of 13.49 is calculated for (h_c+h_r).

In this technique, a sample of the board is partially coated with matt black lacquer made by 3M whose emissivity is very nearly 1 [1]. The surface is heated and the current outputs are measured for the coated part (I_C) and immediately adjacent to the coated part (I_S). A reading is also taken for the background radiation (I_b) by directing the pyrometer at the walls of the chamber. The nett current output from the pyrometer is directly proportional to the emissivity of the surface described by the following relationship:

$$\frac{\varepsilon_{surface}}{\varepsilon_{paint}} = \frac{I_S - I_b}{I_C - I_b} \qquad A5.1$$

A piece of copper clad board was partially coated with the paint and heated by passing of electric current through the copper layer. The specimen was left to reach a steady-state condition and the pyrometer was used to measure temperature outputs on the coated, bare copper and the background.These temperatures were then converted into the the corresponding current outputs using the data supplied by the manufacturers. A graph was produced from the data supplied shown in figure (A5.1) which made it possible to accurately carry out the conversions.

The procedure was repeated at increasing electric power inputs and hence increasing temperature levels. The currents measured and subsequent emissivities are given in Table (A5.1). The mean and standard deviation from the mean of the results is also given in the last row of the table.

Table (A5.1) Results of Emissivity Measurements for Copper Cladding boards			
I_S (mA)	I_C (mA)	I_b (mA)	Emissivity
3.082	0.638	0.418	0.082
3.84	0.69	0.418	0.0796
4.33	0.744	0.418	0.083
4.91	0.827	0.418	0.091
5.524	0.914	0.418	0.097
6.438	0.914	0.418	0.0824
Mean SD 0.086 ± 0.007			

Figure (A5.1) Current/Temperature Response of Pyrometer

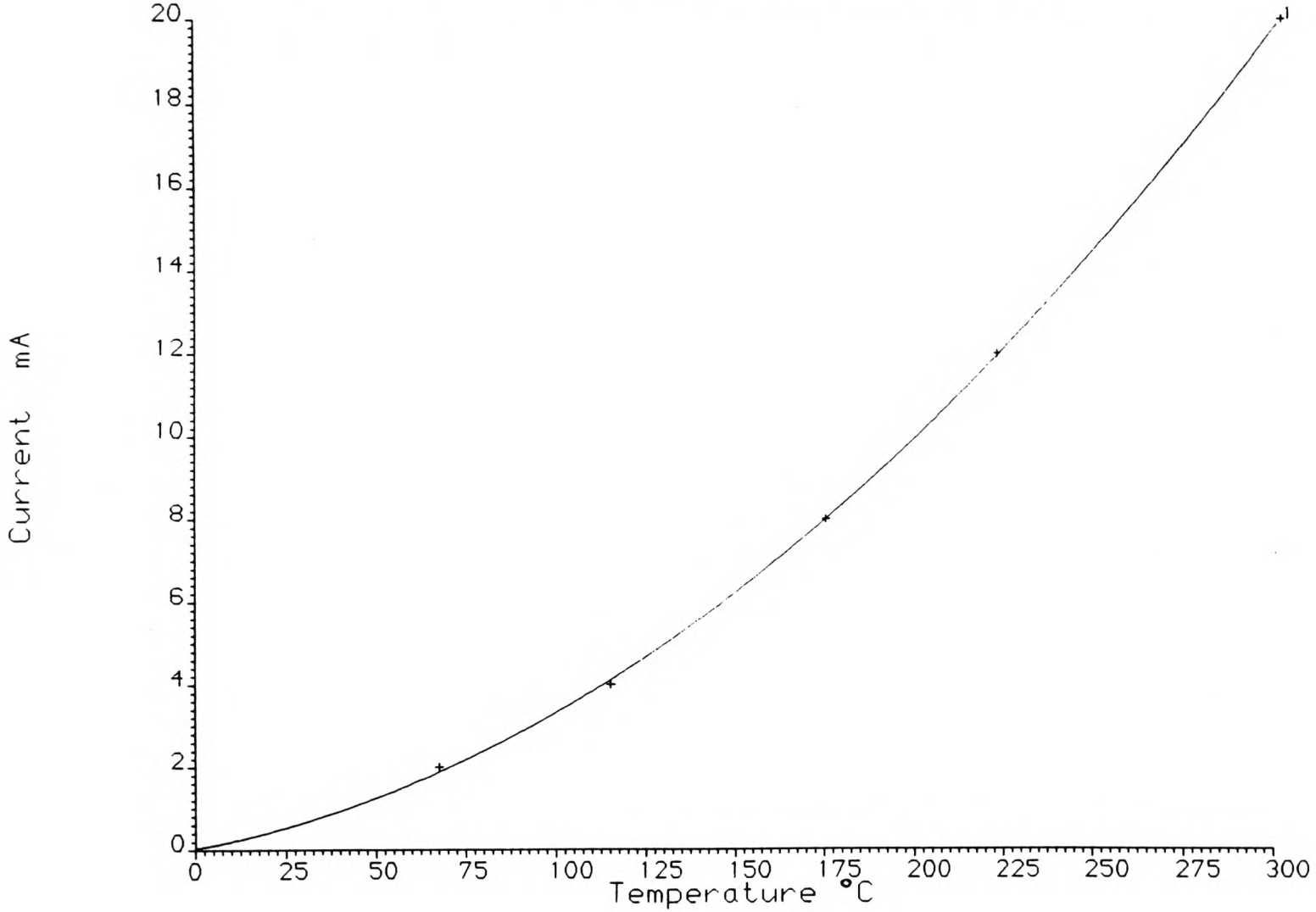

APPENDIX 6: The Raw Results for Thermal Conductivity Measurement of PTFE Normal to its Plane

Table (A6.1) Results for PTFE of thickness 1.58 *mm*						
Test No.	*VI* Watts	T_a °C	T_1 °C	T_2 °C	T_3 °C	*K* *W/mK*
1	9.045	21.8	83.35	80.1	71.0	0.278
2	8.98	22.0	84.5	80.1	71.1	0.277
3	9.012	21.90	83.35	80.0	71.0	0.279
4	9.03	21.95	83.30	80.05	71.0	0.280
Average *K* *W/mK*	0.279 ± 0.014					

Table (A6.2) Results for PTFE of thickness 3.32 *mm*						
Test No.	*VI* Watts	T_a °C	T_1 °C	T_2 °C	T_3 °C	*K* *W/mK*
1	9.075	23.25	86.0	83.8	67.50	0.305
2	9.075	23.30	86.1	84	67.50	0.301
3	9.075	23.30	86.1	84	67.75	0.306
4	9.075	23.20	86.2	84	67.50	0.301
Average *K* *W/mK*	0.304 ± 0.015					

Table (A6.3) Results for PTFE of thickness 7.446 *mm*						
Test No.	*VI* Watts	T_a °C	T_1 °C	T_2 °C	T_3 °C	*K* *W/mK*
1	9.098	23	86.20	84.7	57.10	0.354
2	9.065	23	86.80	85.0	57.55	0.356
3	9.098	23	86.65	85.0	57.55	0.357
4	9.065	23	86.90	85.0	57.80	0.361
Average *K* *W/mK*	0.357 ± 0.018					

APPENDIX 7: The Error Calculations for Thermal conductivity Measurements using the Lees' Disc Apparatus

---

The errors are estimated for test No. 1 in Table (A6.2) by inserting the following errors in equations (7.1) and (7.2):

Error in Voltage = 0.1%

Error in Current = 0.3%

Error in Thermometer Readings = 0.25 °C

Error in Micrometer = 0.005 *mm*

Using the above errors the following errors are obtained for each term in equations (7.1) and (7.2):

$VI = 9.075 \pm 0.4\%$

$A_1(T_1-T_a) = 0.252 \pm 0.845\%$

$A_2(T_2-T_a) = 0.121 \pm 0.88\%$

$A_3(T_3-T_a) = 0.1774 \pm 0.605\%$

$A_4[(T_2+T_3)/2-T_a)] = 0.0277 \pm 1.11\%$

$A(T_2-T_3)/t = 9.868 \pm 3.18\%$

Substituting these in equation (7.1) a value is obtained for e and its percentage error :

$$e = \frac{9.075 \pm 0.4\%}{0.5778 \pm 0.79\%} = 15.7 \pm 1.2\%$$

This is then inserted in equation (7.2) along with the other terms to calculate the value

and error in the thermal conductivity K:

$$K = \frac{(15.7 \pm 1.2\%)[(0.0138 \pm 1.11\%) + (0.1774 \pm 0.605\%)]}{9.868 \pm 3.18\%}$$

$$= 0.304 \pm 5.0\%$$

$$= 0.304 \pm 0.015 \quad W/m^2K$$

APPENDIX 8: The Raw Results for Thermal Conductivity Measurements of FR4 Boards Normal to their Plane

Table (A8.1) Results for FR4 board of thickness 1.5 *mm*						
Test No.	*VI* Watts	T_a °C	T_1 °C	T_2 °C	T_3 °C	*K* *W/mK*
1	9.403	22.6	84.1	81	74.0	0.366
2	9.403	22.8	84.3	81.05	73.9	0.358
3	9.403	22.8	84.5	81.05	74.0	0.363
Average *K* *W/mK*	0.362 ± 0.018					

Table (A8.2) Results for FR4 board of thickness 3 *mm*						
Test No.	*VI* Watts	T_a °C	T_1 °C	T_2 °C	T_3 °C	*K* *W/mK*
1	9.464	22.7	85.0	82.05	69.20	0.378
2	9.420	21.75	84.8	81.90	68.90	0.372
3	9.420	21.80	84.75	81.90	68.95	0.374
Average *K* *W/mK*	0.375 ± 0.019					

Table (A8.3) Results for FR4 board of thickness 4.5 *mm*						
Test No.	*VI* Watts	T_a °C	T_1 °C	T_2 °C	T_3 °C	*K* *W/mK*
1	9.467	21.95	86.1	83.4	66.0	0.401
2	9.454	22.00	86.1	83.2	65.9	0.403
3	9.454	22.10	85.8	82.9	65.9	0.410
Average *K* *W/mK*	0.405 ± 0.02					

Table (A8.4) Results for FR4 board of thickness 6 *mm*						
Test No.	*VI* Watts	T_a °C	T_1 °C	T_2 °C	T_3 °C	*K* *W/mK*
1	9.467	24.4	88	85.5	64	0.412
2	9.467	24.3	88.05	85.6	64.05	0.411
3	9.467	24.3	88.1	85.75	64.2	0.412
4	9.477	20.9	85.25	82.9	61.2	0.410
Average *K* *W/mK*	0.411 ± 0.02					

APPENDIX 9: Results of Temperature Measurements at Various Pressures for Determination of Thermal Conductivity Along the Plane of Fibre-Glass Boards (§7.3)

The following tables give the measured temperatures for each fibre-glass specimen at various vessel pressures with reference to figure (7.6). The last column in each table represents the temperature of the particular point at zero vessel pressure. these were determined via fitting a best curve through the points and extrapolating back to zero pressure.

Table (A9.1) Temperatures along 1st 3 *cm* sample as measured via Thermocouples at various Vessel Pressures

Pressure Torr Temperature °C	Zero Extrapolated	10 Measured	161 Measured	312 Measured	616 Measured
T_0	95.39	94.95	82.37	76.13	68.07
T_1	66.13	65.73	53.51	47.83	40.75
T_2	47.59	47.33	36.38	32.22	27.66
T_3	29.21	29.16	22.47	20.87	19.36
T_4	22.32	22.36	18.75	18.25	17.45
T_5	19.27	19.26	17.65	17.25	16.75
T_6	17.83	17.85	16.85	16.75	16.45
T_7	16.77	16.85	16.45	16.55	16.20
T_8	16.43	16.45	16.25	16.25	15.99

Table (A9.2) Temperatures along 2nd 3 *cm* sample as measured via Thermocouples at various Vessel Pressures							
Pressure Torr Temperature °C	Zero	9.25	159.25	311.25	463.25	615.25	762
T_0	75.91	75.07	64.94	60.25	56.16	53.22	50.19
T_1	53.87	53.03	43.40	38.97	35.69	33.13	30.84
T_2	40.04	39.27	30.74	27.46	25.07	23.37	21.77
T_3	26.18	25.66	20.27	19.05	17.85	17.06	16.35
T_4	21.00	20.67	17.35	16.85	16.15	15.64	15.14
T_5	18.39	18.24	16.55	16.25	15.54	15.14	14.73
T_6	17.28	17.15	15.84	15.74	15.24	14.83	14.43
T_7	16.38	16.35	15.64	15.34	15.04	14.63	14.23
T_8	15.99	16.05	15.44	15.24	14.83	14.53	14.02

Table (A9.3) Temperatures along 1st 4 *cm* sample as measured via Thermocouples at various Vessel Pressures						
Pressure Torr Temperature °C	Zero	12	154.5	305.5	459.5	762
T_0	77.81	76.63	63.68	59.38	55.96	50.96
T_1	54.32	53.22	42.03	37.98	35.5	31.63
T_2	40.98	40.06	30.74	28.05	26.56	23.96
T_3	28.62	28.15	22.67	21.47	20.37	19.66
T_4	23.76	23.46	20.27	19.86	19.56	18.65
T_5	21.56	21.37	19.36	19.26	19.15	18.24
T_6	20.40	20.27	18.85	18.85	18.75	17.94
T_7	19.45	19.36	18.55	18.45	18.45	17.75
T_8	19.57	18.05	18.24	18.24	18.24	17.45

Table (A9.4) Temperatures along 2nd 4 *cm* sample as measured via Thermocouples at various Vessel Pressures							
Pressure Torr Temperature °C	Zero	10	147	298	374	600	762
T_0	90.11	89.2	76.04	70.21	66.20	62.99	60.45
T_1	61.22	60.35	47.63	42.23	39.17	36.78	35.20
T_2	45.63	44.27	32.07	29.26	27.46	26.16	25.46
T_3	30.53	29.65	22.36	20.98	20.47	19.97	20.06
T_4	24.22	23.66	19.26	18.75	18.65	18.55	18.65
T_5	21.46	21.07	18.14	17.94	17.94	17.94	18.14
T_6	20.07	19.76	17.55	17.45	17.65	17.55	17.84
T_7	18.53	18.75	17.15	17.06	17.25	17.25	17.55
T_8	18.05	18.24	16.96	16.85	17.06	17.15	17.35

Table (A9.5) Temperatures along 1st 5 *cm* sample as measured via Thermocouples at various Vessel pressures							
Pressure Torr Temperature °C	Zero	11.5	158.5	301.5	453.5	605.5	763.5
T_0	101.03	99.34	84.03	76.73	71.47	67.29	63.68
T_1	52.83	51.25	38.18	34.21	31.73	30.25	29.26
T_2	33.03	32.12	25.07	23.96	23.17	22.87	22.57
T_3	25.09	24.67	21.47	21.17	20.87	20.87	20.77
T_4	21.88	21.67	20.17	19.96	19.96	19.96	20.07
T_5	20.15	20.17	19.56	19.56	19.26	19.56	19.66
T_6	18.86	18.85	18.95	19.05	19.05	19.16	19.26
T_7	18.42	18.45	18.65	18.75	18.85	18.95	18.95

Table (A9.6) Temperatures along 2nd 5 *cm* Sample as measured via Thermocouples at various Vessel Pressures							
Pressure Torr Temperature °C	Zero	13	152	303	455	607	762
T_0	78.29	76.92	66.21	60.94	56.93	54.28	51.75
T_1	42.64	41.54	33.33	30.05	28.15	27.26	26.06
T_2	28.02	27.46	23.47	22.37	21.76	21.58	21.07
T_3	22.33	22.16	20.67	20.27	19.86	20.17	19.76
T_4	19.97	19.96	19.66	19.56	19.36	19.26	19.26
T_5	18.67	18.7	19.26	19.26	18.95	19.16	19.16
T_6	17.75	17.94	18.95	18.85	18.75	18.85	18.75
T_7	17.45	17.65	18.65	18.65	18.45	18.65	18.55

Table (A9.7) Temperatures along 2nd 6 *cm* sample as measured via Thermocouples at various Vessel Pressures							
Pressure Torr Temperature °C	Zero	10.25	162.25	313.25	465.25	616.25	769.25
T_0	93.60	92.11	77.02	70.50	65.83	61.91	58.70
T_1	48.96	47.53	33.72	29.16	26.56	24.77	23.27
T_2	31.88	30.84	21.62	19.36	18.55	17.65	17.05
T_3	24.28	23.66	18.11	16.75	16.25	15.74	15.34
T_4	20.74	20.27	16.25	15.54	15.24	14.83	14.53
T_5	18.68	18.34	15.44	14.93	14.73	14.33	14.02
T_6	16.99	16.75	14.73	14.33	14.23	13.92	13.62
T_7	16.34	16.15	14.33	13.82	13.72	13.62	13.22

Figure (A9.1) Temperature Vs Pressure For 1st 10cmx3cm Sample

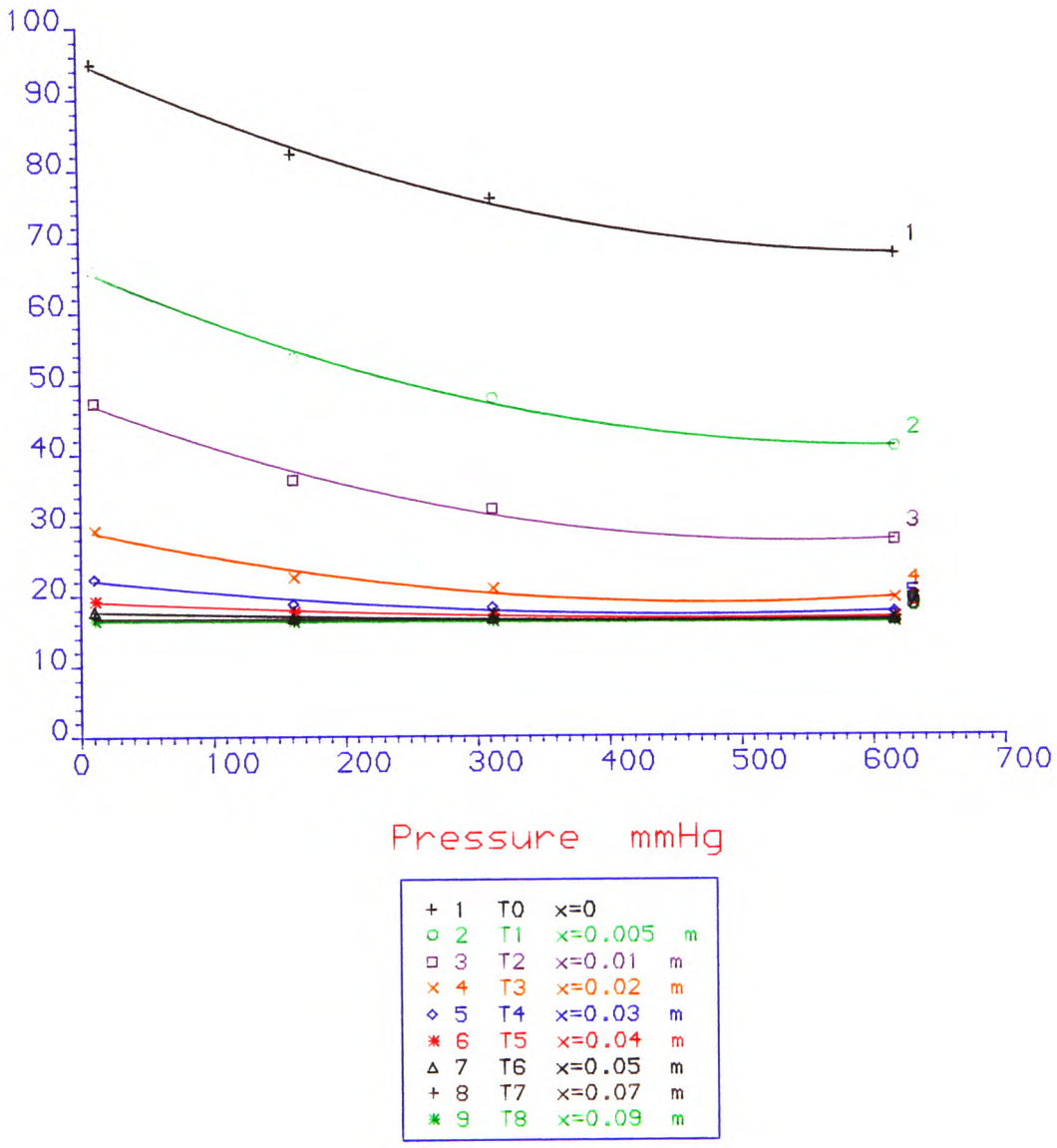

FSARVAR [ELEC] 10-FEB-1992 13:55:39.43

Figure (A9.2) Temperature Vs Pressure For 2nd 10cmx3cm Sample

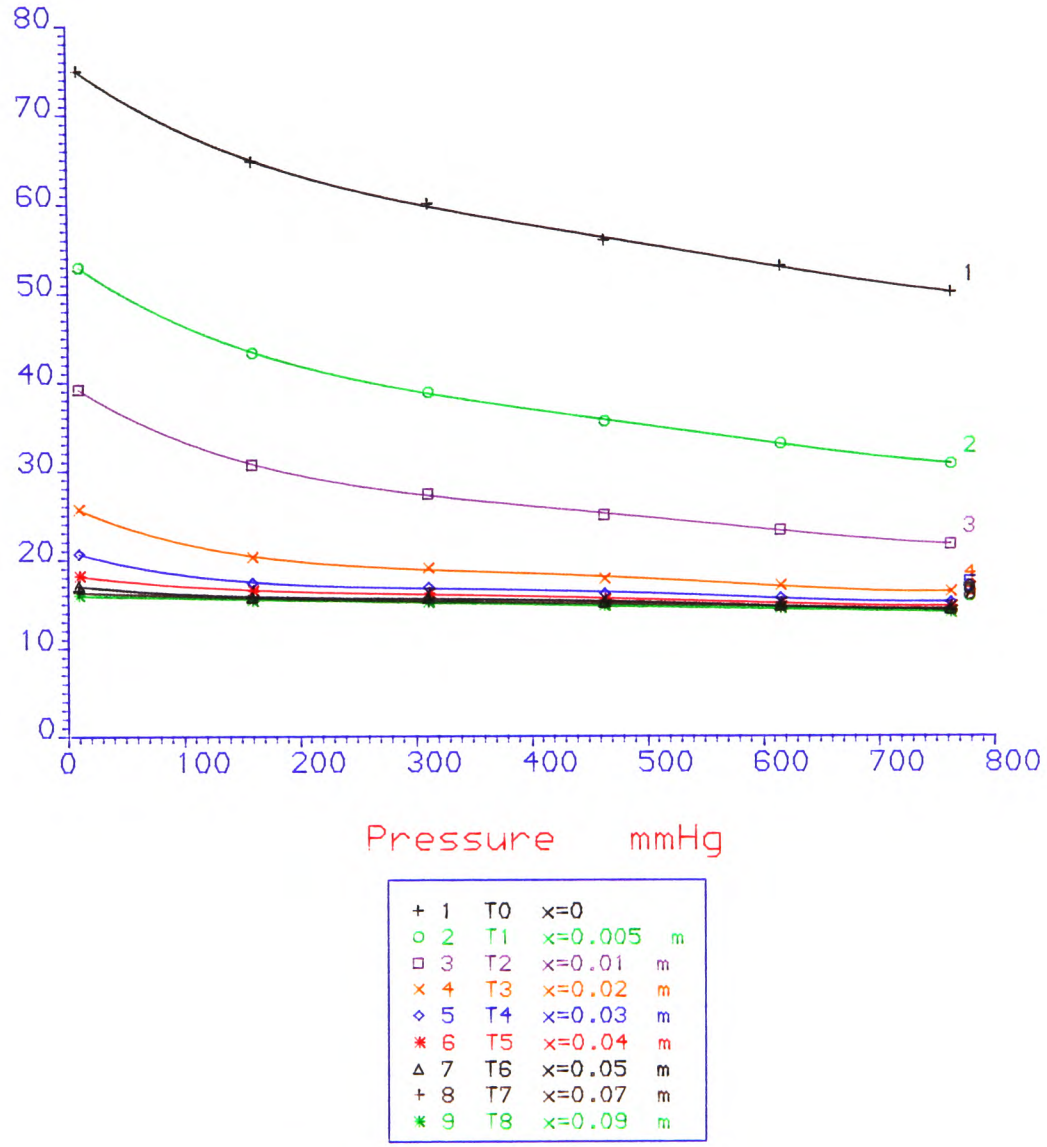

Figure (A9.3) Temperature Vs Pressure For 1st 10cmx4cm Sample

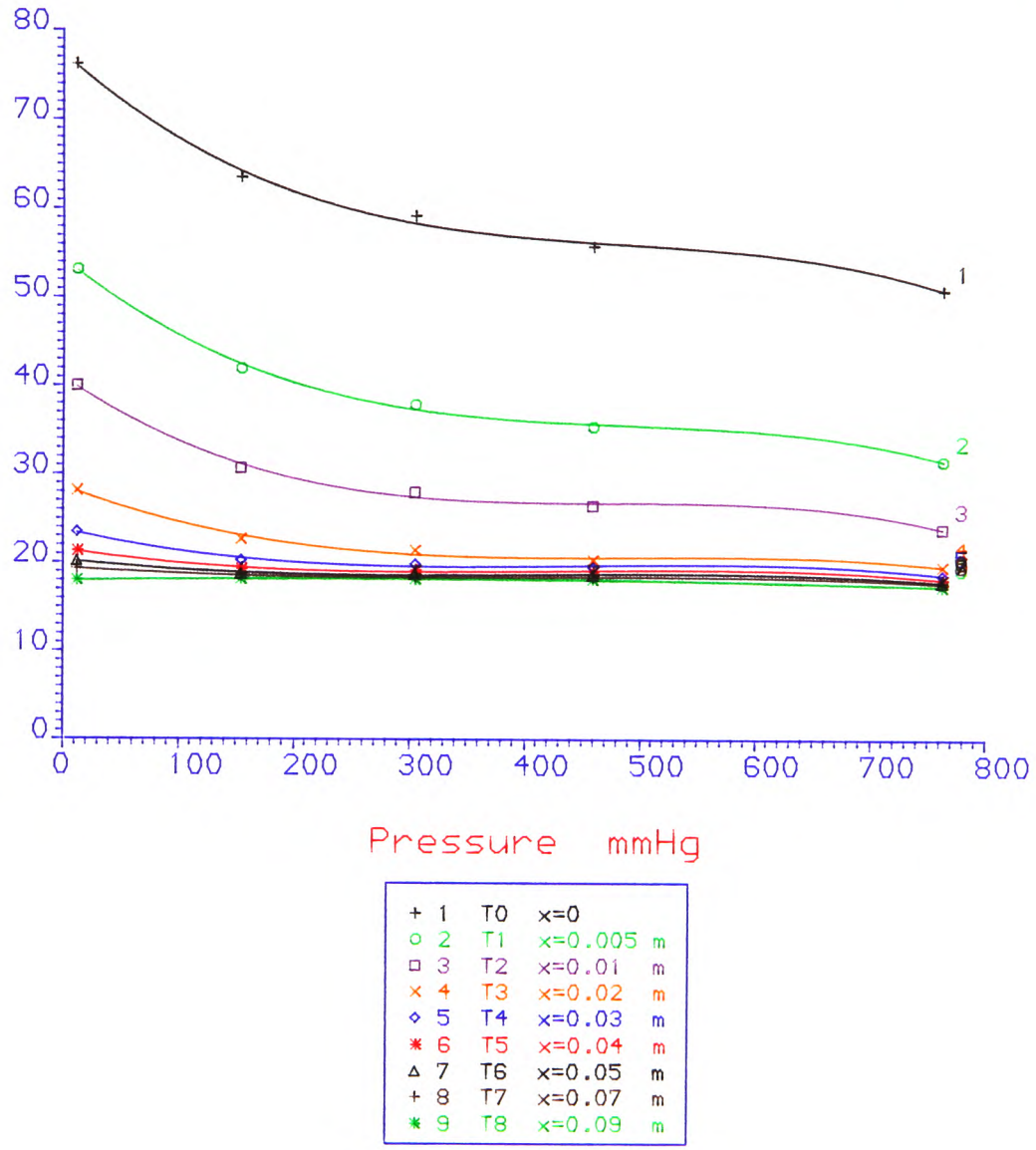

FSARVAR [ELEC] 10-FEB-1992 14:32:50.04

Figure (A9.4) Temperature Vs Pressure For 2nd 10cmx4cm Sample

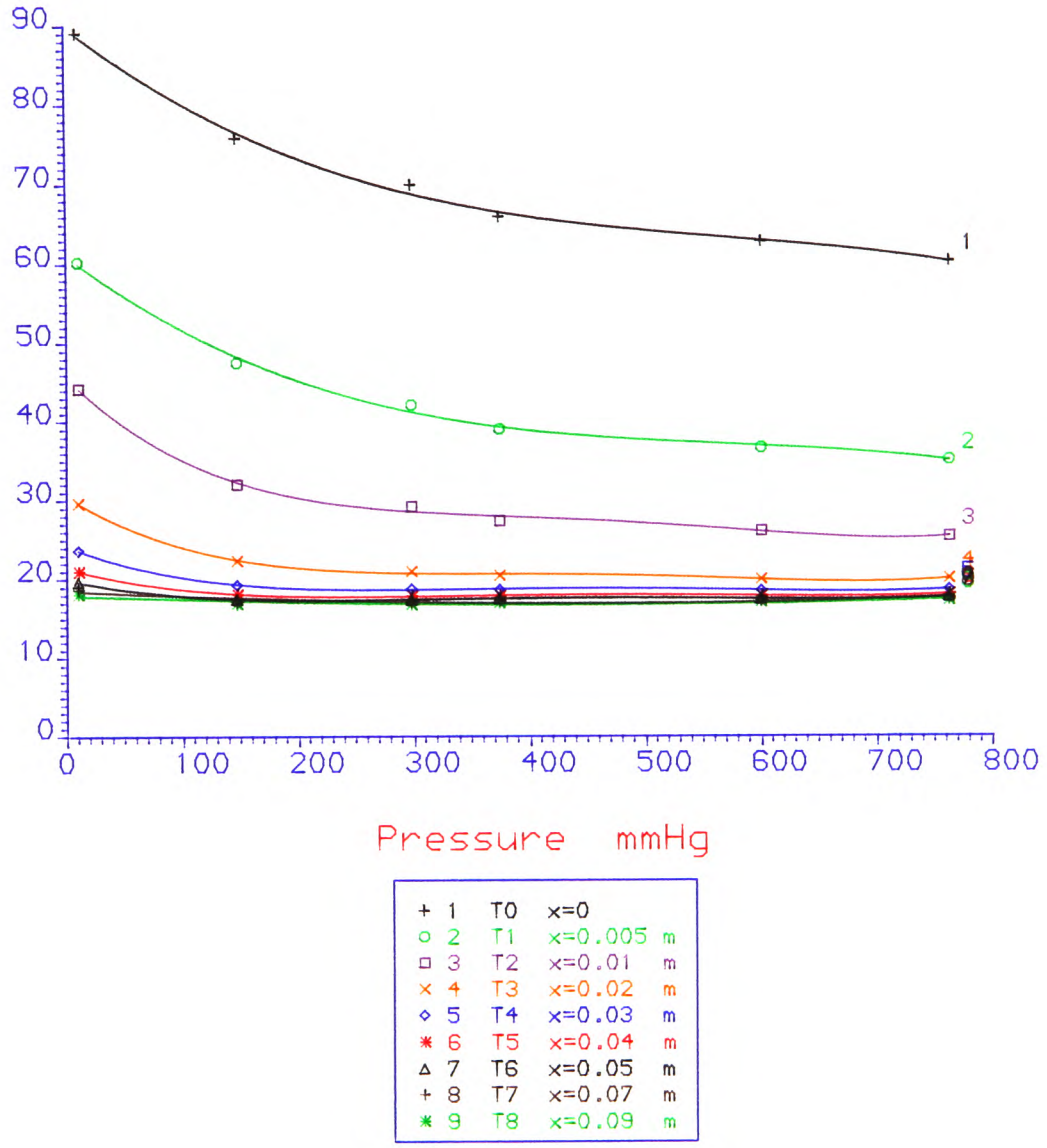

Figure (A9.5) Temperature Vs Pressure For 1st 10cmx5cm Sample

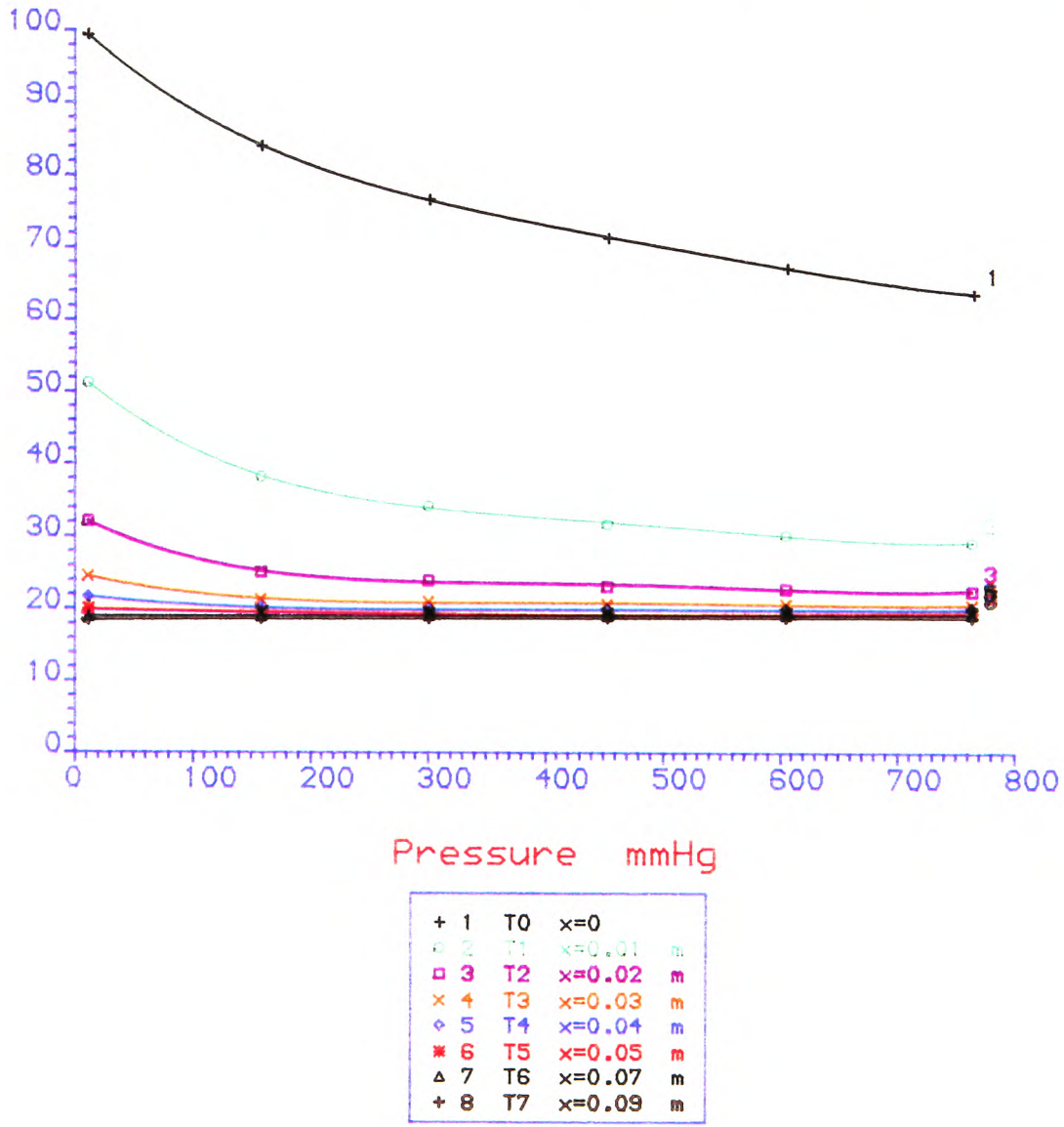

FSARVAR [ELEC] 8-AUG-1989 11:58:05.58

Figure (A9.6) Temperature Vs Pressure For 1st 10cmx6cm Sample

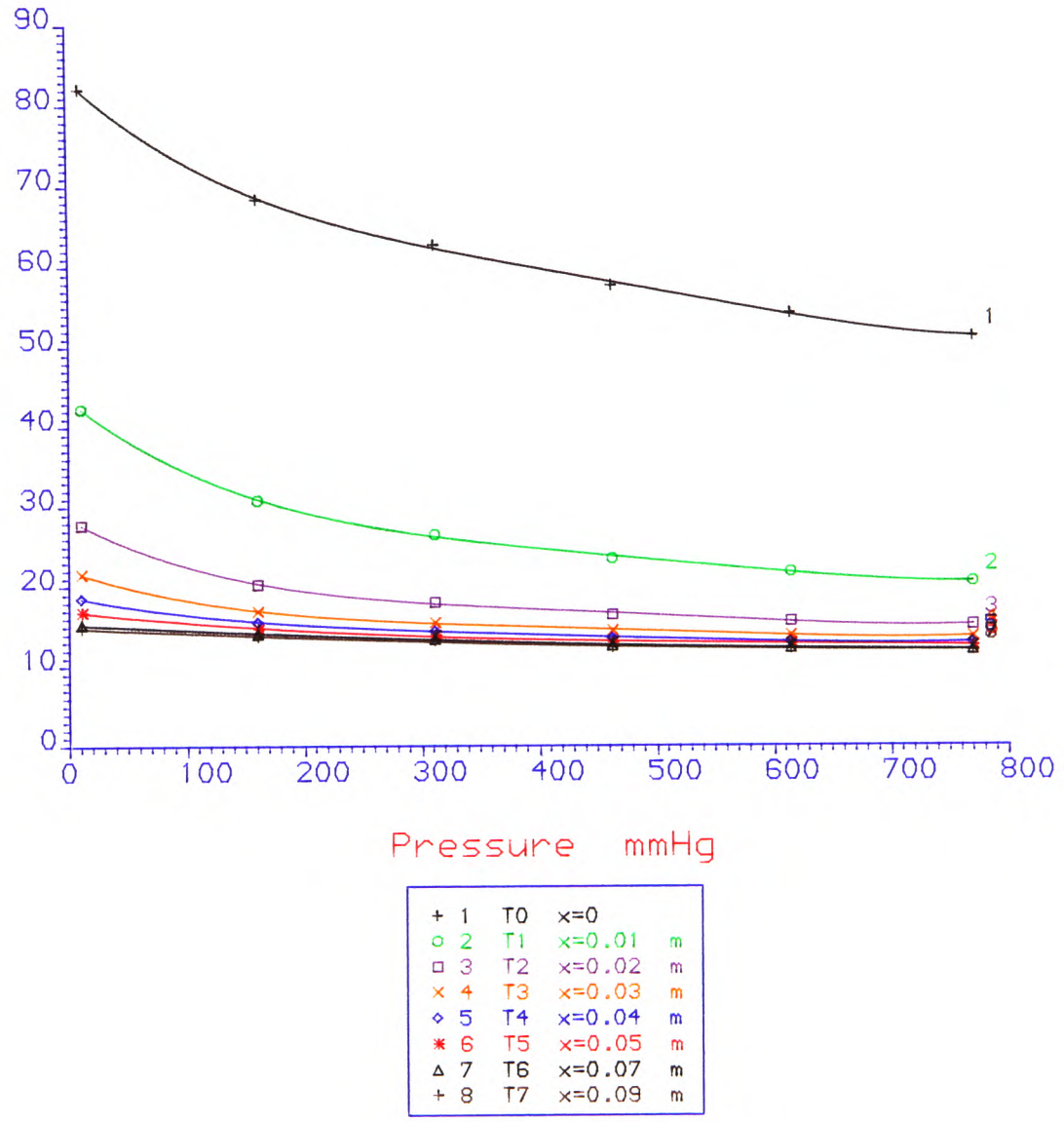

FSARVAR [ELEC] 10-FEB-1992 15:17:30.86

Figure (A9.7) Temperature Vs Pressure For 2nd 10cmx6cm Sample

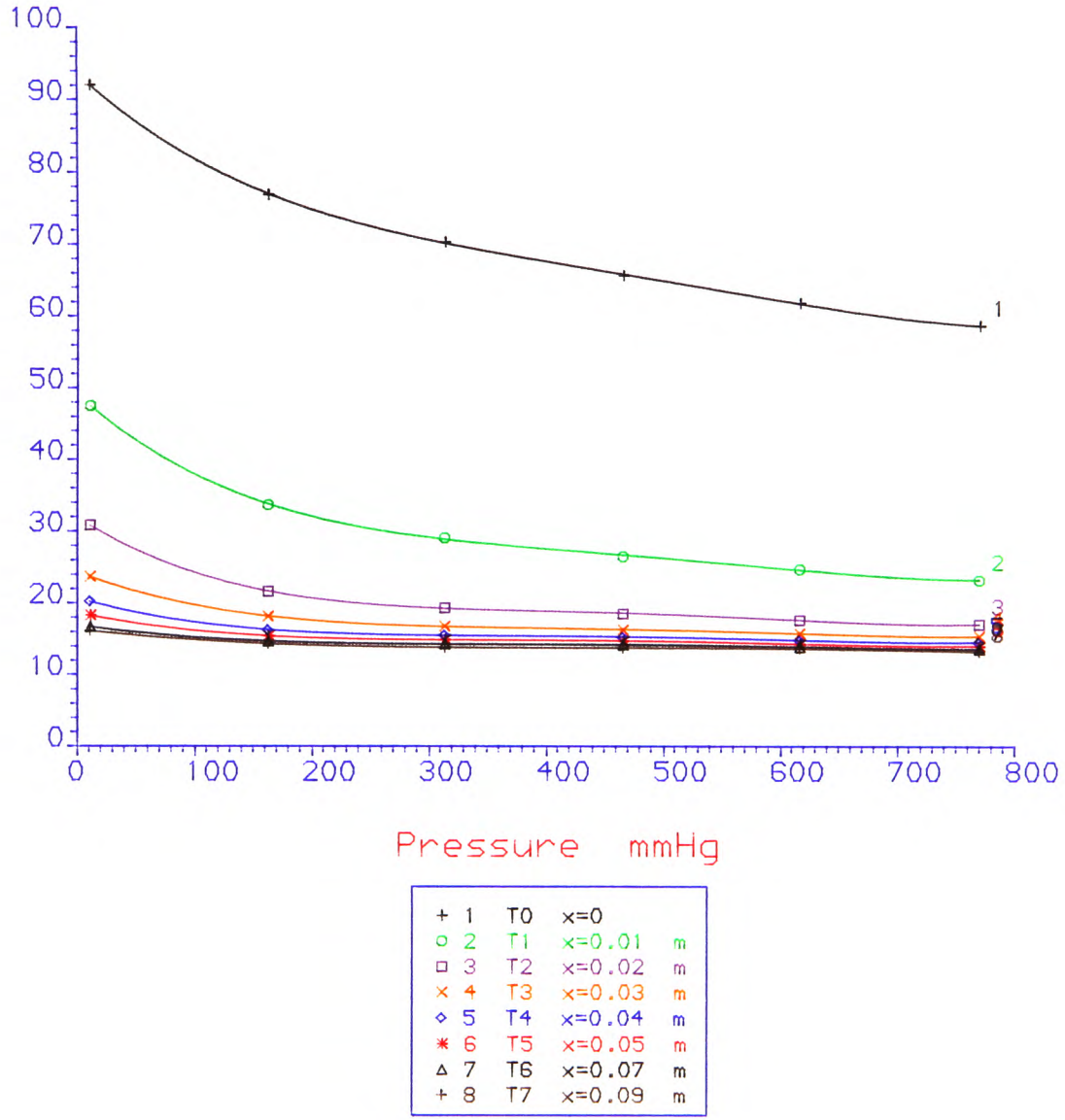

FSARVAR [ELEC] 10-FEB-1992 15:54:04.59

Radiation

The radiation coefficient h_r is determined from the following equation (§ 3.3):

$$h_r = \sigma\varepsilon(T_s^2 + T_a^2)(T_s + T_a)$$

Substituting values of 0.95 for emissivity, 120 °C for surface temperature and 23.2 °C for the ambient temperature a radiation heat transfer coefficient of 9 W/m^2K is obtained for the ceramic package.

Convection

The convective heat transfer coefficient h_c is calculated using the relationships recommended in Chapman [8] for natural convection from a horizontal flat plate with the heated surface facing upwards. The air properties are taken from the appropriate tables [8] at the mean film temperature $T_f=(T_s+T_a)/2$ which is 71.6 °C in this case.

Pr=0.707 K=29.32×10^{-3} W/mK ν=20×10^{-6} m^2/sec

The characteristic length is recommended as $l=A/p$ where A and P are the surface area and perimeter respectively. A width of 0.015 m and 0.03 m yields a value of 0.005 m for l. Rayleigh number is defined as:

$Ra = l^3 \beta g \Delta T Pr/\nu^2$

where $\beta = 1/T_f$

substituting for all the parameters a value of 608.57 is calculated for Rayleigh number which is the laminar range [8] for which the following relationship is recommended:

$Nu = 0.54\, Ra^{1/4} = 2.682$

Since $h_c = NuK/l$ a value of 15.72 W/m^2K is obtained for the convective heat transfer coefficient from the ceramic package.

POOLE N J, SARVAR F, WITTING P A and McKENZIE W H: 'Thermal Modelling Using ASTEC3 Software', *Int. J. of Numerical Modelling*, Volume 1, 103-113, 1988.

POOLE N J and SARVAR F: 'Fundamentals of Heat Transfer', *IEE Colloquium on Thermal Design of Electronic Systems*, London, March 1989.

WITTING P A and SARVAR F: 'Electro-thermal Simulation of Hybrid and VLSI Circuits', *IEE Colloquium on Thermal Design of Electronic Systems*, London, March 1989.

SARVAR F, POOLE N J: 'Simultaneous Modelling of Thermal and Electrical Characteristics Using ASTEC3 Software', *Digest of the Nasecode VI Software Forum*, Dublin, pp. 149-154, 1989.

WITTING P A, SARVAR F, POOLE N J: 'Electro-thermal Simulation of Hybrid and VLSI Circuits', *Proceedings of the IASTED Conference*, Lugano, June 1989.

SARVAR F, POOLE N J, WITTING P A: 'PCB Glass-Fibre Laminates: Thermal Conductivity Measurements and Their Effect on Simulation', *AIME Journal of Electronic Materials*, Volume 19, N0. 12, 1990.

INTERNATIONAL JOURNAL OF NUMERICAL MODELLING : ELECTRONIC NETWORKS, DEVICES AND FIELDS,
Vol. 1, 103–113 (1988)

THERMAL MODELLING USING ASTEC3 SOFTWARE

N. J. POOLE, F. SARVAR, P. A. WITTING AND W. H. McKENZIE*

*Department of Electrical and Electronic Engineering, Polytechnic of Wales, Pontypridd, Mid Glamorgan CF37 1DL, Wales, U.K., and *Department of Mechanical Engineering, Polytechnic of Wales, U.K.*

SUMMARY

This paper describes the application of ASTEC3, a general purpose analogue electronic circuit simulation package, to the analysis of thermal properties of given structures. The modelling of each system is considered for both conduction and convection mechanisms, radiation being assumed to play a very minor role in heat dissipation from most electrical circuits. A procedure is given for the modelling of one-, two- and three-dimensional thermal problems which is then used for the simulation of relatively simple examples. The results obtained with ASTEC3 are compared with results determined by using more traditional and independent techniques.

1. INTRODUCTION

For many years designers have faced the problem of thermal dissipation in semiconductor devices, including hybrid circuits, and the prediction of any heat sources within these circuits. This has become a more important issue as industrial manufacturers try to reduce the physical size of these devices and increase their packing density.[1, 2]

Heat generation is dependent on the electrical activity of the various components in the circuits. The simulation of the electronic aspects of the circuit operation is well catered for by a number of computer packages, but there are no general purpose packages which also include the prediction of any local temperature rise. Current practice in industry appears to be either to apply a crude 'rule-of-thumb' to estimate the heat dissipation, or to use a separate modelling package to calculate the average heat dissipation and to guess the size of all electronic heat sources.

ASTEC3 is a powerful circuit analysis package, capable of performing transient, a.c. small-signal and d.c. steady-state simulations.[3, 4] ASTEC3 is also suitable for providing solutions to differential equations, and any system defined by this format can be solved. As the electrical and thermal characteristics of any given network can be written in terms of differential equations, this allows for the possibility of simulating both phenomena with ASTEC3.

There are three basic processes of heat transfer: conduction, convection and radiation. In conduction thermal energy is transferred through the lattice structure, either by means of free-electrons or as vibrational energy, or both.[5, 6]

The basic equations of heat conduction have been well documented.[7–11] In one dimension the rate of heat transfer through a given area A is given by

$$q_x = -KA\frac{\partial T}{\partial x} \tag{1}$$

where K is the thermal conductivity of the material, T is the temperature and x is the displacement through the material of area A, equal to $\Delta y\ \Delta z$.

The general equation of conduction in three dimensions for a uniform body with constant thermal conductivity is given by[7–11]

$$K\left(\frac{\partial^2 T}{\partial x^2} + \frac{\partial^2 T}{\partial y^2} + \frac{\partial^2 T}{\partial z^2}\right) + q^* = \rho C_p \frac{\partial T}{\partial t} \tag{2}$$

where q^*, ρ and C_p are the heat generation per unit volume, the density and the specific heat capacity of the material, respectively.

0894-3370/88/020103-11$05.50

Received 26 January 1988
Revised 12 May 1988

The rate of change of energy stored in a volume element ΔV is given by[10]

$$q = \rho C_p \Delta x \Delta y \Delta z \frac{\partial T}{\partial t} \tag{3}$$

where ΔV is represented by $\Delta x \Delta y \Delta z$.

Another mode of heat transfer is convection, whereby heat is exchanged between a solid body and an adjacent fluid. There are two types of convection: free convection and forced convection. Free convection takes place as a consequence of density differences caused by temperature gradients between the fluid and the body, and with the fluid itself; forced convection occurs when the fluid motion is induced by an external force. The rate of heat flow at the surface is conventionally described by the equation[7-11]

$$q = hA(T_f - T_s) \tag{4}$$

where A is the area exposed to heat transfer (given by $\Delta y \Delta z$), T_f and T_s are the fluid and surface temperatures, respectively, and h is an average value for the convective heat transfer coefficient.

2. THERMAL SYSTEM MODELLING

The thermal performance of a given system can be written as an electrical analogy by a suitable change of variables. The simple Ohm's law equation can be compared with equations (1) and (4) for conductive and convective heat transfer, respectively. This gives equivalent electrical resistances of

$$R_{\text{conduction}} = \frac{\Delta x}{K \Delta y \Delta z} = R_{\text{th}} \tag{5}$$

$$R_{\text{convection}} = \frac{1}{hA} \tag{6}$$

for conductive and convective processes, respectively.

Also, by comparing the equation for the current in a charging capacitor[12] with equation (3), an equivalent electrical capacitance can be found and used to represent the thermal capacitance of a cell of volume ΔV of a body

$$C_{\text{th}} = \rho C_p \Delta V = \rho C_p \Delta x \Delta y \Delta z \tag{7}$$

Since the flow of heat through a thermal resistance is analogous to the flow of current through an electrical resistance, any form of heat flow into or out of a system can be modelled as sources of current. Similarly, there is an analogy between temperature in a thermal system and electrical voltage, and fixed temperatures at a boundary can therefore be modelled as a voltage source of the same value. By these comparisons, simple electrical equivalent models for thermal characteristics can be constructed, using the analogous thermal resistance and capacitance quantities.

The ASTEC3 input language is based on a conventional circuit diagram, with the positions of each element defined by the nodes at its connections. Figure 1 illustrates the electrical configuration for a cell in 3D conduction.

If the value of convective heat transfer coefficient h is known, convection at the boundaries can be modelled using resistors of values $1/hA$, where A is the convection surface area. In one dimension this reduces to $1/h$ as Δy and Δz are taken as unity, and in two dimensions to $1/h\Delta y$.

3. VALIDATION OF ASTEC3 MODELLING

To verify the validity of ASTEC3 in thermal modelling, the results must be compared with those obtained by some standard techniques. This is carried out for 1D, 2D and 3D heat flow problems, as follows.

3.1. *One dimension*

Consider a slab of width 50 mm with uniform thermal conductivity of 17·3 W/mK, specific heat capacity of 0·444 kJ/kgK and density of 8656 kg/m^3, where heat is generated at a constant rate of

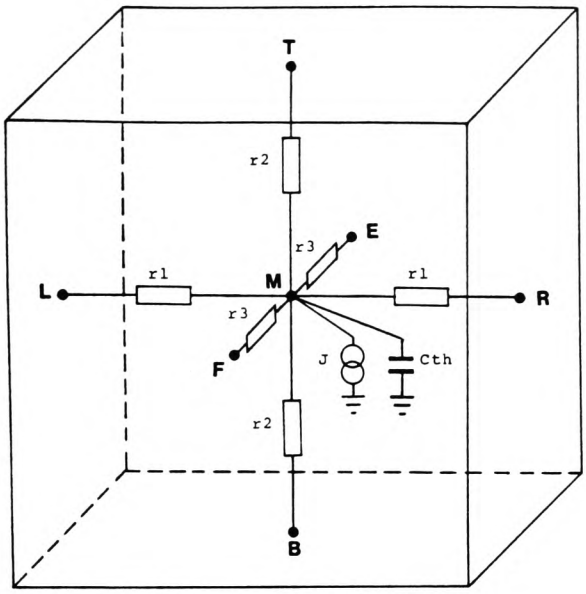

$r1 = \frac{1}{2} Rth_x$

$r2 = \frac{1}{2} Rth_y$

$r3 = \frac{1}{2} Rth_z$

Figure 1. The electrical equivalent model for a cell in 3D conduction

2·06 MW/m^3. The temperature distribution in the slab is to be found when constant temperature sources at 60°C and 20°C are applied to its boundary surfaces.

To achieve an ASTEC3 solution of this problem, the slab is divided into five segments of 10 mm length each. R_{th} and C_{th} are calculated for a 1D cell using equations (5) and (7), and five such cells are connected in series as shown in Figure 2. The resistors in the dotted areas will be used for incorporating convection into the system, as described below.

The simulation is initially carried out with zero heat generation, and the nodal temperatures are recorded until a steady state is reached. This first stage of the operation obviates the need to calculate and specify the initial temperature distribution in the slab. The simulation continues from this condition, with heat generation switched on, to a final steady state.

To validate these results a finite-difference technique was also used to determine the temperatures of the four interior nodes from an initial linear steady-state condition to a final steady state

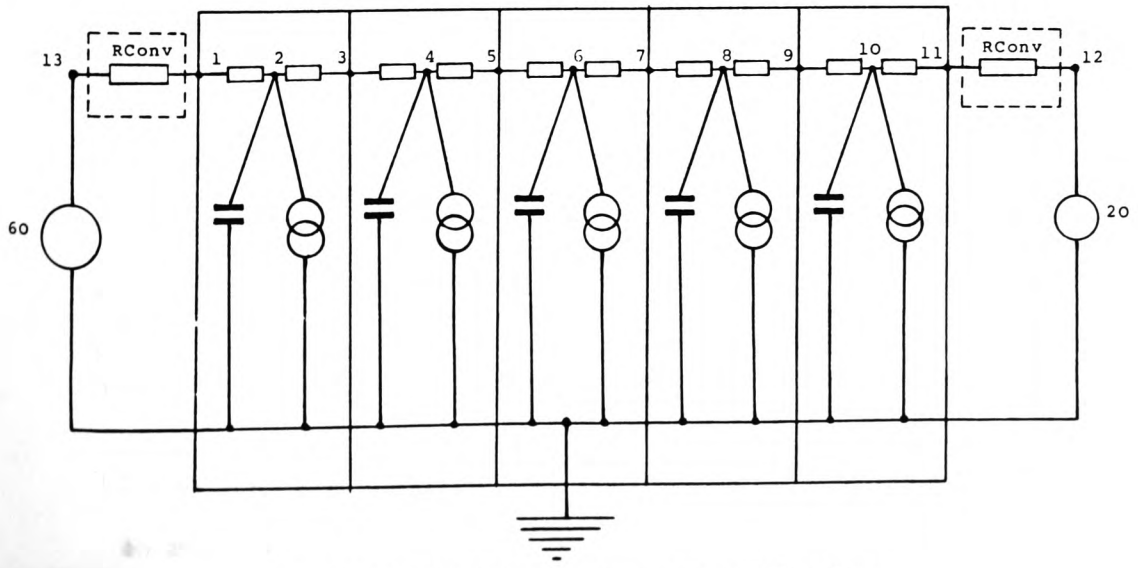

Figure 2. The electrical configuration used for the 1D problem

Table I. Results for the 1D problem with conduction only

Node	Initial temperature (°C)	Final temperature (°C) ASTEC3	Finite difference
1	60·0	60·0	60·0
3	52·0	75·8	75·8
5	44·0	79·7	79·7
7	36·0	71·1	71·7
9	28·0	51·8	51·8
11	20·0	20·0	20·0

Table II. Results for the 1D problem, including conduction and convection

Node	Initial temperature (°C)	Final temperature (°C) ASTEC3	Finite difference
13	60·0	60·0	60·0
1	57·6	67·9	67·9
3	50·5	84·7	84·7
5	43·4	89·5	89·5
7	36·5	82·5	82·5
9	29·5	63·6	63·6
11	22·4	32·7	32·7
12	20·0	20·0	20·0

in steps of Δt. This is a method whereby the partial differential equation of heat conduction is replaced by a system of linear algebraic equations.[7, 11] A comparison of temperatures for identical nodes at equivalent times within both ASTEC3 and the finite-difference technique is given in Table I.

It can be seen from Table I that there is no difference between the results obtained from the two techniques, suggesting that the errors in ASTEC3 modelling are of the same order of magnitude as those in the finite-difference method, with a maximum order of $(\Delta x)^2$.[9]

A more accurate assessment of the errors within ASTEC3 for 1D simulations can be found by comparison with an analytical solution. The steady-state solution to the 1D conduction equation is of the form

$$T = -\tfrac{1}{2}(q^*/K)x^2 + Bx + C$$

where B and C are constants with values of 2176·88 and 60, respectively, determined from the specified boundary conditions. There was no difference between the temperatures calculated from the above expression and those calculated with ASTEC3, to three significant figures.

The above problem can be considered with convection at the boundaries with a heat transfer coefficient of 5 kW/mK from both ends.

Convection at the boundaries is incorporated into the network by adding resistors of values $1/h$ to the two outer nodes, as illustrated by the dotted lines in Figure 2. The steady-state temperatures obtained from ASTEC3 and finite-differencing are given in Table II; again, the results are identical.

3.2. *Two dimensions*

To assess the performance of ASTEC3 in 2D heat transfer problems, the heat flow in a rectangular plate (Figure 3) is simulated. Three sides of a rectangular plate 50 mm wide and

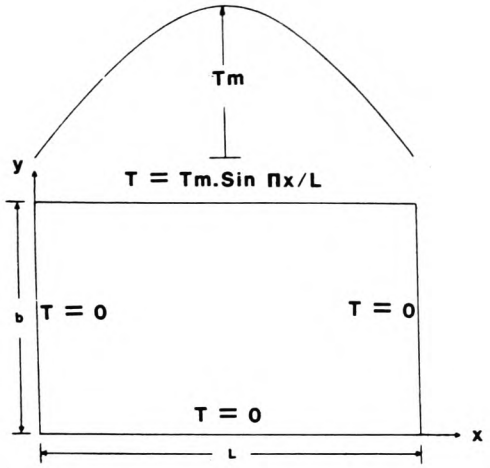

Figure 3. Rectangular plate showing the parameters and symbols used in the general solution to the 2D problem

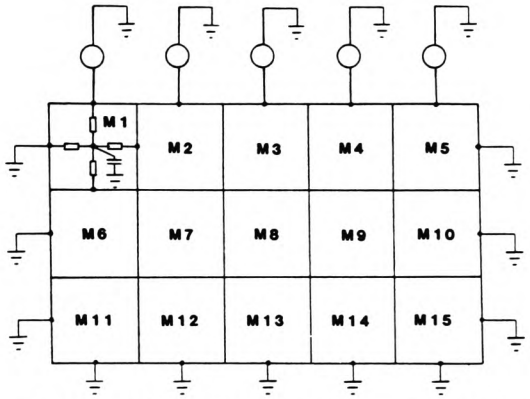

Figure 4. The electrical equivalent model of the rectangular plate as used in the ASTEC3 simulation of the problem

30 mm high are maintained at a constant temperature of 0°C. The upper side has a sinusoidal temperature distribution imposed upon it. The final steady-state temperature distribution in the plate is to be found. Values of 0·05 W/mK, 150 kg/m^3 and 1·88 kJ/kgK are taken for the thermal conductivity, density and specific heat capacity of the solid, respectively.

For ASTEC3 modelling, the plate is divided into 15 square cells of dimensions 10 × 10 mm. R_{th} and C_{th} are calculated using expressions (5) and (7) and an electrical network is constructed by connecting 15 such cells, as shown in Figure 4. Average values are calculated for each segment of the sine function, and applied as voltage sources to the five nodes on the upper side of the circuit, and the outer nodes of the three remaining sides are tied to ground, representing a temperature of 0°C. Figure 5 shows a contour map, plotted using the steady-state temperatures of the mid-nodes of the cells.

The general solution to this problem has been derived analytically in various textbooks;[8,11] a method of separation of variables is used to solve the 2D steady-state heat conduction equation. The general solution is given below, with reference to Figure 3, which shows the boundary conditions and other parameters

$$T(x,y) = T_m \frac{\sinh(\pi y/L)}{\sinh(\pi b/L)} \sin(\pi x/L) \tag{8}$$

The above expression can be used to determine the final temperature of any point in the plate. A comparison between the temperatures of the mid-nodes of the cells obtained from ASTEC3 and equation (8) is given in Table III (with reference to Figure 4).

To reduce the resolution errors, it is possible to replace a single cell by multiple units. Illustrated in Figure 6 is the breakdown of a single unit from Figure 4 into four cells. The improved accuracy

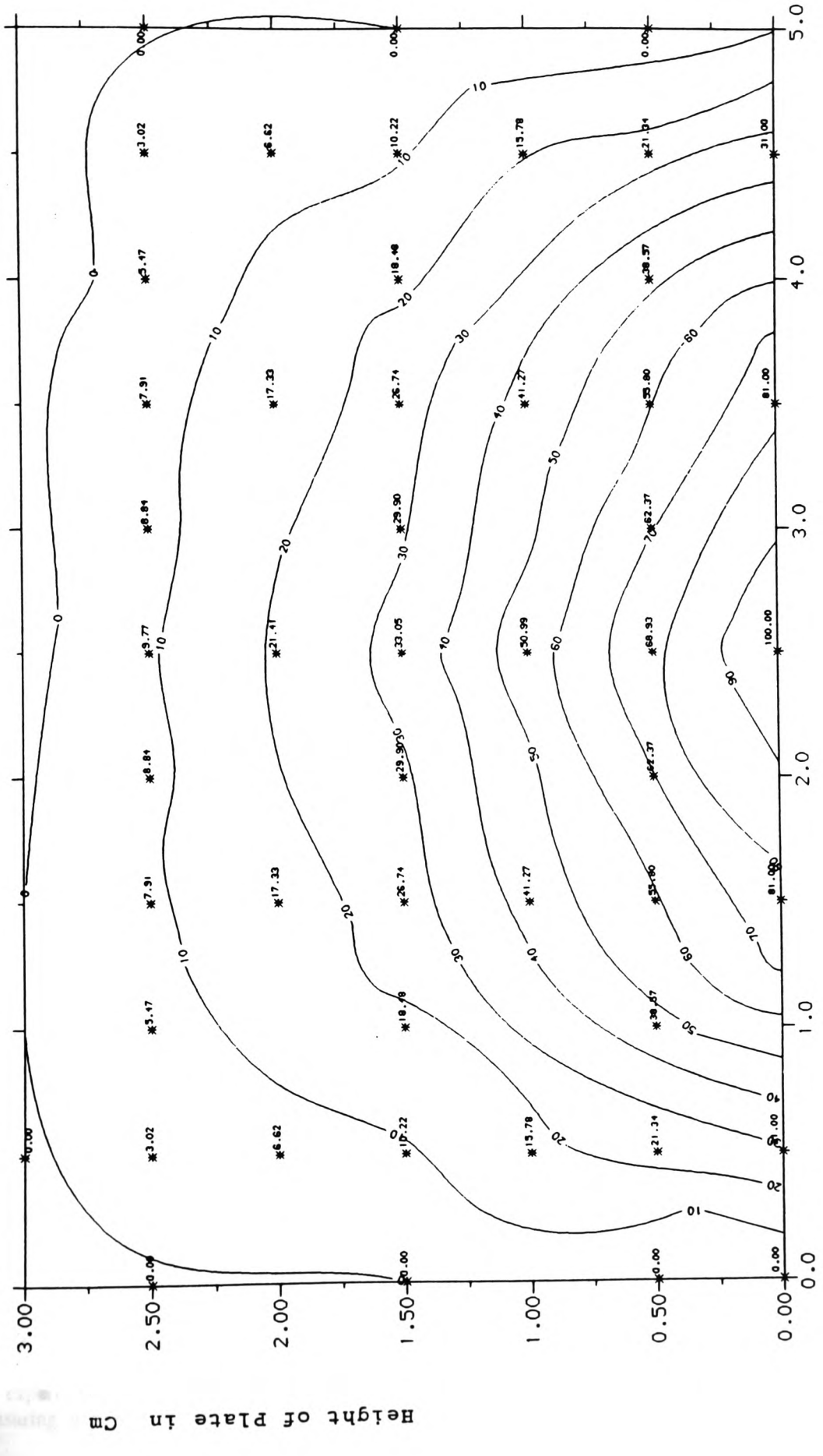

Figure 5. Contour map of the final temperature distribution for the 2D problem, using a coarse-mesh model

Table III. Solution to the 2D problem, using a coarse-mesh model

Mid-node cell	Final temperature (°C)		Temperature difference (°C)
	ASTEC3	Analytical	
M1	21·34	22·1	0·76
M2	55·8	57·84	2·04
M3	68·93	71·53	2·60
M4	55·8	57·84	2·04
M5	21·34	22·1	0·76
M6	10·22	10·45	0·23
M7	26·74	27·37	0·63
M8	33·05	33·82	0·77
M9	26·74	27·37	0·63
M10	33·05	10·45	0·23
M11	3·021	3·067	0·05
M12	7·91	8·03	0·12
M13	9·77	9·93	0·16
M14	7·91	8·03	0·12
M15	3·021	3·067	0·05

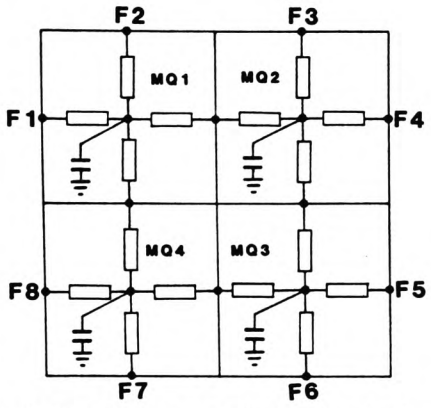

Figure 6. The electrical equivalent model of a fine cell

is demonstrated by the results given in Table IV. Figures 5 and 7 illustrate contour plots for the coarse- and fine-mesh simulations, respectively. The fine-mesh results show a marked reduction in the errors, which are in the range 0·8 °C at the top of the plate to 0·01 °C at the bottom.

3.3. *Three dimensions*

An attempt has been made to check the correct operation of the 3D modelling. The main verification of 3D simulations has been made against experimental arrangements.

A block of material 50 × 30 × 20 mm was assumed to have five of its faces insulated, and a sinusoidal temperature profile imposed upon one of its 30 × 20 mm faces. The same thermal parameters as in the 2D problem were used. The block was divided into cubes of equal dimensions of 10 mm, and an electrical network constructed in the same way as before. The temperature distribution plot of the final steady-state results obtained from ASTEC3 simulation for the upper face is shown in Figure 8.

4. COMPARISON BETWEEN EXPERIMENTAL AND SIMULATED STUDIES

An experiment was set up using a Heimann KT14 infrared radiation pyrometer, capable of measuring up to 400 °C with an accuracy better than 1·5 °C, to measure the temperature at various

Table IV. Solution to the 2D problem, using a fine-mesh model

Mid-node cell	Final temperature (°C)		Temperature difference (°C)
	ASTEC3	Analytical	
M 1.MQ1	13·25	13·0	0·25
M 1.MQ2	38·46	38·0	0·46
M 2.MQ1	59·91	59·2	0·71
M 2.MQ2	75·49	74·7	0·79
M 3.MQ1	83·68	82·8	0·88
M 1.MQ4	9·40	9·30	0·10
M 1.MQ3	27·29	27·0	0·29
M 2.MQ4	42·51	42·1	0·40
M 2.MQ3	53·56	53·1	0·46
M 3.MQ4	59·38	58·8	0·58
M 6.MQ1	6·49	6·44	0·05
M 6.MQ2	18·83	18·7	0·13
M 7.MQ1	29·30	29·1	0·20
M 7.MQ2	36·97	36·7	0·27
M 8.MQ1	40·97	40·7	0·27
M 6.MQ4	4·22	4·20	0·02
M 6.MQ3	12·28	12·2	0·08
M 7.MQ4	19·09	19·0	0·09
M 7.MQ3	24·04	23·9	0·14
M 8.MQ4	26·65	26·5	0·15
M11.MQ1	2·38	2·37	0·01
M11.MQ2	6·89	6·86	0·03
M12.MQ1	10·74	10·7	0·04
M12.MQ2	13·54	13·5	0·04
M13.MQ1	15·0	14·9	0·10
M11.MQ4	0·76	0·76	0·00
M11.MQ3	2·22	2·22	0·00
M12.MQ4	3·46	3·45	0·01
M12.MQ3	4·37	4·35	0·02
M13.MQ4	4·84	4·82	0·02

points on the surface of a thin strip of copper cladding. This was the type used for printed circuit boards, and consisted of a very thin layer of copper 15 μm thick on a fibre-glass base 1·6 mm thick. Electric currents were passed through the strip, causing a rise in its temperature due to the conversion of electrical to thermal energy.

The apparatus was placed inside a chamber which was subsequently sealed very carefully in order to avoid any air currents, and also to establish a quiescent, fairly constant temperature environment. Thus only natural convection could occur, and this is rather simpler to account for in the calculations than is forced convection or a mixture of both.

A schematic diagram of the apparatus is presented in Figure 9. A rectangular strip (140 mm × 26 mm × 15 μm) made of copper cladding is mounted horizontally. Glass wool is used to insulate the underside of the strip, restricting the heat losses by convection to the upper surface. The infrared pyrometer is positioned with its axis perpendicular to the plane of the surface. The distance L between the edge of the lens barrel and the surface is set to exactly 80 mm, as specified by the manufacturers. For a current of 30 A a steady-state temperature of 125 °C was measured at all points along the strip.

The thermal characteristics of the above experiment were simulated by applying the procedure described in Section 3 for 3D conduction. The strip was divided into 15 equal segments, each a cuboid of dimensions (28 mm × 8·67 mm × 15 μm). The thermal resistances in the x, y and z directions and the thermal capacitance of each cell was calculated from equations (5) and (7).

The rate of heat generation in the strip was calculated under the assumption that all the electric power supplied to the strip was converted into thermal energy, and therefore that in steady-state conditions the total heat generation was simply given by I^2R, where I is the current in amperes and R the electric resistance of the copper plate in ohms.

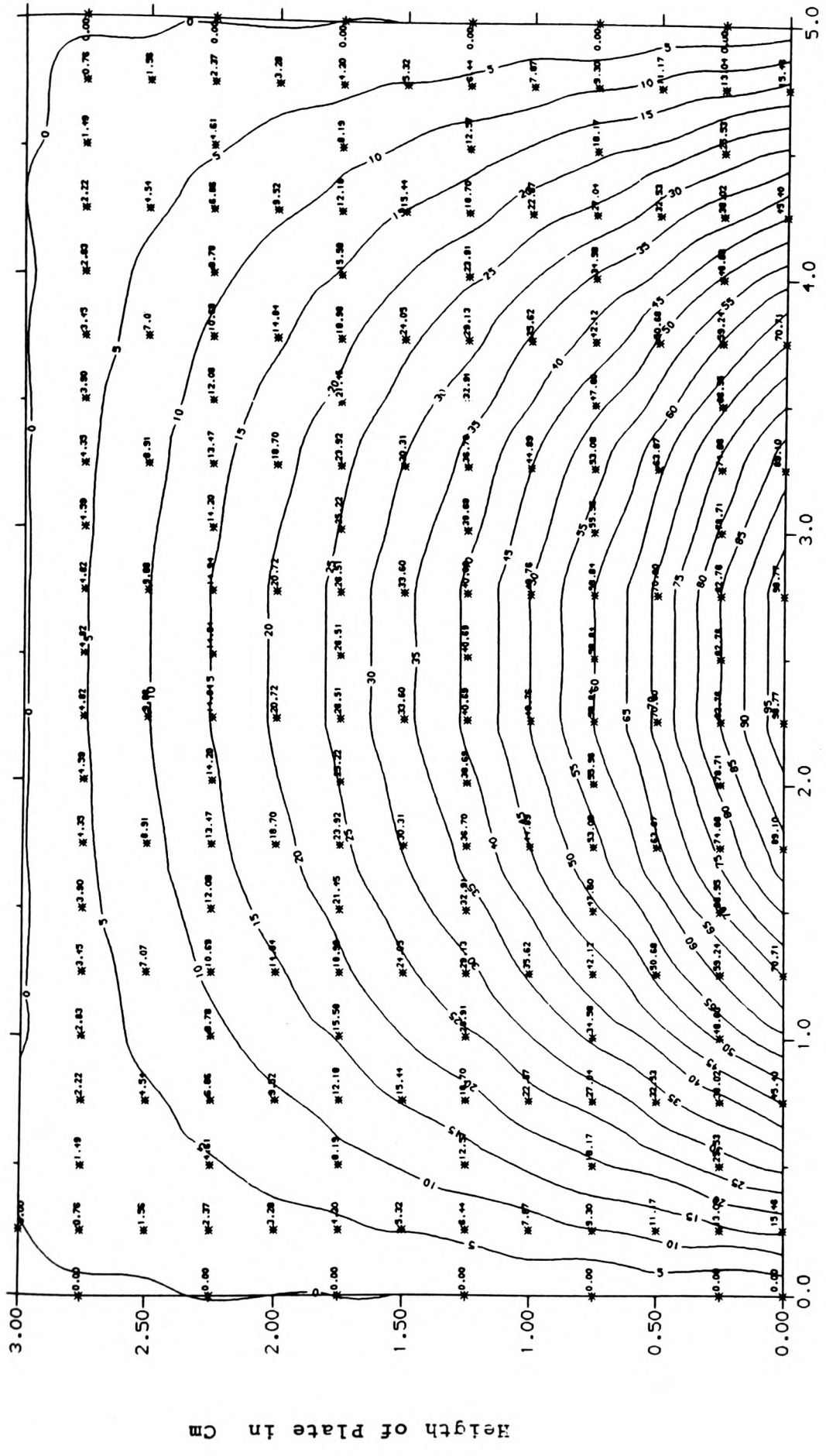

Figure 7. Isothermal lines for the final temperatures in the rectangular plate of the 2D problem

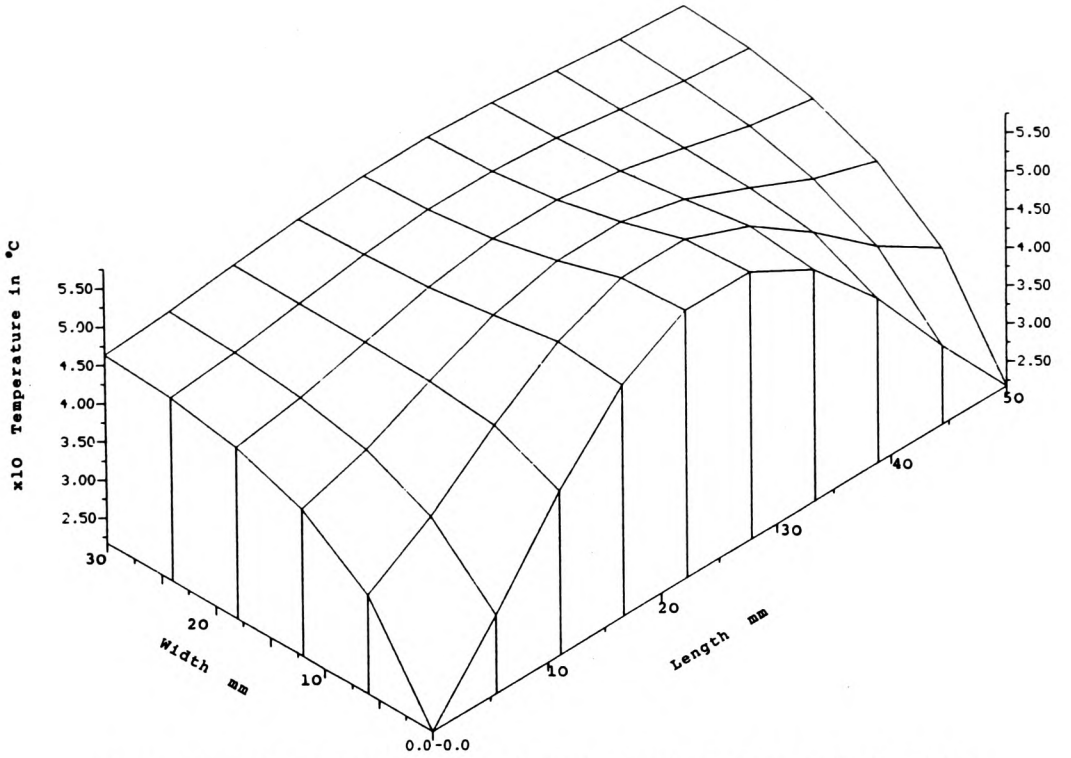

Figure 8. The final steady-state temperature distribution for the upper face in the 3D problem

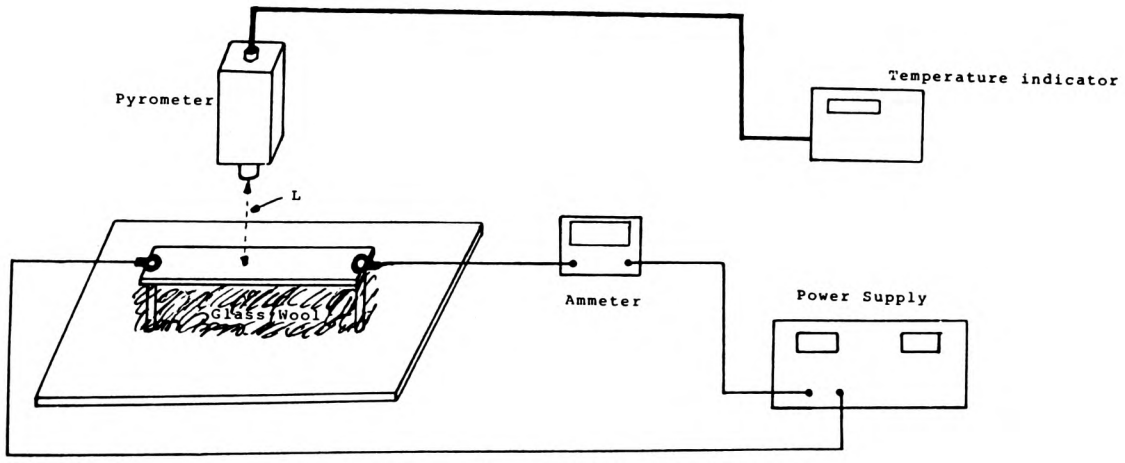

Figure 9. Schematic diagram of the heat transfer experiment

To estimate the convective heat transfer coefficient and thus the value of thermal resistance $R_{convection}$ for the ASTEC3 model, use was made of correlations derived by other workers[9] for natural convection from uniformly heated horizontal surfaces. These gave an average value of 14·95 W/m^{2}K for the heat transfer coefficient which, when incorporated in the ASTEC3 model, yielded a uniform temperature of 125·8 °C, showing an excellent agreement with the measured values.

5. CONCLUSIONS

This paper has described a method of simulating and predicting the temperature distribution in one-, two- and three-dimensional heat transfer systems involving conduction and convection, using the electronic simulation package ASTEC3.

The numerical results presented for a 1D problem for both conduction and convection were exactly the same as a finite difference solution. The results for the 2D problem using a coarse mesh showed very good agreement with the analytical solution. The small errors observed were due to the resolution errors in ASTEC3 modelling, which were reduced when a finer mesh was employed. The modelling procedure was tested against a very simple experimental arrangement, which showed an error of 0·8 °C.

It is the intention of the authors to use ASTEC3 modelling of the thermal structures described in this paper for the simulation and experimental verification of some real circuits. Comparison will of course be made between the ASTEC3 results and measurements carried out by conventional techniques. Other numerical methods might also be employed, if possible, to find solutions to the same problem.

REFERENCES

1. P. Gregory, 'Thermal characteristics of a hybrid microcircuit', in Proc. 11th Seminex Conf. on Advances in Electron Components and Systems, 1982, pp. 347–357.
2. E. Wehrhahn, 'Temperature distribution on substrate of hybrid integrated circuits', in Proc. 5th European Microelectronics Conf., 1985, pp. 288–295.
3. *ASTEC3 User Manual*, SIA Computer Services, London, 1984.
4. P. A. Witting, 'Electronic circuit and system simulation with ASTEC3', *Computer-Aided Eng. J.*, **2**(6), 186–191 (1985).
5. C. Kittel, *Introduction to Solid State Physics*, Wiley, New York, 1976.
6. J. R. Backhurst, J. H. Harker and J. E. Porter, *Problems in Heat and Mass Transfer*, Edward Arnold, London, 1974.
7. A. J. Chapman, *Heat Transfer*, 4th Edn, McGraw-Hill, New York, 1984.
8. J. P. Holman, *Heat Transfer*, 6th Edn, McGraw-Hill, New York 1986.
9. F. J. Bayley, *Heat Transfer*, Nelson, London, 1972.
10. M. N. Ozisik, *Basic Heat Transfer*, McGraw-Hill, New York, 1977.
11. F. Kreith, *Principles of Heat Transfer*, Harper and Row, New York, 1973.
12. R. J. Smith, *Circuits, Devices and Systems*, Wiley, New York, 1976.

Fundamentals of Heat Transfer

N.J. Poole, F. Sarvar

There are three basic processes of heat transfer namely conduction, convection and radiation. In most problems of practical importance two or sometimes all of these modes may occur simultaneously.

Conduction is a heat flow mechanism whereby thermal energy is transferred through a material from a region of high temperature to a region of lower temperature. In electrically conducting solids, heat is carried through the lattice structure simultaneously by means of free electrons and vibrational energy (phonons) [1,2]. In non-metallic or dielectric materials heat is conveyed only by means of phonons [1]. In one dimension the rate of heat transfer through a given area A is given by the Fourier rate equation:

$$q_x = -KA \frac{\partial T}{\partial x} \qquad \text{- - - - - (1)}$$

where K is the thermal conductivity of the material, T is the temperature and x is the displacement through the material of area A equal to $\Delta y \, \Delta z$.

Equation (1) assumes that temperature varies only along the x direction and does not change with time. The general equation of conduction in three dimensions for a uniform body with constant thermal conductivity and with heat sources present within the body [3,4] is given by:

$$K \left(\frac{\partial^2 T}{\partial x^2} + \frac{\partial^2 T}{\partial y^2} + \frac{\partial^2 T}{\partial z^2}\right) + q^* = \rho C_p \frac{\partial T}{\partial t} \qquad \text{- - - - - (2)}$$

where q^*, ρ and C_p are the heat generation per unit volume, density and the specific heat capacity of the material respectively.

The terms on the left hand side of equation represent the heat gains by conduction and generation respectively and the right hand side represents the rate of change of temperature with time in the solid.

Convection is another mode of heat transfer where heat is exchanged between a solid body and an adjacent fluid. Heat transfer between the fluid and the solid surface takes place because of a combination of conduction within the fluid and energy transport which is due to the fluid motion.

There are two types of convection namely free convection and forced convection. Free convection takes place as a consequence of density differences caused by temperature gradients between the fluid and the body and within the fluid itself. Forced convection occurs when the fluid motion is induced by an external force. The rate of heat flow at the surface is conventionally described by the equation [3,4]:

$$q = h_c A (T_f - T_s) \qquad \text{- - - - - (3)}$$

The Polytechnic of Wales, Dept. of Electrical & Electronic Engineering, Pontypridd, CF37 1DL

where A is the solid surface area exposed to the fluid. h_c is the convective heat transfer coefficient and T_f and T_s are the fluid and surface temperatures respectively.

The determination of the temperature distribution in the fluid and hence the true local heat transfer coefficient involves the solution of the complete fluid mechanics problem in the region near the surface.

In general, this would involve the simultaneous solution of equations for conservation of mass, momentum and energy and also the equations of state of fluid [3,5].

Because of the complexity of the equations of motion and energy, it is extremely difficult to solve convective heat transfer problems by the above method except for very simple, idealised situations. For most cases of practical interest convective heat transfer problems have been studies experimentally and the results are then presented in the form of empirical equations that involve some dimensionless groups. In natural convectors the dimensionless numbers are related by:

$$Nu = C\ (Gr.Pr)^n \qquad ----- (4)$$

where C and n are constants. Nu, Gr and Pr are Nusselt, Grashof and Prandtl numbers respectively given by:

$$Nu = h_c l/K \qquad ----- (5)$$

$$Gr = \Delta T \beta g l^3/\nu^2 \qquad ----- (6)$$

$$Pr = \mu C_p/K \qquad ----- (7)$$

where the parameters are as given below:

β The coefficient of cubical expansion
g Acceleration due to gravity
l Characteristic length for bodies with geometrically similar shapes
ν The coefficient of kinematic viscosity
μ Coefficient of dynamic viscosity
C_p The specific heat capacity of the fluid
K Fluid thermal conductivity
h_c The heat transfer coefficient

The physical significance of Nusselt number may easily be arrived at by writing equation (5) in the following form:

$$Nu = \frac{h_c A \Delta T}{K A \Delta T/l} \qquad ----- (8)$$

which can be interpreted as the ratio of the heat transfer by convection to heat transfer by conduction across a fluid layer of thickness l.

Equation (7) describing Prandtl number can also be rearranged in the following form by introducing the fluid density ρ:

$$Pr = \frac{\mu C_p}{K} = \frac{\mu/\rho}{K/(\rho C_p)} \qquad ----- (9)$$

The Prandtl number represents the ratio of kinematic viscosity and thermal diffusivity; the first of which affects the velocity distribution and the second which influences the temperature profile in the fluid.

Finally, the Grashof number is a dimensionless group representing the ratio of the buoyancy forces to the viscous forces in natural convection systems.

The third mode of heat transfer is thermal radiation. This is a process in which bodies emit thermal energy by means of electromagnetic radiation. This type of radiation is emitted in all possible directions and if it strikes another body, it may be partly absorbed, partly reflected and partly transmitted. The absorbed part of thermal radiation will appear as heat within the absorbing body.

In contrast to conduction and convection where the transfer of energy from one body to another can occur only through a material medium, electromagnetic radiation may pass from one body to another without the need of a transport medium.

There is a maximum rate at which thermal radiant energy can be emitted and consequently absorbed by a body at a certain temperature. The surfaces which interchange radiant energy at such rates are called black bodies and it can be shown [6] that the radiation emitted by such surfaces at temperature T is given by the Stefan-Boltzmann law:

$$E_b = \sigma A T^4 \qquad -----(10)$$

where σ is the Stefan-Boltzmann constant, T is the absolute temperature in Kelvins, E_b is the black-body emissive power and A is the area of the radiating surface.

In practice there are no surfaces that behave as a black-body and the radiation flux emitted by a "grey body" is always less than a black-body and is given by:

$$q = \varepsilon E_b \qquad -----(11)$$

where ε is called the emissivity which relates the radiation of the grey surfaces to that of a black surface.

For a body at temperature T_1, totally enclosed in another much larger surface maintained at T_2, the net radiant energy exchanged is given by:

$$q = \varepsilon\sigma A(T_1^4 - T_2^4) \qquad -----(12)$$

where A is the surface area of the enclosed body.

Similar to convection, a radiation heat-transfer coefficient h_r may be defined as:

$$q_{rad} = h_r A(T_1 - T_2) \qquad -----(13)$$

where T_1 and T_2 are the temperatures of the two bodies exchanging heat by radiation. h_r may be determined for different surfaces with varying shapes and geometries [3]. By comparing equations (10) and (11) the following expression is obtained for the heat transfer coefficient as:

$$h_r = \varepsilon\sigma(T_1^2 + T_2^2)(T_1 + T_2) \qquad -----(14)$$

References

1. KITTEL, C.,: 'Introduction to Solid State Physics', New York, Wiley and Sons, 5th edition, 1976.

2. BACKHURST, J.R., HARKER, J.H. and PORTER, J.E.,: 'Problems in Heat and Mass Transfer', London, Arnold, 1974.

3. CHAPMAN, A.J.: 'Heat Transfer', New York, McGraw-Hill, 1984.

4. KREITH, F.,: 'Principles of Heat Transfer', New York, Harper and Row, 1973.

5. OZISIK, M.N.,: 'Basic Heat Transfer', New York, McGraw-Hill, 1977.

6. HOLMAN, J.P.: 'Heat Transfer', New York, McGraw-Hill, 1981.

ELECTRO-THERMAL SIMULATION of HYBRID and VLSI CIRCUITS

P A WITTING, F SARVAR

INTRODUCTION

For many years designers of integrated[1] and hybrid circuits[2][3] have faced the problem of predicting the temperature rise within their devices under operational conditions. This has become a more important issue as the packing density of the devices has increased[4][5]. The tendency to carry out all design work in the simulation domain and to then move, without iteration, to the production of finished devices has increased the need for a simulation tool capable of predicting the local temperature within an operational device. It is also important that such a tool should not be over conservative in its predictions, since this could be wasteful.

Current practice in industry appears to be to either guess at the average heat dissipation in each section of a circuit or to carry out a electrical(only) simulation to determine the average dissipation. These *average values* of heat dissipation are then input to a quite separate thermal model to predict the temperature rise. Since such methods take no account of the phasing of the heat dissipation it is possible for the predictions to over- or under-estimate the true situation.This is clearly shown by an example system with two heat generating islands. The heat sources are pulsed and in phase (a), pulsed and out of phase (b) and constant (c); all with the same average heat input. The maximum temperatures reached are, however, very different being 179°C, 177°C and 83°C respectively. This situation will become worse as the devices get smaller and the averaging effect of their thermal mass is less powerful.

The Polytechnic of Wales is currently engaged in a research project to develop a simulation tool which combines the electrical and thermal simulation functions. The work is based around the Astec3 circuit simulator and relies heavily on the simple but powerful modelling capabilities of this package. The overall objectives of this project are as follows:-

1. To develop a method of creating one-, two- and three-dimensional thermal models using Astec3
2. To validate these models against simple macro-scale structures which are amenable to both theoretical and empirical checking
3. To develop a two-layered model capable of combining both the electrical and thermal aspects
4. To produce isothermal contours for the device being simulated

The Polytechnic of Wales, Pontypridd, Mid Glamorgan, CF37 1DL, UK

5. To estimate the computing resource required to achieve a realistic simulation

6. To develop a means of semi-automatically generating the description of the structure to be simulated

7. To carry out simulations of hybrid structures to establish the validity of the modelling procedure at this scale

8. To likewise carry out investigations on integrated circuits

9. To develop interactive input and colour-graphic output facilities

The final objective represents a major challenge in its own right and work in this area has been deferred to a future project. This paper presents the results achieved to date on the first five objectives.

VALIDATION of ASTEC3 in THERMAL MODELLING

The methods used to carry out the simulations will be discussed in the presentation. The methods have been tested against theoretical predictions for some simple arrangements and good agreement obtained, comparable to that achieved by finite difference techniques. These results have been further tested against macro-scale physical systems. For simple arrangements good agreement has been obtained, but some anomalies have been observed in more complex situations. Recent work has elaborated the models to remove these anomalies with the result that work will soon commence on hybrid-scale systems.

COMPUTATIONAL ASPECTS

Measurements of computation time demonstrate that, for a given computer system, the computation time is proportional to the number of cells being computed - up to a certain limit imposed by the memory availability in the particular computer. Measurements on three different computers from the DEC vax range of machines indicates that the computation rate (cells per second) is proportional to the computer's power rating in Mflops, being approximately 29.2 cell/sec/Mflop.

A further restriction, in the case of the vax computers, is an limit on the number of equations that may be included in any one model. This is 32,767 corresponding to approximately 3150 2-D cells. It will be seen therefore that there is a strong motivation to reduce the number of cells used. This has lead to the development of mixed-mesh models where fine mesh cell are used in areas of high temperature gradient with a coarser cell structure being used elsewhere. A range of interface cells have been

developed to permit this mixing.

The specification of the mesh structure for complex systems is clearly time consuming and error prone. A semi-automatic method of producing the required description files has been devised and is in routine use.

CONCLUSION

It has been demonstrated that the simulation of the electrical and thermal aspects of circuit behaviour can be combined via the ASTEC3 software system. The finer the cell mesh the more accurate the results obtained, at the expense of extending the computation. The use of mixed coarse/fine cells reduces this problem and a semi-automatic method of generating the mesh file has been developed.

The results obtained from the simulations have been shown to correspond to theoretical predictions and, with some reservations, to the experimental situation. However, further work needs to be done on the effects of convection before the method is fully developed.

The advantages of the combined simulation is seen to be a more realistic estimation of the thermal effects as a result of being able to take account of the phasing of the heat generation processes.

[1]**HEIN V L, LENZI V D:**'Thermal Analysis of Substrates and Integrated Circuits', Proceedings of Electronic Component Conference, May 1969, pp 166-177

[2]**DAVID, R F:**'Computerised Thermal Analysis of Hybrid Circuits', Trans IEEE on Parts, Hybrids and Packaging,**vol PHP-3, no 3** , Sept 1977, pp 283-289

[3]**SBERGOVIC S, BOSNJAK K M:**'Computer application in Thermal Analysis of Passive Components in Hybrid Microelectronic Circuits, International Colloquium on New Orientations of Passive Components, 1982, p 415

[4]**GREGORY P:**'Thermal Characteristics of a Hybrid Microcircuit', Proceedings of 11th Seminex Conference on Advances in Electronic Components and Systems, 1982, pp 347-357

[5]**WEHRHAHN E:** 'Temperature Distribution on Substrate of Hybrid Electronic Circuits', Proceedings of the 5th European Microelectronics Conference, 1985, pp 288-295

LECTURE NOTES AND DIGEST OF THE NASECODE VI ASSOCIATED SHORT COURSE AND SOFTWARE FORUM — Edited by W. Crans—Dublin (Ireland) 10th-12th July 1989 — Boole Press Ltd.

Simultaneous modelling of thermal and electrical characteristics using ASTEC 3 software

F. SARVAR, N.J. POOLE, AND P.A. WITTING

Department of Electrical and Electronic Engineering, Polytechnic of Wales, Pontypridd, Mid Glamorgan CF37 1DL, Wales, U.K.

ABSTRACT

It is difficult for designers to predict average temperature rise due to thermal dissipation in semiconductor integrated circuits and also hybrid microcircuits. Similarly the prediction and subsequent prevention of localised hot spots is quite crucial since their effect could very well cause the failure of the whole device. These hot spots may also affect the tolerance of circuit components which can cause drastic changes in the device characteristics. This has become more of an important issue as industrial manufacturers have tried to reduce the physical size of devices and therefore increase their packing density.

Heat generation in electronic circuits is dependent on the electrical activity of the various components in the circuit. Whilst the simulation of the electronic aspects of the circuit operation is well catered for by a number of computer packages there are no general purpose packages which also facilitate the prediction of the local temperature rise.

The purpose of this research is to be able to predict thermal and electrical characteristics of the given devices using the simulation package.

These new results show that it is possible for ASTEC3 to be used as a thermal simulation package. Using these techniques it will soon be possible to predict device reliability due to thermal dissipation.

ASTEC3 is particularly well suited to this task as it incorporates two features of special significance in addition to its highly efficient electronic simulation capabilities. These are its powerful sub-modelling facility and its ability to handle large sets of first order differential equations. Within these equations there is no upper limit to the number of components that may be used for simulations.

INTRODUCTION

For many years designers have faced the problem of thermal dissipation in semiconductor devices, including hybrid circuits, and the prediction of any heat sources within these circuits. This has become a more important issue as industrial manufacturers try to reduce the physical size of these devices and increase their packing density [1,2].

Heat generation is dependent on the electrical activity of the various components in the circuits. The simulation of the electronic aspects of the circuit operation is well catered for by a number of computer packages, but there are no general purpose packages which also include the prediction of any local temperature rise. Current practice in industry appears to be either to apply a crude rule-of-thumb to estimate the heat dissipation or to use a separate modelling package to calculate the average heat dissipation and to guess the size of all electronic heat sources.

ASTEC3 is a powerful circuit analysis package, written in Fortran 77, capable of performing transient, a.c. small-signal and d.c. steady-state simulations [3]. ASTEC3 is also suitable for providing solutions to differential equations, and any system defined by this format can be solved. As the electrical and thermal characteristics of any given network can be written in terms of differential equations, this allows for the possibility of simulating both phenomena with ASTEC3.

The circuit description is written in ASTEC3 syntax which is based on a conventional circuit diagram with the position of each element defined by the nodes at its connections. ASTEC3 is a software language that is possible to run on IBM, VAX and CRAY mainframe machines. ASTEC3 is currently run on either a VAX 11/785 or a VAX 8650, these machines requiring 2,000,000 bytes of memory for ASTEC3 and 1,000,000 bytes has proved sufficient memory to run our application circuits.

THERMAL SYSTEM MODELLING

The basic equations of heat transport have been well documented [4]. It is possible to make thermal analysis of a given system in terms of electrical parameters by a suitable change of variables. The simple Ohm's law equation can be compared with conductive and convective heat transfer, respectively. This gives equivalent electrical resistances of

$$R_{conduction} = \frac{\Delta x}{K\Delta y\Delta z} = R_{th} \qquad (1)$$

$$R_{convection} = \frac{1}{hA} \qquad (2)$$

for conductive and convective processes, respectively.

The current in a charging capacitor is analogous to the rate of change of energy stored in a volume element ΔV giving a thermal capacitance:

$$C_{th} = \rho C_p \Delta V = \rho C_p \Delta x \Delta y \Delta z \qquad (3)$$

Since the flow of heat through a thermal resistance is analogous to the flow of current through an electrical resistance, any form of heat flow into or out of a system can be modelled as sources of current. Similarly, there is an analogy between temperature in a thermal system and electrical voltage, and fixed temperatures at a boundary can therefore be modelled as a voltage source of the same value. By these comparisons, simple electrical equivalent models for thermal characteristics can be constructed using the analogous thermal resistance and capacitance quantities.

The ASTEC3 input language is based on a conventional circuit diagram, with the positions of each element defined by the nodes at its connections. Figure 1 illustrates the electrical configuration for a cell in 3D conduction.

If the value of convective heat transfer coefficient h is known, convection at the boundaries can be modelled using resistors of values $1/hA$, where A is the convection surface area. In one dimension this reduces to $1/h$ as Δy and Δz are taken as unity, and in two dimensions to $1/h\Delta y$.

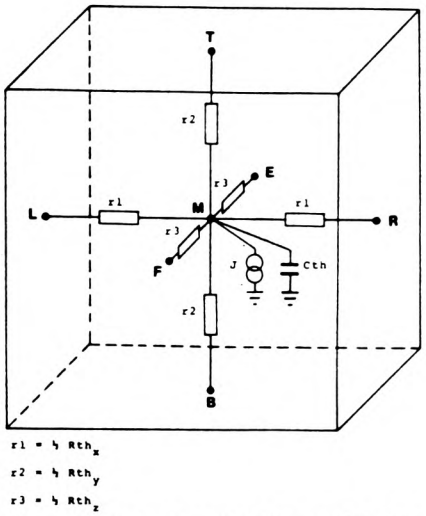

Figure 1. The electrical equivalent model for a cell in 3D conduction

COMPARISON BETWEEN EXPERIMENTAL AND SIMULATED STUDIES

Verification of the results obtained using ASTEC3 were compared to standard techniques for one and two dimensional problems and have been previously documented [5]. Three dimensional simulation studies have been used to model experiments.

An experiment was set up using a Heimann KT14 infrared radiation pyrometer, capable of measuring up to 300°C with an accuracy better than 1.5 °C, to measure the temperature at various points on the surface of a thin strip of copper cladding. This was the type used for printed circuit boards, and consisted of a very thin

layer of copper 15 μm thick on a fibre-glass base 1.6 mm thick. Electric currents were passed through the strip, causing a rise in its temperature due to the conversion of electrical to thermal energy.

The apparatus was placed inside a chamber which was subsequently sealed very carefully in order to avoid any air currents, and also to establish a quiescent, fairly constant temperature environment. Thus only natural convection could occur, and this is rather simpler to account for in the calculations than is forced convection or a mixture of both.

A schematic diagram of the apparatus is presented in Figure 2. A rectangular strip (140 mm x 26 mm x 15 μm) made of copper cladding is mounted horizontally. Glass wool is used to insulate the underside of the strip, restricting the heat losses by convection to the upper surface. The infrared pyrometer is positioned with its axis perpendicular to the plane of the surface. The distance L between the edge of the lens barrel and the surface is set to exactly 80 mm, as specified by the manufacturers. For a current of 30 A a steady-state temperature of 125°C was measured at all points along the strip.

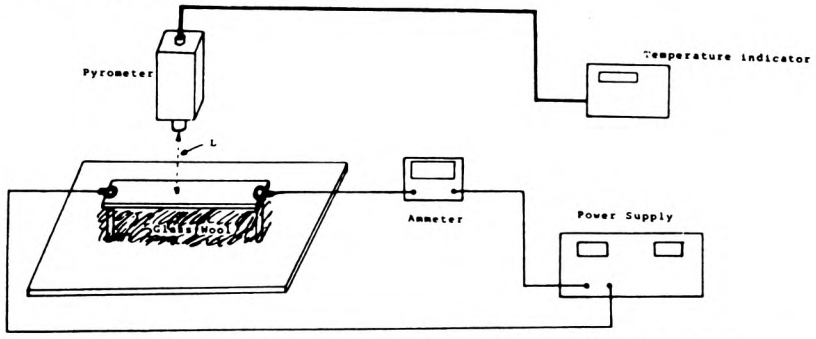

Figure 2. Schematic diagram of the heat transfer experiment

The thermal characteristics of the above experiment were simulated by applying the procedure described previously. The strip was divided into 15 equal segments, each a cuboid of dimensions (28 mm x 8.67 mm x 15 μm). The thermal resistances in the x, y and z directions and the thermal capacitance of each cell was calculated from the given equations. The rate of heat generation in the strip was calculated under the assumption that all the electric power supplied to the strip was converted into thermal energy, and therefore that in steady-state conditions the total heat generation was simply given by I^2R, where I is the current in amperes and R the electric resistance of the copper plate in ohms.

To estimate the convective heat transfer coefficient and thus the value of thermal resistance $R_{convection}$ for the ASTEC3 model, use was made of correlations derived by other workers for natural convection from uniformly heated horizontal surfaces. These gave an average value of 14.95 W/m^2K for the heat transfer coefficient which, when incorporated in the ASTEC3 model, yielded a uniform temperature of 125.8°C,

showing an excellent agreement with the measured values.

A more complicated system of experimentation was devised where use was made of the same rig described in the previous section. The systems designed take into account the type of thermal problems which may be encountered when simulating the thermal characteristics of semiconductor devices. Rectangular plates (140 mm x 120 mm) of PCB were used where islands were cut into the conducting layer of the boards but not into the insulation. This was achieved by etching very thin grooves all around the islands to isolate them from the rest of the copper layer. These islands were heated by passing an electric current through them and the infra-red pyrometer was used to measure the steady-state temperatures at selected points on the surface. These thermal structures were also simulated using ASTEC3 by dividing the plates into a (6 x 7) mesh.

Two types of configurations were tested. Figure 3 represents the modal pattern of the rectangular plate.

(a) One heated island (20 mm x 100 mm) in different positions on the plate using a heating current of 30 Amps. Position 1 used nodes 37-41 inclusive and Position 2 used nodes 30-34 inclusive as illustrated in Figure 3. Table 1 gives the measured and simulated results for comparison.

(b) Two heated islands (100 mm x 20 mm) and (20 mm x 40 mm) are cut using nodes 30-34 inclusive for island 1 and 13-20 for island 2 as represented in Figure 3. These islands were heated by passing currents of 30 and 10 Amps through the larger and smaller islands respectively. The results of these measurements are given in table 2 along with the simulation results. These show good agreement with a maximum difference of 8°C.

36	37	38	39	40	41	42
29	30	31	32	33	34	35
22	23	24	25	26	27	28
15	16	17	18	19	20	21
8	9	10	11	12	13	14
1	2	3	4	5	6	7

Figure 3. Modal Pattern of Rectangular Plate

Using Vax machines running under VMS operating system, the CPU computation times for a typical hybrid circuit (400mm^2 with a minimum feature size 0.01mm^2) are 1957 secs and 6849 secs for Vax 8650 and Vax 11/785 respectively. ASTEC3 is available in a compiled version under academic licence.

Table 1. Measured and Simulated Results for one heated island

Position One				Position Two		
Surface Node No.	Measured Temp. °C	Simulated Temp. °C	Temp. Difference	Measured Temp. °C	Simulated Temp. °C	Temp. Difference
4	28	24.8	3.2	31	25.4	5.7
8	27.8	25.1	2.7	31	25.7	5.3
20	30	25.9	4.1	33.2	27.1	6.1
24	27.7	33.2	5.5	40.7	29.8	10.9
26	27.7	35.2	7.5	-	-	-
32	44.9	30.8	14.1	67.4	76.7	9.3
33	42.8	30.7	12.1	71.6	77.3	5.7
39	85.6	81.3	4.3	48.1	35	13.1

Table 2. Measured and Simulated Results for 2 heated islands

Surface Node No.	Measured Temp. °C	Simulated Temp °C	Temp. difference °C
4	29.9	27.9	2
8	32.1	28	4.1
20	31	34	3
24	41	32.4	8.6
26	40.7	33.1	7.6
33	71.7	80.5	8.8
32	75	81.1	6.1
39	41.7	35.7	6.0

CONCLUSIONS

This paper has described a method of simulating and predicting the temperature distribution in one, two and three dimensional heat flow system using electronic simulation package ASTEC3. The modelling system is verified by comparison with finite difference techniques and analytical solutions of well known heat transfer problems. Various experiments have also been carried out which show very good agreement with the simulated results. It has been shown that both electrical and thermal simulation can be performed on any electrical circuit simultaneously. Tests will be carried out on real hybrid circuit and semiconductor devices in the near future.

REFERENCES

1. P. Gregory, Thermal characteristics of a hybrid microcircuit . Proc. 11th Seminex Conf. on Advances in Electron Components and Systems, 1982, pp. 347-357.
2. E. Wehrhahn. 'Temperature distribution on substrate of hybrid integrated circuits', in Proc. 5th European Microelectronics Conf., 1985, pp. 288-295.
3. ASTEC3 User Manual, SIA Computer Services, London, 1984.
4. A.J. Chapman, Heat Transfer, 4th Edn, McGraw-Hill, New York, 1984.
5. N.J. Poole, F. Sarvar, P.A. Witting, & W.H. McKenzie, Int.J.of.Num.Mod., Vol. 1, 103-113 (1988).

ELECTRO-THERMAL SIMULATION of HYBRID and VLSI CIRCUITS

P A WITTING, F SARVAR, N J POOLE

The Polytechnic of Wales, Pontypridd, Mid-Glamorgan, UK

ABSTRACT

This paper introduces a method of carrying out combined electrical and thermal simulations. This is of particular value for vlsi and hybrid circuits since it allows a more realistic estimate of thermal stresses to be obtained. Practical problems such as the automatic generation of meshes, the estimation of convective heat loss coefficients and computation time are considered.

INTRODUCTION

For many years designers of integrated[1] and hybrid circuits[2][3] have faced the problem of predicting the temperature rise within their devices under operational conditions. This has become a more important issue as the packing density of the devices has increased[4][5]. The tendency to carry out all design work in the simulation domain and to then move, without iteration, to the production of finished devices has increased the need for a simulation tool capable of predicting the local temperature within an operational device. It is also important that such a tool should not be over conservative in its predictions, since this could be wasteful.

Current practice in industry appears to be to either guess at the average heat dissipation in each section of a circuit or to carry out an electrical(only) simulation to determine the average dissipation. These *average values* of heat dissipation are then input to a quite separate thermal model to predict the temperature rise. Since such methods take no account of the phasing of the heat dissipation it is possible for the predictions to over- or under-estimate the true situation. This is clearly shown in figure 1 which depicts a system with two heat generating islands. The heat sources are pulsed and in phase (a), pulsed and out of phase (b) and constant (c); all with the same average heat input. The maximum temperatures reached are, however, very different being 179°C, 177°C and 83°C respectively. This situation will become worse as the devices get smaller and the averaging effect of their thermal mass is less power '.

The Polytechnic of Wales is currently engaged in a research project to develop a simulation tool which combines the electrical and thermal simulation functions. The work is based around the Astec3 circuit simulator and relies heavily on the simple but powerful modelling capabilities of this package. The overall objectives of this project are as follows:-

1. To develop a method of creating one-, two- and three-dimensional thermal models using Astec3
2. To validate these models against simple macro-scale structures which are amenable to both theoretical and empirical checking
3. To develop a two-layered model capable of combining both the electrical and thermal aspects
4. To produce isothermal contours for the device being simulated
5. To estimate the computing resource required to achieve a realistic simulation
6. To develop a means of semi-automatically generating the description of the structure to be simulated
7. To carry out simulations of hybrid structures to establish the validity of the modelling procedure at this scale
8. To likewise carry out investigations on integrated circuits
9. To develop interactive input and colour-graphic output facilities

To date considerable progress has been made with the first five objectives and attention is now being directed towards items six and seven. The final objective represents a major challenge in its own right and work in this area has been deferred to a future project. This paper presents the results achieved to date on the first five objectives.

SUITABILITY of ASTEC3

Astec-3 is a general purpose analogue electronic circuit simulation package capable of performing nonlinear DC, nonlinear transient and small signal AC analysis. The package was developed by the French atomic energy authority (CEA) ...d has been available in the UK for some six years.

Originally developed for the IBM range of computers, Astec-3 is now available for Cray and VAX machines, including the VAX workstation. The simulator offers a number of advantages over more

established simulators (such as SPICE in the electronics domain). Among Astec-3's principal advantages are its efficiency, the simple way in which models may be created, and the fact that very little in-house expertise is required since the package is fully supported by the vendors.

An important consideration in the current application is that data output from the simulator is not confined to simple circuit values (such as voltages) but may also include component values etc. Furthermore, the results of a simulation may be combined according to any user-defined function allowing such parameters as power dissipation to be displayed. One of the principal features of Astec-3 is the ease with which users can create models. The modelling and library facilities allow users to construct personalised system simulators , as discussed by Charnley[6]. . These models are written in the system description language itself and no specialised knowledge is generally necessary. They are, therefore, analogous to the subroutines of a high-level computer language and can be used to 'hide' the detail of a simulation (of, say, a servo valve) so that it may be treated as a 'black box' with access only available via the defined external connections. Such models may have parameters passed to them as well as having default values. In addition, complex models with many parameters to be passed may be defined as 'types' (ie instances of the model with parameters pre-defined).

As described above, the models must be defined within the simulation to which they relate. However, provision is made to place such models into a personal library. This is a special file, separate from Astec-3, from which model descriptions may be recalled into any simulation. There is also a system library containing models of a wide variety of electronic devices. Users can apply these models but cannot write to the system library.

In the application described in this paper it is necessary that both the thermal and electrical characteristics of a component be modelled. The instantaneous heat generation due to the passage of a current may be calculated as a parameter in Astec3 from the the values of the circuit parameters. The value of this parameter can then be assigned to the heat generator in the thermal model. In this way a "2-layer" combined electro-thermal model is produced. An example of this approach is shown in figure 2 which portrays the two-layer structure for a simple amplifier. In this example the circuit is assumed to be a very simple hybrid common-emitter amplifier. The electrical circuit is modelled in the upper part of figure 2(b) and the heat generated in the transistor chip is given by:

power dissipated =

$$(vn3 - vn4)ir1 + (vn2 + vn3)(ir1 - ir4) = ptr1$$

The thermal model of the transistor chip is given in the lower part of figure 2(b) where the current source represents the heat generator and is made equal to ptr1 and the thermal capacity of the chip is represented by the capacitor. Heat transfer to the surrounding atmosphere and the substrate is accounted for by R_{conv} and R_{cond} respectively. In some situations the values of the electrical parameters can be dependent on the their temperature. In such circumstances the values of the electrical components would not be constants but would be dependent on the values of the relevant node in the thermal part of the model. This approach has been used in research on fuse behaviour within the department.

A fuller description of the Astec-3 system has been given elsewhere[7][8][9]

VALIDATION OF ASTEC3 in THERMAL MODELLING

The approach used in the current project is to create an electrical analogy of the thermal system. There are three basic processes of heat transfer namely conduction, convection and radiation.

The basic equations of heat conduction have been well documented[10]and in one dimension the heat transfer through an area, A (dy,dz), is given by:

$$q_x = -K A \frac{\partial T}{\partial x} \qquad (1)$$

Where K is the thermal conductivity in the x direction, q_x is the energy flow in the x direction(normal to A) and T is the temperature. The equivalent equation for three dimensions is:

$$\rho C_p \frac{\partial T}{\partial t} = q^{\bullet} + K\left(\frac{\partial^2 T}{\partial x^2} + \frac{\partial^2 T}{\partial y^2} + \frac{\partial^2 T}{\partial z^2}\right) \qquad (2)$$

Where C_p, ρ and $q^{\bullet}$ are the specific heat, density and heat generation per unit volume respectively.

By taking voltage, current electrical capacitance and electrical resistance as analogous to temperature, heat flow thermal capacity and thermal resistance respectively one arrives at the electrical model for conduction in an elemental cube as shown in figure 1 where

$$C_{th} = \rho C_p \Delta x \Delta y \Delta z \qquad (3)$$

$$R_{conduction} = \frac{\Delta x}{K \Delta y \Delta z} = R_{th} \qquad (4)$$

The rate of heat transfer from a surface at temperature T_s to a fluid at temperature T_f by convection is given by the equation

$$q = hA(T_f - T_s) \qquad (5)$$

The model for convection is thus as shown in figure 2 with

$$R_{convection} = \frac{1}{hA} \qquad (6)$$

The determination of the value of h in equation 6 from theoretical considerations is, in practice, very difficult except for certain very simple situations. In most practical situations an empirical approach is used[11][12].

The final mode of transfer is radiation which may be described by the well known Stefan-Boltzmann law:

$$q = \varepsilon \sigma A(T1^4 - T2^4) \qquad (7)$$

where T1 is the temperature of the surface, T2 that of the surroundings, σ is the Stefan-Boltzmann constant and ε is the emissivity of the surface.

This may be put into a form similar to the equation for convection which is useful if the temperature variations of the surface are small:

$$q_{radiation} = h_r A(T1 - T2) \quad (8)$$

where

$$h_r = (T1^2 + T2^2)(T1 + T2) \quad (9)$$

In such circumstances the surface loss by both radiation and convection may be combined into a single model such as that in figure 2 with an equivalent h-factor, h_{equiv} given by:

$$h_{equiv} = h_r + h \quad (10)$$

Test Examples. The above principles were verified in the context of ASTEC3 modelling by applying them to a number of situations which could be computed directly from theory or by separate and widely accepted methods. This approach was carried out for one- and two-dimensional arrangements.

In one dimension the temperature distribution in a uniform slab with the following properties:

width 50mm density 8656kg/m³

thermal conductivity 17.3W/mK

specific heat capacity 0.444kJ/kgK

rate of internal heat generation 2.06MW/m³

boundary surface temperatures 20°C and 60°C

A five cell model was used in the simulation as shown in figure 4, with R_{conv} set to zero to indicate perfect contact with the boundary temperatures. The model was started from the initial equilibrium temperatures occurring for the case of zero internal heat generation. Heat generation was initiated at t=0 and a series of temperature distributions obtained for various elapsed times. The final temperature distribution was compared with that obtained via the analytical solution:

$$T = -0.5(q^*/K)x^2 + Bx + C \quad (11)$$

where B = 2176.88
C = 60
K = 17.3
$q^* = 2.06 \times 10^6$

for the given problem. The results obtained via ASTEC3, a finite difference technique and the analytical solution are shown below:

node	initial temperature °C	final temperature °C: ASTEC3	finite difference method	analytical method
1 (0mm)	60.0	60.0	60.0	60.0
3 (10mm)	52.0	75.8	75.8	75.8
5 (20mm)	44.0	79.7	79.7	79.7
7 (30mm)	36.0	71.7	71.7	71.7
9 (40mm)	28.0	51.8	51.8	51.8
11(50mm)	20.0	20.0	20.0	20.0

As can be seen, the simulation agrees with the theoretical results to better than 0.1°C. Further, the errors are similar to those obtained by the finite difference technique[5][13]. If convection is introduced at the ends of the plate then R_{conv} is no longer zero. The resulting steady-state distribution if the convective loss coefficient is 5kW/mK is given below:

node	13	1	3	5	7	9	11	12
ASTEC3	60.0	67.9	84.7	89.5	82.5	63.6	32.7	20.0
finite	60.0	67.9	84.7	89.5	82.5	63.6	32.7	20.0

To verify the simulation performance in two dimensions the temperature distribution in a rectangular plate of side 50mm x 30mm has been simulated as shown in figure 5. Three sides of the plate are held at 0°C while the top side has a sinusoidal distribution applied. A 15 cell model was used with the following parameters:

thermal conductivity 0.05 W/mK
density 150 kg/m³
specific heat capacity 1.88 kJkgK

The sinusoidal temperature distribution is imposed by the voltage sources along the top edge with each being set to the average value applicable to the relevant cell. The theoretical distribution is given[8][12] as

$$T(x,y) = T_a \frac{\sinh(\pi y/L)}{\sinh(\pi b/L)} \sin(\pi x/L) \quad (12)$$

and the symbols are defined on the diagram.

The resulting temperature distribution is shown in figure 6 which was obtained by transferring the ASTEC3 results to the Gino plotting routines. This was arranged to happen automatically by executing ASTEC3 through a batch file containing the necessary additional commands.

The maximum error obtained was 2.6°C near the point of maximum temperature gradient. to reduce this error the linear resolution of the model was doubled, with the result that the maximum error was reduced to 0.9°C. This was, of course, achieved at the cost of increased computing time.

Empirical Tests. While the modelling technique may be shown to give good agreement with theory it is also necessary to demonstrate close agreement with practical arrangements. Deviations from a true representation may occur not only due to theoretical problems, but also due to the models not covering the full spectrum of significant phenomena. In order to assess this possibility it is necessary to carry out measurements on practical structures alongside the simulations. Initially, in order to avoid the problems of measuring surface temperatures of very small areas, a large scale physical model was used for the experiments. The nature of this model was similar to that of a hybrid circuit with heat generating elements being mounted in good thermal contact with an insulating substrate.

The actual arrangement is shown in figure 7 which is a simple resistor mounted on a substrate and heated by means of the current flowing through it. The material used was a piece of copper-clad glass fibre laminate as used for printed circuit boards. The 'resistor' was isolated from the surrounding copper by etching a fine line around it. The model is three dimensional, having two layers - one for the copper and one for the substrate. Thermal connection between the 'resistor' and the

surroundings is via the glass fibre laminate only. the underside of the laminate was well insulated so that negligible heat was lost through this route. Heat generation only occurred in the 'resistor' area due to the passage of current and the whole assembly was enclosed in a large cabinet to reduce extraneous environmental effects.

The temperature at the position of the mid-point of each cell was measured using a calibrated Heimann KT14 infra-red pyrometer (accuracy 1.5°C). The measurements were compared with those obtained from the simulation. The simulation accounted for the thermal conduction in each of the two dissimilar layers (each assumed to be isotropic) and convection from the copper surface, the edges of the board being considered insignificant. The convection coefficients were computed using the empirical techniques detailed in various sources[13]. This approach had previously proved successful in other, simpler, arrangements[14].

Initial agreement between the measured and simulated results was not good. Experiments to vary the conduction and convection coefficients in order to achieve agreement disclosed that the results were far more sensitive to the convection coefficient. However, this coefficient is the most difficult to determine with any precision. It was further determined that increasing the conductivity in the substrate gave better agreement. Further detailed measurements indicated that the reinforced board was strongly anisotropic with the conduction normal to the board approximating that of epoxy resin and that tangential to the surface being close to that of glass.

The model was, therefore amended to include this anisotropy and to include an assessment of the radiative loss from each area of surface. This then only left the convection losses unknown. Manipulation of these coefficients in the model in a systematic and physically justifyable manner is now bringing much closer agreement. Once this is completed it is expected that the distribution of coefficients will provide a means of predicting suitable values on an a-priori basis. To this end measurements on the 'convection plume' associated with the experimental rig are in hand.

The results obtained will, of course, be subject to scaling effects when applied to actual size hybrid and vlsi circuits, it may well be that the convection regime on the micro - scale will be far simpler.

COMPUTATIONAL ASPECTS

It was mentioned above that errors can be reduced by using more cells. For simple cases it has been demonstrated that the errors are comparable in size with those obtained via finite difference analysis. Furthermore, the greatest errors occur at points of high temperature gradient. Measurements of computation time demonstrate that, for a given computer system, the computation time is proportional to the number of cells being computed - up to a certain limit imposed by the memory availability in the particular computer. Measurements on three different computers from the DEC vax range of machines indicates that the computation rate (cells per second) is proportional to the computer's power rating in Mflops, being approximately 29.2 cell/sec/Mflop.(figure 8)

For hybrid circuits the number of cells required may be estimated as follows

minimum feature size to be resolved 0.1mm

substrate size 20mm

number of cells 200x200 = 40,000

computation time(sec)	
57	Cray xmp2
114	Cray 1s
1957	vax8650
6849	vax11/785+fpa

Simulations on vlsi circuits would involve slightly lower substrate dimensions and much smaller feature sizes. Thus the number of cells involved would be significantly greater with a corresponding effect on computation times.

A further restriction, in the case of the vax computers, is a limit on the number of equations that may be included in any one model. This is 32,767 corresponding to approximately 3150 2-D cells. It will be seen therefore that there is a strong motivation to reduce the number of cells used. This has lead to the development of mixed-mesh models where fine mesh cell are used in areas of high temperature gradient with a coarser cell structure being used elsewhere. A range of interface cells have been developed to permit this mixing.

The specification of the mesh structure for complex systems is clearly time consuming and error prone. A semi-automatic method of producing the required description files has been devised and is in routine use.

CONCLUSION

It has been demonstrated that the simulation of the electrical and thermal aspects of circuit behaviour can be combined via the ASTEC3 software system. The finer the cell mesh the more accurate the results obtained, at the expense of extending the computation. The use of mixed coarse/fine cells reduces this problem and a semi-automatic method of generating the mesh file has been developed.

The results obtained from the simulations have been shown to correspond to theoretical predictions and, with some reservations, to the experimental situation. However, further work needs to be done on the effects of convection before the method is fully developed.

The advantage of the combined simulation is seen to be a more realistic estimation of the thermal effects as a result of being able to take account of the phasing of the heat generation processes.

[1]**HEIN V L, LENZI V D:**'Thermal Analysis of Substrates and Integrated Circuits', Proceedings of Electronic Component Conference, May 1969, pp 166-177

[2]**DAVID, R F:**'Computerised Thermal Analysis of Hybrid Circuits', Trans IEEE on Parts, Hybrids and Packaging,vol PHP-3, no 3 , Sept 1977, pp 283-289

[3]**SBERGOVIC S, BOSNJAK K M:**'Computer application in Thermal Analysis of Passive Components in Hybrid Microelectronic Circuits, International Colloquium on New Orientations of Passive Components, 1982, p 415

[4]**GREGORY P:**'Thermal Characteristics of a Hybrid Microcircuit', Proceedings of 11th Seminex Conference on Advances in Electronic Components and Systems, 1982, pp 347-357

[5]**WEHRHAHN E:** 'Temperature Distribution on Substrate of Hybrid Electronic Circuits', Proceedings of the 5th European Microelectronics Conference, 1985, pp 288-295

[6]**Charnley, M.** 'A model design approach to electronic CAE', Computer-Aided Engineering Journal, Vol 2, No 6, pp 192-199, 1985

[7]**WITTING, P A** 'Astec3 Introductory Manual', SIA Computer services,London , England, 1984

[8]'Astec3 User Manual, SIA Computer Services, London, England, 1984

[9]**WITTING, P A** 'Electronic Circuit Simulation With Astec3', Computer-Aided Engineering Journal,**vol 12 no 6**, pp186-191, 1985

[10]**HOLMAN J P**, 'Heat Transfer', 6th edn, McGraw-Hill, New York, 1986

[11]**CHAPMAN A J:** 'Heat Transfer', McGraw-Hill, New York, 1984

[12]**OZISIC M N:**, 'Fundamentals of Heat and Mass Transfer, McGraw-Hill, New York, 1977

[13]**BAYLEY, F J** 'Heat Transfer',Nelson, London, 1972

[14]**POOLE, N J;SARVAR, F;WITTING, P A;McKENZIE, W H'**Thermal Modelling Using ASTEC3 Software' Int. Journal of Numerical Modelling: Electronic Networks, Devices and Fields, **vol 1** pp 103-113, 1988

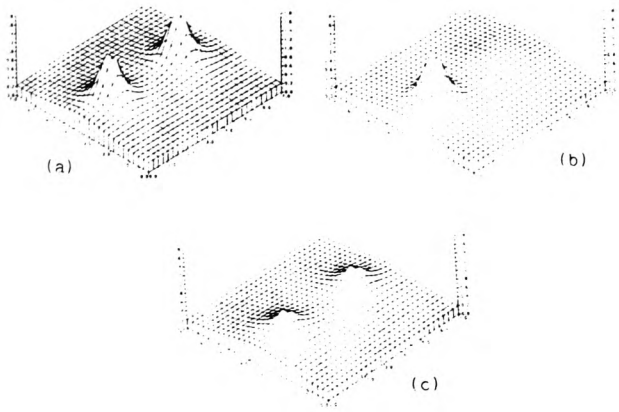

Figure 1

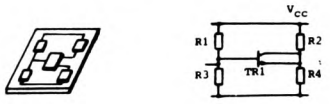

Figure 2

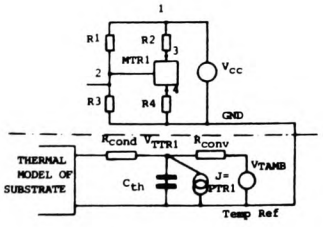

Figure 3

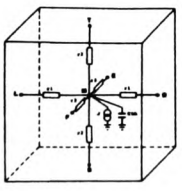

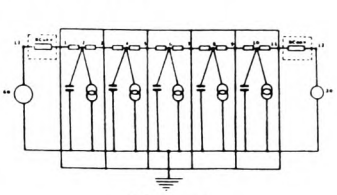

Figure 4

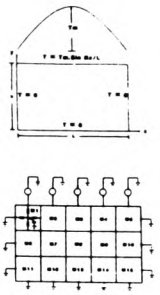

Figure 5

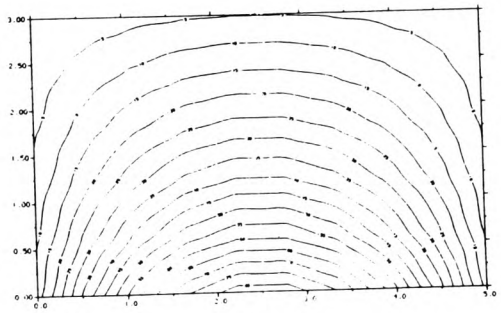

Figure 6

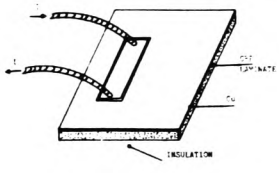

Figure 7

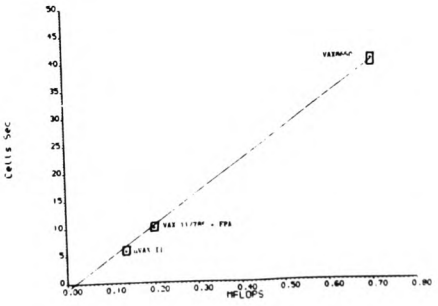

Figure 8

Journal of Electronic Materials, Vol. 19, No. 12, 1990

PCB Glass-Fibre Laminates: Thermal Conductivity Measurements and Their Effect on Simulation

F. SARVAR, N. J. POOLE and P. A. WITTING

Department of Electronics and Information Technology
Polytechnic of Wales, Pontypridd, Mid Glamorgan, CF37 1DL, Cymru, United Kingdom

Accurate values of thermal conductivity are required for the simulation of temperature phenomena in electronic circuits. This paper presents the results of measurements carried out to determine the thermal conductivity along and normal to the plane of fibre glass laminates used in the manufacture of printed circuit boards. It has been found that the reinforced fibre-glass substrates used in PCBs are strongly anisotropic with the conductivity normal to the boards being much smaller than tangential to it. The test samples were type FR4 epoxy/glass laminates. An experiment has been designed which determines the thermal conductivity in-the-plane of the laminates by matching the measured temperature distribution along a heated specimen with a finite difference solution. An electrically heated Lees' disc apparatus is also used to measure the thermal conductivity of these boards in a direction normal to their plane. The samples tested yielded values of 0.343 W/mK and 1.059 W/mK for thermal conductivity through and along the plane of the boards, respectively.

Key words: Thermal conductivity, PCB, substrate, glass-fibre

INTRODUCTION

A modelling technique has been devised for thermal analysis of semiconductor devices as well as printed circuit boards.[1] This is based on analogy between thermal and electrical systems. The structure is divided into a number of cuboidal "conduction cells," Fig. 1, and thermal resistances are used to construct an equivalent electrical network of the thermal structure. This is subsequently simulated for temperatures at the required points via ASTEC3 software which is an electronic analysis program.

In the course of experiments on a specially designed test specimen, unusually large differences were observed between the expereimentally measured and simulated temperatures. These experiments were performed on copper clad printed circuit boards (PCB). The rectangular PCB had dimensions of (14 × 12 cm) and consisted of a base of 1.6 mm FR4 epoxy/glass laminate[2] with 35 μm of copper cladding. An electrically isolated island (10 × 2 cm) resembling a resistor was cut into the copper layer of the plate as illustrated in Fig. 2. The 'resistor' was then Joule heated by passage of electric current of 30 A. As the island is electrically isolated, heat conduction from the heated area to the surrounding board is through the glass-fibre substrate. The surface temperatures were measured at selected points using an HEIMANN infrared pyrometer type KT14. This pyrometer is capable of measuring up to 300° C to an accuracy of 1.5° C and has a focal diameter of 4 mm.[3]

A three-dimensional, two layer thermal model of the structure consisting of the copper layer and the fibre-glass backing was constructed by dividing each layer into (7 × 6) thermal cells. In the model, thermal conduction in the x, y, and z directions, Fig. 1, in each of the copper and fibre-glass layers were taken into account using a value of 0.343 W/mK for the thermal conductivity in all directions within the fibre-glass layer assuming that it was isotropic. This value had been measured using a Lees' disc apparatus as described in later sections. Convection and radiation from the copper surface were also accounted for.

The results of the initial simulations are given in Table I along with the measured temperatures. This is an overhead view of the plate where in each cell the top figure represents the measured and the bottom value a simulated top-node, Fig. 1, temperature.

These show simulated temperatures of greater than 38% above the experimental results inside the heated island shown in Table I surrounded by double lines. The temperatures computed anywhere else on the plate are just above ambient which was measured at 23° C; these observations lead to the conclusion that the heat generated in the islands was not conducted away and therefore resulted in excessive temperatures simulated in these areas.

One possible reason for the observed results was anisotropy of thermal conductivity in the PCB. The viability of the explanation was tested by simulation. The in-the-plane thermal conductivity of the fibre-glass layer was varied but the normal component was held constant at its measured value of 0.343 W/mK. Table II gives such results for the midpoint of the heated island where a temperature of 70.6° C was obtained experimentally.

These show that closer agreement could be obtained by assuming anisotropy and therefore a procedure was devised to measure the in-the-plane component as described in the following section. A further section is also included which gives the re-

(Received April 13, 1989; revised July 5, 1990)

0361-5235/1990/1401-1345$5.00©90 AIME

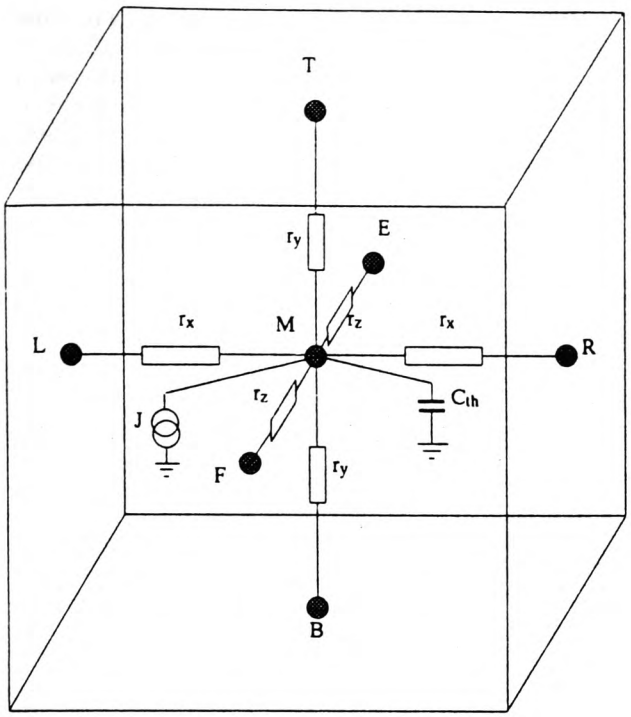

$r_x = 1/2\ R_{thx}$

$r_y = 1/2\ R_{thy}$

$r_z = 1/2\ R_{thz}$

Fig. 1 — The electrical equivalent model for a cell in three-dimensional conduction.

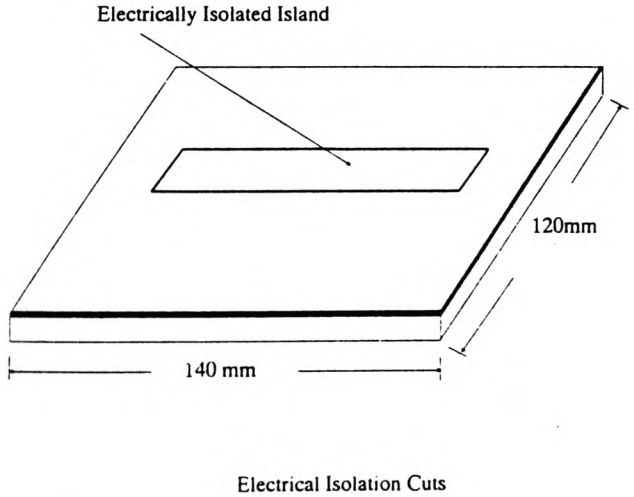

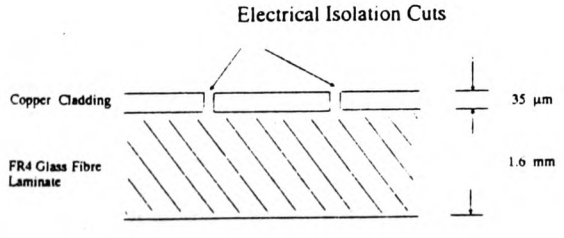

Fig. 2 — The layout of the PCB plate used in the heat transfer experiment.

Table I. Simulation and Experimental Results using Isotropic Thermal Conductivity Values K = 0.343 W/mK

33.2	34.3	35.8	37.4	36.4	35.3	33.8
25.9	26.2	26.4	26.5	26.4	26.2	25.9
33.2	38.5	41.7	43.9	41.7	38.0	34.3
26.3	27.1	27.4	27.5	27.4	27.1	26.3
	55.6	66.3	70.6	66.3	55.6	
	96.2	97.4	97.7	97.4	96.2	
34.3	38.5	41.0	42.8	41.7	39.6	39.6
25.9	26.5	26.8	26.9	26.8	26.5	25.9
33.2	34.3	35.3	36	36.4	34.8	33.8
25.2	25.4	25.5	25.6	25.5	25.4	25.2
32.1	33.2	33.2	34.3	33.2	33.2	32.1
24.8	24.9	25.0	25.0	25.0	24.9	24.8

Top Figure: Experimental
Bottom Figure: Simulated

sults of a Lees' disc experiment for the normal component of thermal conductivity.

THERMAL CONDUCTIVITY ALONG THE PLANE OF THE BOARDS

An experiment was set up for the measurement of thermal conductivity in-the-plane of the glass fibre boards. Rectangular samples of FR4 board were heated at one end and temperatures were measured along their lengths. These measured temperatures were then matched with a finite-difference solution of the equation defining the flow along the specimen. The thermal conductivity value in the equation was varied and the resulting temperatures were monitored until the square-root-error between the measured and the calculated values were minimised. This value of thermal conductivity was then taken to be that of the test sample. Finite-difference is a method where a particular structure is divided into small regions called "nodes" and heat balances are made on each of the nodes. This gives rise to a set of linear algebraic equations which can be solved simultaneously for temperatures at the required points. Errors in the order of $(\Delta x)^{2\,4}$ are normally expected with the one-dimensional form of this technique, Δx being the space increment.

The experiment was designed in such a way that the heat flow situation was as simple as possible to analyse numerically. The samples were heated uniformly along their widths so that the heat would be travelling along their lengths in a parallel fashion

Table II. Simulated Temperatures Obtained at the Mid-point of the Heated Island in Fig. (2) by Varying the Thermal Conductivity in the Plane of the FR4 Laminate

In-Plane Thermal Conductivity (W/mK)	0.7	1.0	1.5
Simulated Temperature (°C)	86.9	80.8	73.6

with negligible flow in the direction normal to the main flow. The chosen samples were of small thicknesses and heated around their perimeter at one end to ensure minimal temperature gradients normal to the faces. Furthermore, the temperatures were determined assuming no convection or conduction from the surface. This was achieved experimentally by enclosing the specimen in vacuum and extrapolating to zero pressure (perfect vacuum). This left radiation as the only heat loss mechanism. As energy loss by radiation is a function of the surface emissivity, the surface was coated with a paint of known emissivity (Black Velvet 2010).

Also to simplify the situation further all the temperatures were recorded at their steady-state value. This along with the criteria given above means that a one-dimensional steady-state heat flow equation with only a radiative heat loss term could be adopted.

Rectangular samples were prepared 15 cm long and with varying widths of 3, 4, 5 and 6 cm. The copper layer of the PCB boards were chemically etched off except very small circular patches of about 3 mm in diameter along the length of the samples in regular intervals of 10 mm as shown in Fig. 3. Thermocouples were then trapped under a very small amount of solder at these positions.

Since the emissivity of the boards were unknown, they were coated with "black velvet" paint 2010 made by 3M and having an emissivity of 0.95.[5] Heating wires were wrapped around the first 50 mm of each fin and connected to a power supply. The specimen was then clamped onto a holder and placed inside a steel pressure chamber as shown in Fig. 4. The inside walls of the vessel were blackened to stop any reflection that may occur. The system was evacuated in order to eliminate the effects of convection and to allow the calculation of the true value of temperature along the sample when radiation is the only heat loss mechanism. The thermocouple wires were taken out through a hole on top of the chamber which was carefully sealed to stop any leakage into the system while pumping down. The output signals of the thermocouples were fed into an AD595AQ thermocouple amplifier circuit with an internal cold junction (ice-point) compensator. A calibrated microvoltmeter was subsequently used to monitor the amplified signal and hence the temperatures along the specimen.

For a constant electrical input power, the variation of steady-state temperatures with pressure was recorded for each thermocouple. Graphs were produced for temperatures for each point vs pressure in the vessel. A sample graph for a 10 cm by 6 cm specimen is shown in Fig. 5 with reference to Fig.

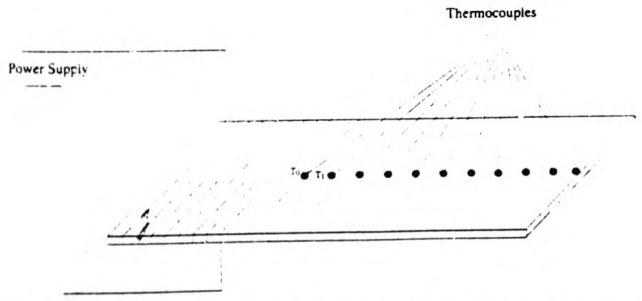

Fig. 3 — A block diagram of the samples used in thermal conductivity measurements in the plane of the boards.

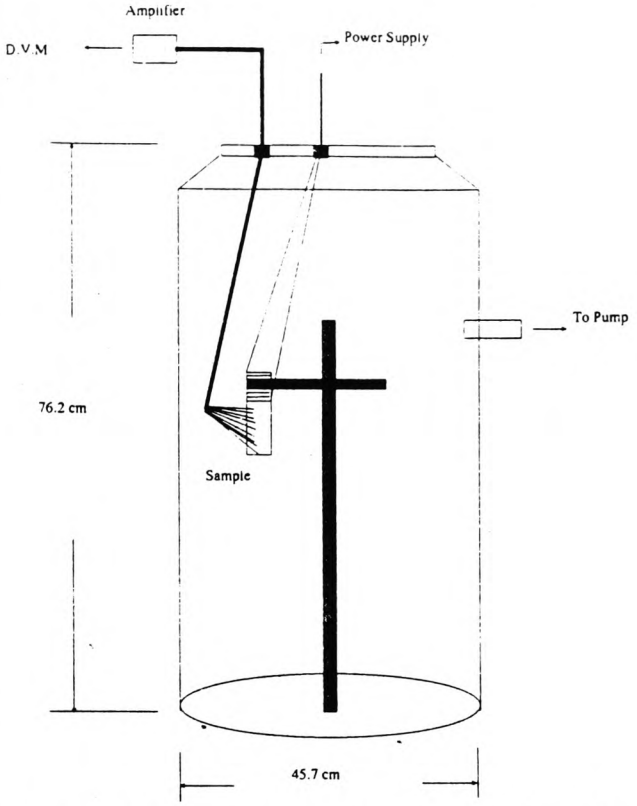

Fig. 4 — A block diagram showing the vacuum chamber and the sample used for thermal conductivity measurements in the plane of the boards.

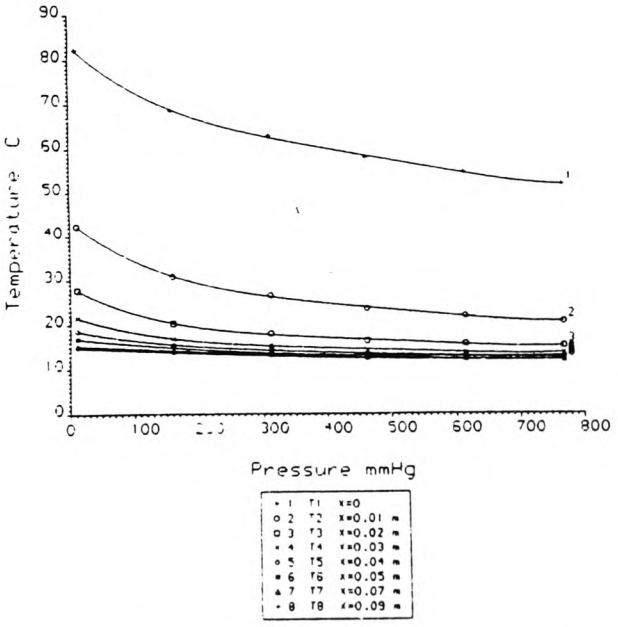

Fig. 5 — Graph of temperature vs pressure for a sample (10 × 6 cm) used in measuring the thermal conductivity tangential to the plane of the fibre-glass laminates.

3. Each line in the graph represents the temperature of each point as a function of pressure in the chamber. By extrapolation, the values of temperature corresponding to zero pressure were obtained for each position. This was done since, at zero pressure, heat losses by conduction and convection are zero.

In the second part of the procedure a finite difference method was used to solve the steady-state one-dimensional heat-conduction equation defining the heat flow in fin-shaped thin rectangular plates where heat is only lost by radiation. The resultant temperature distribution was then compared with that found in practice and the only unknown quantity, the in-plane thermal conductivity, varied to obtain a best fit.

The finite difference is a method whereby the partial differential equation of conduction is replaced by a system of linear algebraic equations for temperatures at a number of nodal points over the region.[6] This gives rise to a set of simultaneous equations which can be solved for temperatures at the required points.

The fins were divided into ten intervals as shown in Fig. 6. The energy balance for an i^{th} node inside the fin is given by:

$$KA\left(\frac{T_{i-1}-T_i}{\Delta x}\right) + KA\left(\frac{T_{i+1}-T_i}{\Delta x}\right) = \sigma\epsilon\,(P\Delta x)(T_i^4 - T_v^4)$$

where σ, ϵ, P and A are Stephan-Boltzmann constant, emissivity, perimeter and the cross sectional area of the sample respectively. K and Δx are thermal conductivity and space increment, T_v is the vessel temperature and T_i represents the temperature at the i^{th} node. The energy equation for the last half element is given by:

$$KA\left(\frac{T_9 - T_{10}}{\Delta x}\right) = \sigma\epsilon\left(A + P\frac{\Delta x}{2}\right)(T_{10}^4 - T_v^4)$$

A set of ten equations were obtained and solved simultaneously by using T_0, the root temperature as measured experimentally. A BASIC program was developed to calculate the other nodel points by stepping through the range of T_1 values, Fig. 3. The program repeats this for a range of thermal conductivity values between 0.8 and 1.4 W/mK. In this way, all node temperatures are determined for a range of thermal conductivities. A mean square error value between the measured (zero pressure) temperatures and calculated temperatures was then computed for each of the values of in-plane thermal conductivity.

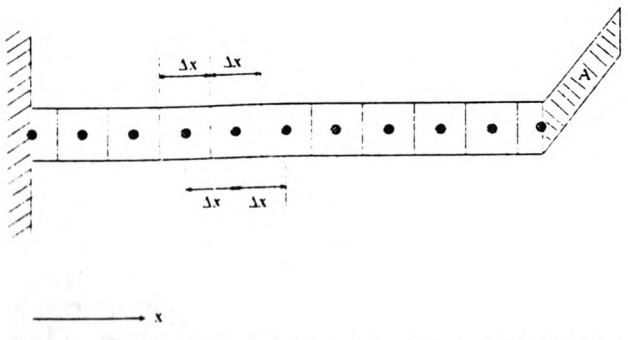

Fig. 6 — The breakdown of the rectangular samples for finite-difference solution.

The program automatically selects the set of calculated results with the smallest errors squared value and prints out the corresponding value of thermal conductivity.

This procedure is repeated for all eight samples, two for each size which gave the following results: an average value of 1.059 W/mK and standard deviation of 0.019 (See Table III). This value is very close to the thermal conductivity of glass reported as 1.1[7] which suggests that, along the plane of the boards, the majority of the heat is conducted by the woven glass-fibre sheets.

THERMAL CONDUCTIVITY NORMAL TO THE PLANE OF GLASS-FIBRE LAMINATES

An electrically heated Lees' disc apparatus was used to estimate the thermal conductivity in a direction normal to the glass fibre boards. The apparatus consisted of three flat circular metal discs of good thermal conductivity, Fig. 7, drilled radially where thermometers were inserted. A circular disc of the sample of exactly the same diameter as the metal slabs is sandwiched between discs 1 and 2 and a heating coil between discs 2 and 3. All these components were clamped firmly together and the outside surfaces were coated white to give them the same total emissivity.

The heater was switched on and the rig was left to stabilise. In a steady state condition, all the electrical energy supplied to the heating coil is lost from the surfaces of the metal discs and the specimen exposed to ambient air. For a voltage V and current I the following equation applies:[8,9]

$$VI = e\left[A_1(T_1 - T_a) + A_2(T_2 - T_a) + A_x\left(\frac{T_2+T_3}{2} - T_a\right) + A_3(T_3 - T_a)\right]$$

Table III. Results of Thermal Conductivity Measurements in the Plane of the FR4 Boards

Sample Width mm	Thermal Conductivity W/mK	
	Sample 1	Sample 2
30	1.09	1.03
40	1.045	1.075
50	1.05	1.055
60	1.055	1.075

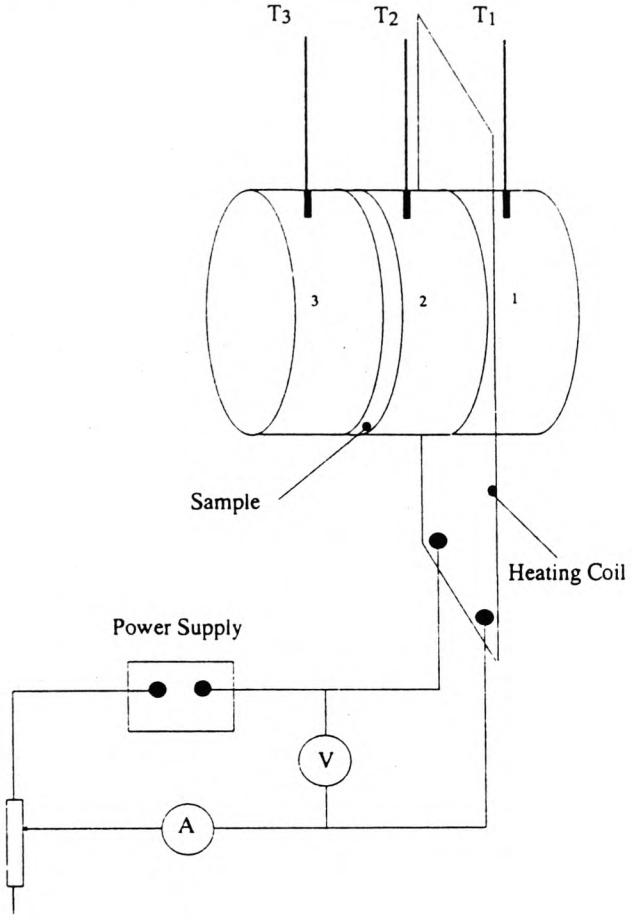

Fig. 7 — A schematic diagram of the electrically heated Lees' disc apparatus.

where T_1, T_2, T_3 and T_a are temperatures of discs 1, 2, 3 and the ambient air, respectively. A_1, A_2, A_3 and A_x are the emissive areas of discs 1, 2, 3 and of the specimen, respectively. From this equation, e, the power loss per unit area per °C above the ambient is obtained.

The heat flowing into the sample from disc 2 is eventually lost from the surfaces of either the sample or disc 3. If the cross sectional area of the sample is A and its thickness t is very small then the thermal conductivity K may be obtained from the following equation:[8,9]

$$KA\frac{(T_2 - T_3)}{t} = e\left[\frac{A_x}{2}\left(\frac{T_2 + T_3}{2} - T_a\right) + A_3(T_3 - T_a)\right]$$

To establish the relationship between thickness of the sample and its measured thermal conductivity for the particular apparatus and also to test its reliability, the inital experiments were carried out on a homogeneous material by using solid sheets of PTFE whose thermal conductivity is well-documented. These tests were carried out on samples of PTFE with varying thicknesses and the resulting

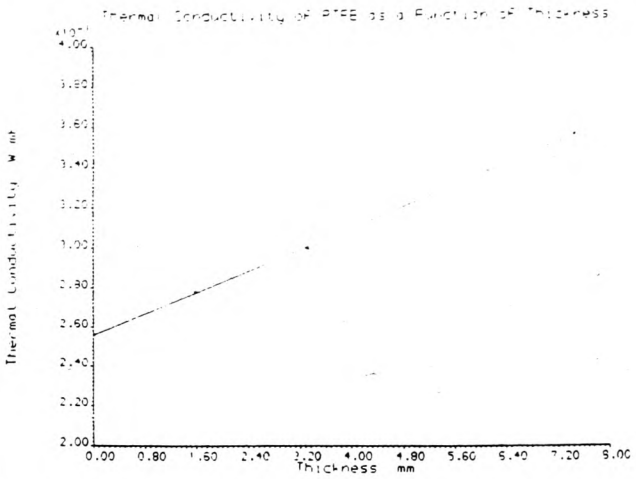

Fig. 8 — Graph showing variation of measured thermal conductivity of PTFE as a function of sample thickness for the Lees' disc apparatus.

thermal conductivities were plotted against the corresponding thicknesses. Figure 8 shows a linear relationship between the two variables and at zero thickness a value of 0.25597 W/mK is found which is in very good agreement with the quoted value of 0.25586 W/mK.[10] The thermal conductivity value was extrapolated to at zero thickness in order to remove the errors associated with finite sample thickness. The equations are derived assuming that the sample is at a uniform temperature given by the average of the two adjacent metal discs. This assumption leads to errors which increase with thickness and it is reduced to a minimum for samples of negligible thicknesses.

The same procedure was repeated to estimate the thermal conductivity of FR4 epoxy/glass laminates. Because of the unavailability of glass fibre sheets in different thicknesses, 1, 2, 3 and 4 discs of the PCB laminates were clamped tightly into position. All discs of the sample were cut from the same sheet of fibre glass to exactly the same diameter as the metal discs. The results are shown in Fig. 9 and af-

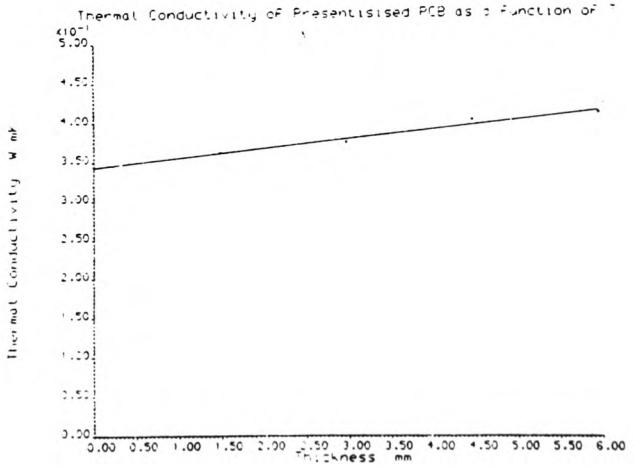

Fig. 9 — Thermal conductivity of PCB as a function of sample thickness for the Lees' disc apparatus.

Table IV. The Measured and Simulated Temperatures using Anisotropic Thermal Conductivities for FR4 Layer in Fig. 2, K_{plane} = 1.059 W/mK K_{normal} = 0.343 W/mK

33.2	34.3	35.8	37.4	36.4	35.3	33.8
29.0	29.6	30.0	30.2	30.0	29.6	29.0
33.2	38.5	41.7	43.9	41.7	38.0	34.3
29.8	31.2	31.9	32.2	31.9	31.2	29.8
	55.6	66.3	70.6	66.3	55.6	
	77.0	79.1	79.7	79.1	77.0	
34.3	38.5	41.0	42.8	41.7	39.6	39.6
29.1	30.2	30.8	30.9	30.8	30.2	29.1
33.2	34.3	35.3	36.0	36.4	34.8	33.8
27.6	28.0	28.3	28.4	28.3	28.0	27.6
32.1	33.2	33.2	34.3	33.2	33.2	32.1
26.9	27.1	27.2	27.3	27.2	27.2	26.9

ter extrapolating to zero thickness a value of 0.343 W/mK was obtained for the conductivity normal to the plane of the boards.

SIMULATIONS OF THE PCB STRUCTURE USING THE ANISOTROPIC THERMAL CONDUCTIVITIES

The computer model of the experimental structure was subsequently amended to account for the anisotropic thermal conductivity. This was carried out by calculating thermal resistances using the measured anisotropic thermal conductivities in the plane and normal directions. The results are given in Table IV which shows a marked reduction in the errors between the simulated and measured temperatures compared to the earlier simulations, which assumed isotropy. For example, this error is 12.9% at the centre point of the 10 × 2 cm island compared to 38.4% simulated previously.

Convective heat transfer coefficients are thought to be responsible for the remaining discrepancies between the experimental and simulated results. This heat loss process is presently being studied using optical techniques which should give an insight into the heat flow mechanism over the plates and an indication of its variation over the surface.

CONCLUSIONS

Anisotropic thermal conductivity of FR4 Epoxy/Glass laminates used for printed circuit boards has been successfully measured. A technique has been developed to measure thermal conductivity along the plane of materials in the shape of a thin flat board. This technique may be used in other areas of research where anisotropic thermal conductivity of materials in the form of thin flat boards is required. An electrically heated Lees' disc apparatus is also used to determine the thermal conductivity normal to their plane. Values of 0.343 W/mK and 1.059 W/mK have been measured for thermal conductivity normal and tangential to PCB laminates showing that the thermal conductivity of these reinforced boards are almost three times greater in the plain of their flats.

ACKNOWLEDGEMENTS

This research is supported by an internal Polytechnic of Wales grant. We wish to thank Mr. W. H. McKenzie for his valuable help and discussions.

REFERENCES

1. HEIMANN Radiation Thermometer KT14 Instruction Manual, HEIMANN GmbH Infrared Measurements, D-6200 Wiesbaden-Dotzheim, West Germany.
2. N. J. Poole, F. Sarvar, P. A. Witting and W. H. McKenzie, Int. J. Numerical Modelling *1*, 103 (1988).
3. private communication, Mica and Micanite (Ireland) LTD., Mallow, Co. Cork, Ireland.
4. F. J. Bayley, J. M. Owen and A. B. Turner, Heat Transfer, Nelson and Sons Ltd., (1972), pp. 90–92.
5. 'Nextel 2010 Velvet Coating' Product Performance Bulletin and Application Instructions, 3M Industrial Chemical Products, 3M Head Office, Bracknell, Berks, England.
6. A. J. Chapman, Heat Transfer, 4th Ed., McGraw-Hill, New York, (1984), p. 131.
7. G. W. C. Kay and T. H. Laby, Tables of Physics and Chemical Constants, 15th Ed., Longman Group Ltd., (1986), p. 69.
8. A. J. Starling and A. J. Woodall, Physics, 2nd Ed. Longmans (1964), pp. 320–321.
9. Equipment Notes No. P28030/1 for Lees' Disc Apparatus from Philip Harris Limited, Shenstone, England.
10. Data Sheet No. PD4/7/82, Polypenco Engineering Plastics Materials Limited, 76 Bridge Road East, Welwyn Garden City, Herts, England.